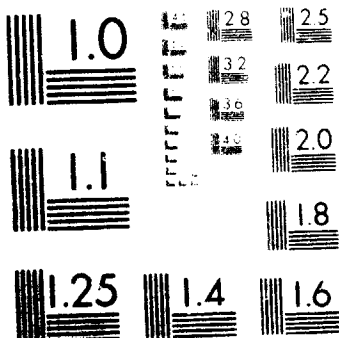


10F2

N8I-23036

UNCLAS



MICROCOPY RESOLUTION TEST CHART
NATIONAL BUREAU OF STANDARDS 1963

NASA Technical Memorandum 81927

(NASA-TM-81927) TWO-DIMENSIONAL AERODYNAMIC
CHARACTERISTICS OF THE NACA 0012 AIRFOIL IN
THE LANGLEY 8 FOOT TRANSONIC PRESSURE TUNNEL
(NASA) 139 p HC A07/MF A01

CSCL 01A

N81-23036

Unclassified
G3/02 42317

TWO-DIMENSIONAL AERODYNAMIC CHARACTERISTICS OF THE NACA 0012 AIRFOIL IN THE LANGLEY 8-FOOT TRANSONIC PRESSURE TUNNEL

CHARLES D. HARRIS

APRIL 1981



National Aeronautics and
Space Administration

Langley Research Center
Hampton, Virginia 23665

TWO-DIMENSIONAL AERODYNAMIC CHARACTERISTICS OF THE NACA 0012 AIRFOIL
IN THE LANGLEY 3-FOOT TRANSONIC PRESSURE TUNNEL

By Charles D. Harris
Langley Research Center

SUMMARY

Results of two-dimensional wind tunnel tests of the symmetrical NACA 0012 airfoil in the Langley Research Center's 8-foot Transonic Pressure Tunnel are reported. Tests were conducted at lift coefficients from near zero through maximum values at Mach numbers from 0.30 to 0.86 for Reynolds numbers of 3.0 million and 9.0 million with transition fixed at 5-percent chord. A limited amount of data was obtained near zero and maximum lift for a Reynolds number of 6.0 million with transition fixed at 5-percent chord. In addition, transition free data were obtained through the Mach number range from 0.30 to 0.86 for zero lift and a Reynolds number of 3.0 million.

INTRODUCTION

Advances in computational methods and increased concern about wind tunnel wall interference effects in the transonic speed range have underscored the need for reliable two-dimensional experimental data. In an effort to provide such data, tests have been conducted on the symmetrical NACA 0012 airfoil in the Langley Research Center's 8-foot Transonic Pressure Tunnel. The 8-foot tunnel was chosen because, although it was not designed as a two-dimensional tunnel, its geometry permits a model of large chord while maintaining a large span-to-chord ratio, both of which are desirable for two-dimensional testing. In addition, the ratio of sidewall-displacement-thickness (δ^*) to tunnel width (b) for the 8-foot tunnel

$(2\delta^*/b = 0.0084)$ is small, which tends to minimize sidewall-boundary-layer effects (ref. 1). The 0012 airfoil was chosen since it has long been a standard two-dimensional model for evaluating wind-tunnel test techniques and computational methods (see, for example, ref. 2) and for making comparisons between data obtained in different wind tunnels.

The purpose of this report is to document the results of these tests. Consequently, results are presented without discussion.

SYMBOLS

Values are given in both SI and U.S. Customary Units. Measurements and calculations were made in U.S. Customary Units.

c_p pressure coefficient, $\frac{p_L - p_\infty}{q_\infty}$

c chord of airfoil, cm (in.)

c_d' section profile-drag coefficient determined from wake measurements (ref. 3),

$$\sum_{\text{wake}} c_d' \frac{\Delta h}{c}$$

c_d' point drag coefficient (ref. 3)

c_m section pitching-moment coefficient,

$$\sum_u c_p \frac{\Delta x}{c} (0.25 - \frac{x}{c}) - \sum_u c_p \frac{\Delta x}{c} (0.25 - \frac{x}{c})$$

c_n section normal-force coefficient,

$$\sum_u c_p \frac{\Delta x}{c} - \sum_u c_p \frac{\Delta x}{c}$$

h vertical distance in wake profile, cm (in.)

M Mach number
p static pressure, N/m² (lb/ft²)
q dynamic pressure, N/m² (lb/ft²)
 R_n Reynolds number based on airfoil chord
x airfoil abscissa, cm (in.)
z airfoil ordinate, cm (in.)
 α angle of attack, angle between airfoil reference line and airstream direction, deg

Subscripts:

L local point on airfoil
l lower surface
u upper surface
∞ undisturbed stream conditions

APPARATUS AND TECHNIQUES

Wind Tunnel Model

A sketch of the 0012 airfoil model is presented in figure 1 and the design and measured section coordinates are presented in table I. The measured coordinates of the experimental model deviated slightly from the design coordinates, but these deviations are small, nowhere greater than $\Delta z/c = 0.0002$ and generally less than 0.0001, and should not significantly affect the results.

The wind-tunnel model spanned the width of the tunnel with a span-chord ratio of 3.43. The body of the model was machined from aluminum with embedded pressure tubes and the leading edge was made of stainless steel. Angle of attack was changed manually by rotating the model about pivots in

the tunnel sidewalls. A sketch of the model installed in the tunnel is shown in figure 2.

Wind Tunnel

The investigation was conducted in the Langley 8-foot transonic pressure tunnel (ref. 4). This tunnel is a continuous flow, variable-pressure wind tunnel with controls that permit the independent variation of Mach number, stagnation pressure and temperature, and dewpoint. The upper and lower test-section walls are axially slotted to permit testing through the transonic speed range. The total slot width at the position of the model averaged about 5 percent of the width of the upper and lower walls. The tunnel has a square test section with filleted corners so that the total cross-sectional area at the beginning of the slots is equivalent to that of a 2.44-meter-diameter (8-foot-diameter) circle.

Measurements

Surface-pressure measurements.- Normal force and pitching moments acting on the airfoil were determined from surface static-pressure measurements. The surface-pressure measurements were obtained from a chordwise row of orifices located approximately $0.32c$ from the tunnel center line. Orifices were more concentrated near the leading and trailing edges of the airfoil to define the pressure gradients in these regions and a rearward facing orifice was included in the trailing edge (identified at an upper surface x/c location of 1.00). Pressures were measured with electronically actuated differential pressure-scanning-valve units with a transducer range of $\pm 68.9 \text{ kN/m}^2$ (10 lb/in.^2). Accuracy of the transducers was within 0.5-percent full scale.

Wake measurements.- Drag forces were determined from vertical variations of the total and static pressures measured across the wake with the profile drag rake shown in figure 3. The profiles, schematically illustrated in figure 4, represent the momentum losses as indicated by stagnation-pressure deficits across the wake. The middle section of these profiles reflects viscous and separation losses in the boundary layer, whereas the "wings" of the profile reflect direct losses in stagnation pressure across the shock waves.

The rake was positioned in the vertical center-line plane of the tunnel, one chord length rearward of the trailing edge of the airfoil. The total-pressure tubes were flattened horizontally and closely spaced vertically (0.36 percent of the airfoil chord) in the region of the wake associated with skin-friction boundary-layer losses. Outside this region, the tube vertical spacing progressively widened until in the region above the wing where only shock losses were anticipated, the total-pressure tubes were spaced apart about 7.2 percent of the chord. Static-pressure tubes were distributed as shown in figure 3. Each static pressure measured was used over a section of the rake to determine local flow conditions in the vicinity of the static-pressure tube rather than using an average of all the static pressures measured. The rake was attached to the conventional center-line sting mount of the tunnel; this arrangement permitted it to be moved vertically to center the close concentration of tubes in the boundary-layer wake.

Total and static pressures in the wake were also measured with electronically actuated differential-pressure scanning valve units. The

range of the transducer in the valve connected to total-pressure tubes intended to measure losses in the boundary-layer wake was $\pm 17.2 \text{ kN/m}^2$ (2.5 lb/in^2); the corresponding range for measuring shock losses and static pressures in the wake was $\pm 6.9 \text{ kN/m}^2$ (1.0 lb/in^2).

Reduction of Data

Calculation of c_n and c_m . - Section normal-force and pitching-moment coefficients were obtained by numerical integration (based on the trapezoidal method) of the local surface-pressure coefficient measured at each orifice multiplied by an appropriate weighting factor (incremental area).

Calculation of c_d . - To obtain section drag coefficients, point drag coefficients were computed for each total-pressure measurement in the wake by using the procedure of reference 3. These point drag coefficients were then summed by numerical integration across the wake, again based on the trapezoidal method.

Wind-Tunnel-Wall Effects

Two-dimensionality of flow. - Observation of the flow over the model and on the tunnel sidewall at Mach numbers from 0.50 to 0.65 using the fluorescent-oil film method described in reference 5 showed the flow to be two-dimensional with no sidewall separation evident at maximum lift conditions.

Corrections. - Because of the uncertainty in wall-induced lift interference effects and solid and wake blockage effects (particularly in the presence of local supercritical flow) the basic experimental data is presented without corrections for wall effects.

An indication of the influence of the tunnel walls on the flow over the model is shown as a dashed line rotation of the normal force angle of attack curves of figures 5 and 6. The dashed lines represent incremental changes in angle of attack due to wall-induced downwash over the model. Using the geometric characteristics of the 8-foot tunnel (slot spacing = 54.31 cm (21.38 in.), tunnel semi-height of 108.61 cm (42.76 in.), and average openness ratio in the vicinity of the model of 0.051) and the analysis of reference 6, the incremental change in angle of attack (in degrees) was estimated to be $\Delta\alpha = -1.55 c_n$.

TEST CONDITIONS

Tests were conducted at lift coefficients from near zero through maximum values at Mach numbers from 0.30 to 0.86 for Reynolds numbers of 3.0 million and 9.0 million with transition fixed at 5-percent chord. A limited amount of data was obtained near zero and maximum lift for a Reynolds number of 6.0 million with transition fixed at 5-percent chord. In addition, transition free data were obtained through the Mach number range from 0.30 to 0.86 for zero lift and a Reynolds number of 3.0 million.

Transition trips consisted of sparsely distributed 0.25-cm-wide (0.10-in.) bands of carborundum grains sized according to the technique of reference 7 and attached to the surface with clear lacquer. No. 54 carborundum grains were used for 3.0-million Reynolds number, No. 80 for 6.0-million and No. 100 for 9.0-million.

The stagnation temperature of the tunnel air was automatically controlled at temperatures which ranged, dependent on Reynolds number and

Mach number, from 311 K (100°F) to 322 K (120°F). The air was dried until the dewpoint in the test section was reduced sufficiently to avoid condensation effects.

PRESENTATION OF RESULTS

The experimental data reported herein are presented without discussion in the following figures:

Figure

| | |
|--|----|
| Force and moment characteristics. $R_n = 3.0 \times 10^6$, transition fixed..... | 5 |
| Force and moment characteristics. $R_n = 9.0 \times 10^6$, transition fixed..... | 6 |
| Effects of Reynolds number on force and moment characteristics. Transition fixed..... | 7 |
| Effects of Reynolds number on drag-rise characteristics..... | 8 |
| Chordwise pressure distribution for $R_n = 3.0 \times 10^6$ and transition fixed, at: | |
| $M = 0.30$ | 9 |
| $M = 0.35$ | 10 |
| $M = 0.50$ | 11 |
| $M = 0.55$ | 12 |
| $M = 0.60$ | 13 |
| $M = 0.65$ | 14 |
| $M = 0.70$ | 15 |
| $M = 0.74$ | 16 |
| $M = 0.76$ | 17 |
| $M = 0.78$ | 18 |

Figure

| | |
|--|----|
| $M = 0.80$ | 19 |
| $M = 0.82$ | 20 |
| $M = 0.84$ | 21 |
| $M = 0.86$ | 22 |
| Chordwise pressure distribution for $R_n = 6.0 \times 10^6$ and transition fixed, at: | |
| $M = 0.30$ | 23 |
| $M = 0.35$ | 24 |
| $M = 0.50$ | 25 |
| $M = 0.55$ | 26 |
| Effect of Mach number on chordwise pressure distributions. | |
| $R_n = 6.0 \times 10^6$, angles of attack near zero, transition fixed..... | 27 |
| Chordwise pressure distribution for $R_n = 9.0 \times 10^6$ and transition fixed, at: | |
| $M = 0.50$ | 28 |
| $M = 0.55$ | 29 |
| $M = 0.60$ | 30 |
| $M = 0.65$ | 31 |
| $M = 0.70$ | 32 |
| $M = 0.74$ | 33 |
| $M = 0.76$ | 34 |
| $M = 0.78$ | 35 |
| $M = 0.80$ | 36 |
| $M = 0.82$ | 37 |

Figure

M = 0.84..... 38

M = 0.86..... 39

Effect of Mach number on chordwise pressure distributions.

$R_n = 3.0 \times 10^6$, angles of attack near zero, transition free..... 40

The pressure distributions presented show disturbances in the airfoil pressure coefficient in some cases near 5-percent-chord. Examination of these disturbances (figs. 15(a), 16(b), 17(a), for example) show that they generally occur when the local velocity is near sonic velocity, and therefore, more sensitive. These disturbances are believed to be caused by the effect of the transition particles on the pressure orifices and may be disregarded.

REFERENCES

1. Barnwell, Richard W.: A Similarity Rule for Compressibility and Sidewall Boundary-Layer Effects in Two-Dimensional Wind Tunnels. AIAA Paper No. 79-0108, Jan. 1979.
2. Experimental Data Base for Computer Program Assessment - Report of the Fluid Dynamics Panel Working Group 04. AGARD-AR-138, May 1979.
3. Baals, Donald D.; and Mourhess, Mary J.: Numerical Evaluation of the Wake-Survey Equations for Subsonic Flow Including the Effect of Energy Addition. NACA WR L-5, 1945. (Formerly NACA ARR LSH27.)
4. Schaefer, William T., Jr.: Characteristics of Major Active Wind Tunnels at the Langley Research Center. NASA TM X-1130, 1965.
5. Loving, Donald L.; and Katzoff, S.: The Fluorescent-Oil Film Method and Other Techniques for Boundary-Layer Flow Visualization. NASA Memo 3-17-59L, 1959.
6. Barnwell, Richard W.: Design and Performance Evaluation of Slotted Walls for Two-Dimensional Wind Tunnels. NASA TM-78648, Feb. 1978.
7. Braslow, Albert L.; and Knox, Eugene C.: Simplified Method for Determination of Critical Height of Distributed Roughness Particles for Boundary-Layer Transition at Mach Numbers From 0 to 5. NACA TN 4363, 1958.

TABLE I.- SECTION COORDINATES OF NACA 0012 SYMMETRICAL AIRFOIL
 [c = 63.5 cm (25 in.)]

| x/c | z/c | | |
|------|--------|----------|--------|
| | Design | Measured | |
| | | Upper | Lower |
| 0.0 | 0.0 | 0.0 | 0.0 |
| .002 | .0078 | .0078 | -.0078 |
| .005 | .0122 | .0121 | -.0121 |
| .01 | .0170 | .0169 | -.0169 |
| .02 | .0236 | .0235 | -.0235 |
| .03 | .0284 | .0283 | -.0283 |
| .04 | .0323 | .0322 | -.0322 |
| .05 | .0355 | .0354 | -.0354 |
| .06 | .0384 | .0383 | -.0383 |
| .08 | .0431 | .0430 | -.0430 |
| .10 | .0468 | .0467 | -.0467 |
| .12 | .0499 | .0498 | -.0498 |
| .14 | .0524 | .0523 | -.0523 |
| .16 | .0544 | .0544 | -.0543 |
| .18 | .0561 | .0561 | -.0560 |
| .20 | .0574 | .0574 | -.0573 |
| .22 | .0584 | .0584 | -.0583 |
| .24 | .0591 | .0591 | -.0590 |
| .26 | .0596 | .0596 | -.0595 |
| .28 | .0599 | .0600 | -.0599 |
| .30 | .0600 | .0601 | -.0600 |
| .32 | .0599 | .0600 | -.0599 |
| .34 | .0597 | .0598 | -.0597 |
| .36 | .0593 | .0594 | -.0592 |
| .38 | .0587 | .0588 | -.0586 |
| .40 | .0580 | .0581 | -.0580 |
| .42 | .0572 | .0573 | -.0572 |
| .44 | .0563 | .0564 | -.0563 |
| .46 | .0553 | .0554 | -.0553 |
| .48 | .0542 | .0542 | -.0542 |
| .50 | .0529 | .0530 | -.0528 |

TABLE I.- SECTION COORDINATES OF NACA 0012 SYMMETRICAL AIRFOIL.- Continued.
 [c = 63.5 cm (25 in.)]

| x/c | z/c | | |
|------|--------|----------|--------|
| | Design | Measured | |
| | | Upper | Lower |
| .52 | .0516 | .0517 | -.0516 |
| .54 | .0502 | .0503 | -.0502 |
| .56 | .0488 | .0489 | -.0487 |
| .58 | .0472 | .0472 | -.0472 |
| .60 | .0456 | .0457 | -.0456 |
| .62 | .0440 | .0441 | -.0440 |
| .64 | .0422 | .0423 | -.0422 |
| .66 | .0404 | .0405 | -.0404 |
| .68 | .0386 | .0387 | -.0386 |
| .70 | .0366 | .0367 | -.0366 |
| .72 | .0347 | .0348 | -.0347 |
| .74 | .0326 | .0327 | -.0326 |
| .76 | .0306 | .0307 | -.0306 |
| .78 | .0284 | .0285 | -.0284 |
| .80 | .0262 | .0263 | -.0262 |
| .82 | .0240 | .0241 | -.0240 |
| .84 | .0217 | .0218 | -.0216 |
| .86 | .0193 | .0194 | -.0192 |
| .88 | .0169 | .0170 | -.0168 |
| .90 | .0145 | .0145 | -.0144 |
| .92 | .0120 | .0120 | -.0119 |
| .94 | .0094 | .0095 | -.0093 |
| .96 | .0067 | .0068 | -.0067 |
| .98 | .0040 | .0042 | -.0040 |
| 1.00 | .0013 | .0015 | -.0013 |

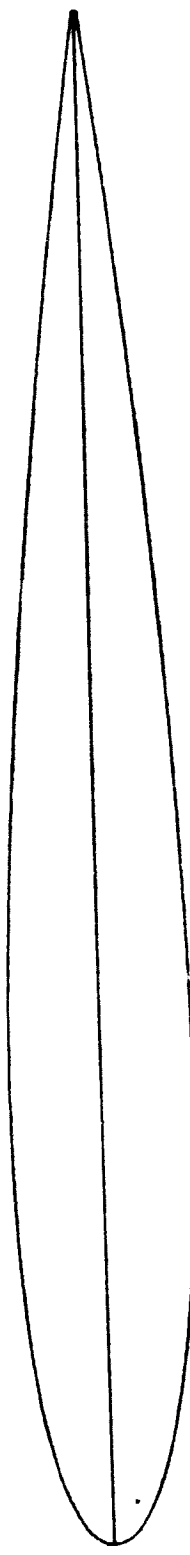


Figure 1.- Sketch of NACA 0012 airfoil.

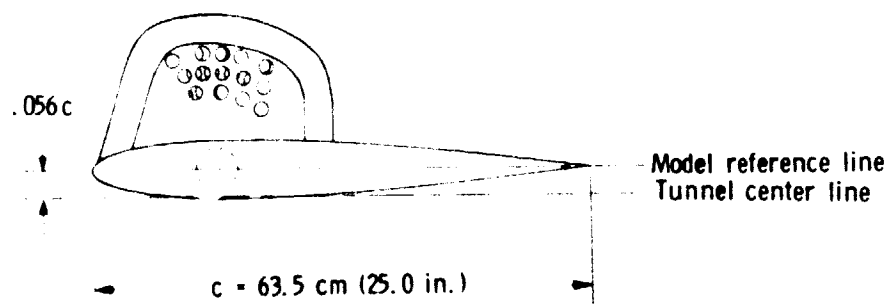
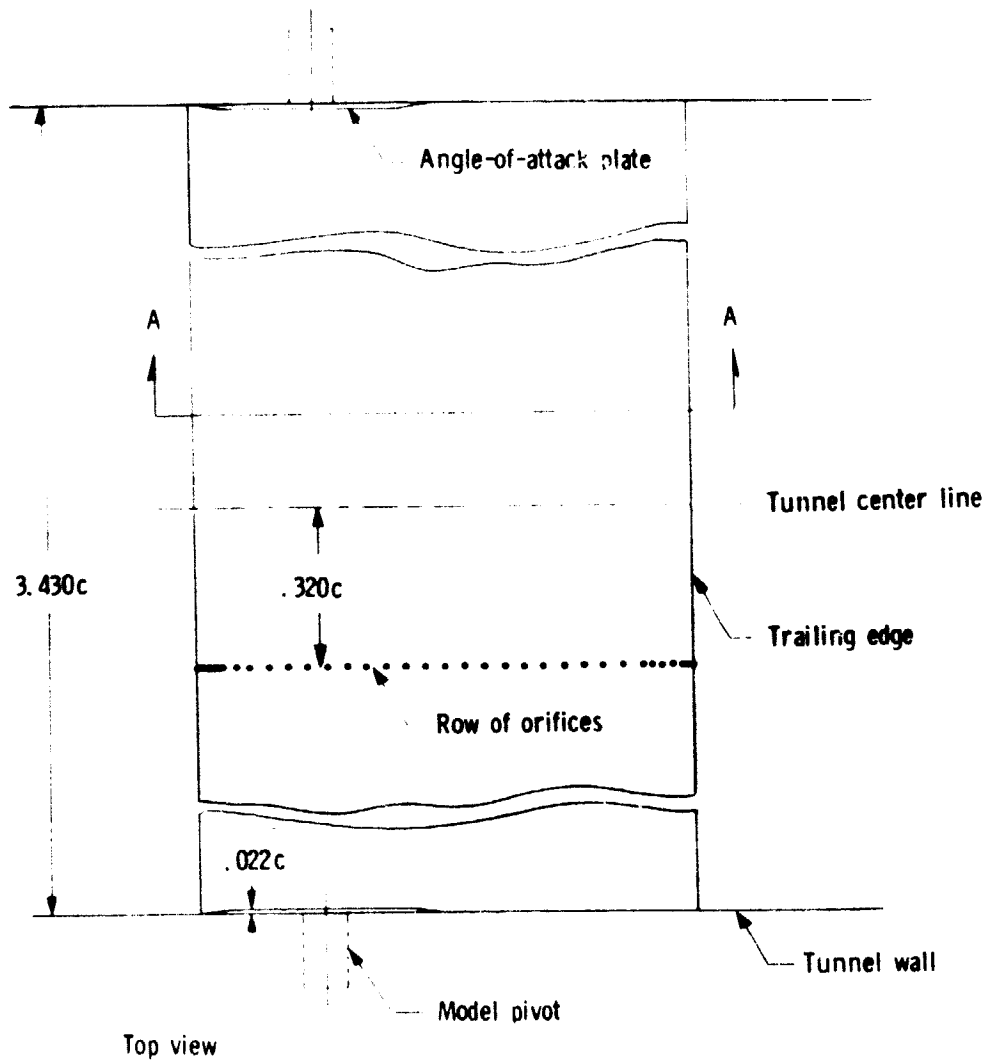


Figure 2.- Sketch of model installed in tunnel
(with angle of attack end plates).

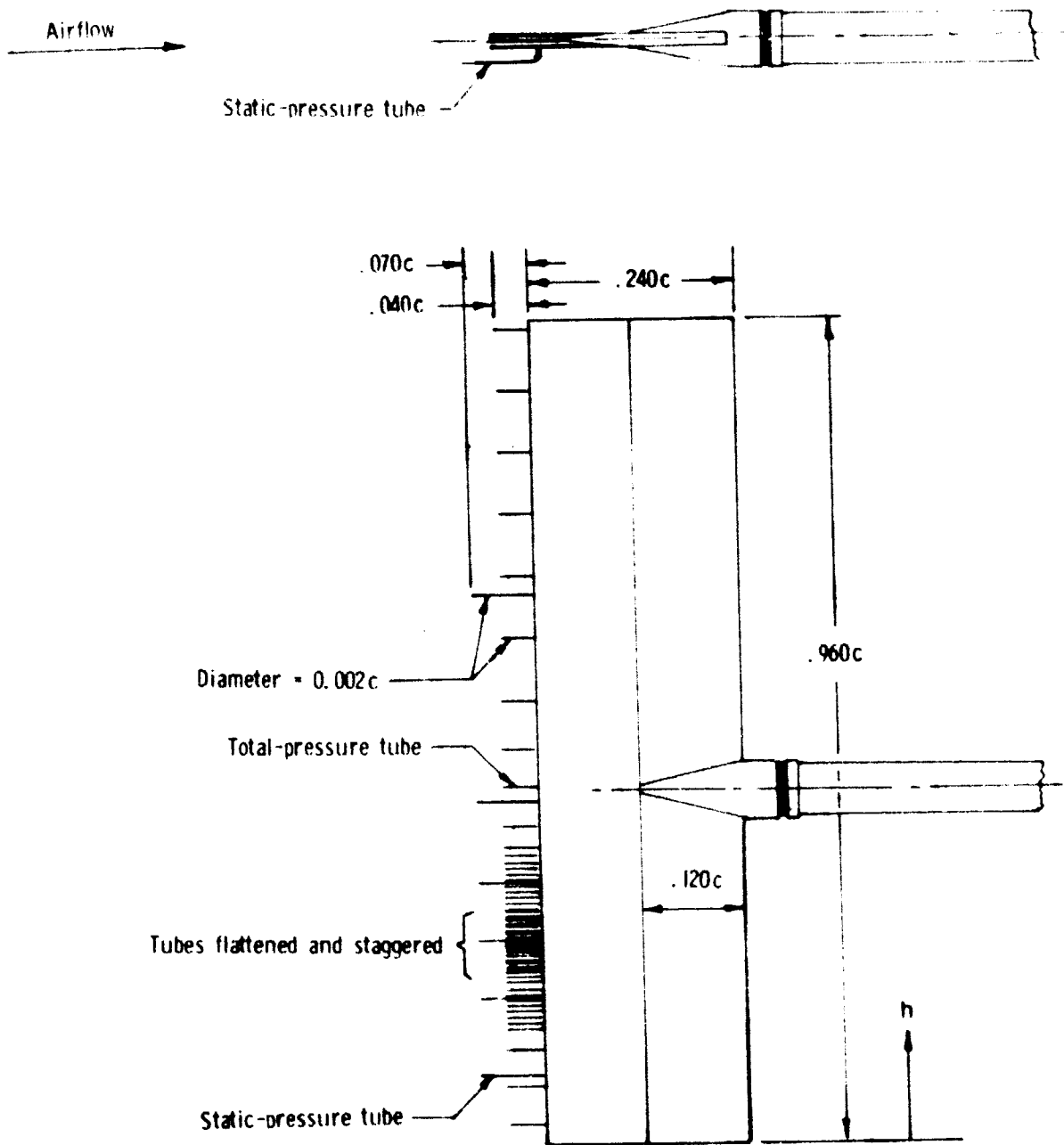


Figure 3.- Profile drag rake.

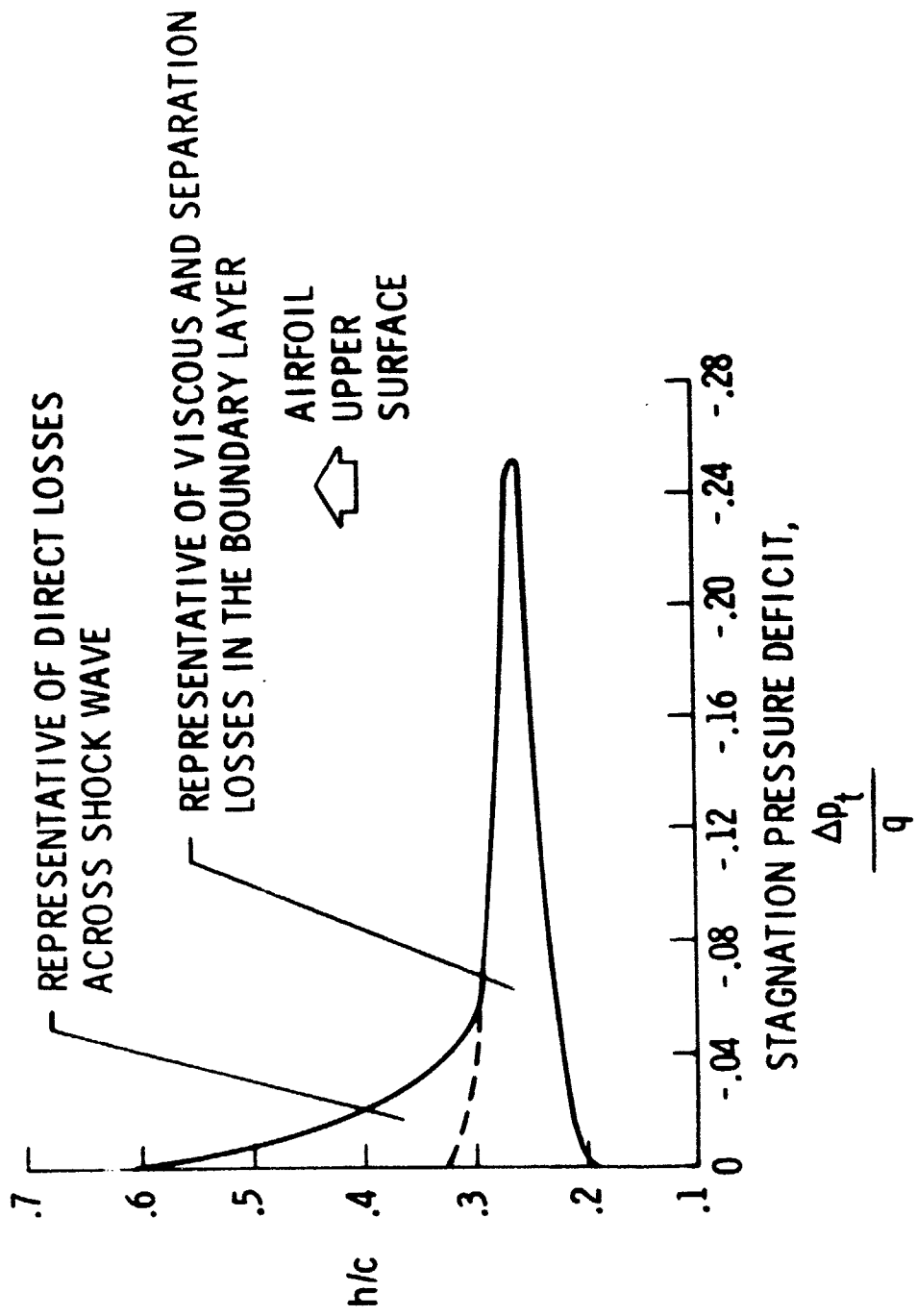
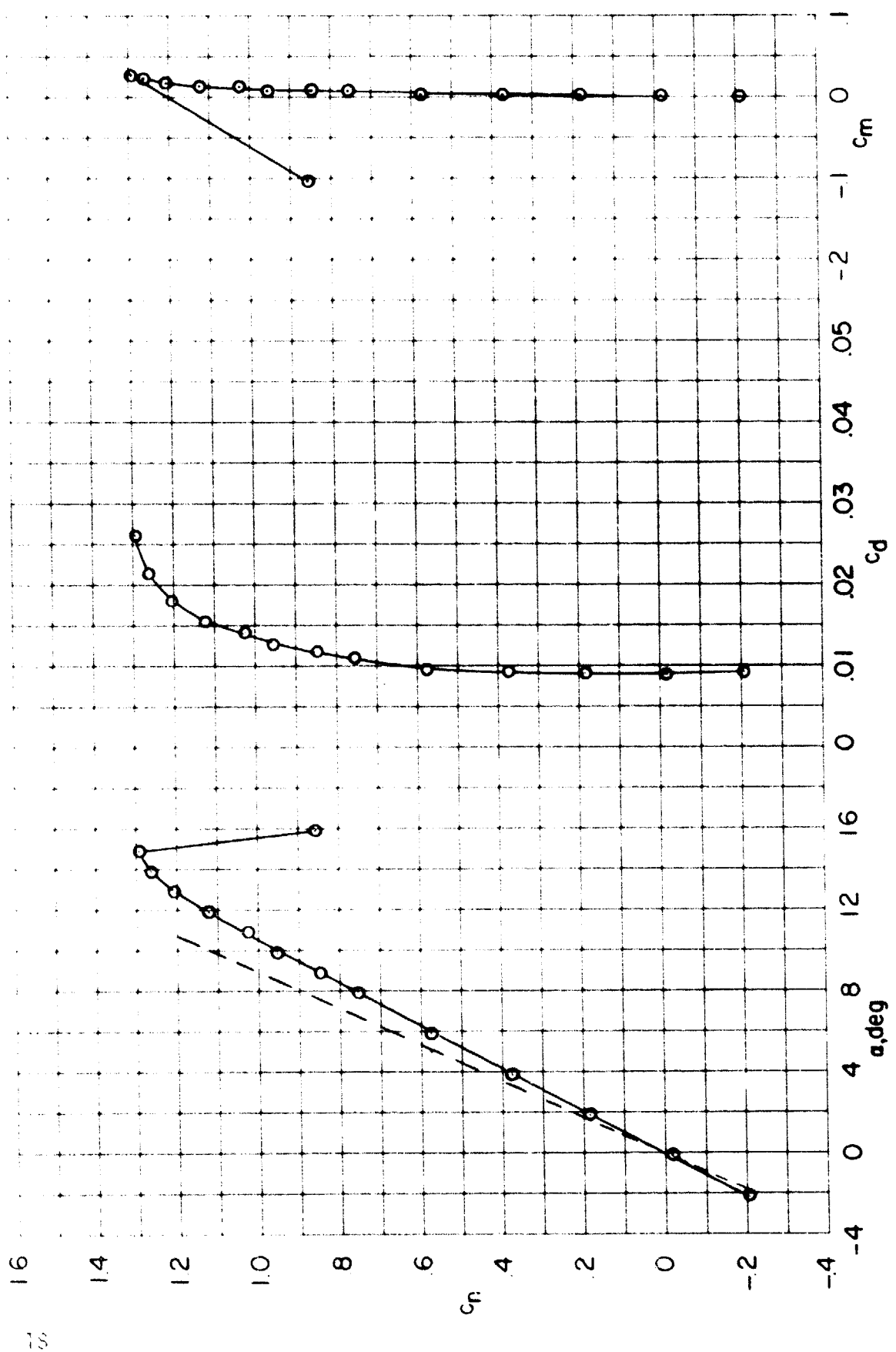
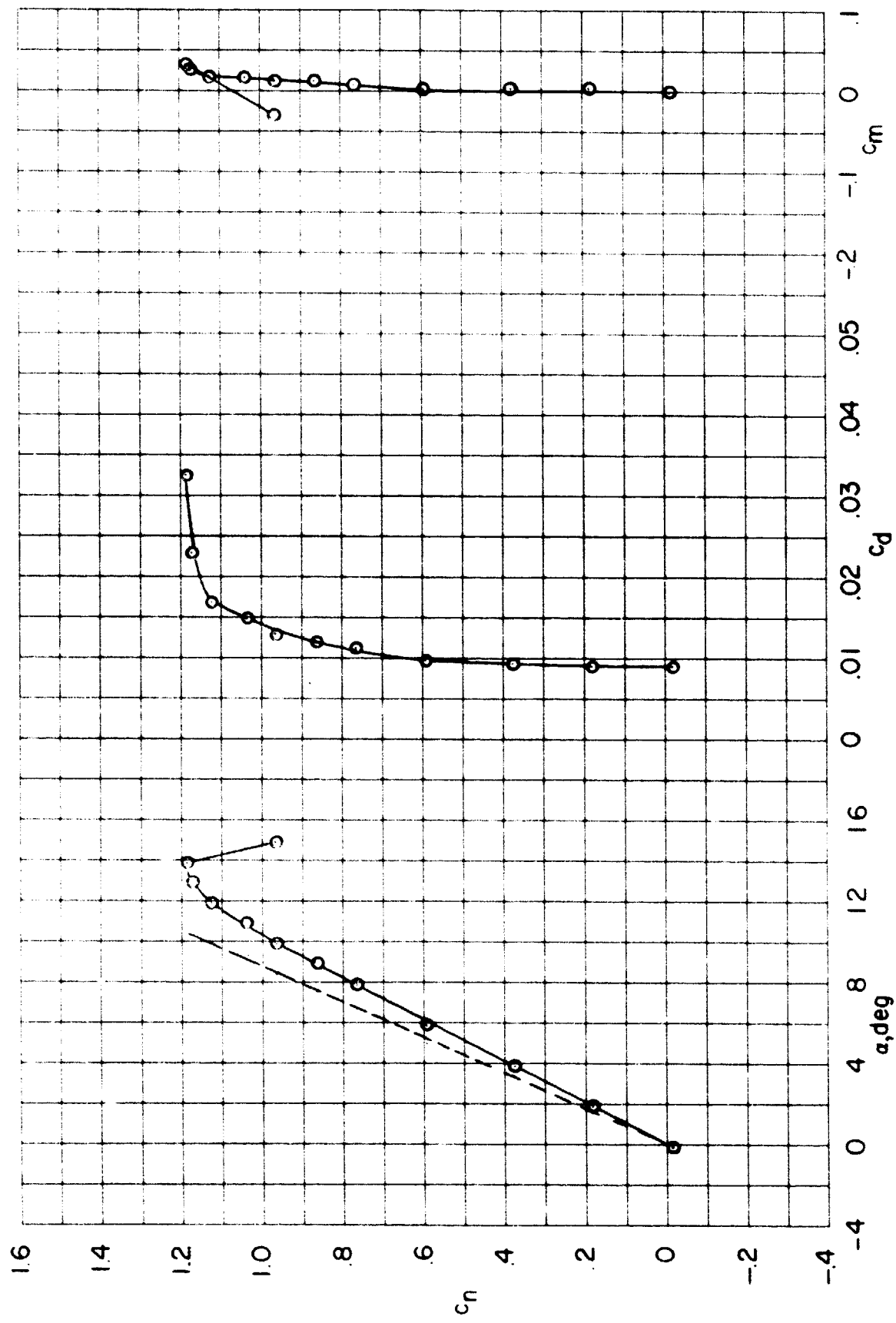


Figure 4.- Wake profile schematic.



(a) $M = 0.30$

Figure 5.- Force and moment characteristics of NACA 0012 airfoil. $Rn = 3.0 \times 10^6$, transition fixed. (dashed line indicates angle of attack correction for wall interference).



(b) $M = 0.35$

Figure 5.- Continued.

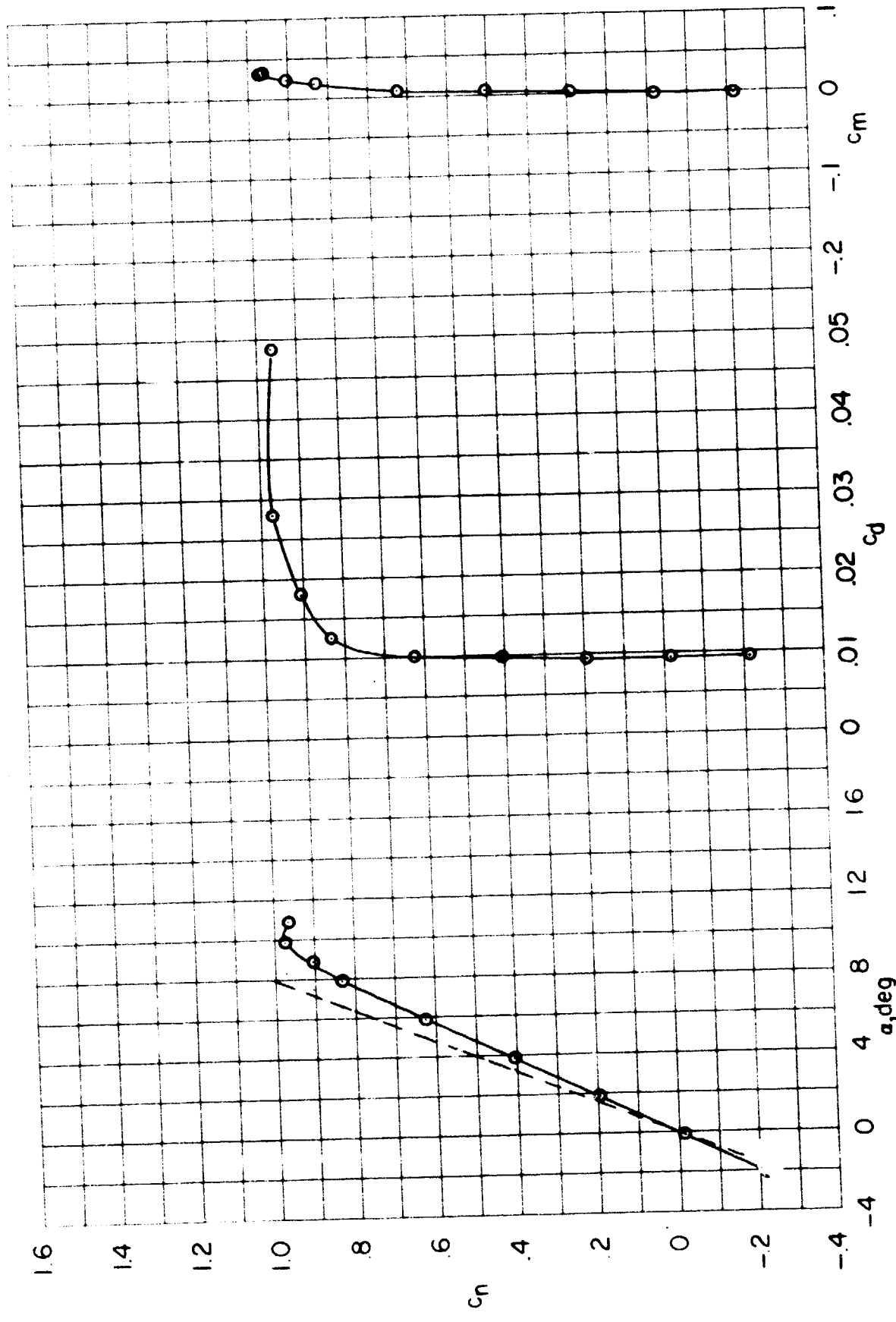
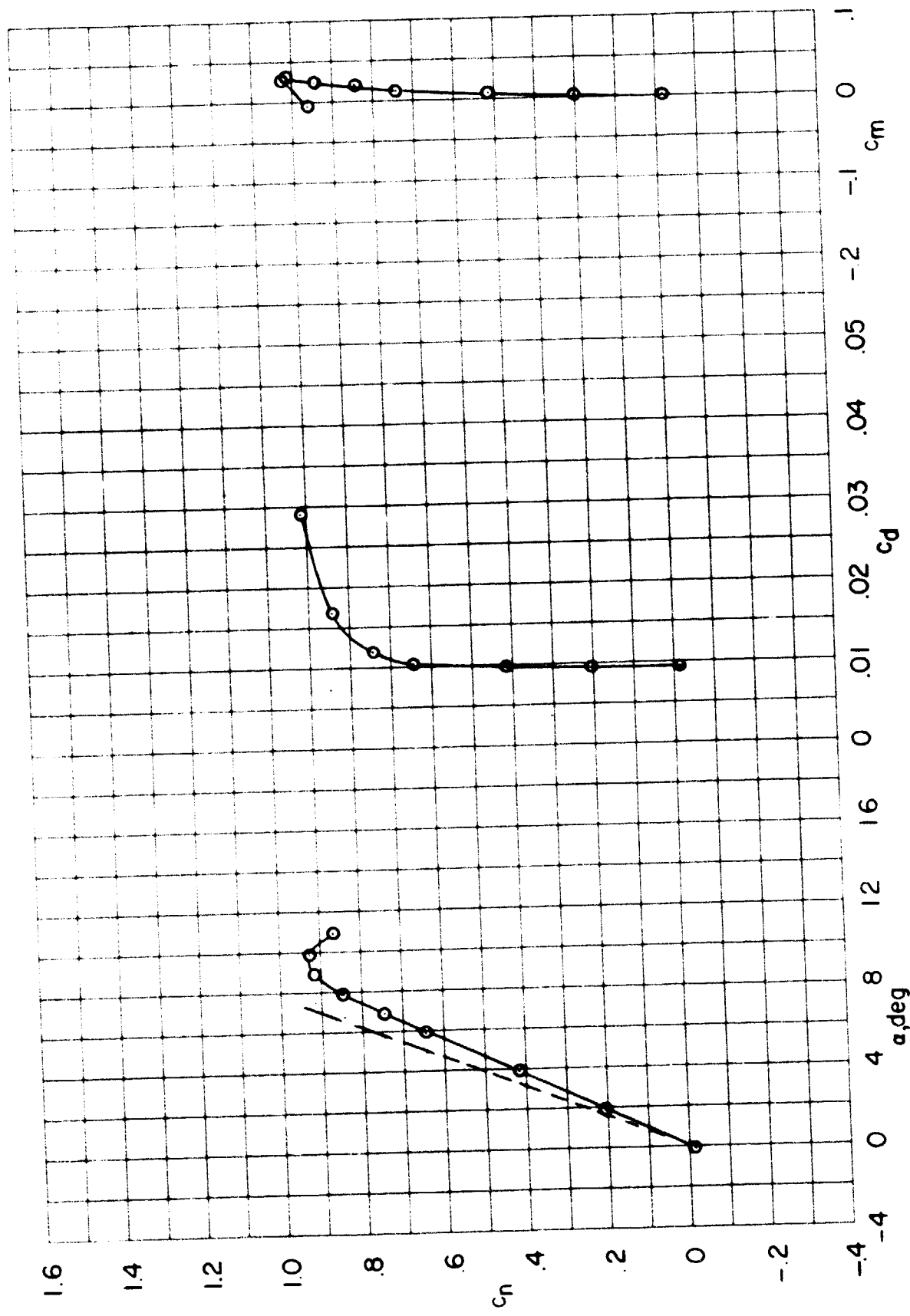
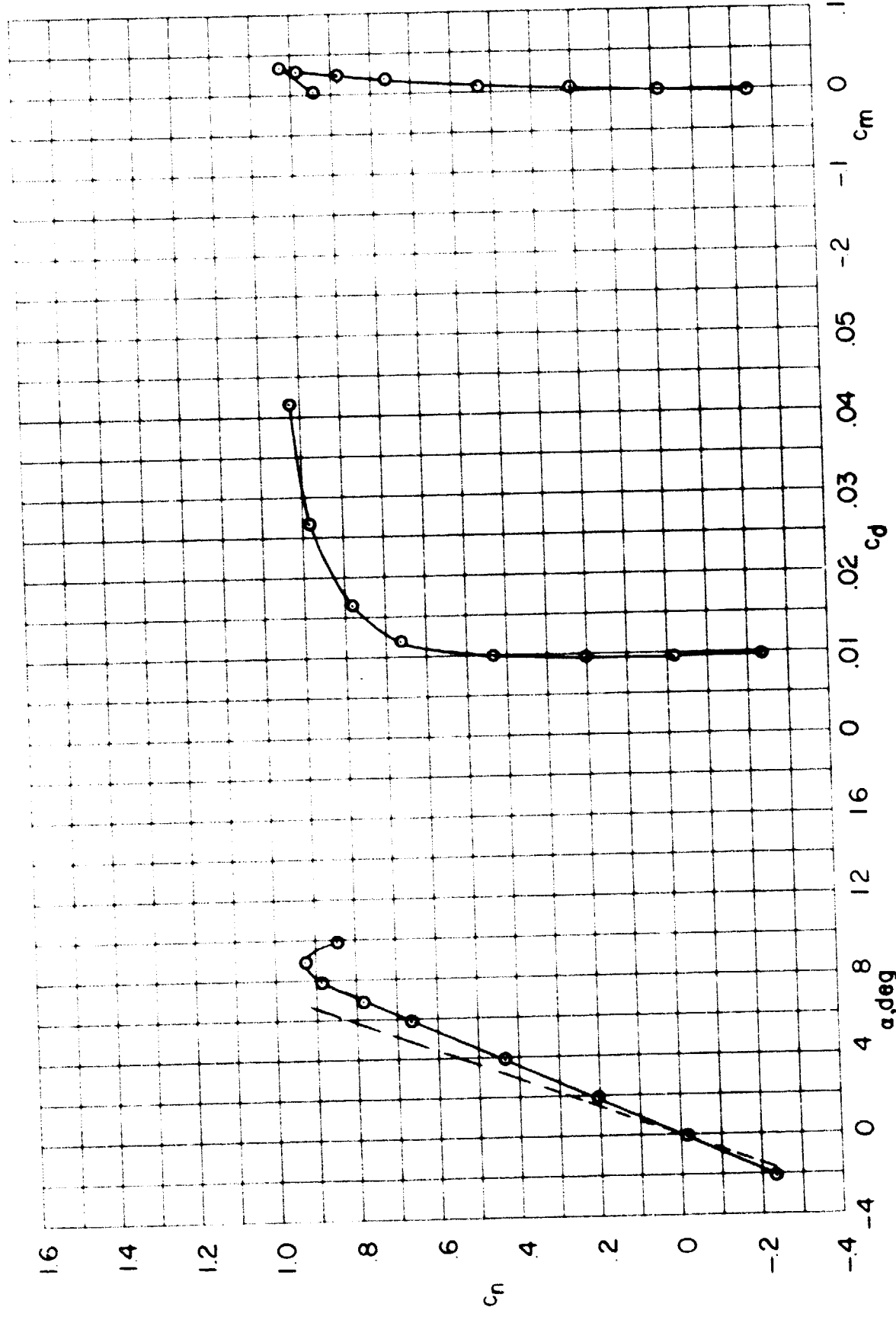


Figure 5.- Continued.



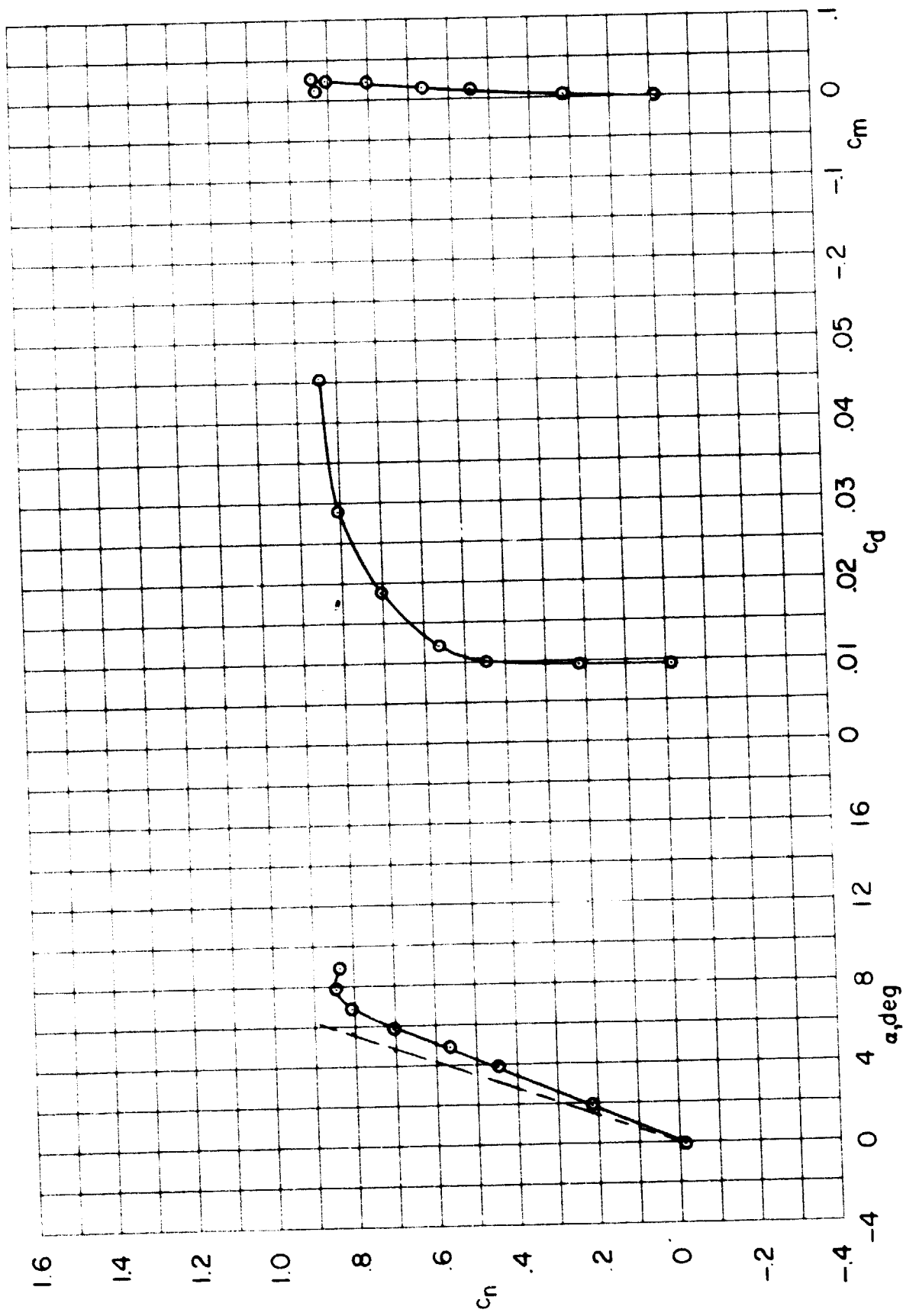
(d) $M = 0.55$

Figure 5.- Continued.



(e) $M = 0.60$

Figure 5.- Continued.



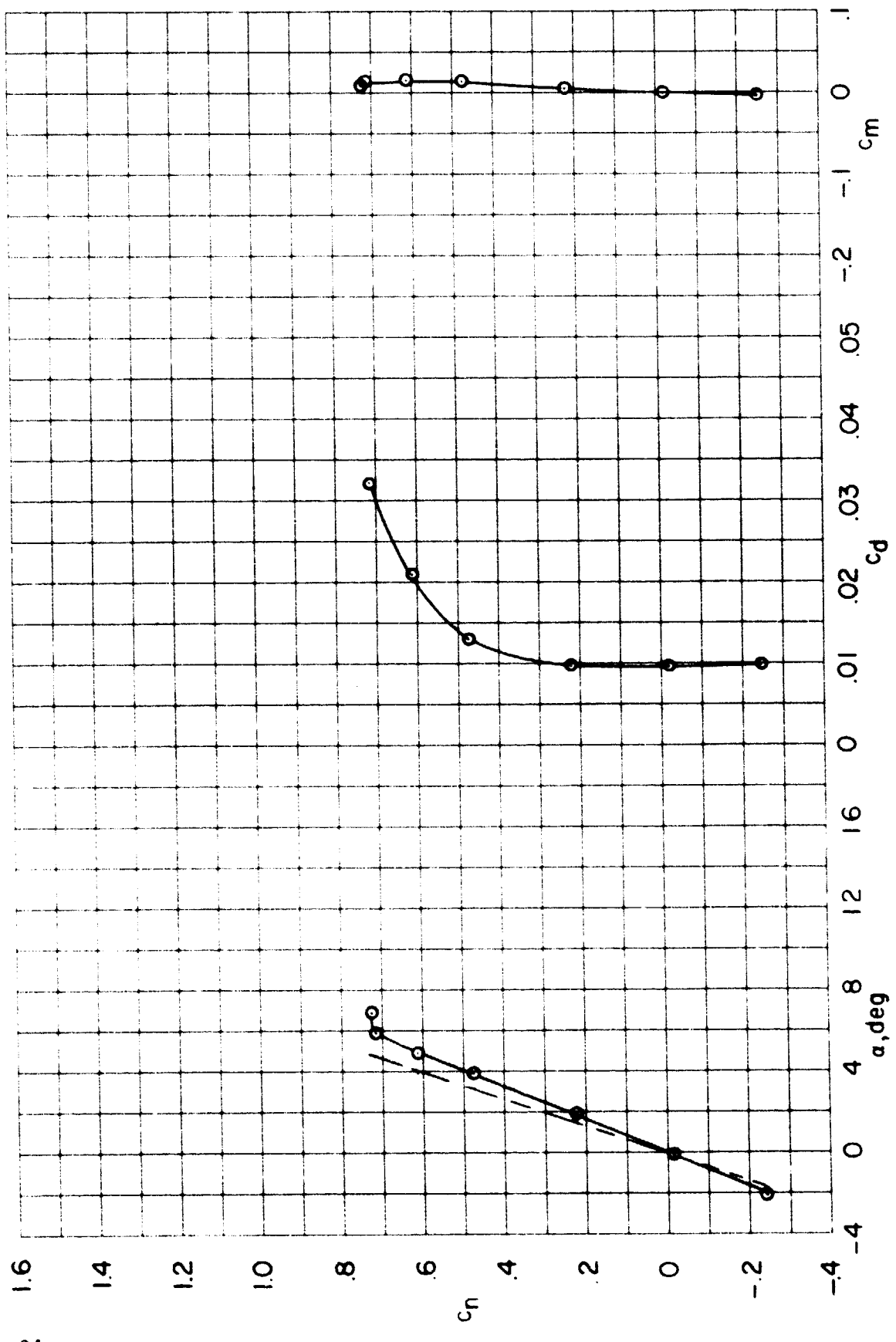
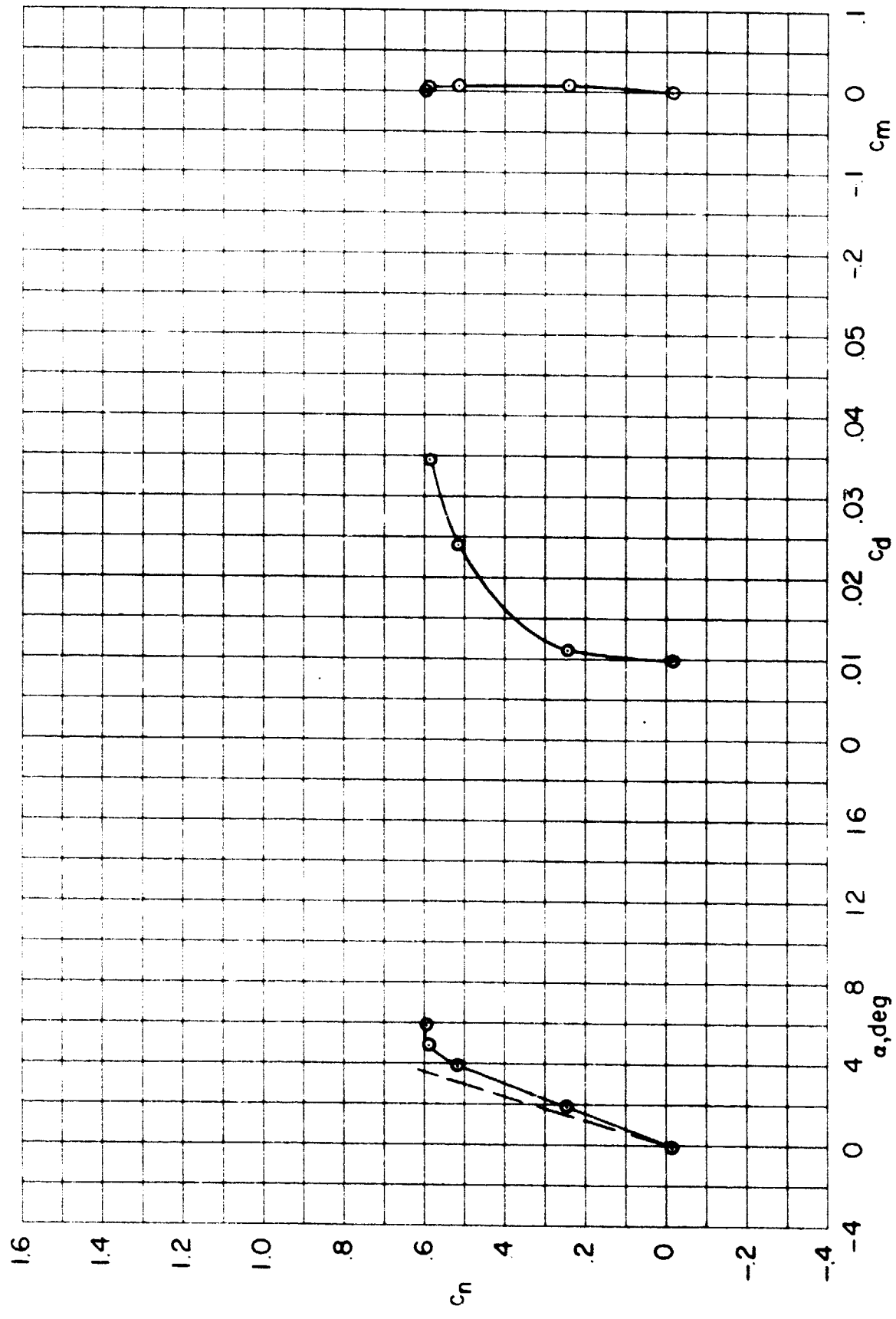
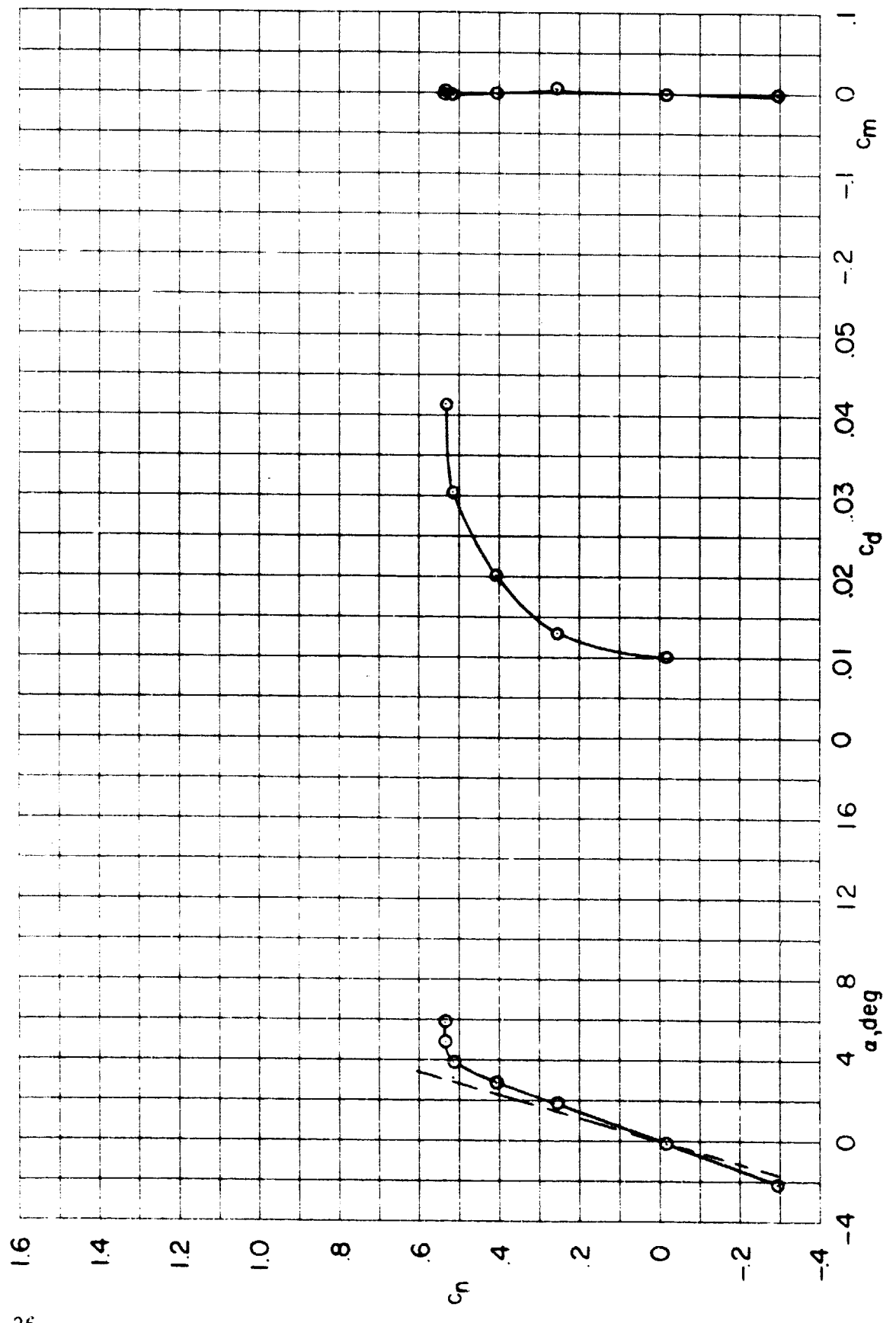


Figure 5. - Continued.

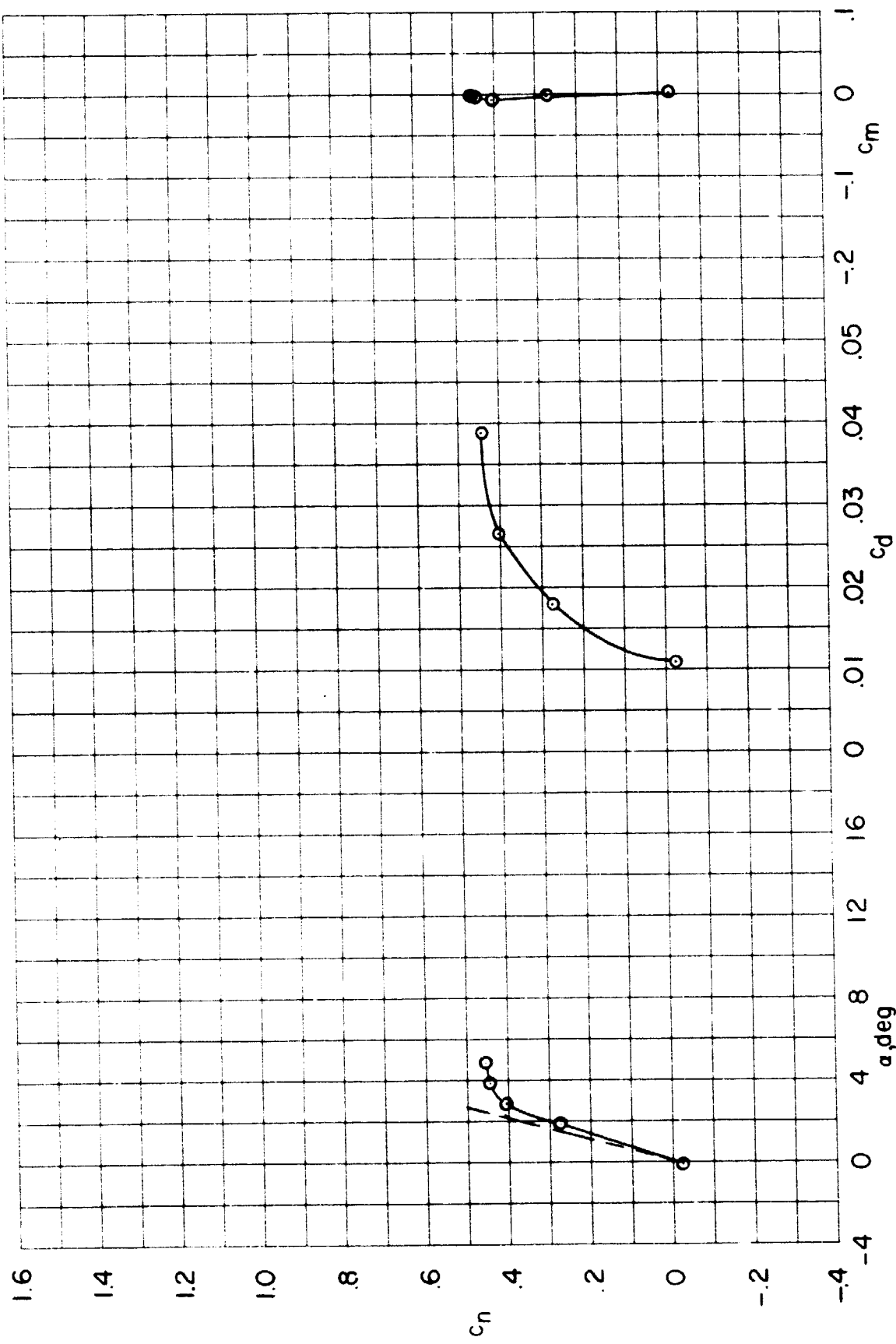


(h) $M = 0.74$



(i) $M = 0.76$

Figure 5.- Continued.



(j) $M = 0.78$

Figure 5.- Continued.

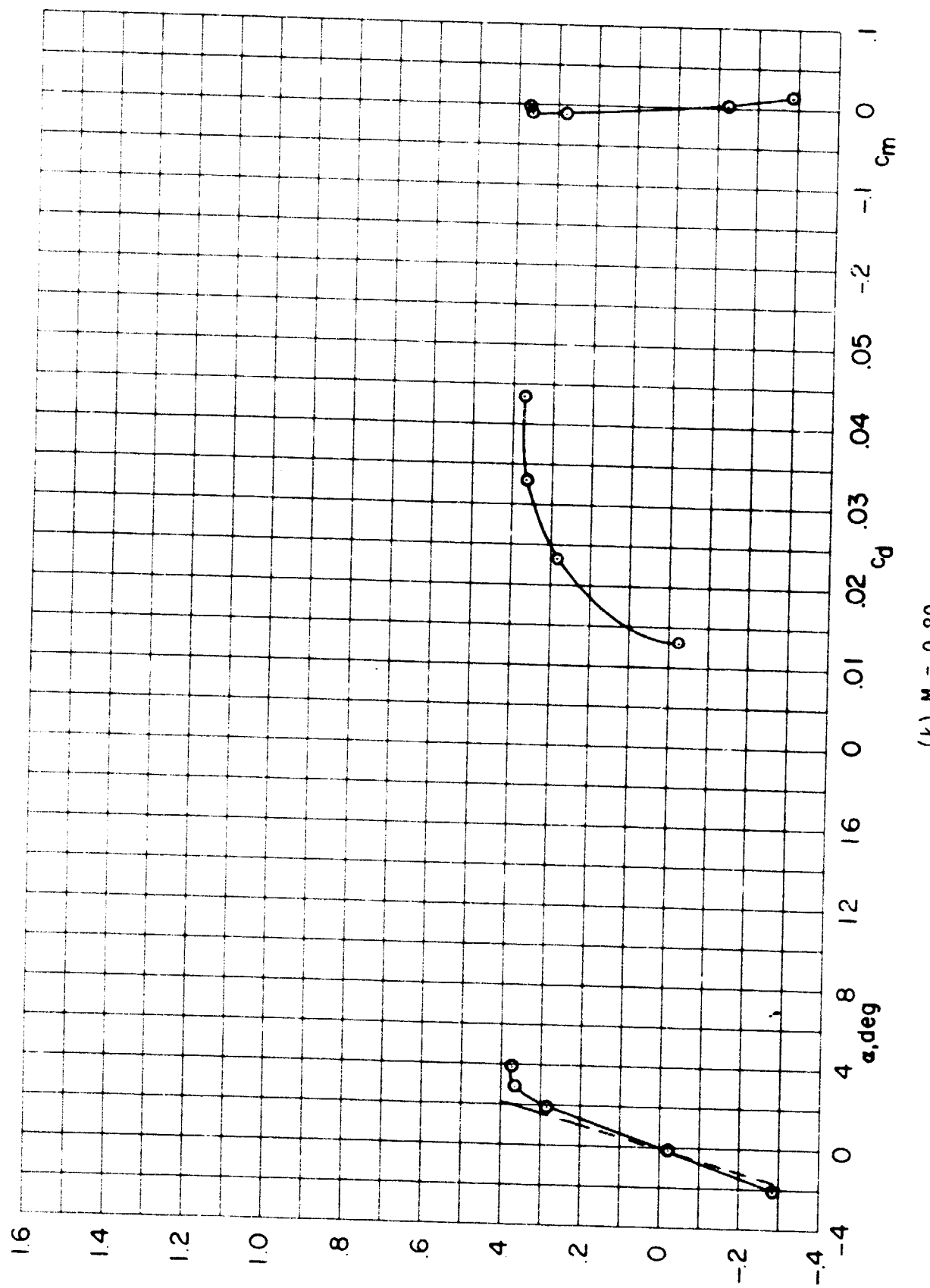
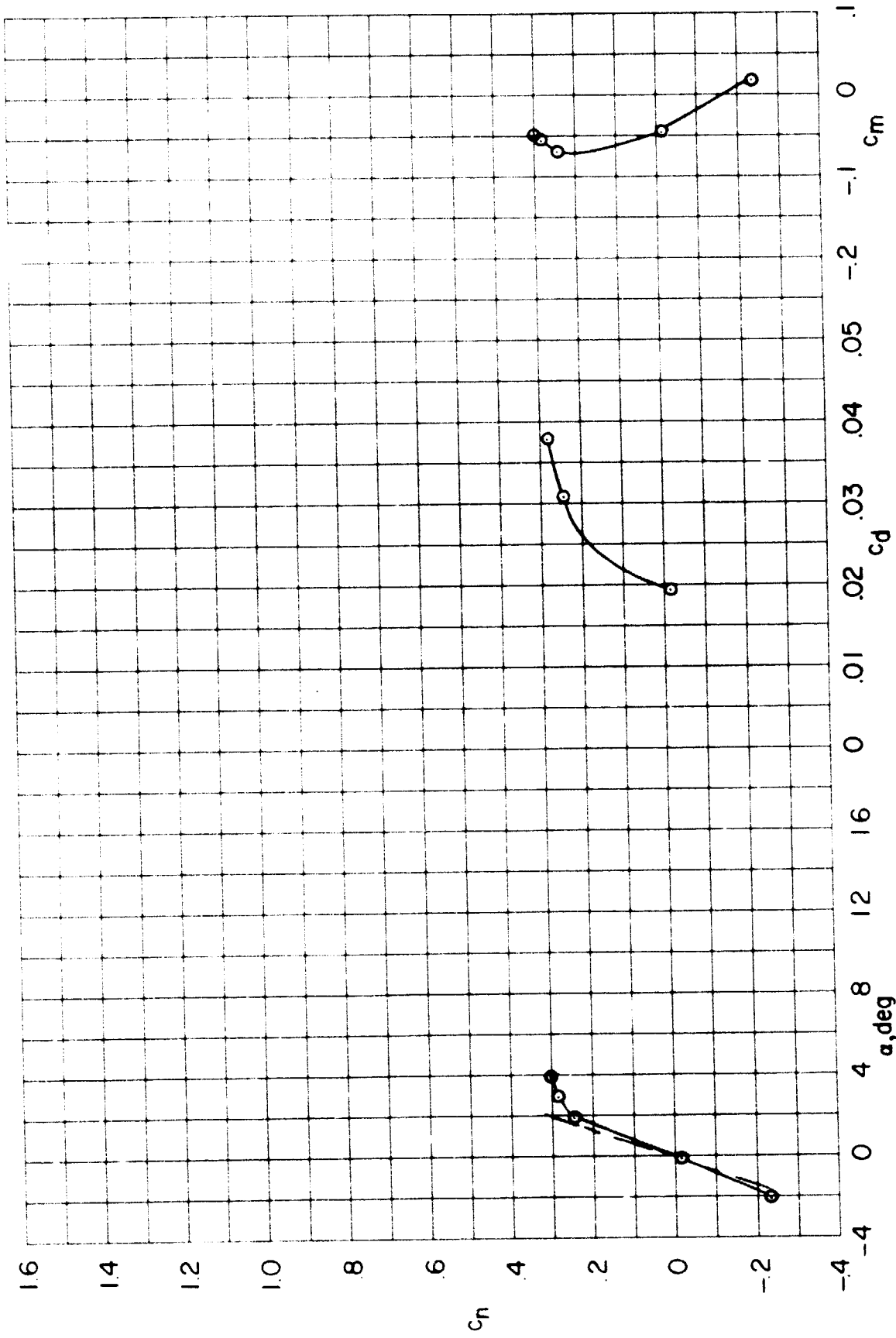


Figure 5.-Continued.



(1) $M = 0.82$

Figure 5.- Continued.

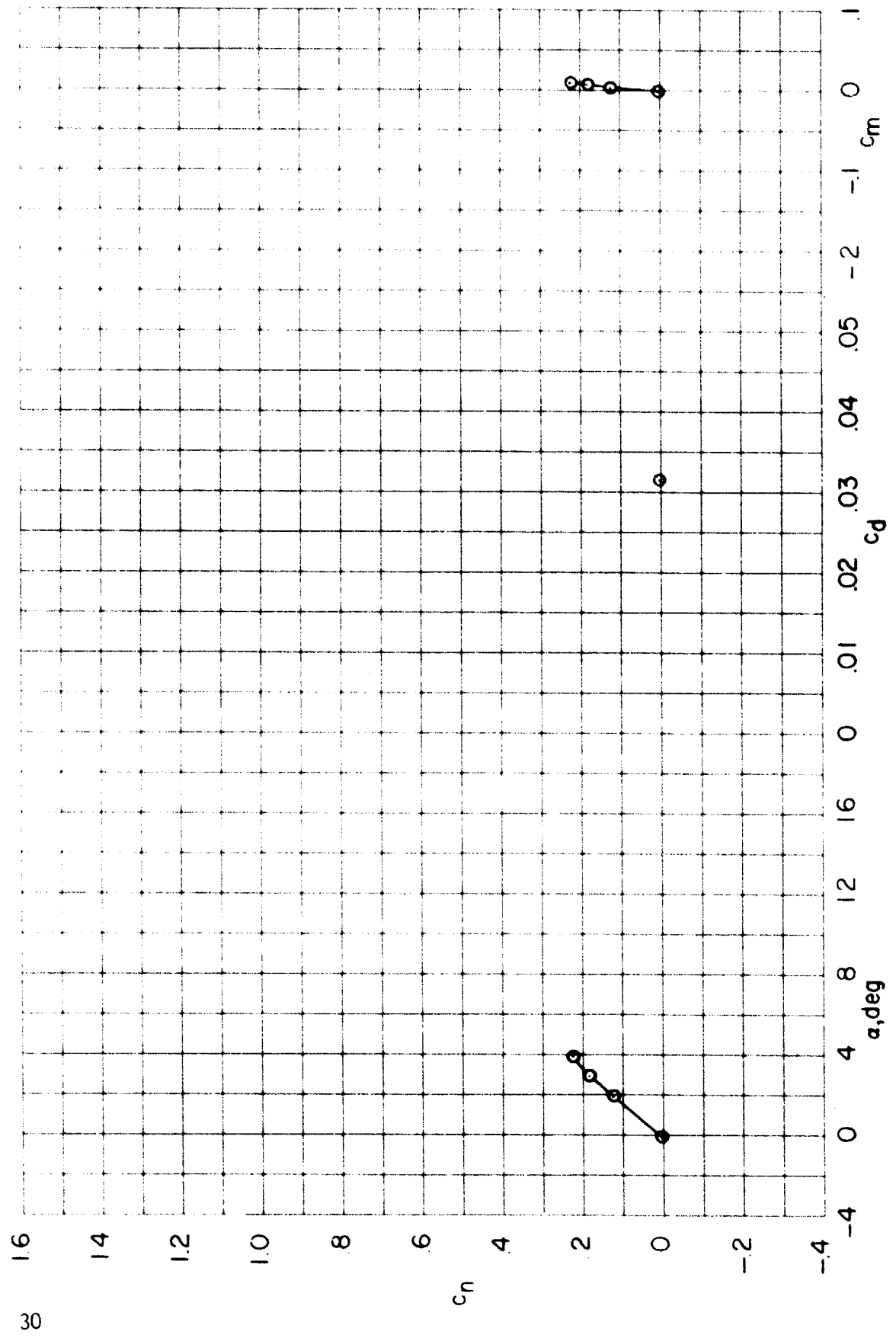
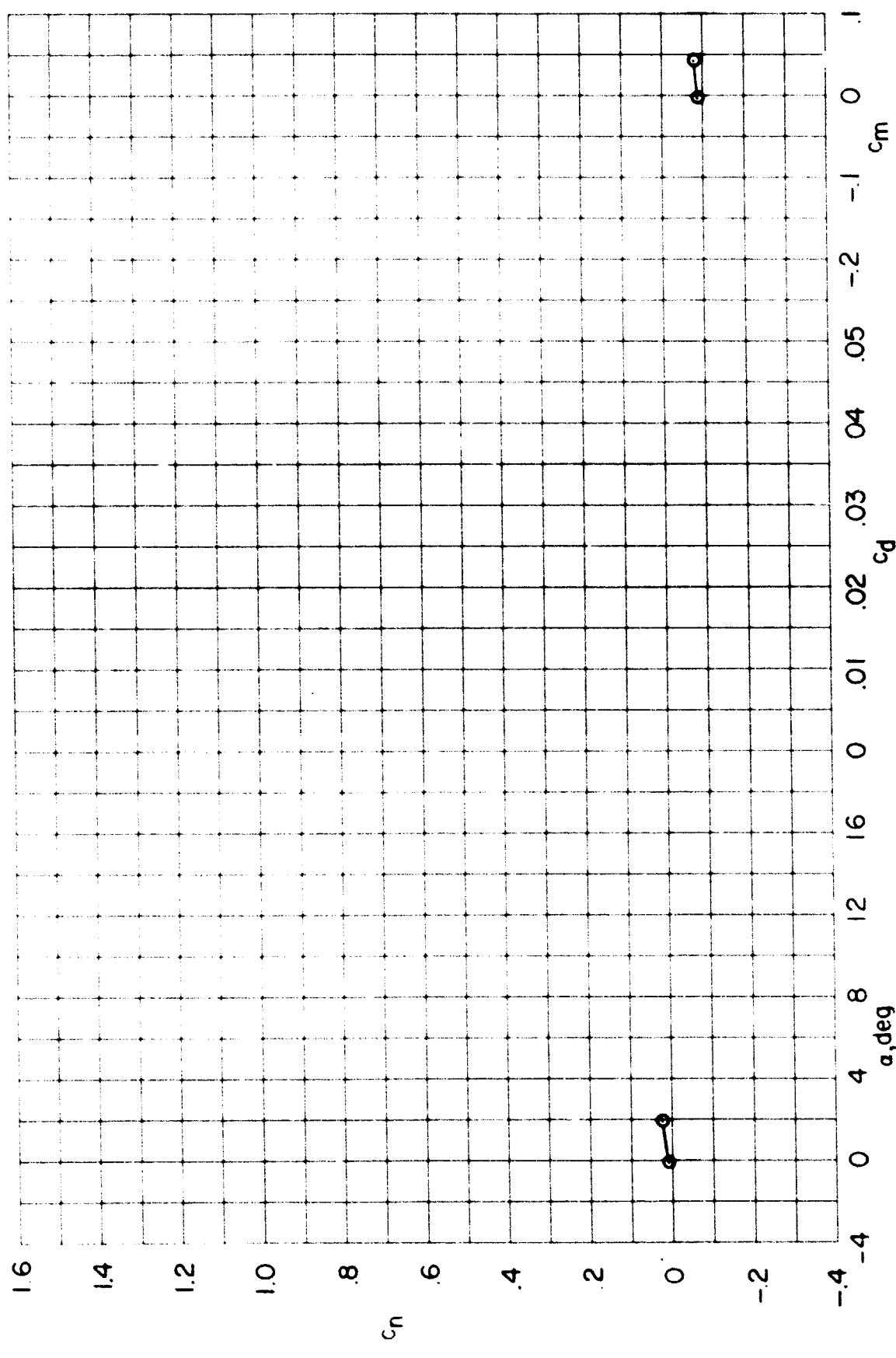
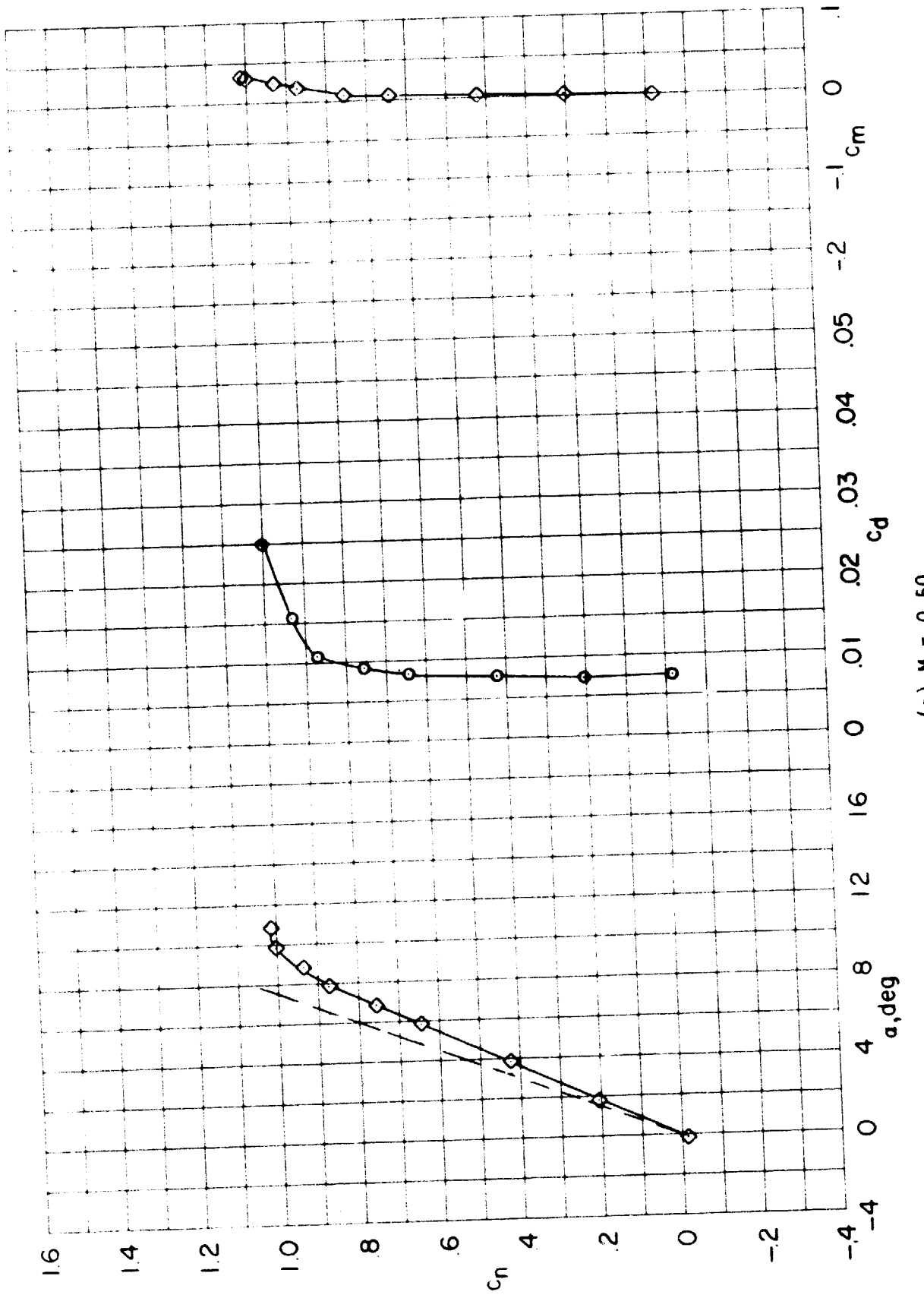


Figure 5.- Continued.
(m) $M = 0.84$



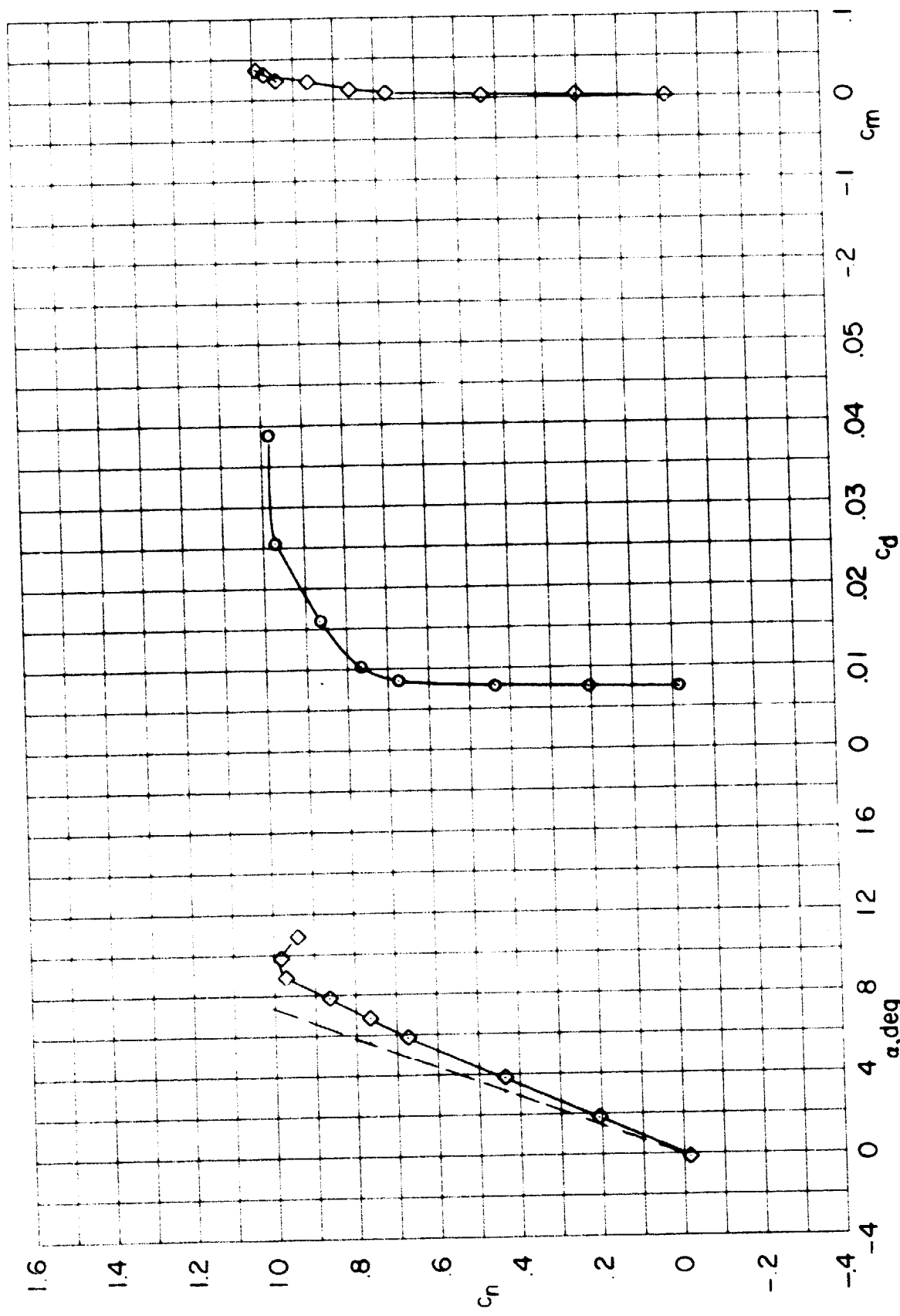
(n) $M = 0.86$

Figure 5.- Concluded.



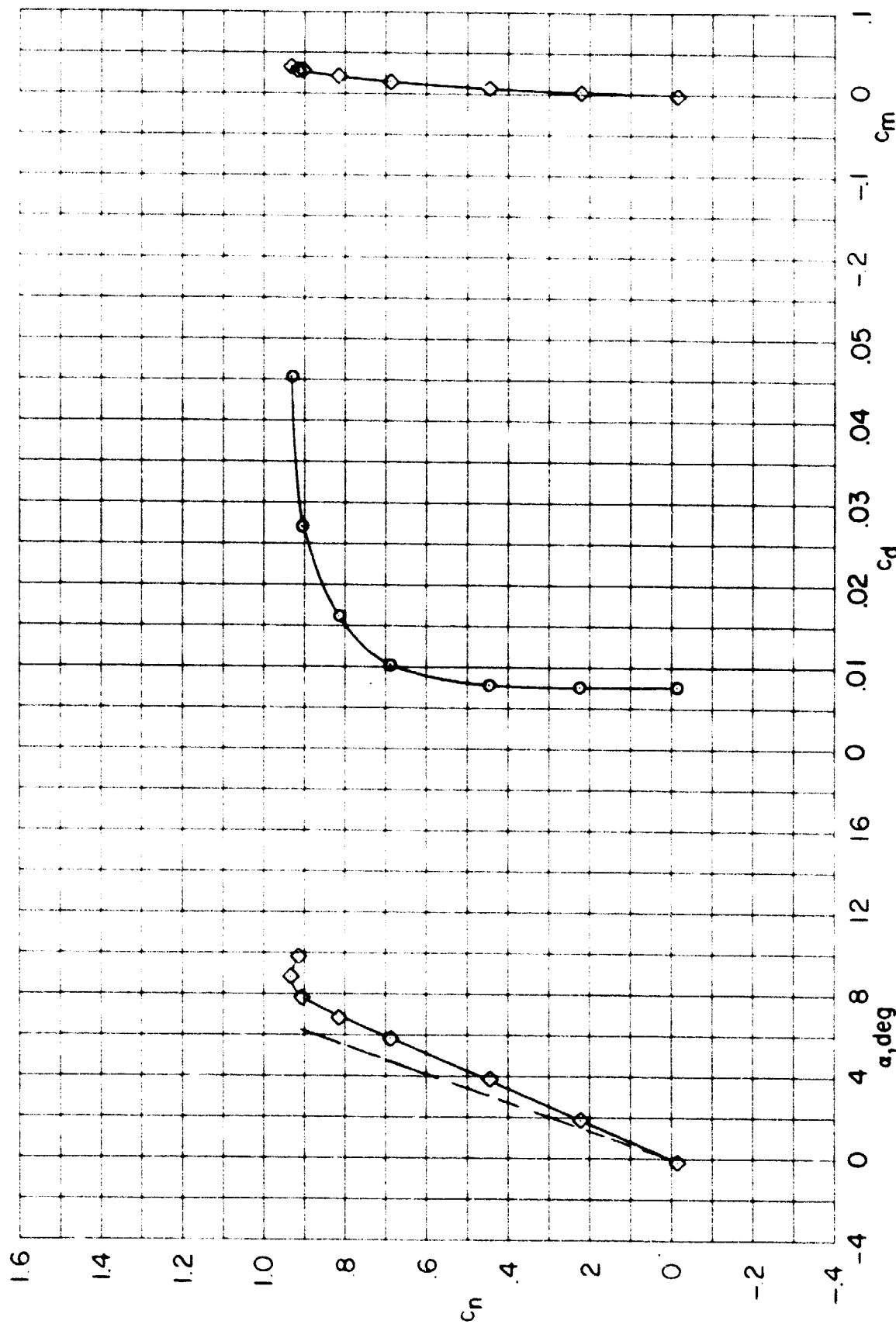
(a) $M = 0.50$

Figure 6.- Force and moment characteristics of NACA 0012 airfoil. $R_n = 9.0 \times 10^6$, transition fixed. (dashed line indicates angle of attack correction for wall interference).

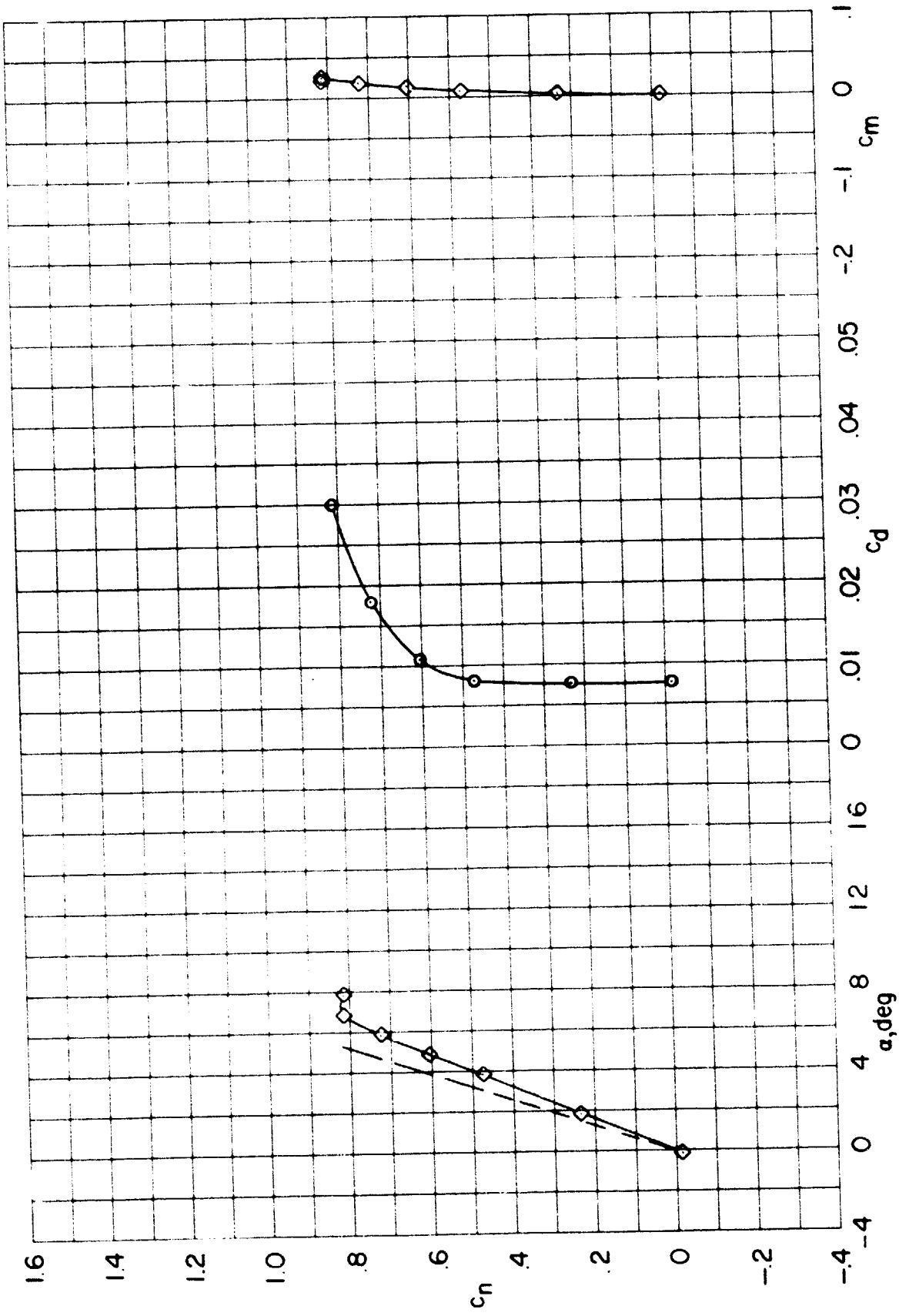


(b) $M = 0.55$

Figure 6.- Continued.

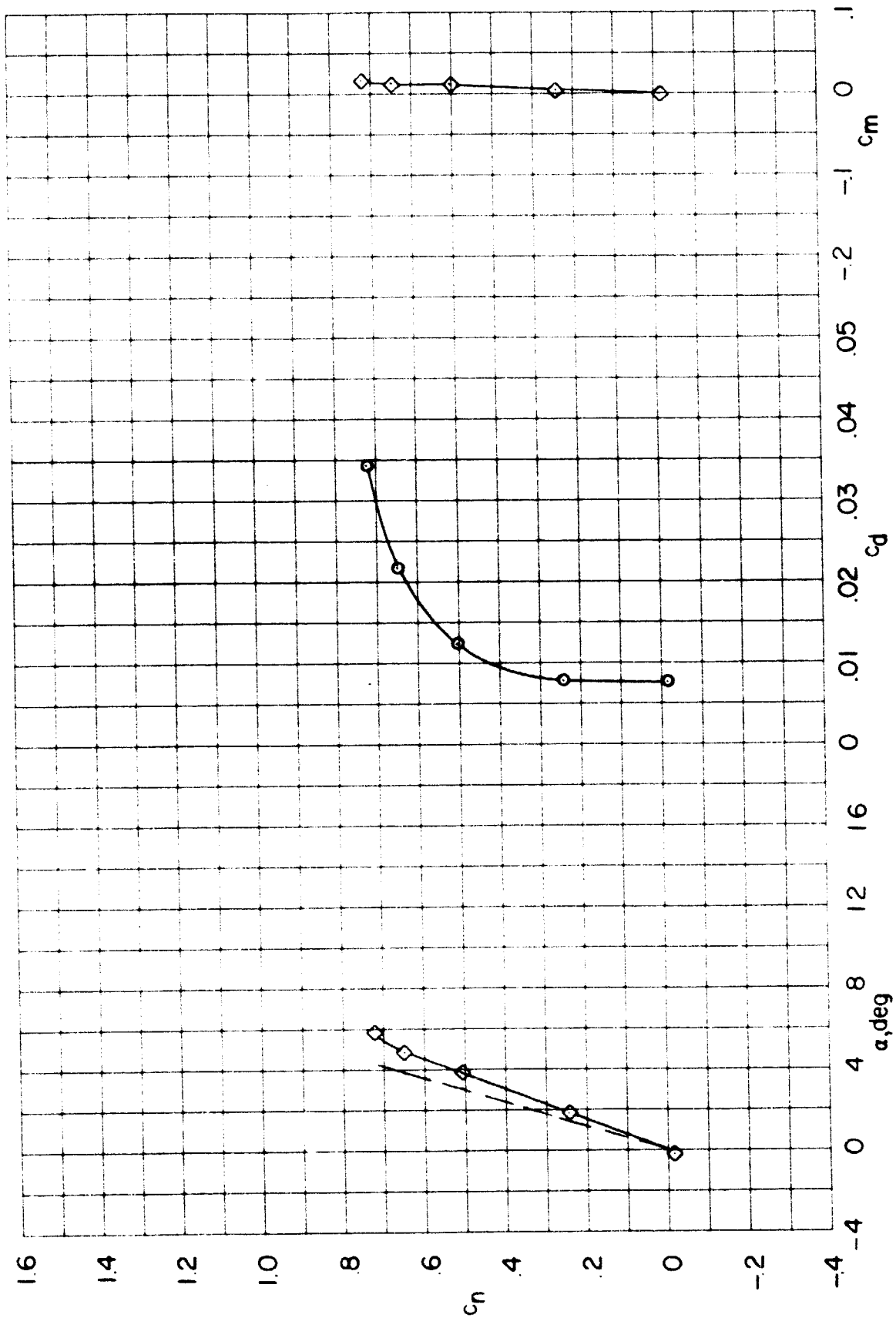


(c) $M = 0.60$
Figure 6.- Continued.



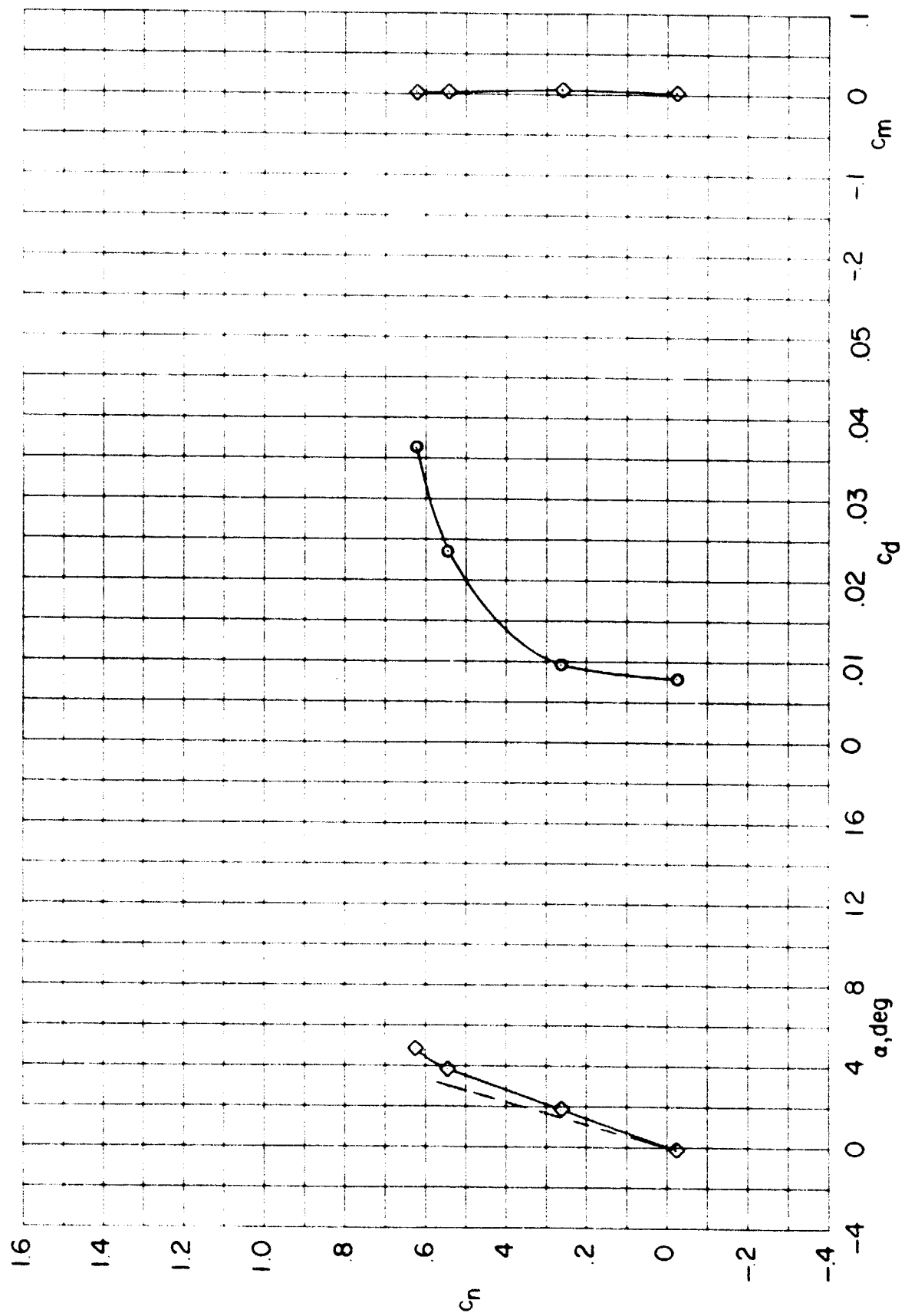
(d) $M = 0.65$

Figure 6.- Continued.



(e) $M = 0.70$

Figure 6.- Continued.



(f) $M = 0.74$

Figure 6.- Continued.

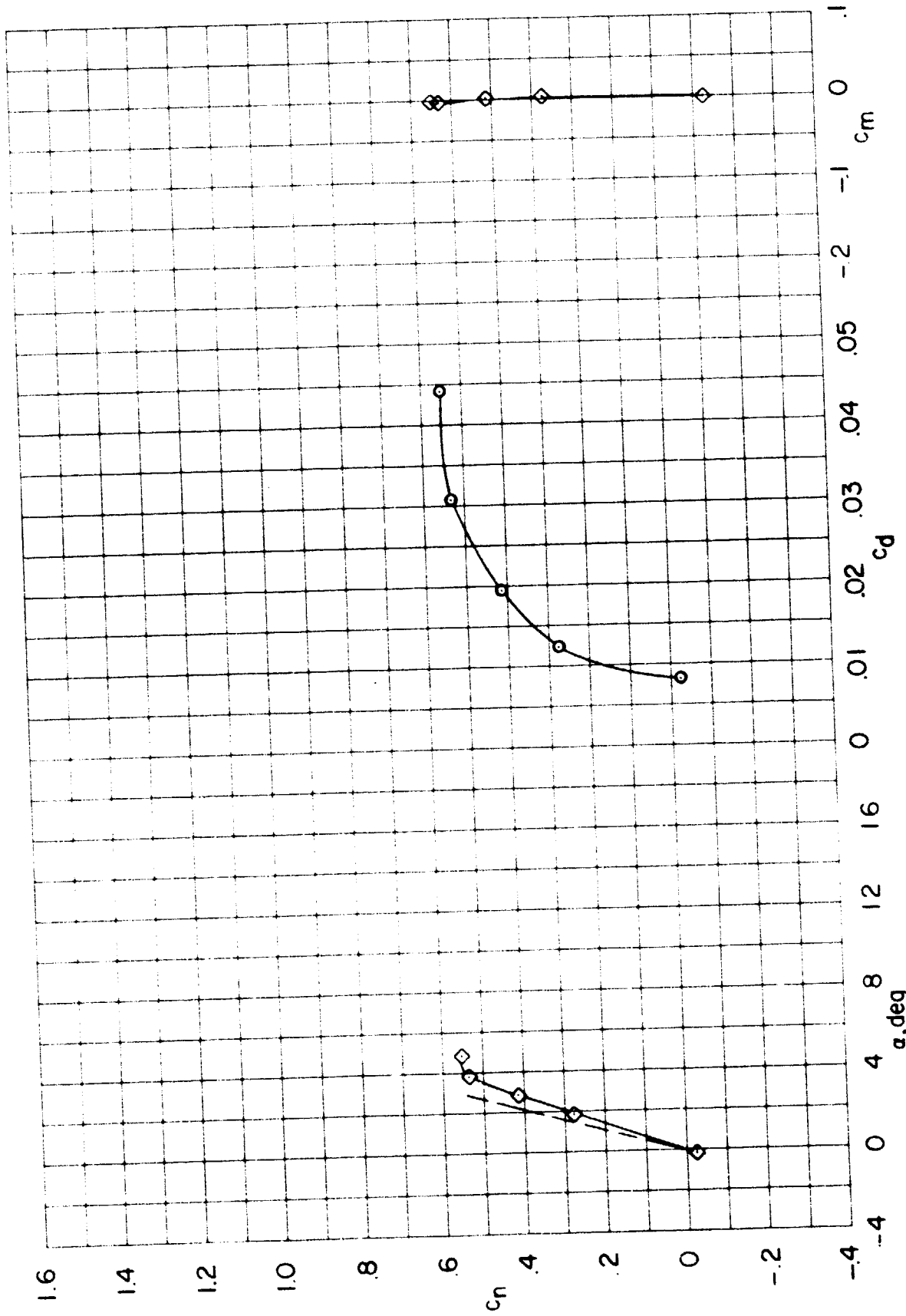


Figure 6.- Continued.
(g) $M = 0.76$

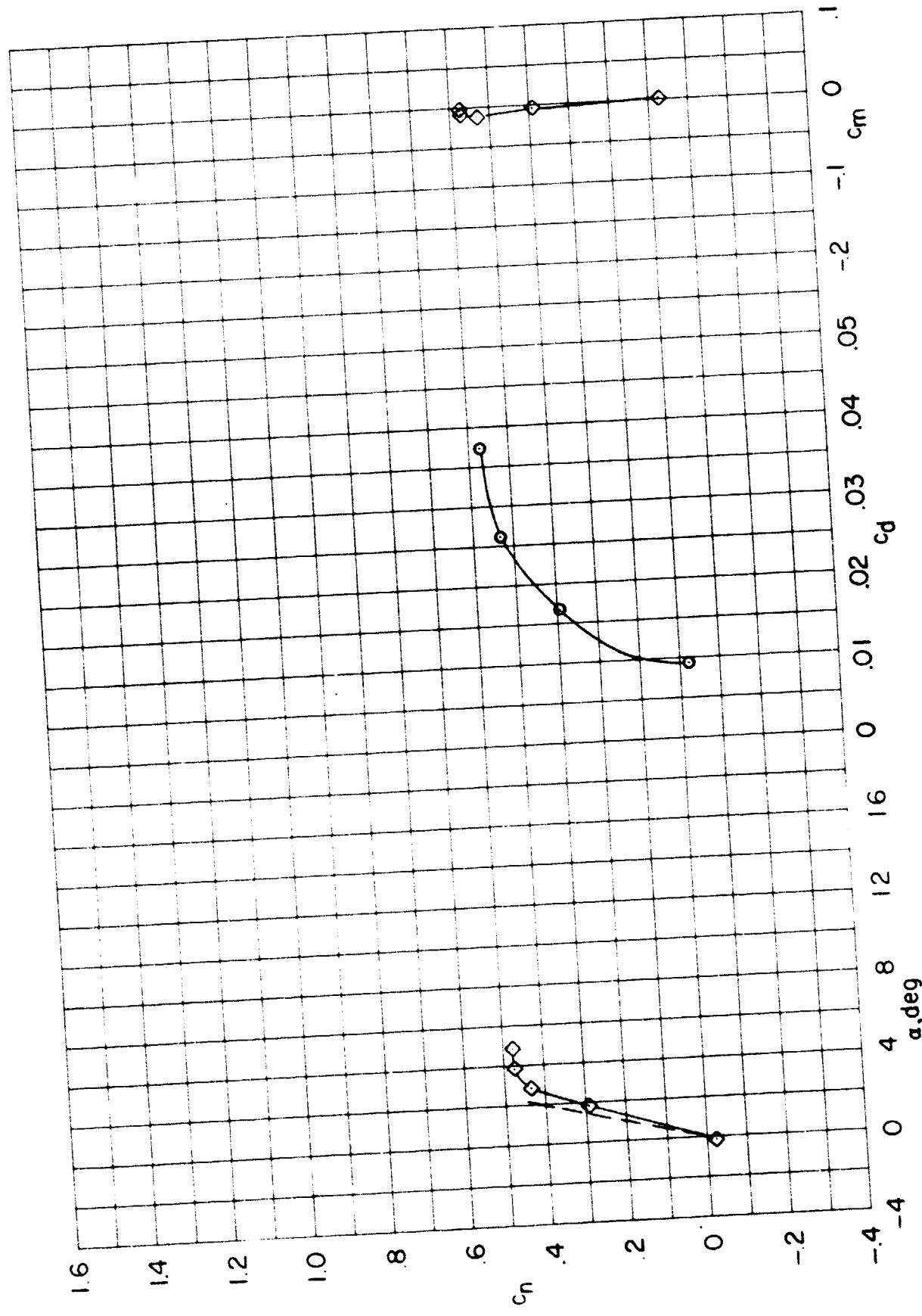
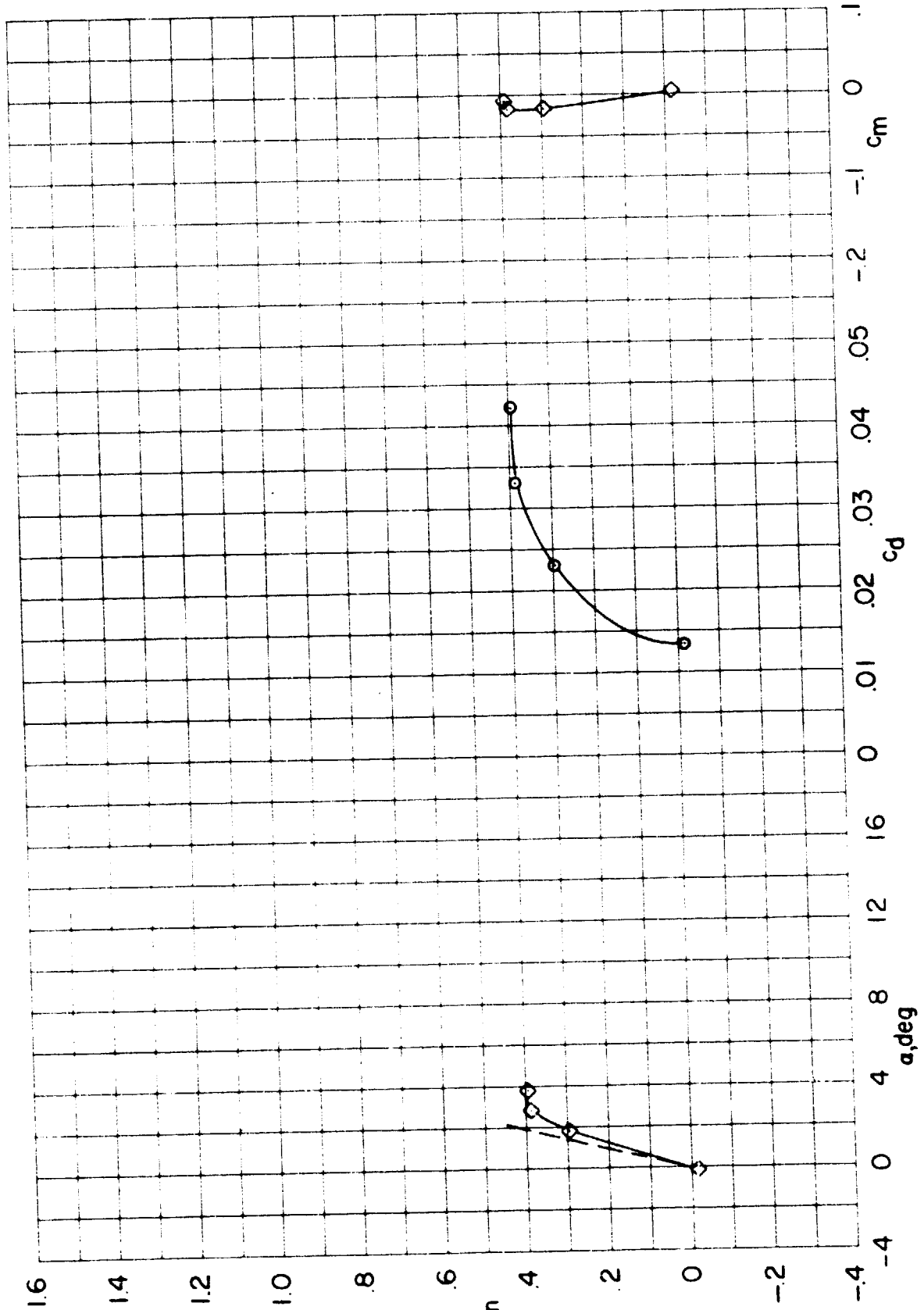
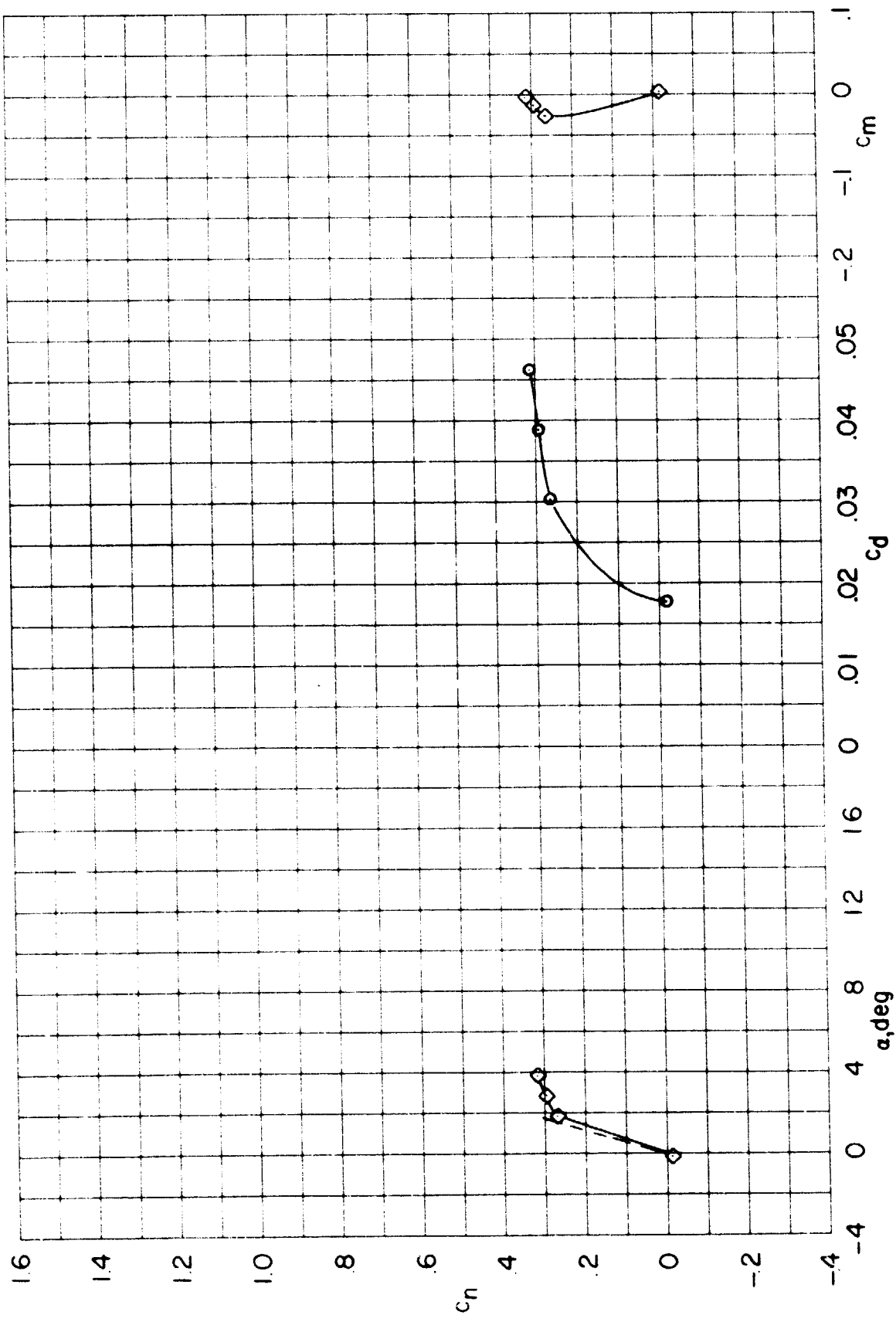


Figure 6.- Continued.



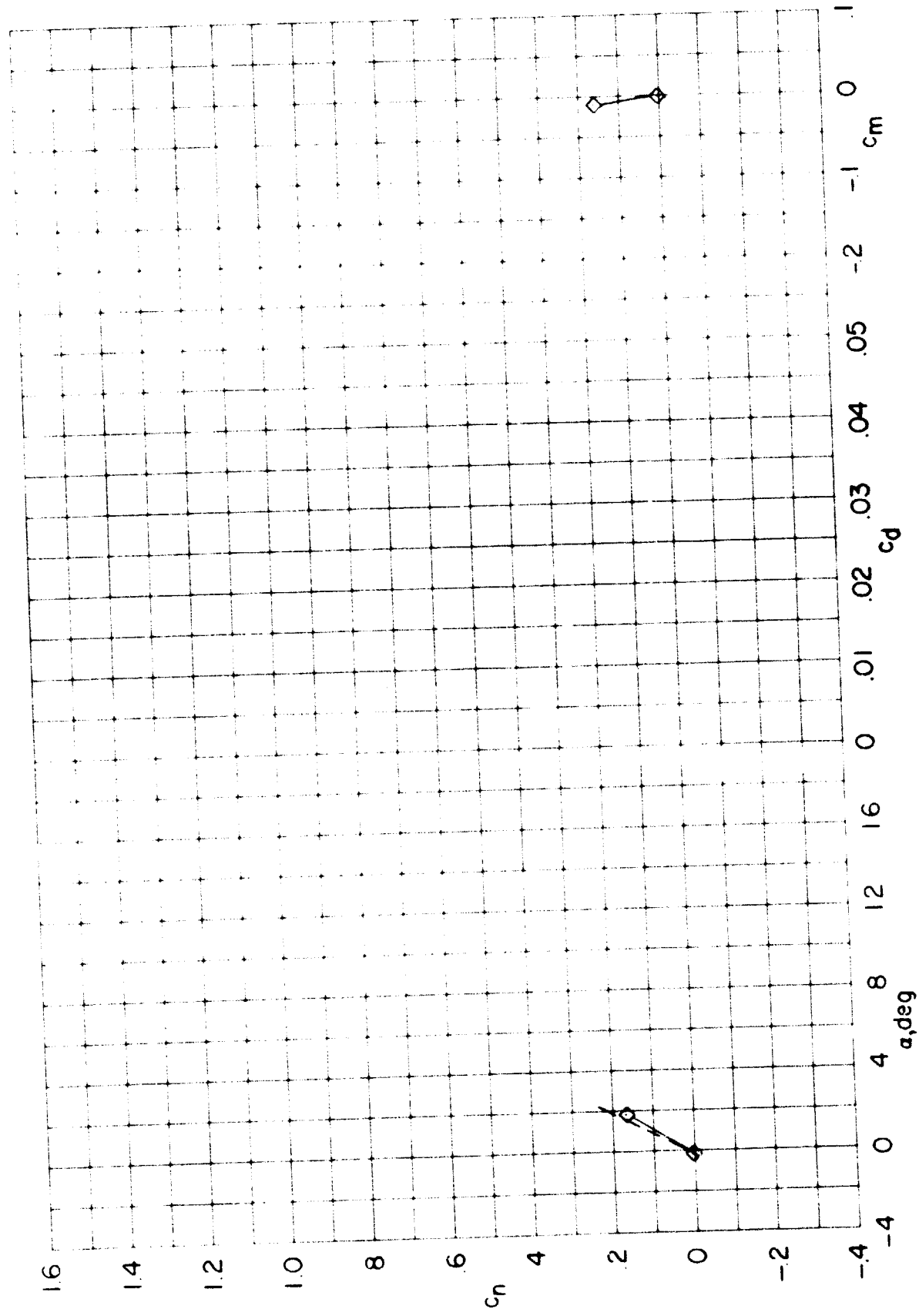
(i) $M = 0.80$

Figure 6.- Continued.



(j) $M = 0.82$

Figure 6.- Continued.



(k) $M = 0.84$

Figure 6.- Concluded.

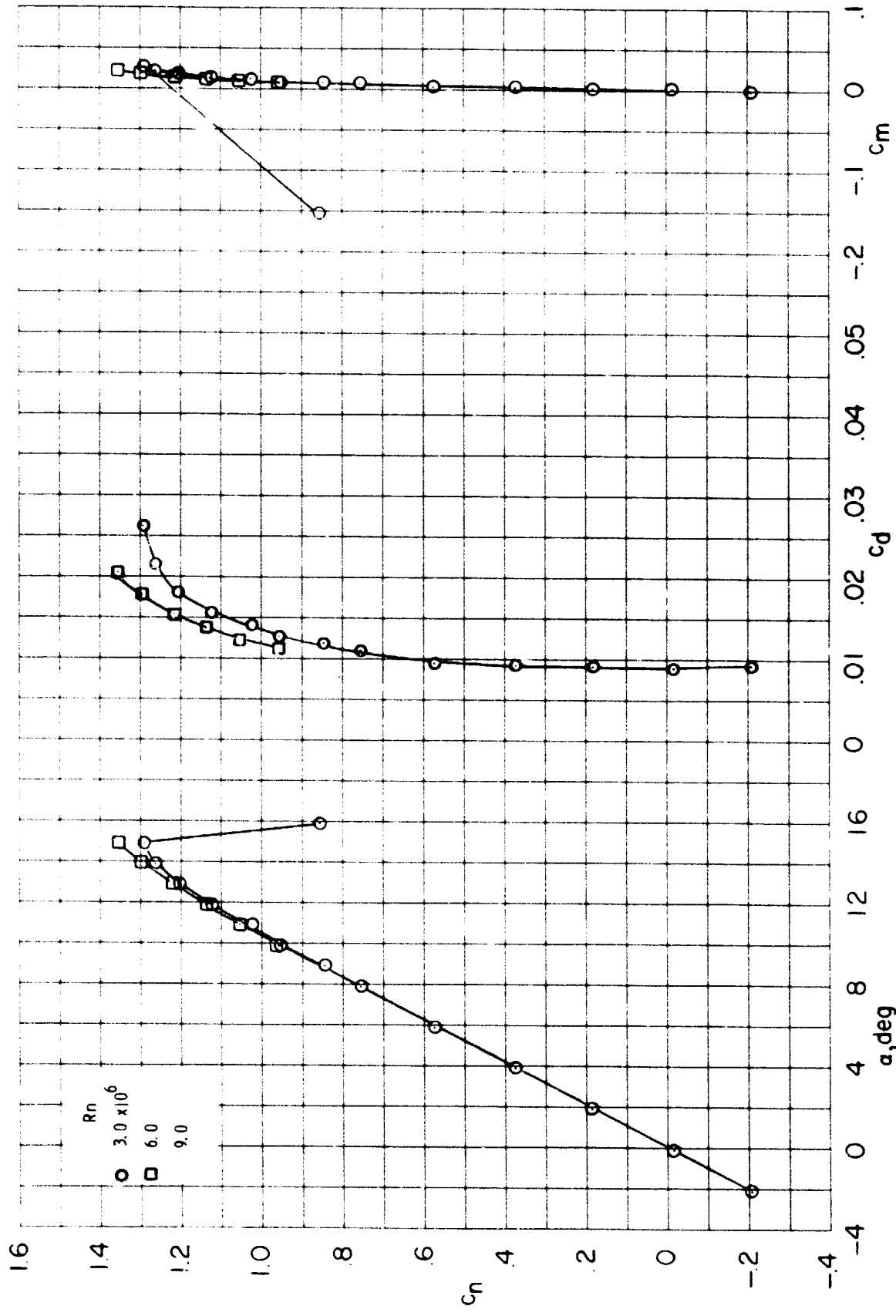


Figure 7. - Effects of Reynolds number on force and moment characteristics of NACA 0012 airfoil. Transition fixed.

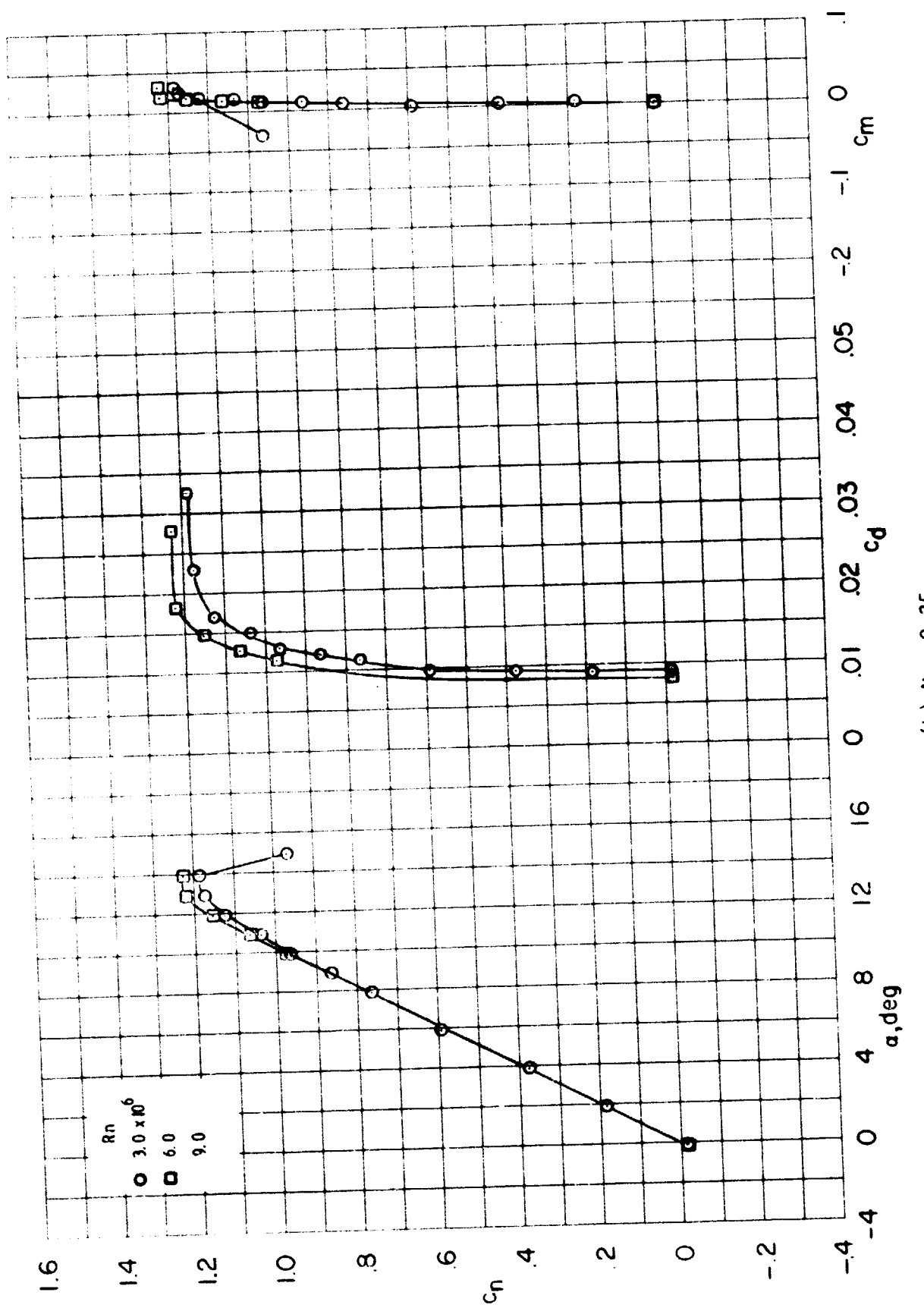
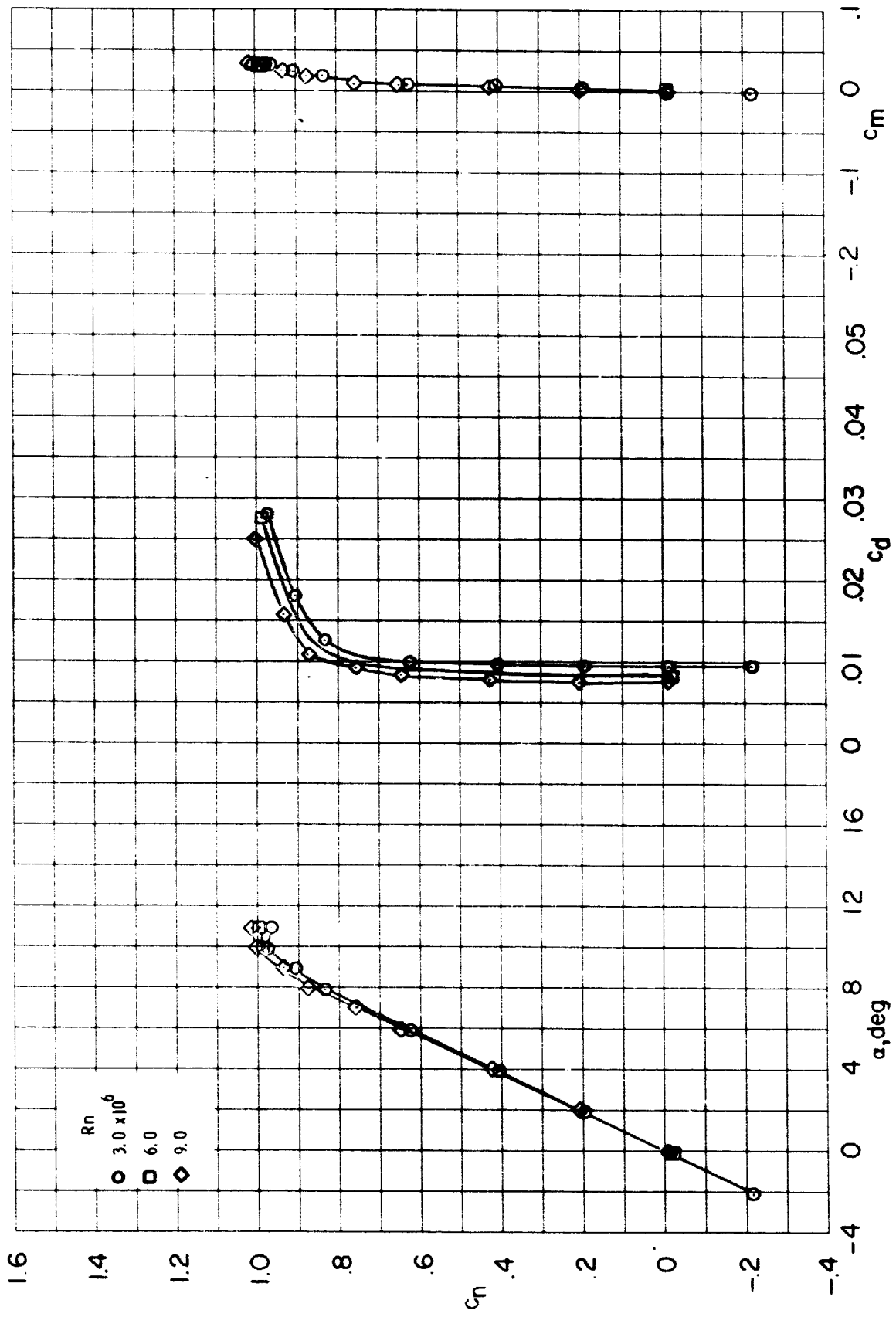


Figure 7.- Continued.
(b) $M = 0.35$



(c) $M = 0.50$

Figure 7.- Continued.

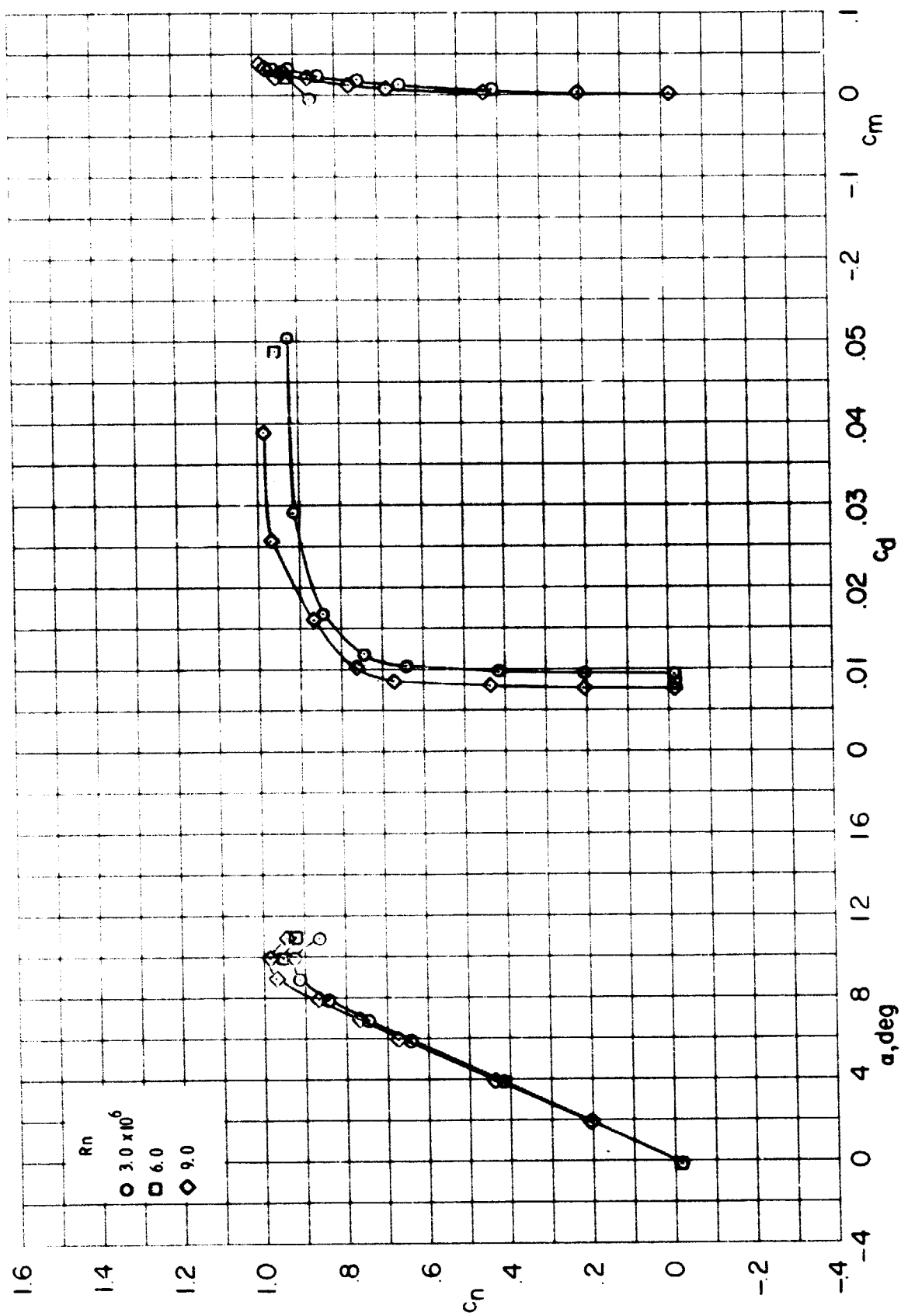


Figure 7.- Continued.
(d) $M = 0.55$

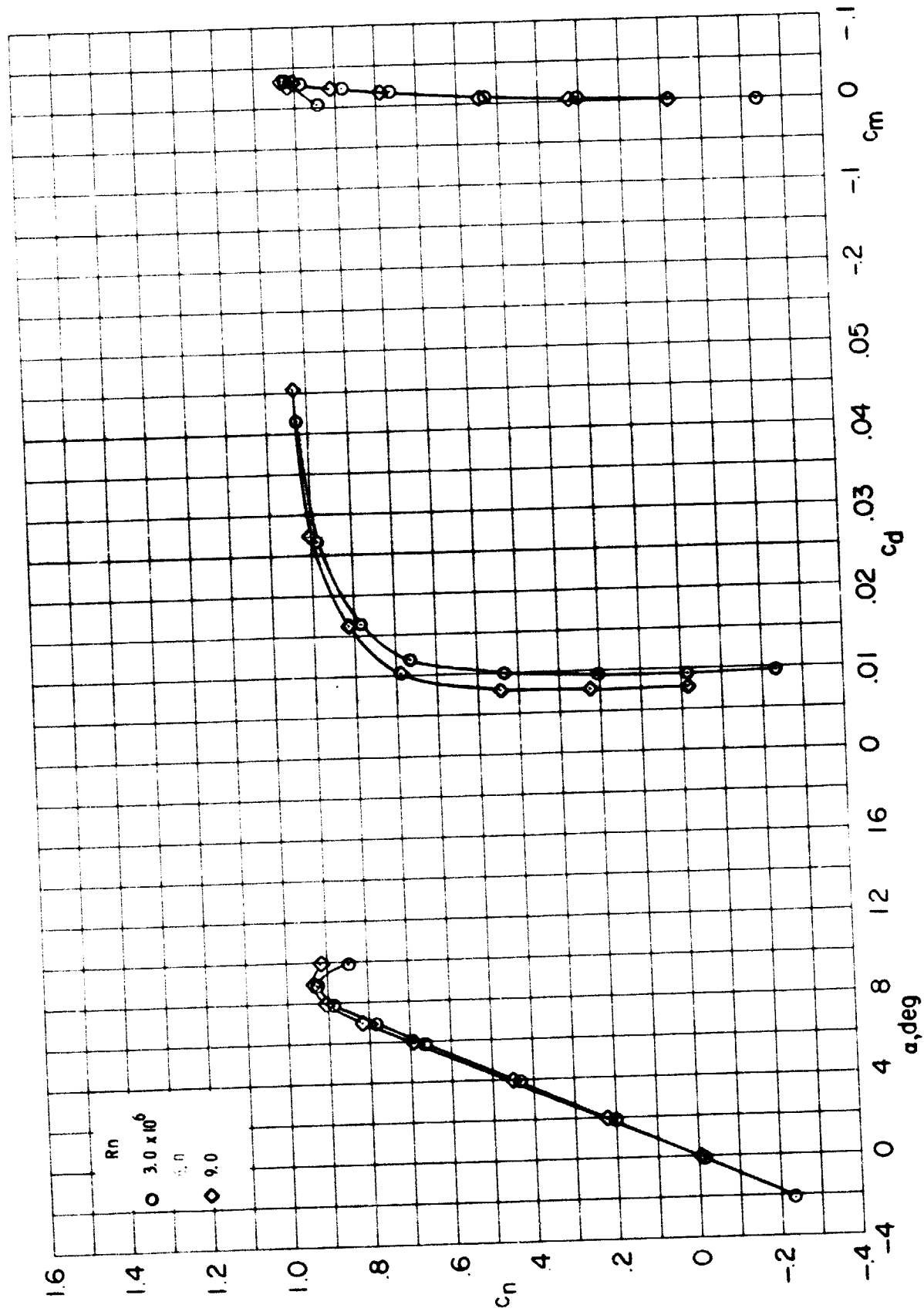
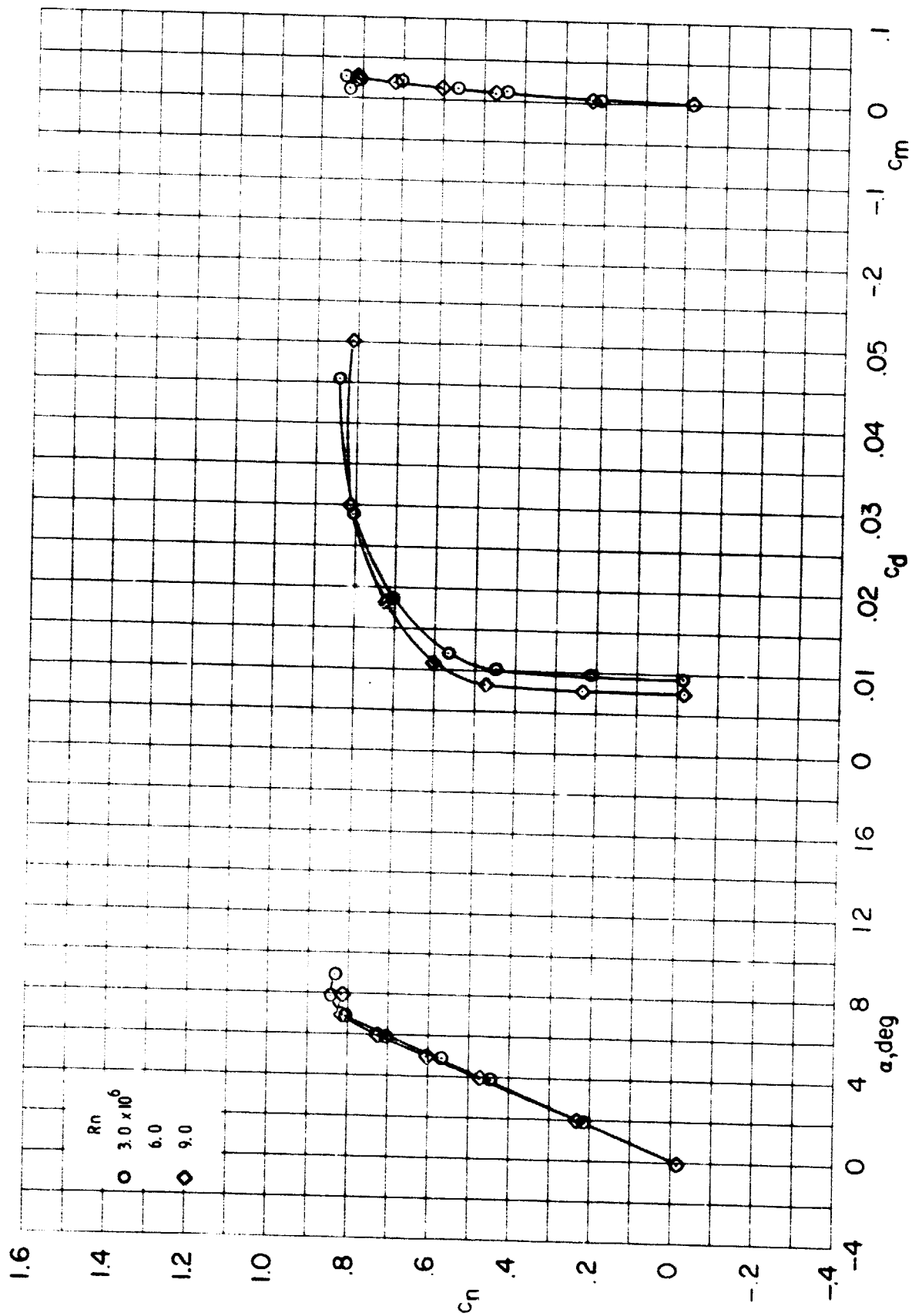


Figure 7.- Continued.



(f) $M = 0.65$
Figure 7.- Continued.

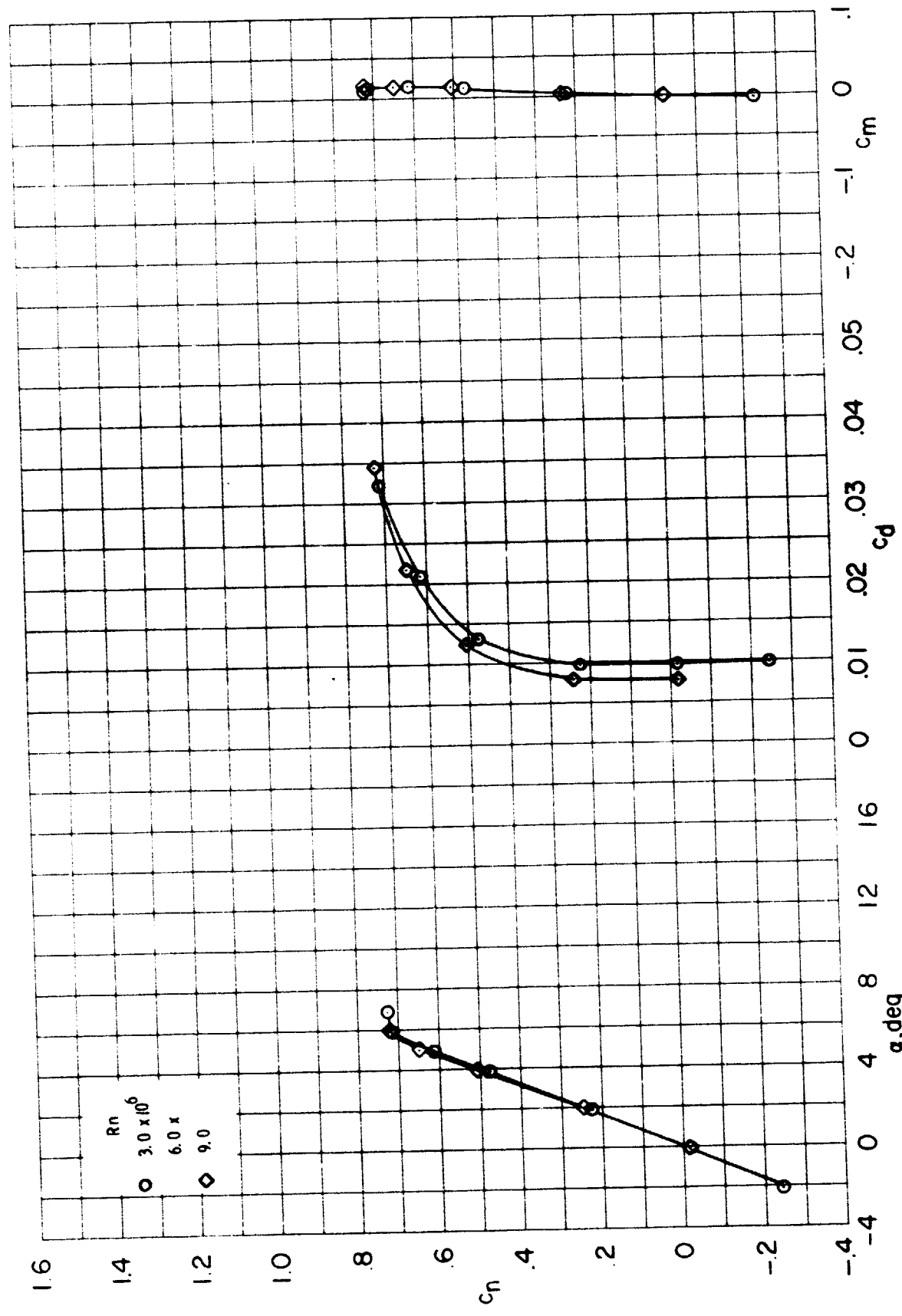


Figure 7.- Continued.

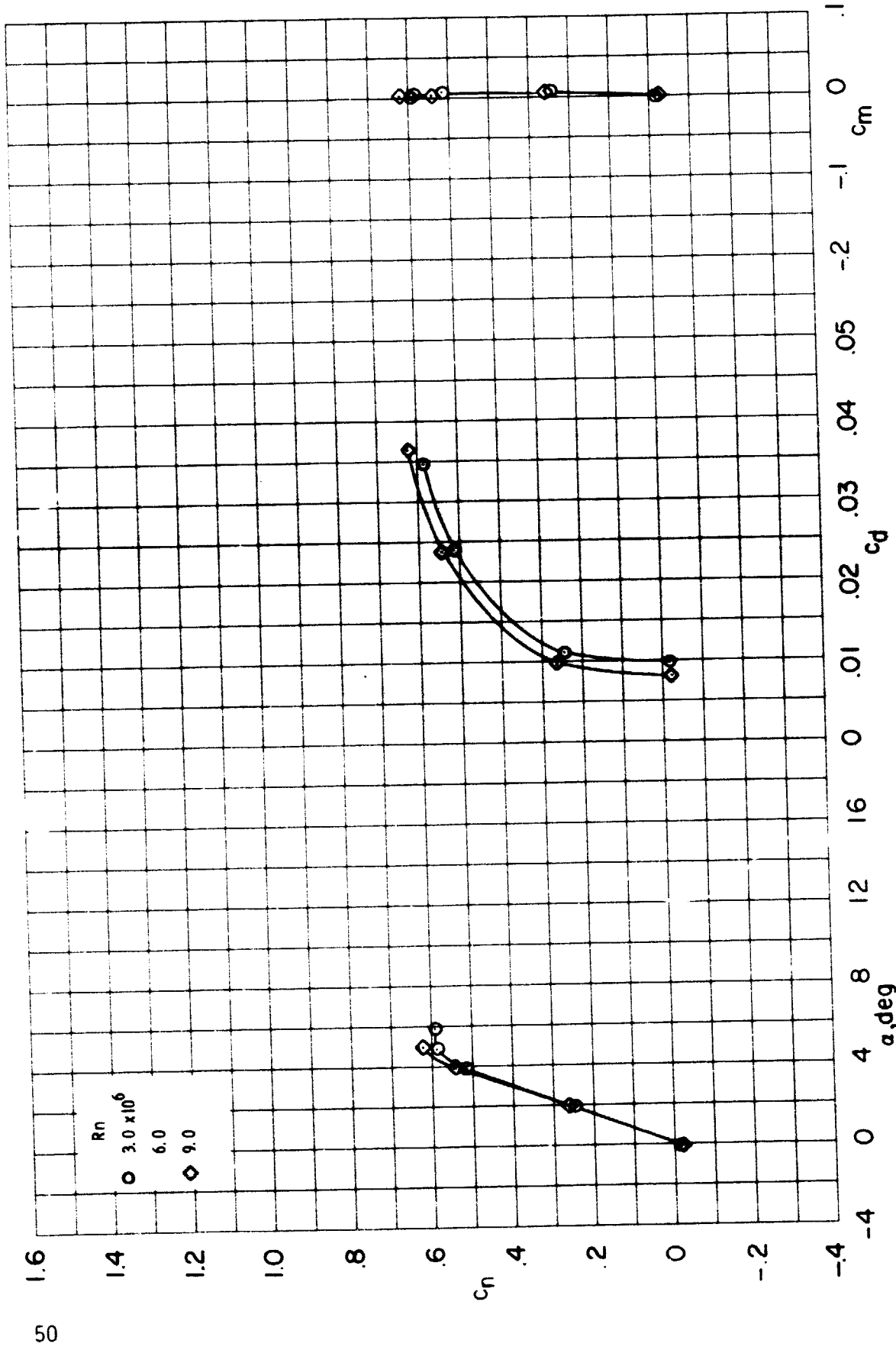
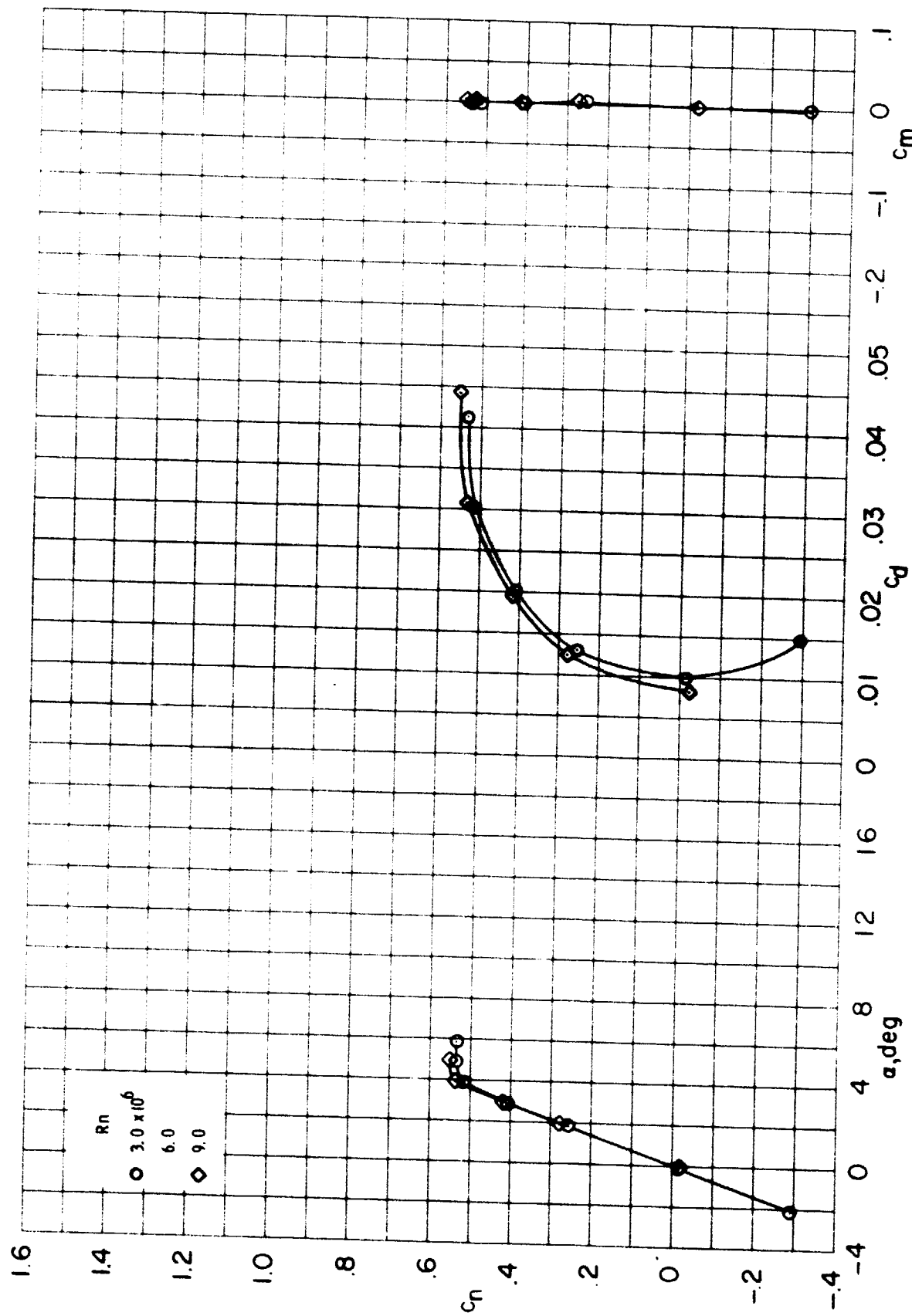


Figure 7. - Continued.
(h) $M = 0.74$



(i) $M = 0.76$

Figure 7.- Continued.

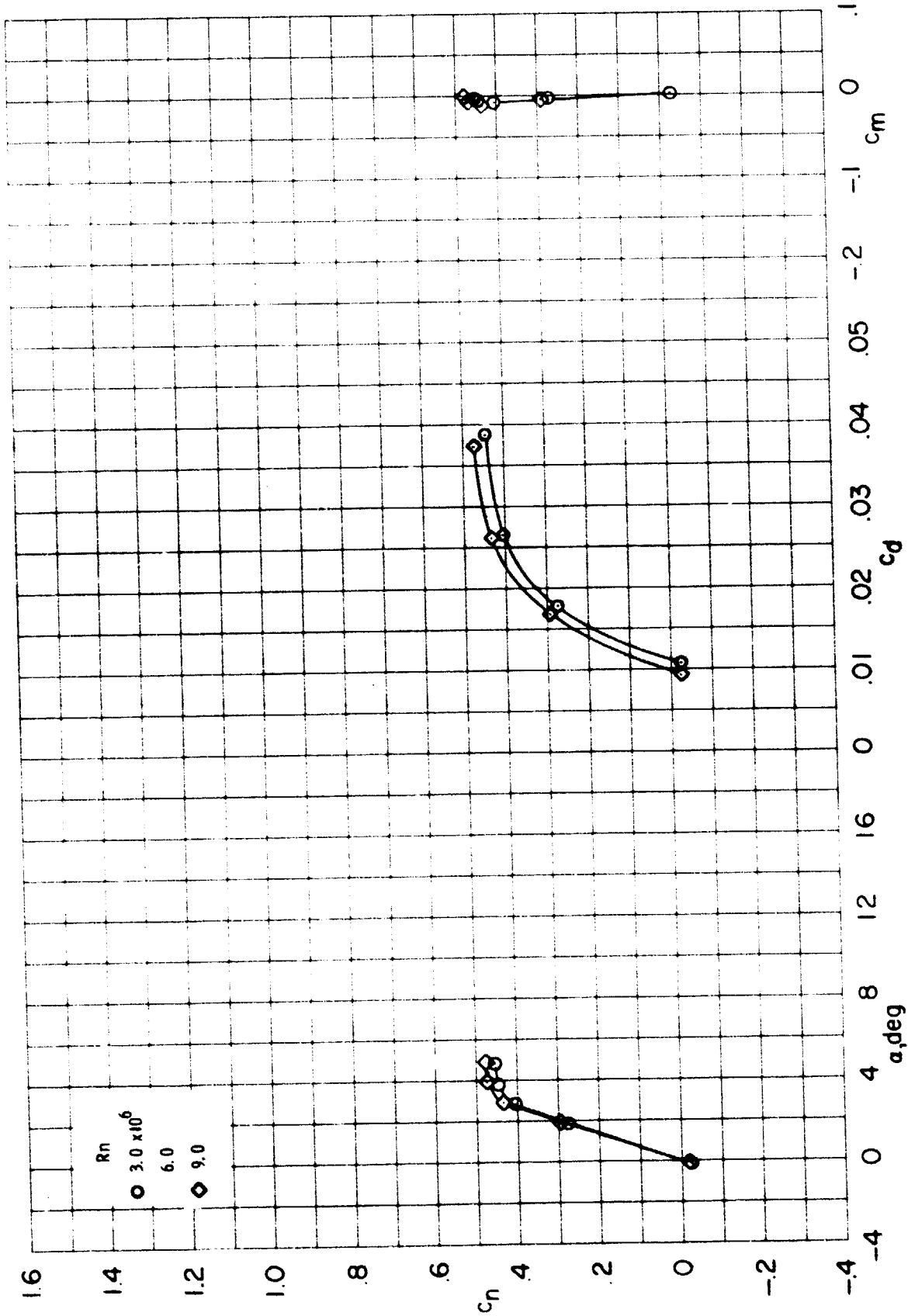
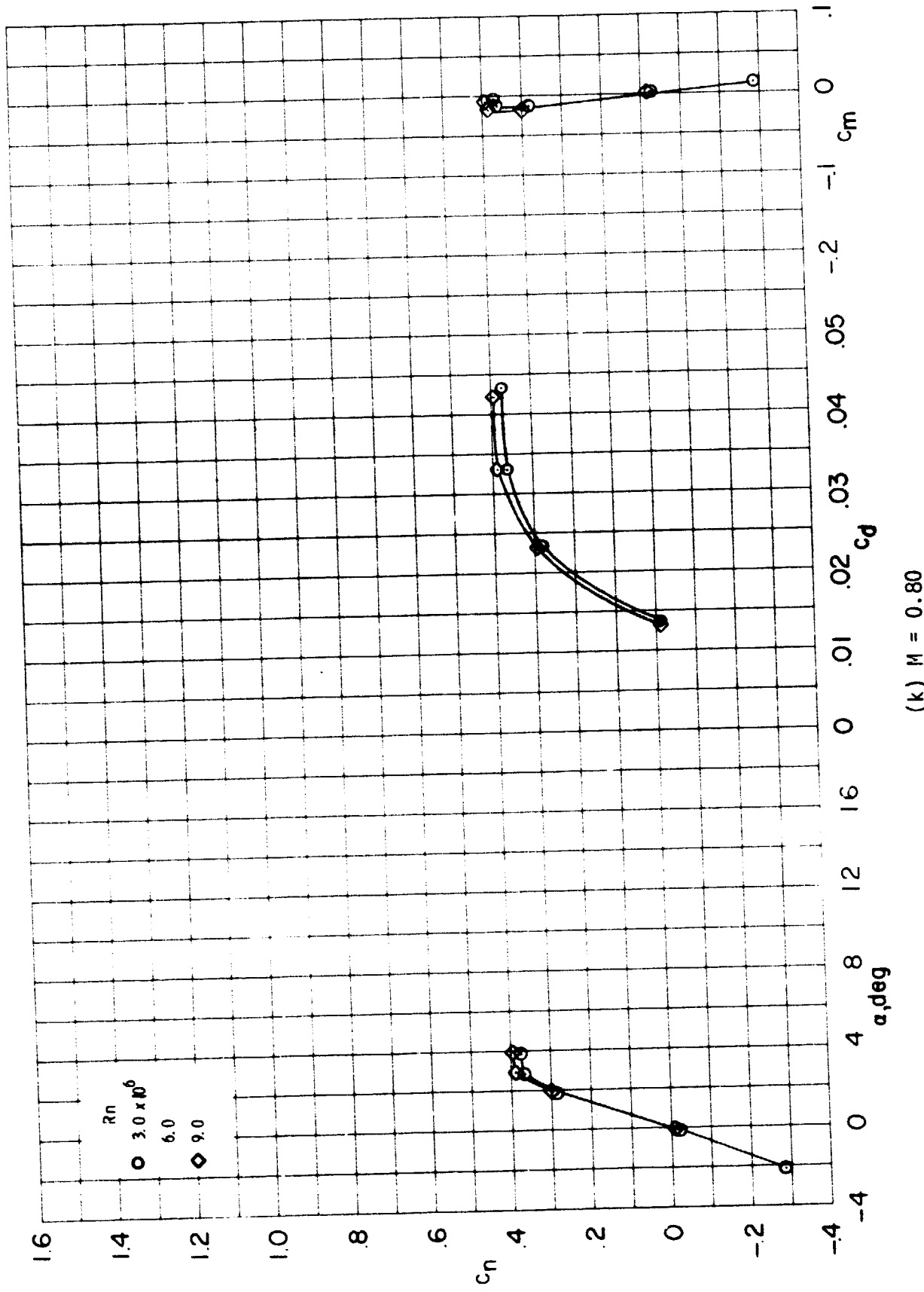


Figure 7.- Continued

(j) $M = 0.78$



(k) $M = 0.80$
Figure 7.- Continued.

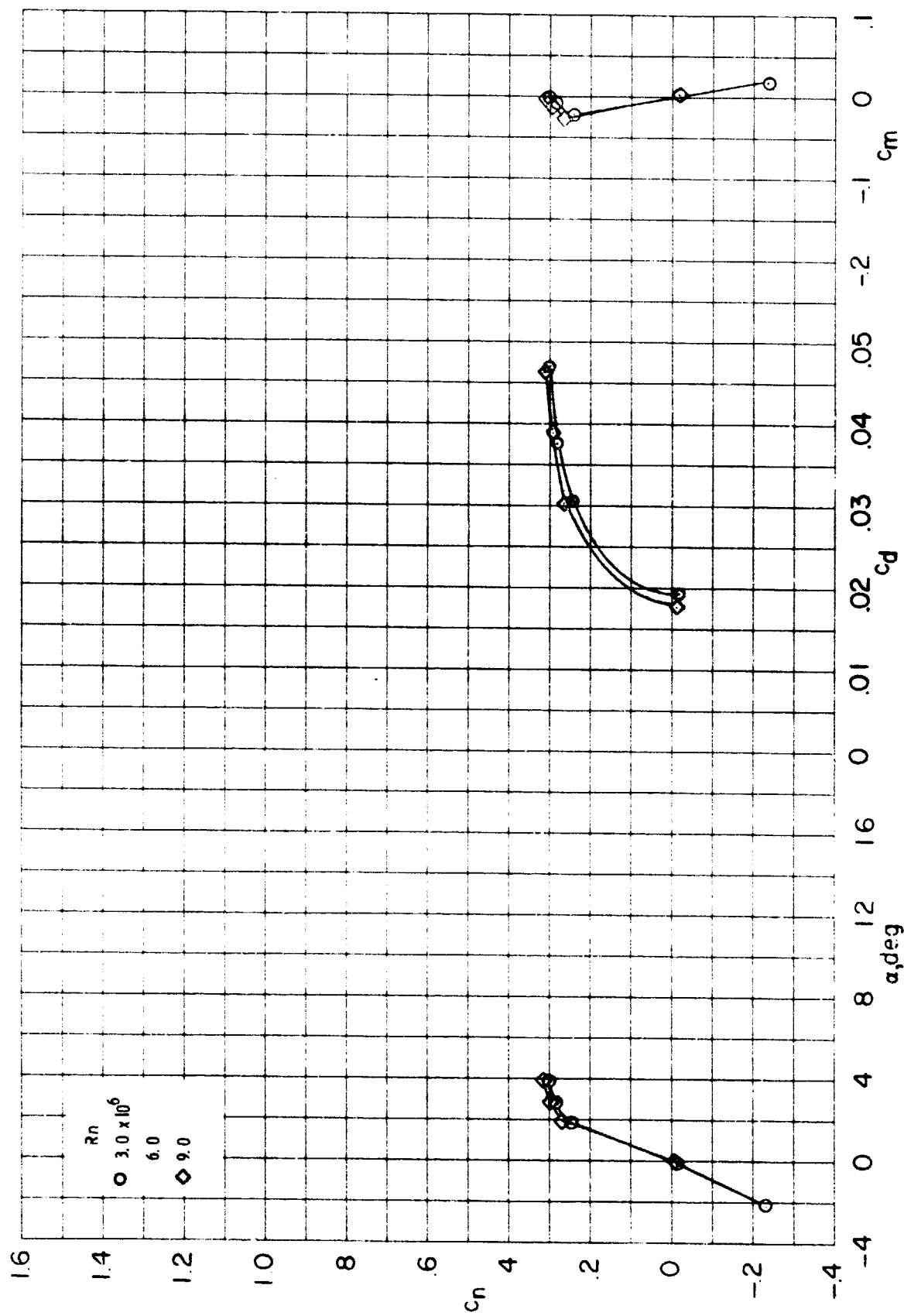
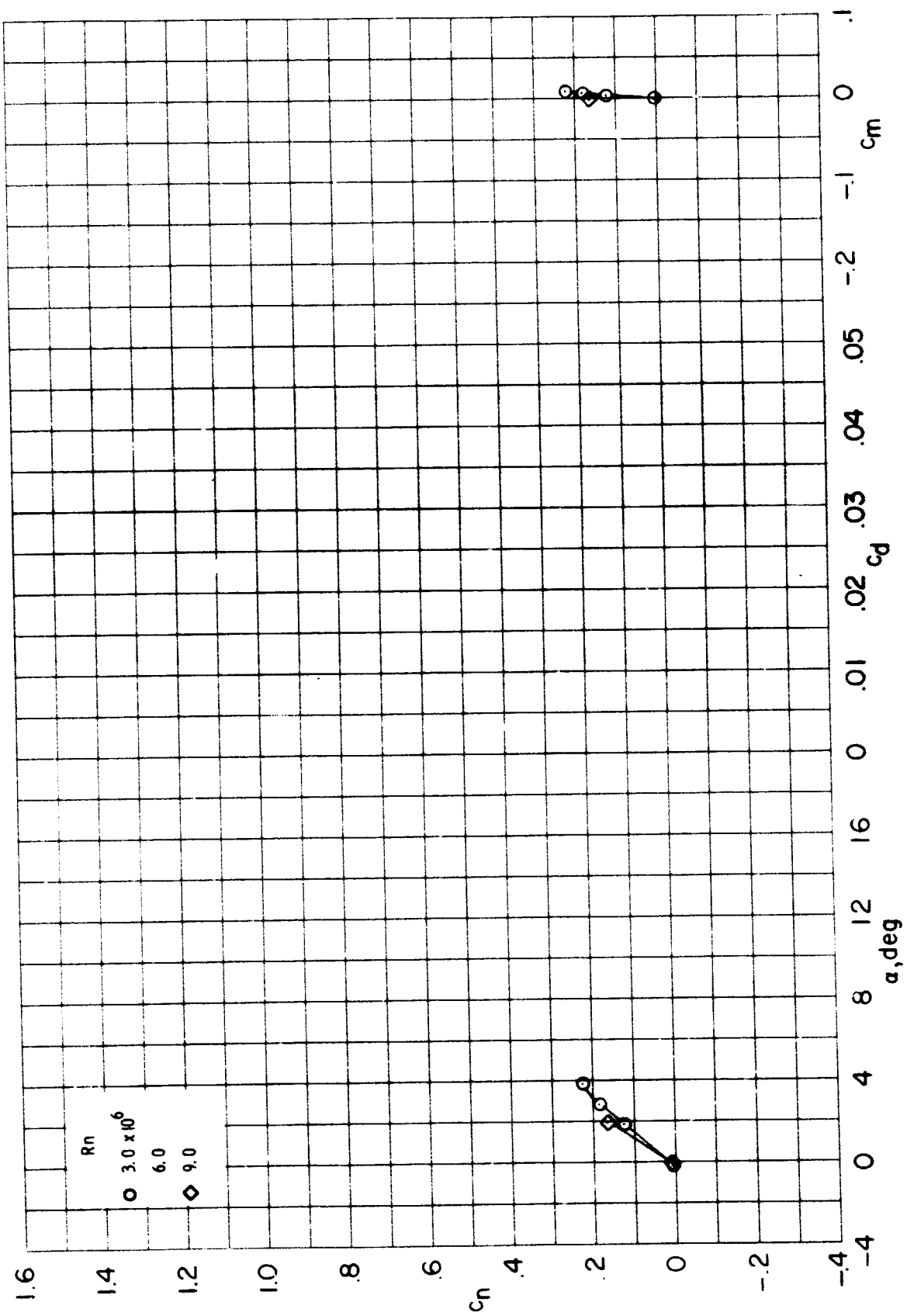


Figure 7.- Continued.

(1) $M = 0.82$



(m) $M = 0.84$

Figure 7.- Concluded.

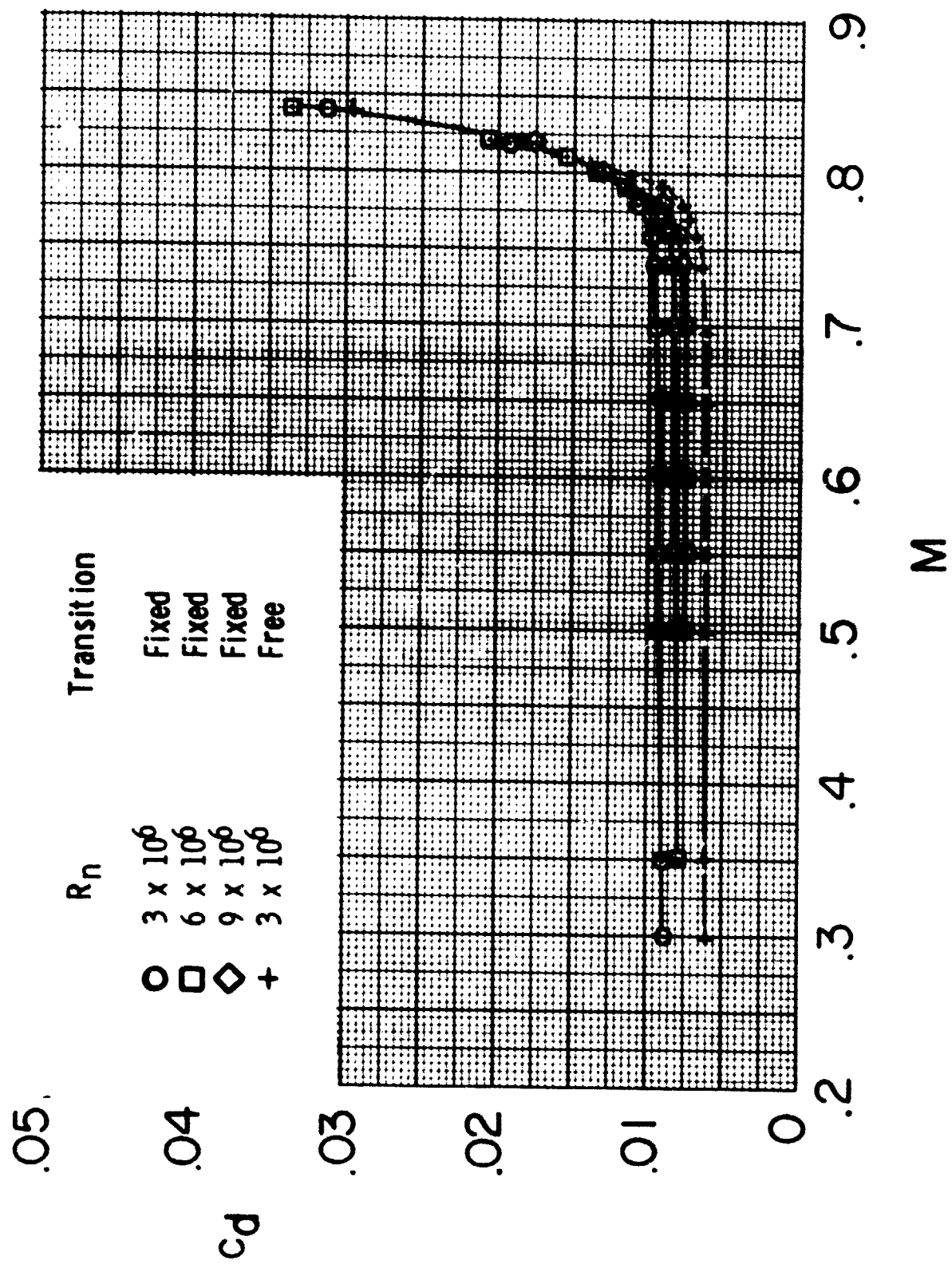


Figure 8.- Effect of Reynolds number on drag-rise characteristics
of NACA 0012 airfoil. $\alpha \approx -0.14$.

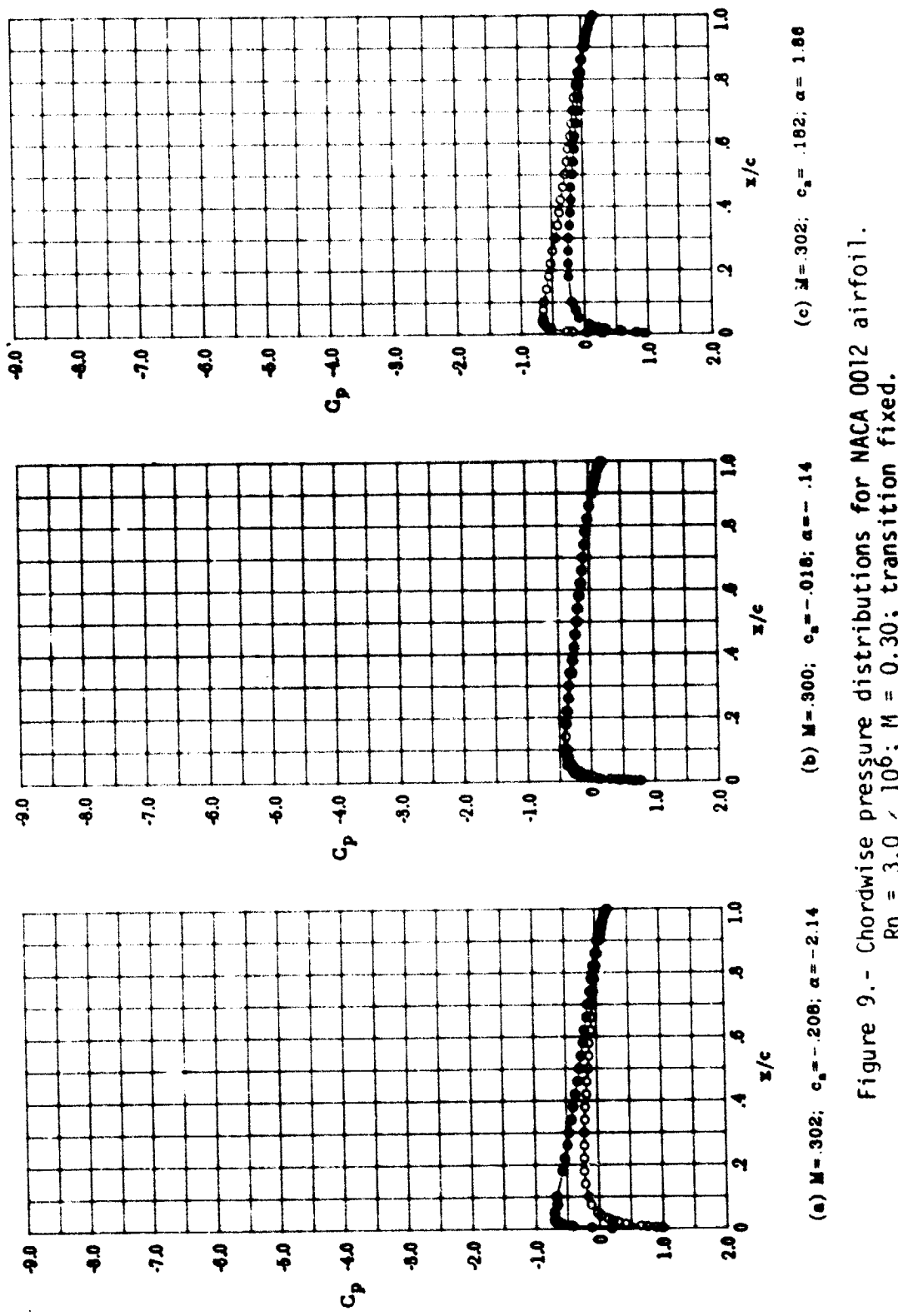


Figure 9. - Chordwise pressure distributions for NACA 0012 airfoil.
 $Rn = 3.0 \times 10^6$; $M = 0.30$; transition fixed.

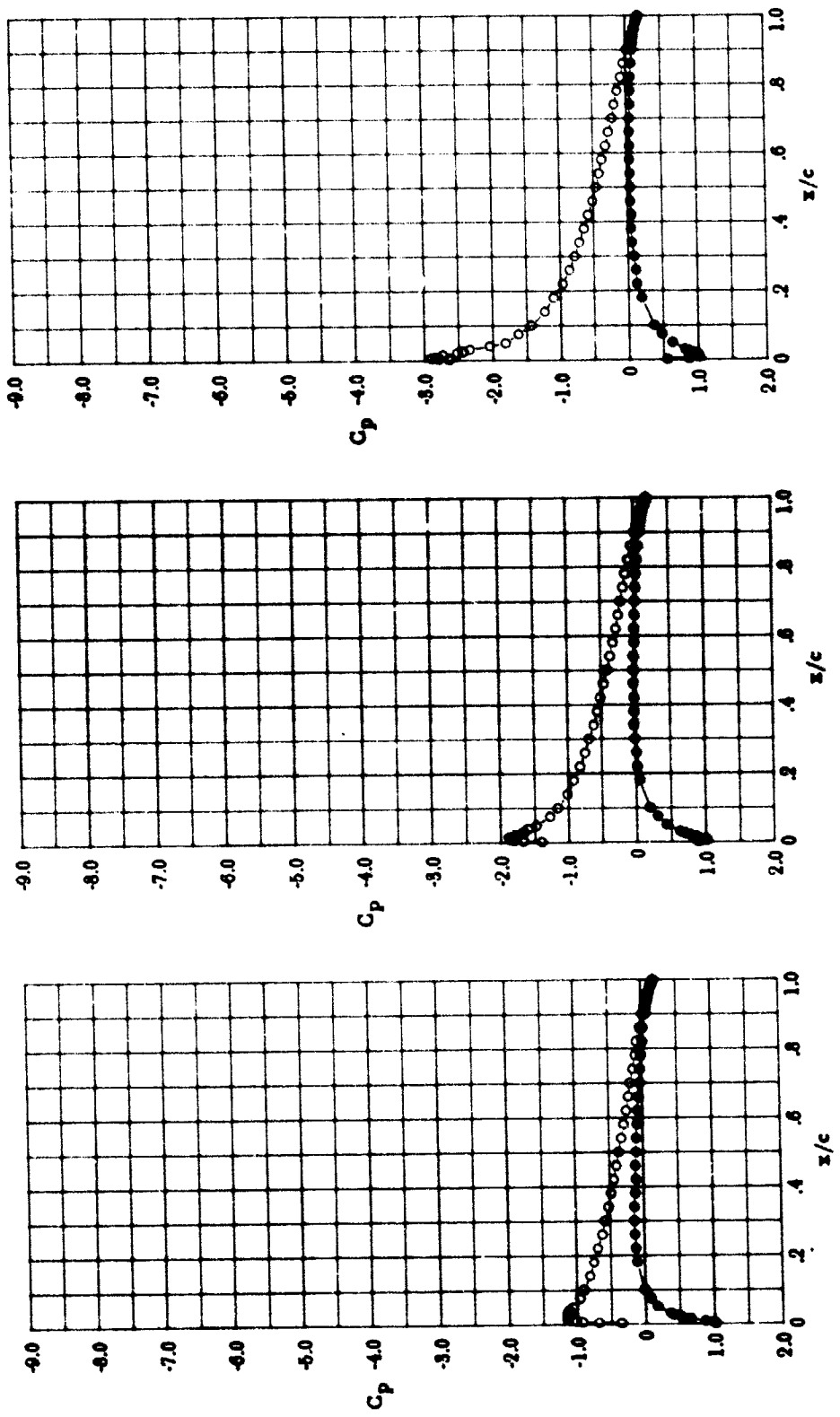


Figure 9.- Continued.

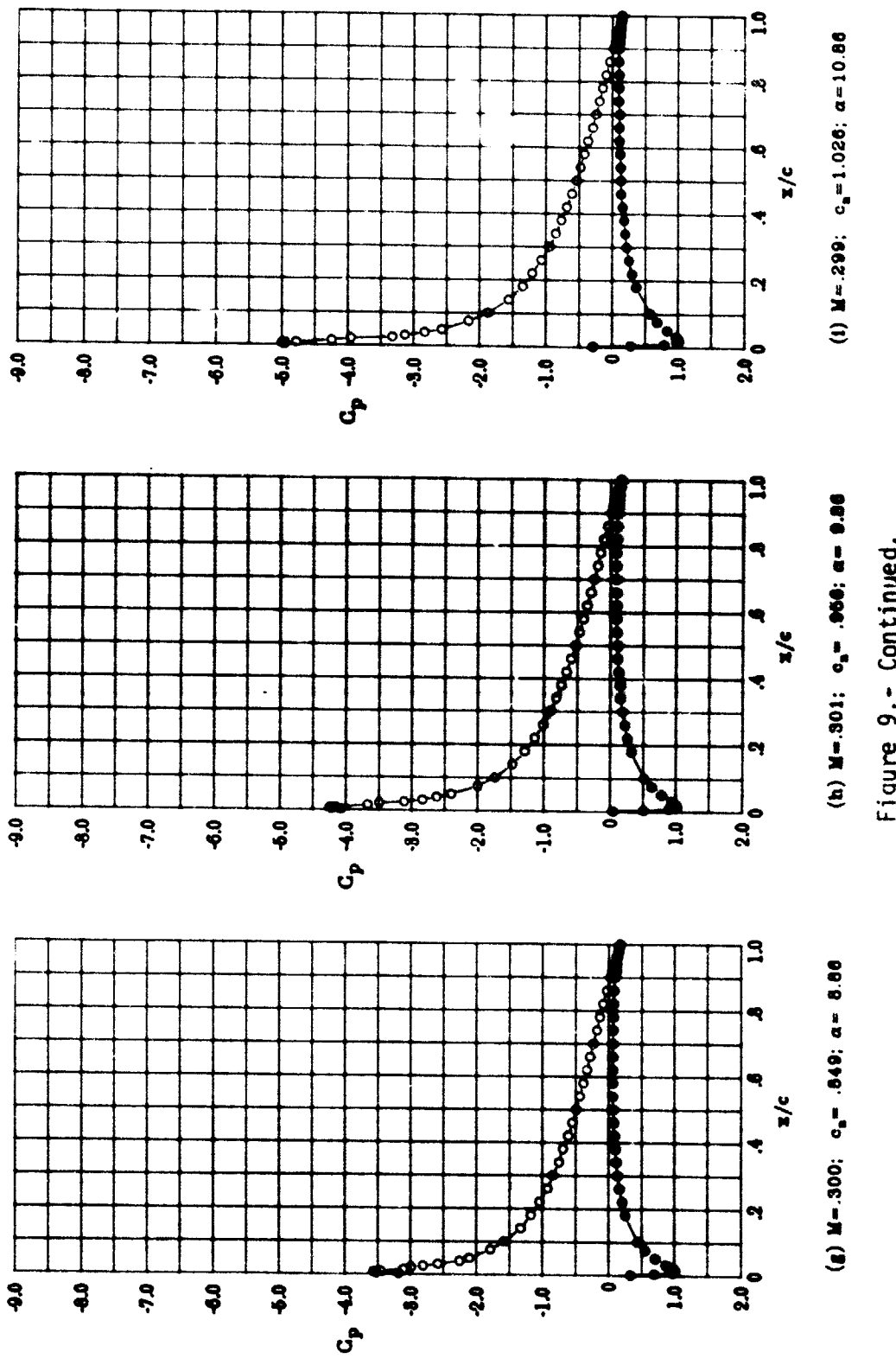


Figure 9.- Continued.

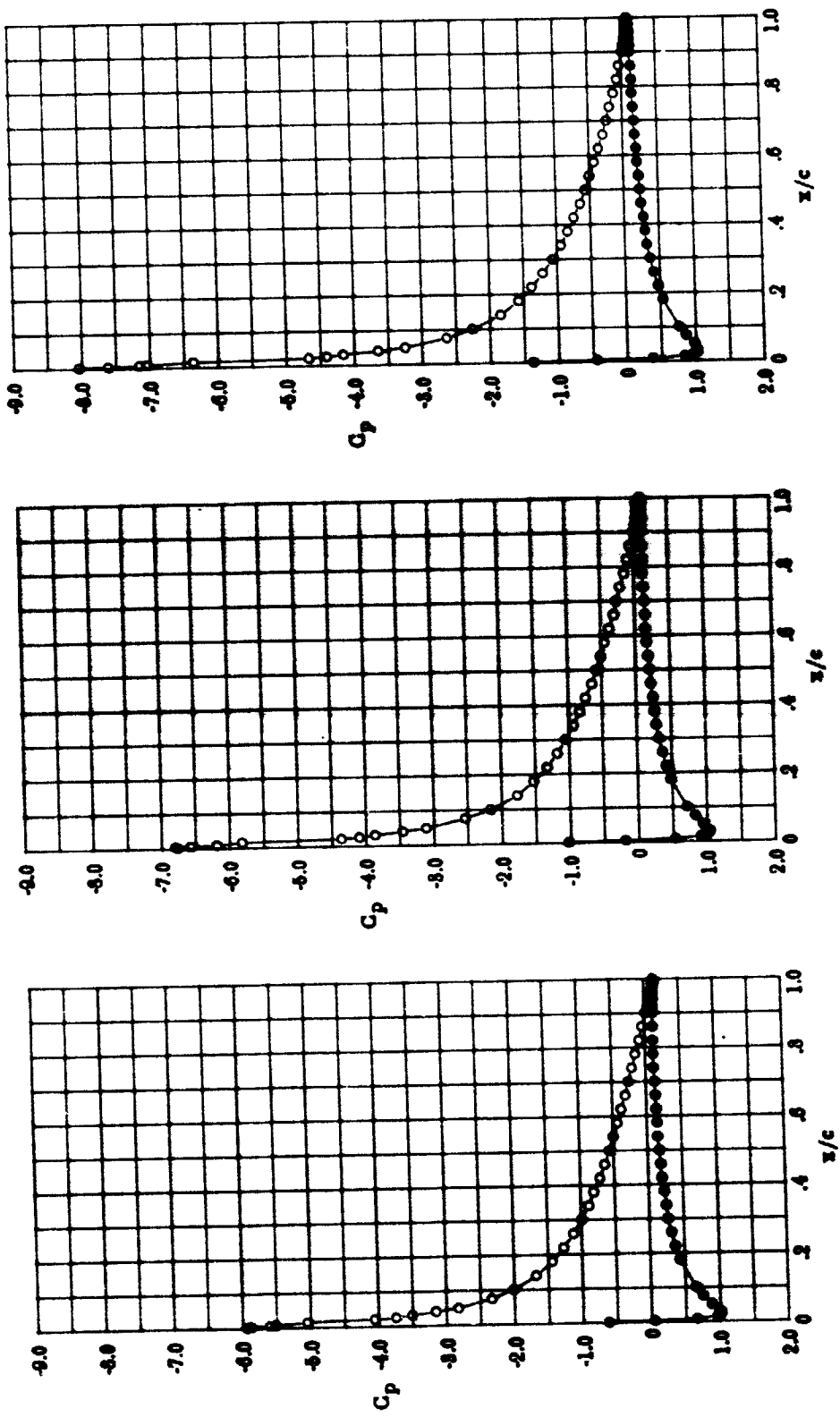


Figure 9.- Continued.

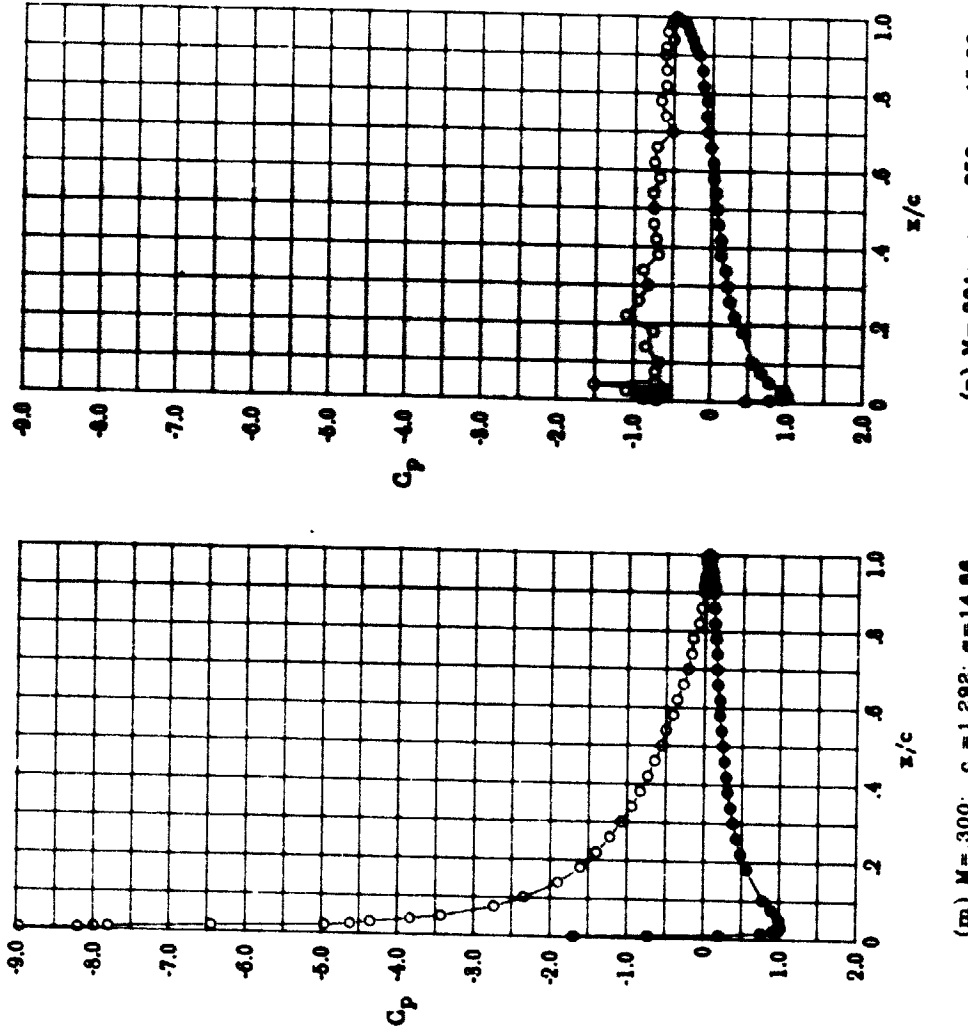


Figure 9.- Concluded.

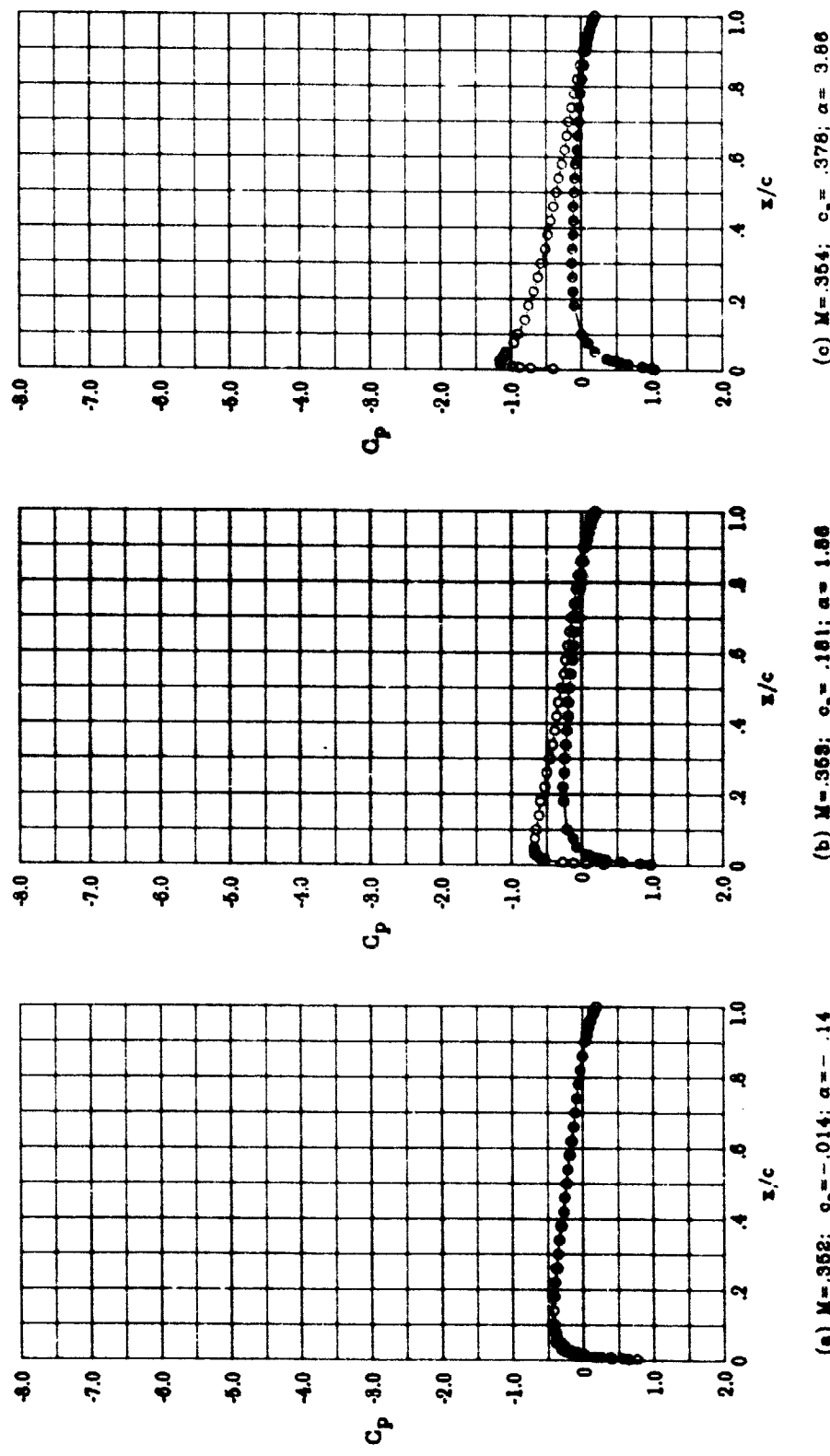


Figure 10.- Chordwise pressure distributions for NACA 0012 airfoil.
 $Rn = 3.0 \times 10^6; M = 0.35$; transition fixed.

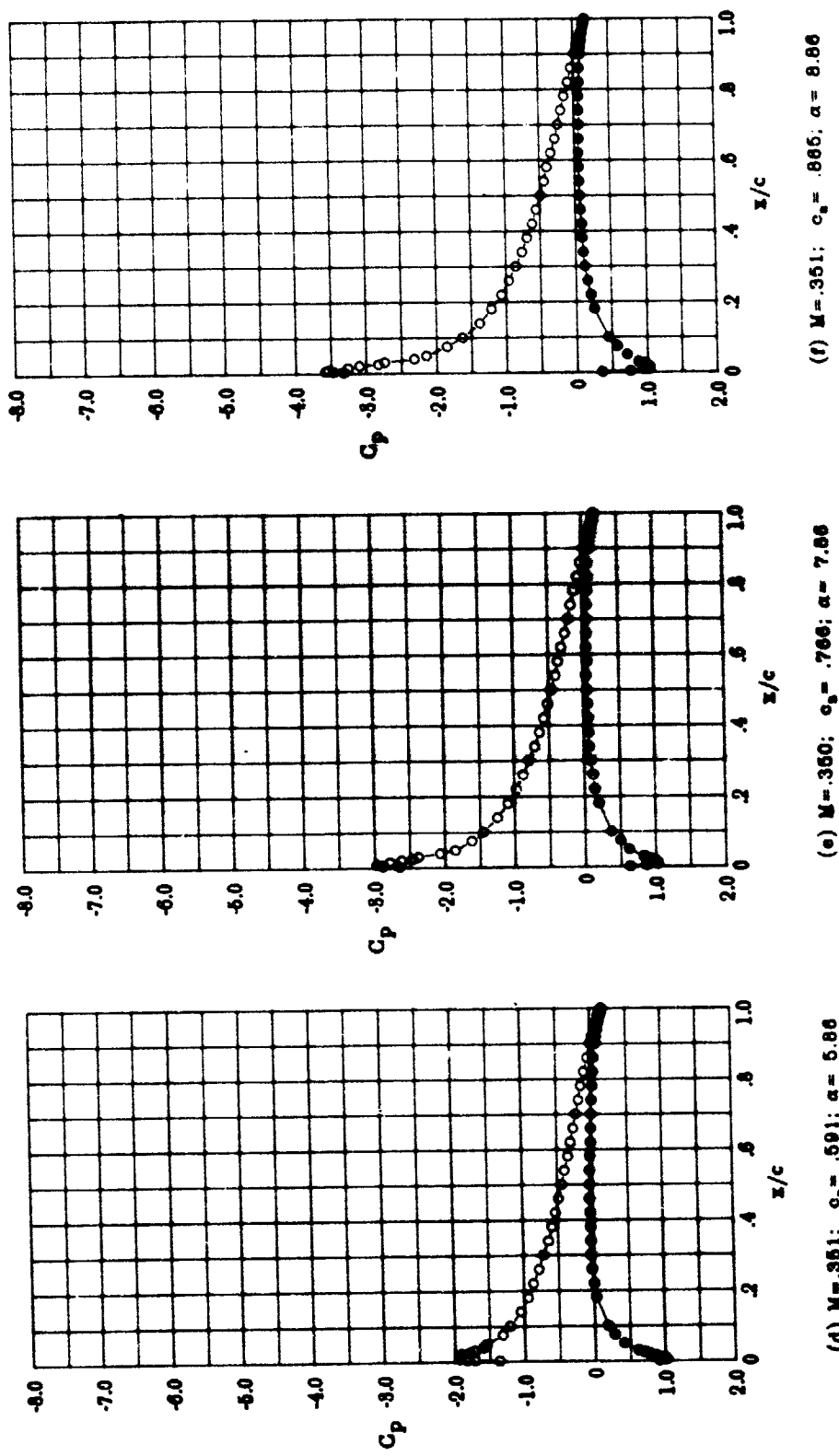


Figure 10.- Continued

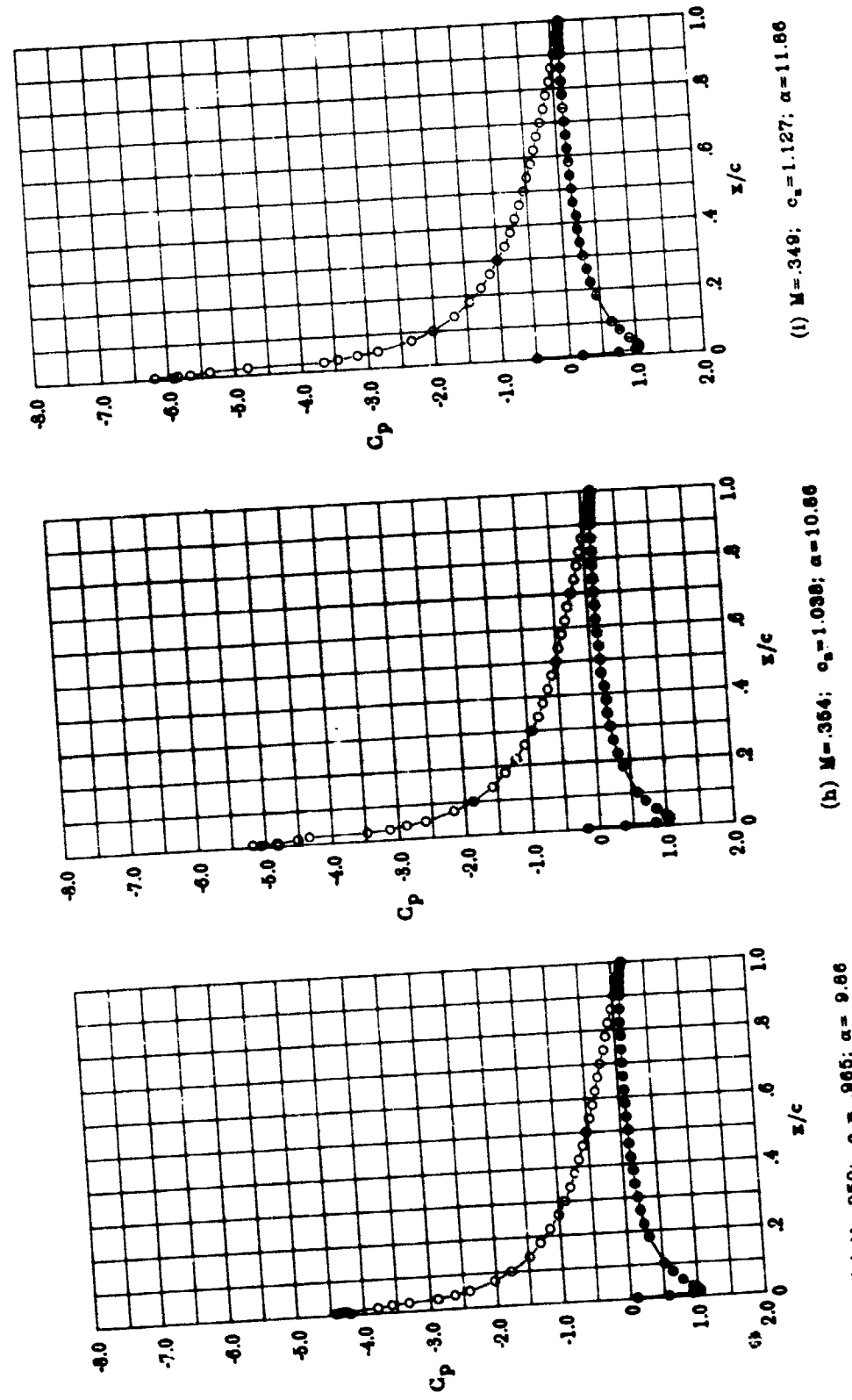


Figure 10.- Continued.

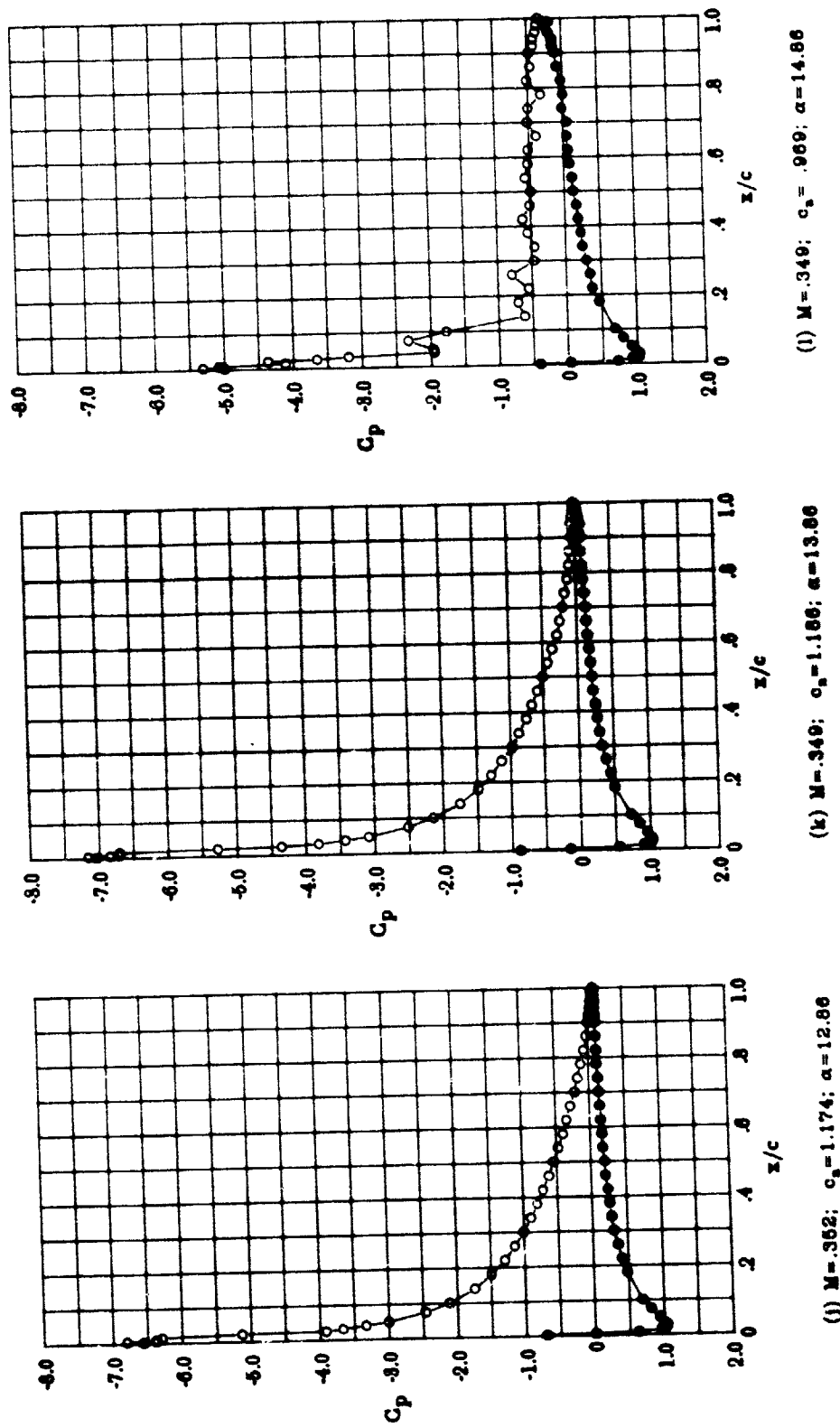


Figure 10.- Concluded.

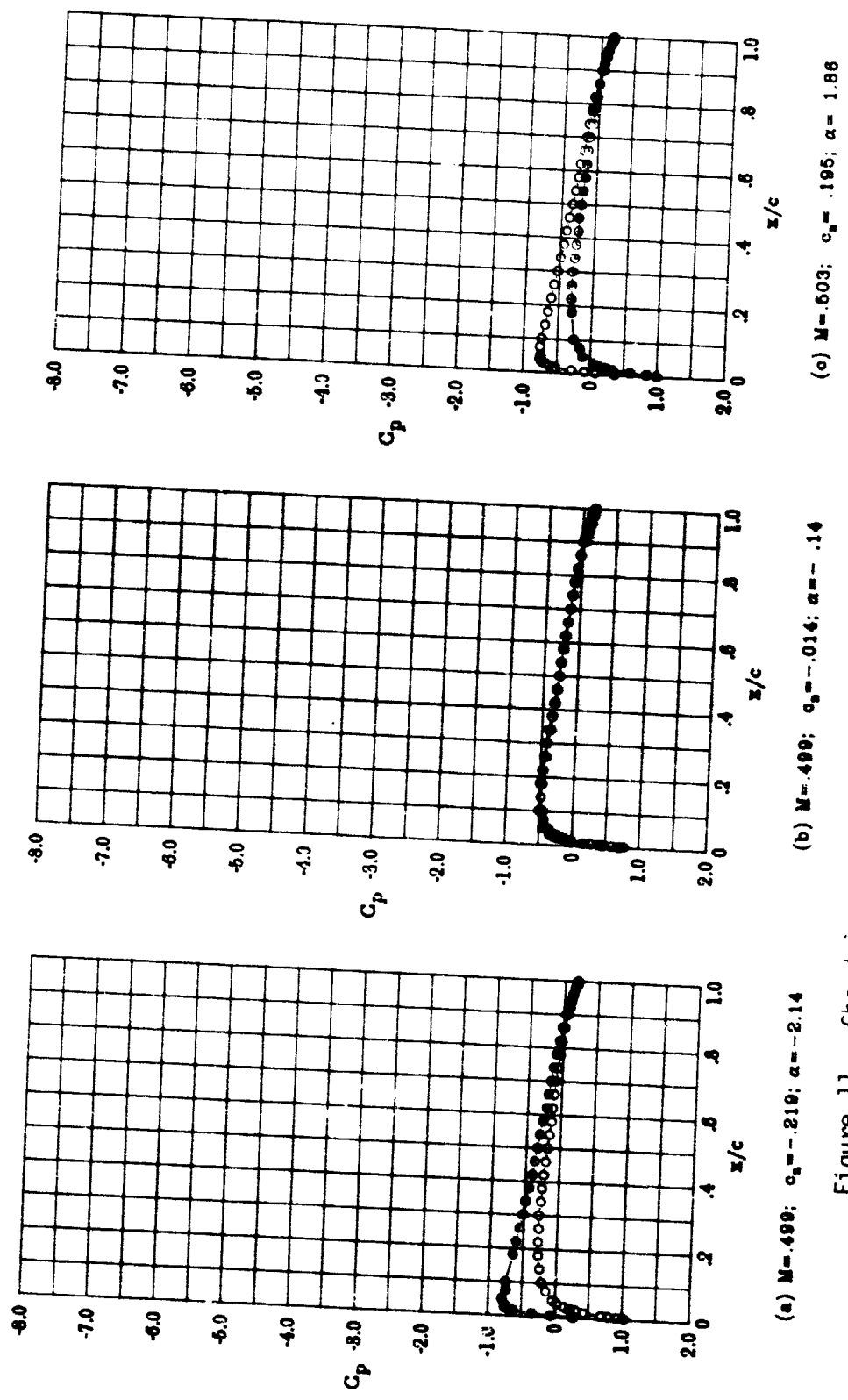


Figure 11.- Chordwise pressure distributions for NACA 0012 airfoil.
 $R_h = 3.0 \times 10^6$; $M = 0.50$; transition fixed.

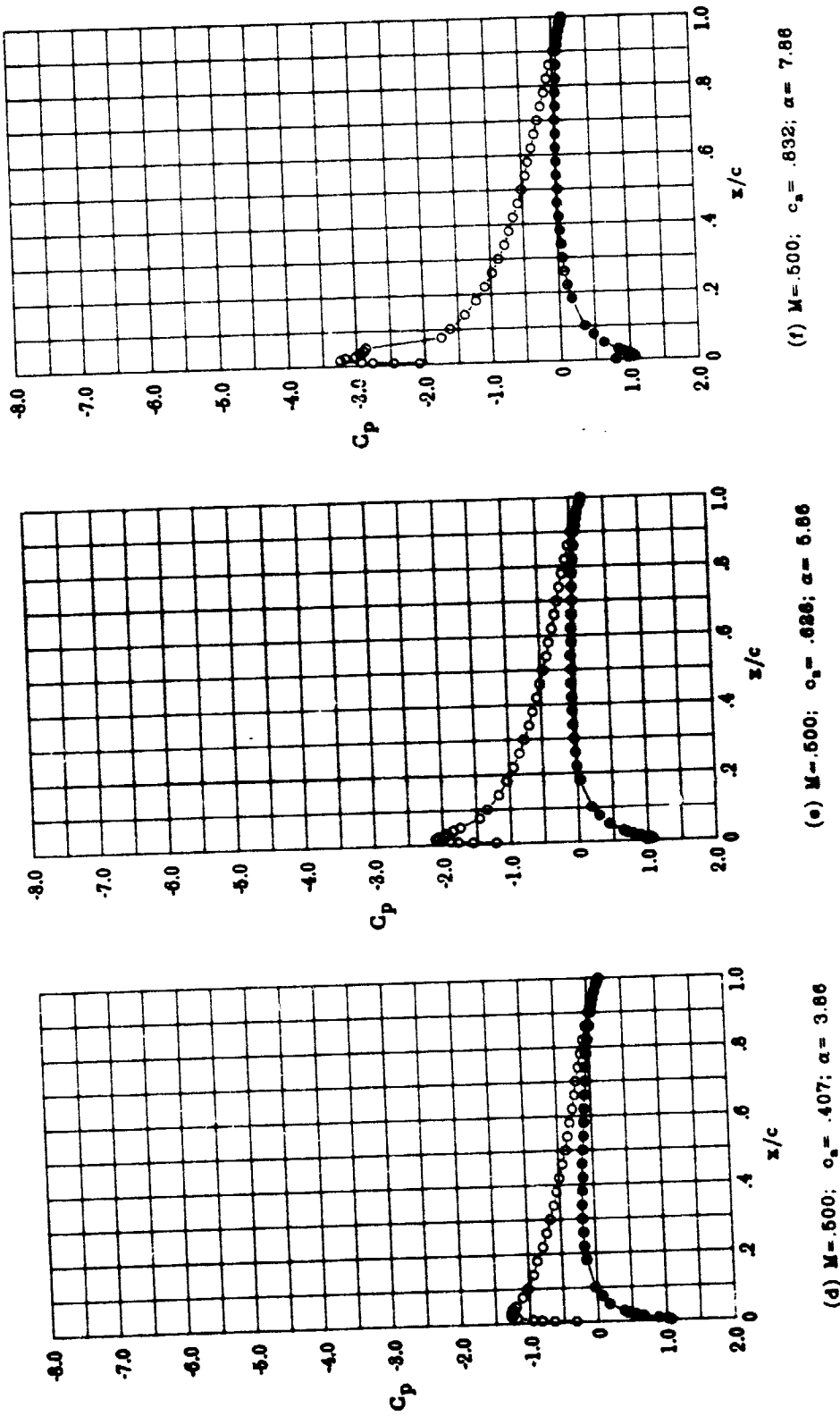


Figure 11.- Continued.

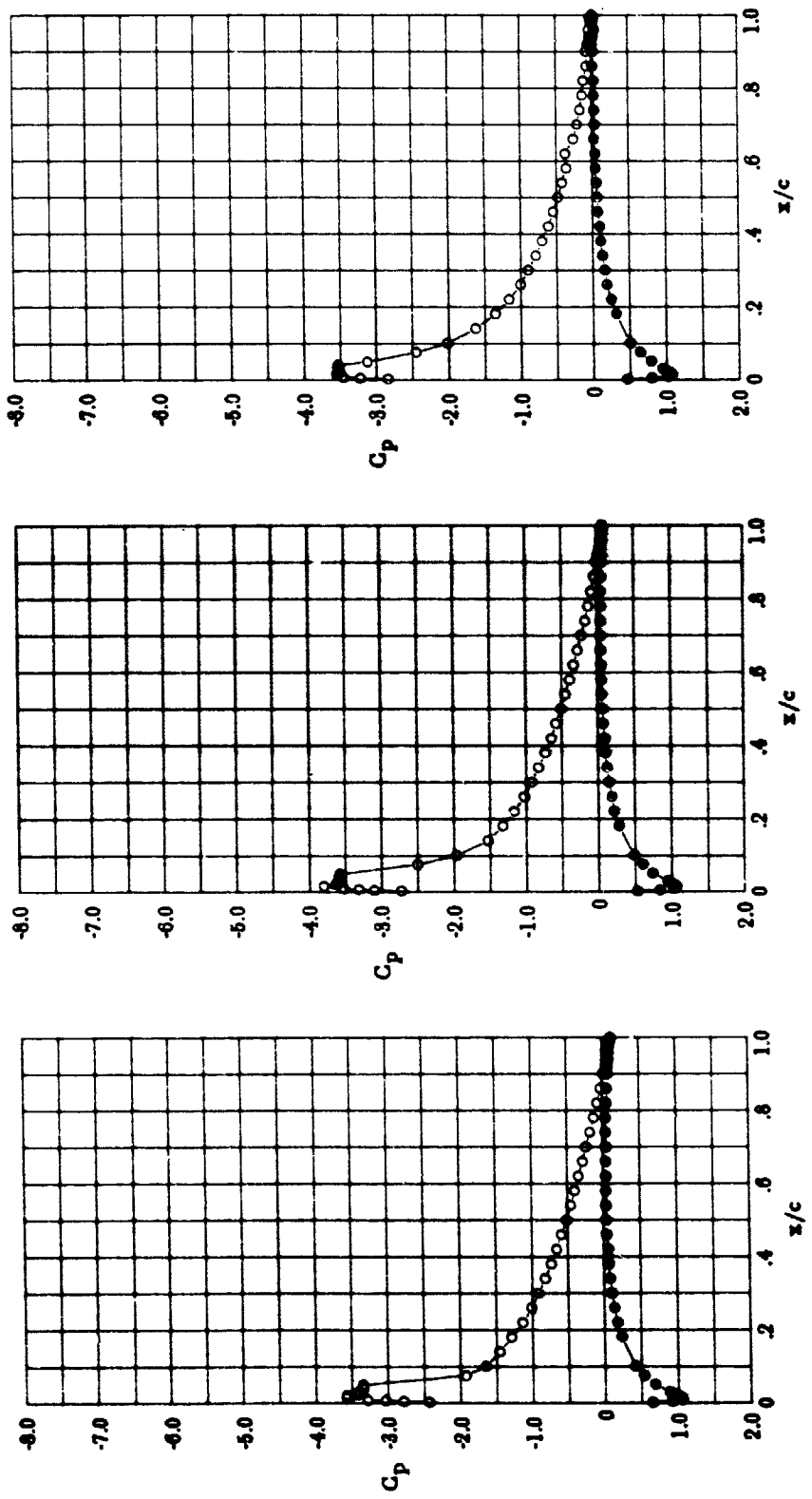


Figure 11.- Concluded.

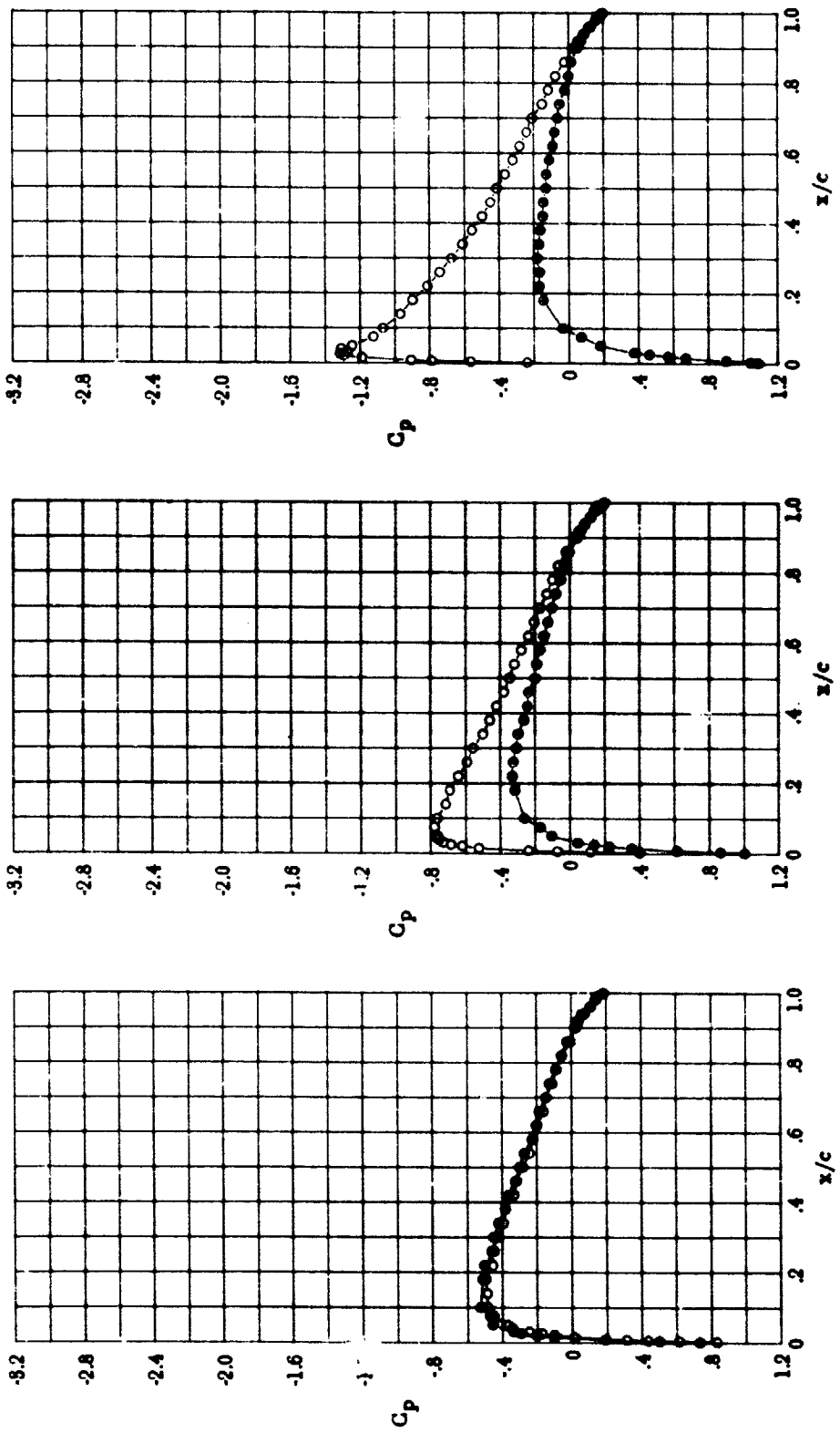


Figure 12.- Chordwise pressure distributions for NACA 0012 airfoil.
 $Rn = 3.0 \times 10^6$; $M = 0.55$; transition fixed.

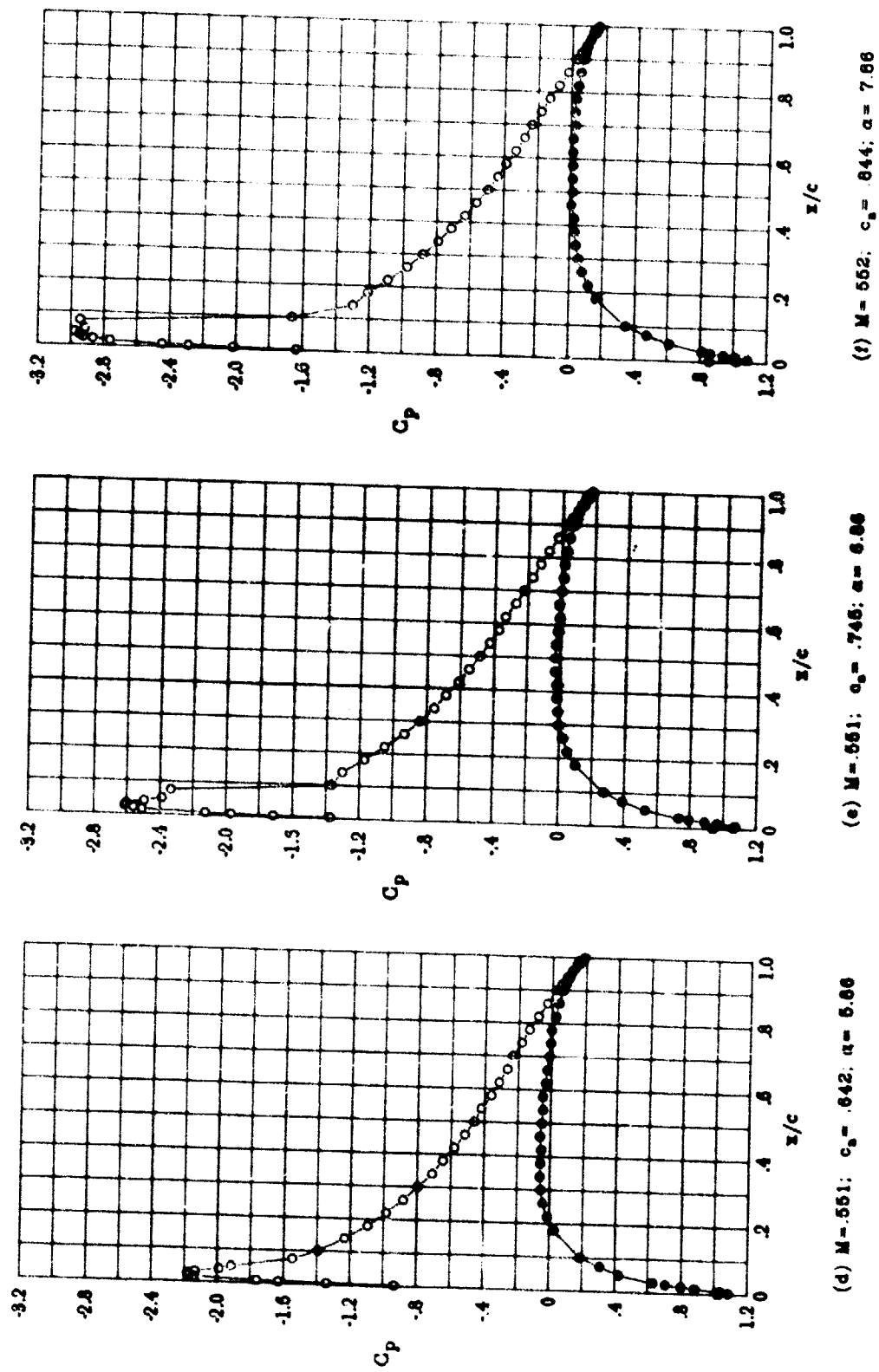
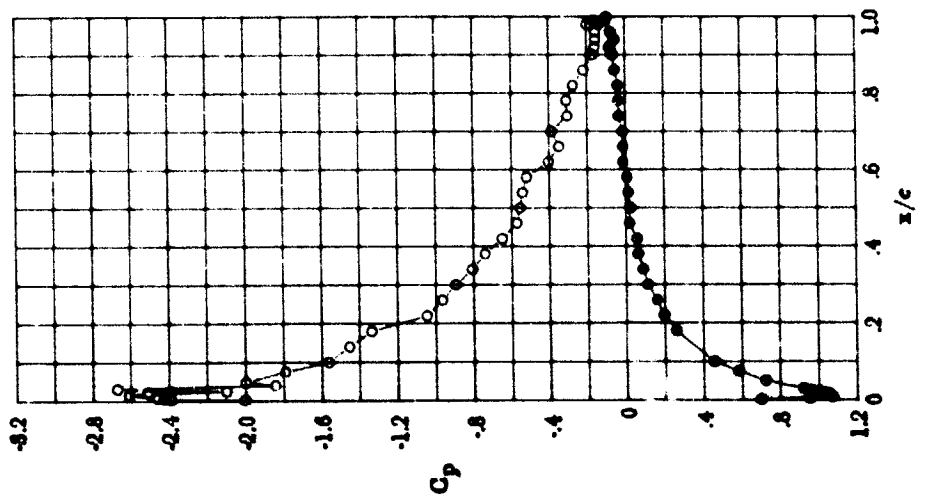
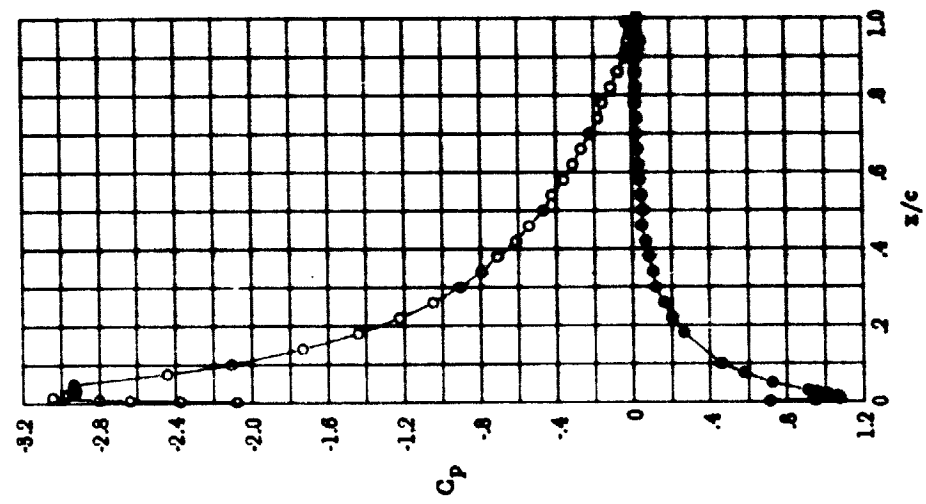


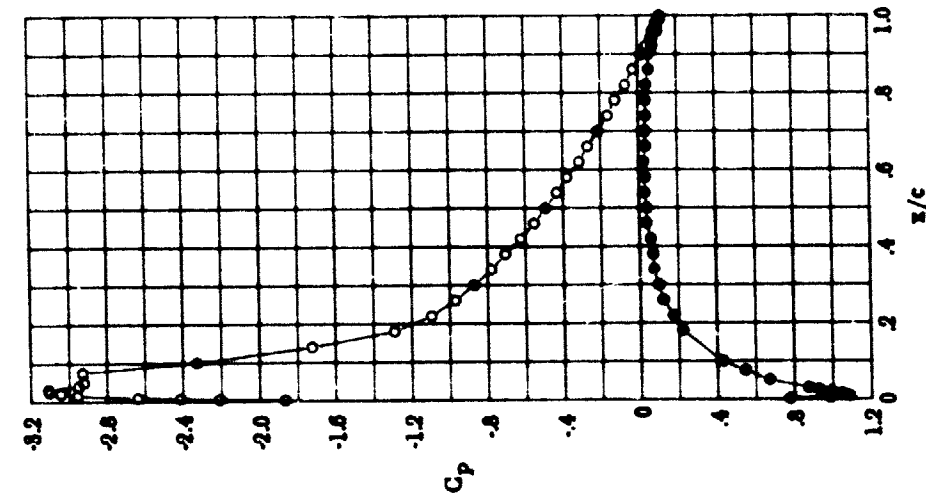
Figure 12. - Continued.



(i) $M = 0.660$; $c_0 = .803$; $\alpha = 10.86$



(h) $M = 0.550$; $c_0 = .927$; $\alpha = 9.86$



(g) $M = 0.563$; $c_0 = .914$; $\alpha = 8.86$

Figure 12.- Concluded.

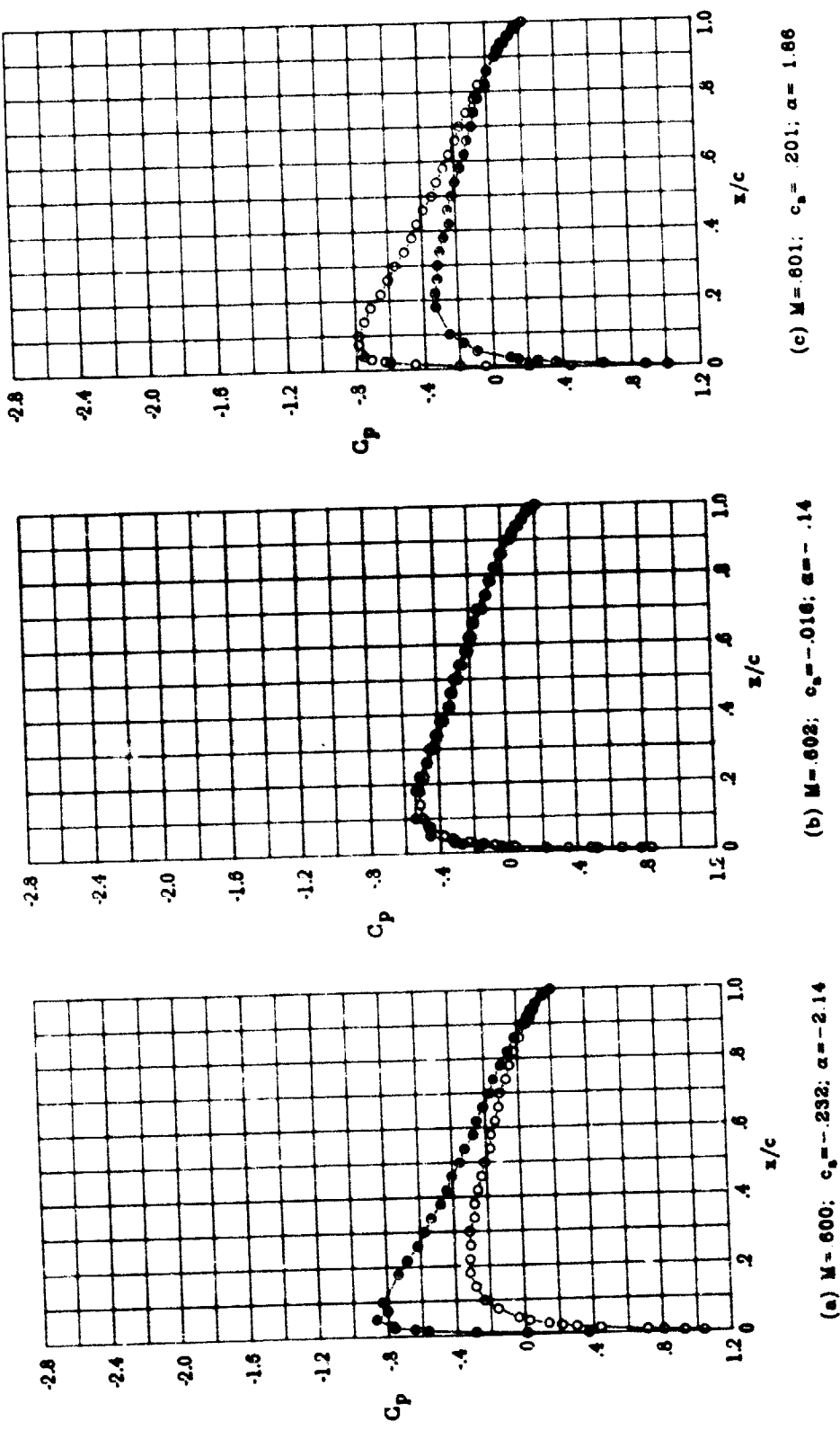


Figure 13.- Chordwise pressure distributions for NACA 0012 airfoil.
 $Rn = 3.0$, 10^6 , $M = 0.60$; transition fixed.

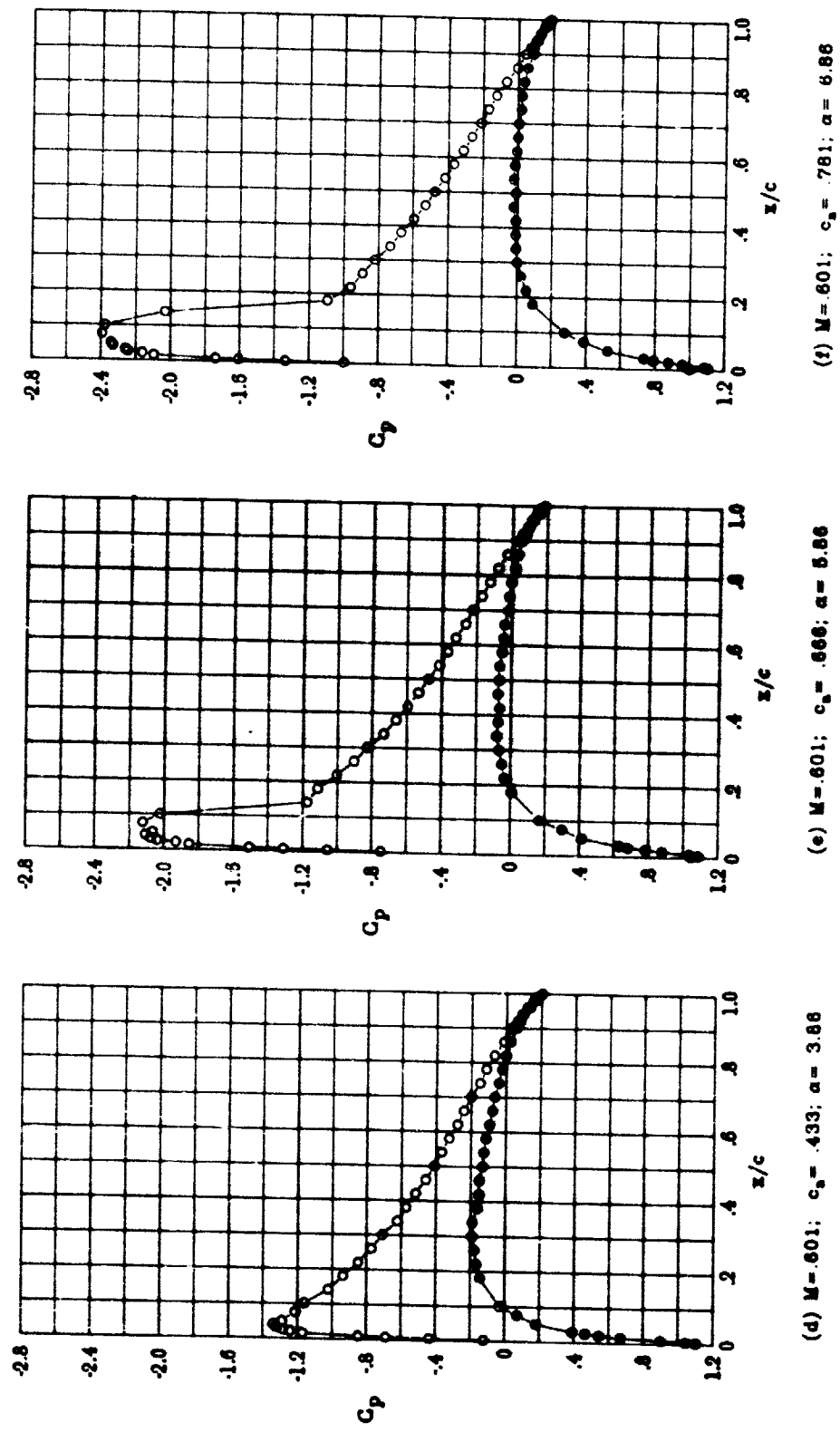
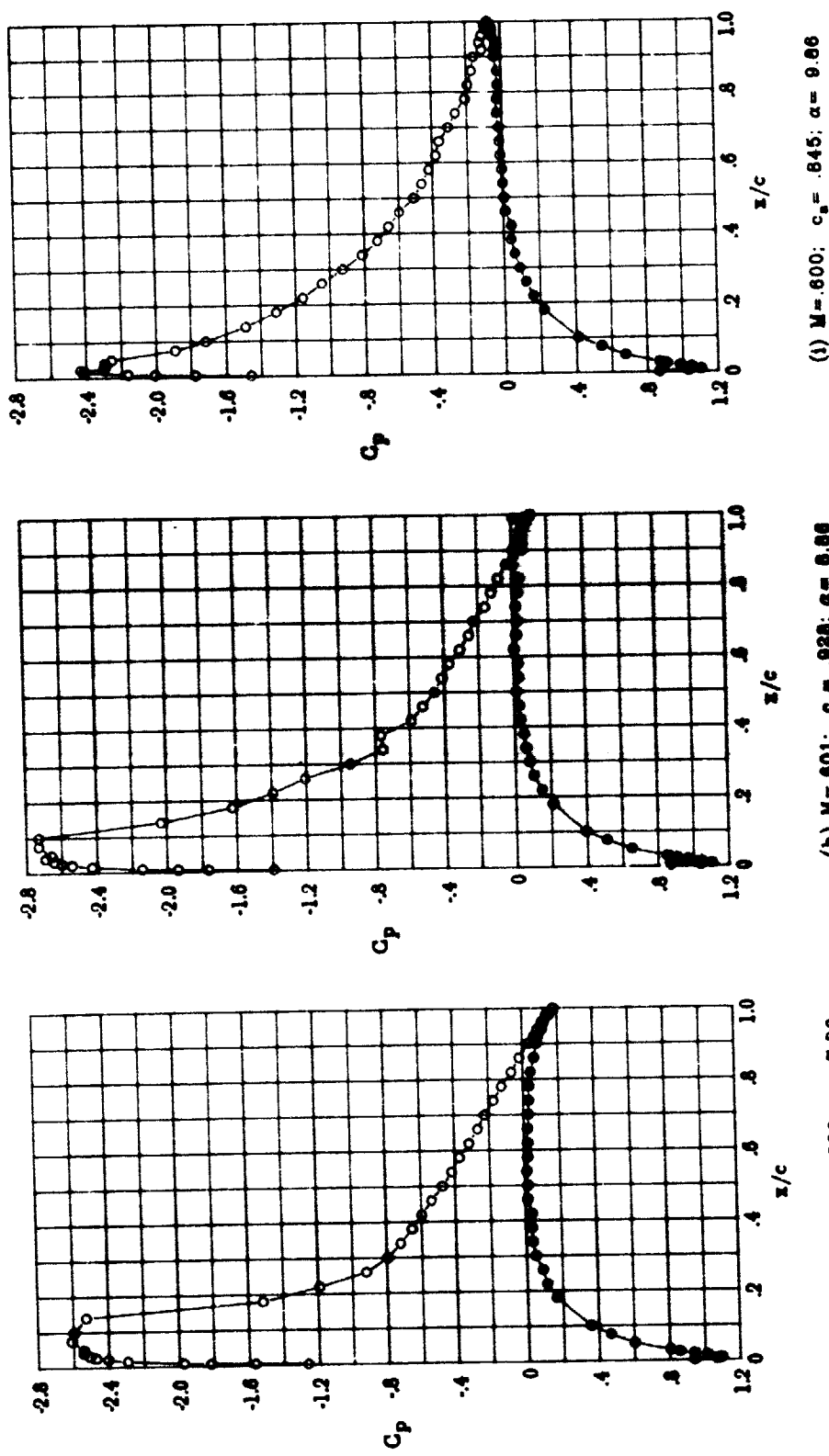


Figure 13.- Continued.



(1) $M = .600; c_0 = .845; \alpha = 9.86$

(b) $M = .601; c_0 = .928; \alpha = 8.86$

Figure 13.- Concluded.

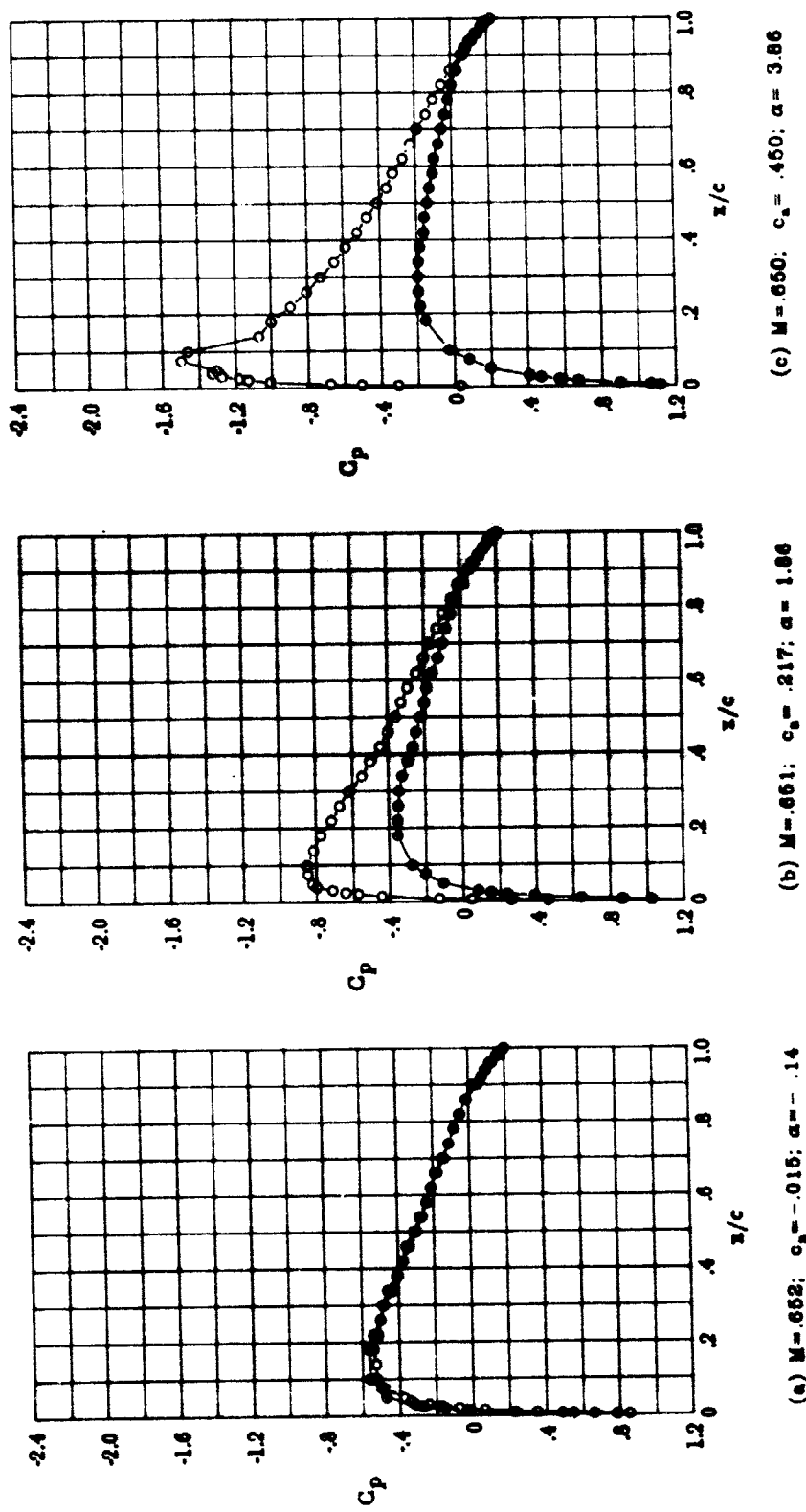
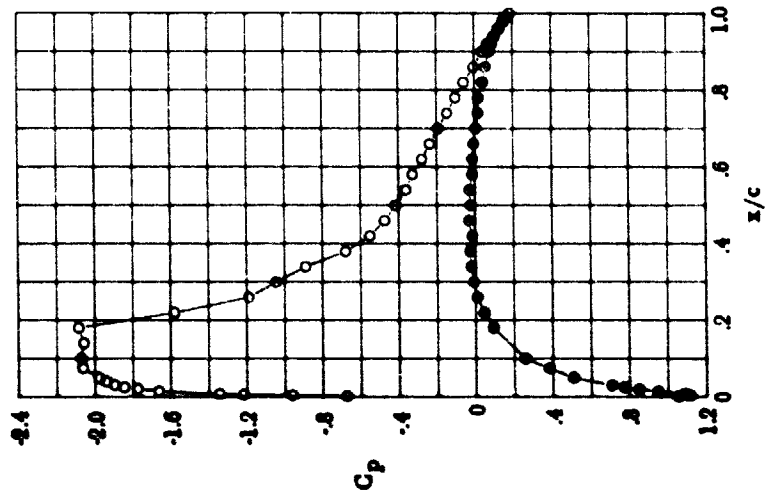
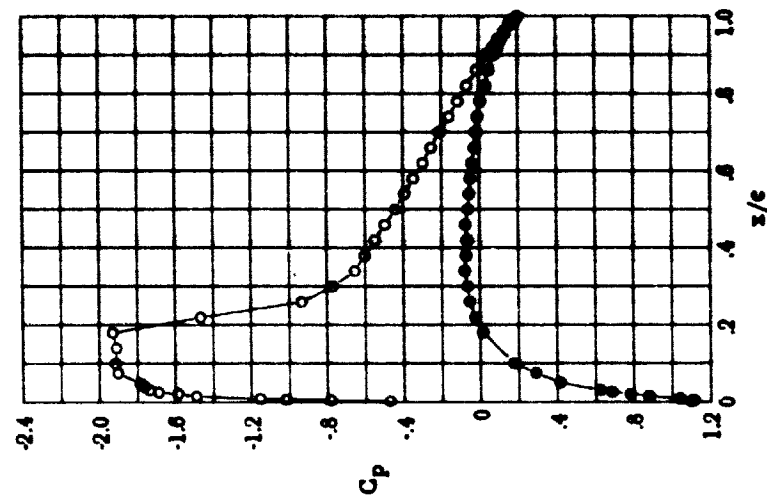


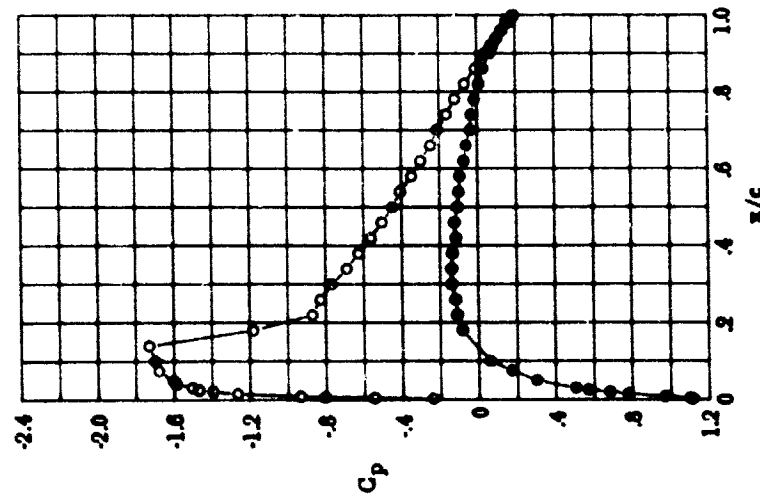
Figure 14.- Chordwise pressure distributions for NACA 0012 airfoil.
 $Rn = 3.0 \times 10^6; M = 0.65$; transition fixed.



(f) $M = 0.651$; $c_a = .809$; $\alpha = 6.86$



(e) $M = 0.652$; $c_a = .704$; $\alpha = 5.86$



(d) $M = .661$; $c_a = .666$; $\alpha = 4.86$

Figure 14. - Continued.

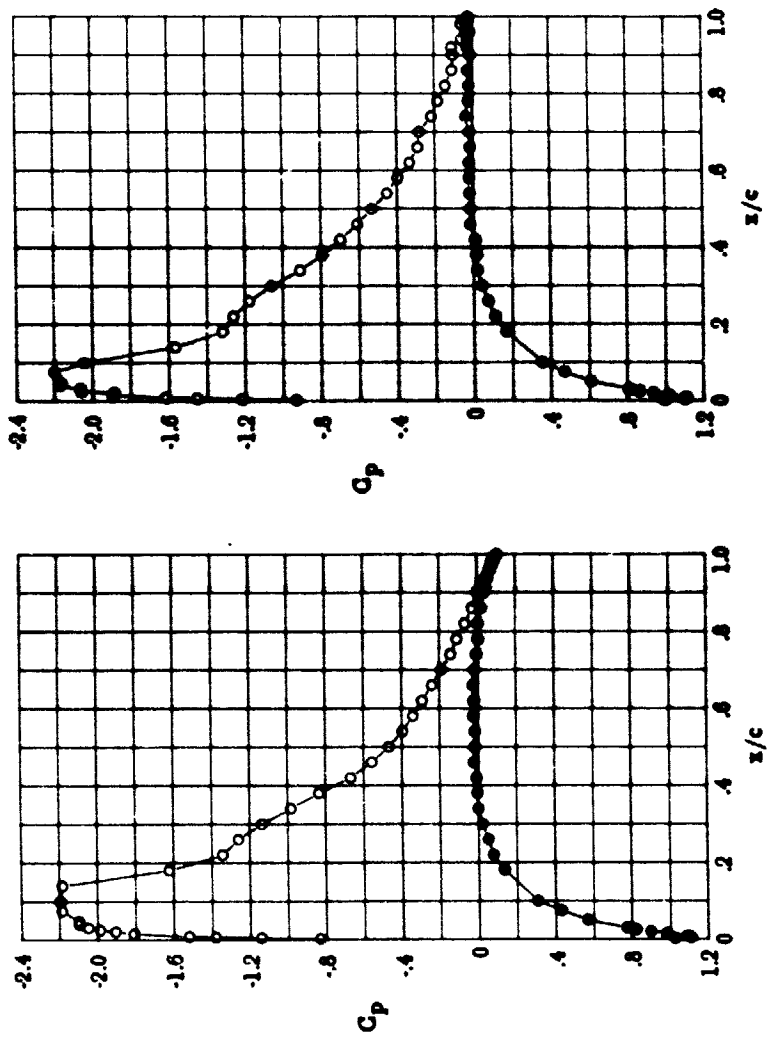


Figure 14.- Concluded.

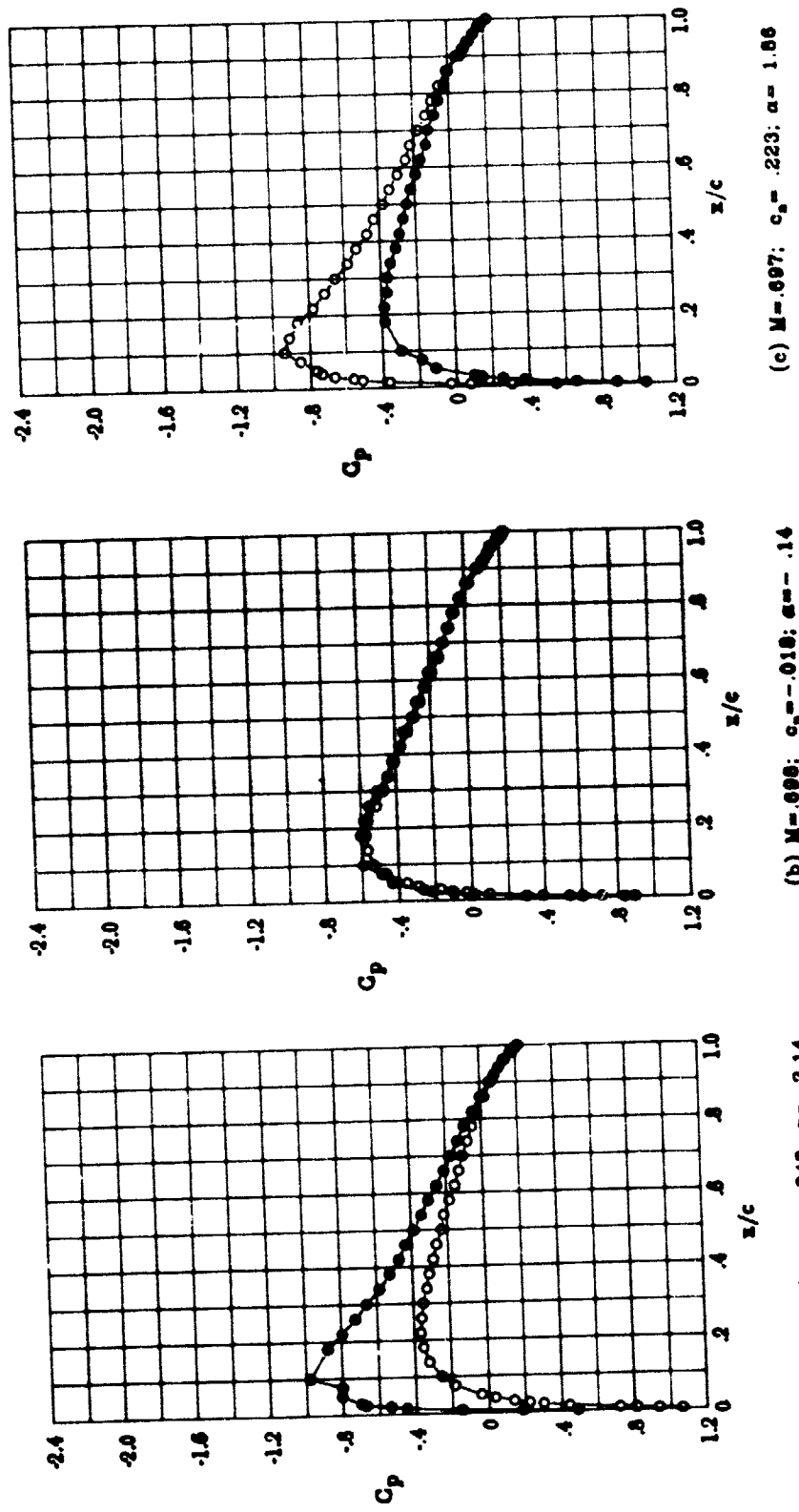


Figure 15.- Chordwise pressure distributions for NACA 0012 airfoil.
 $R_n = 3.0$, $M = 0.70$; transition fixed.

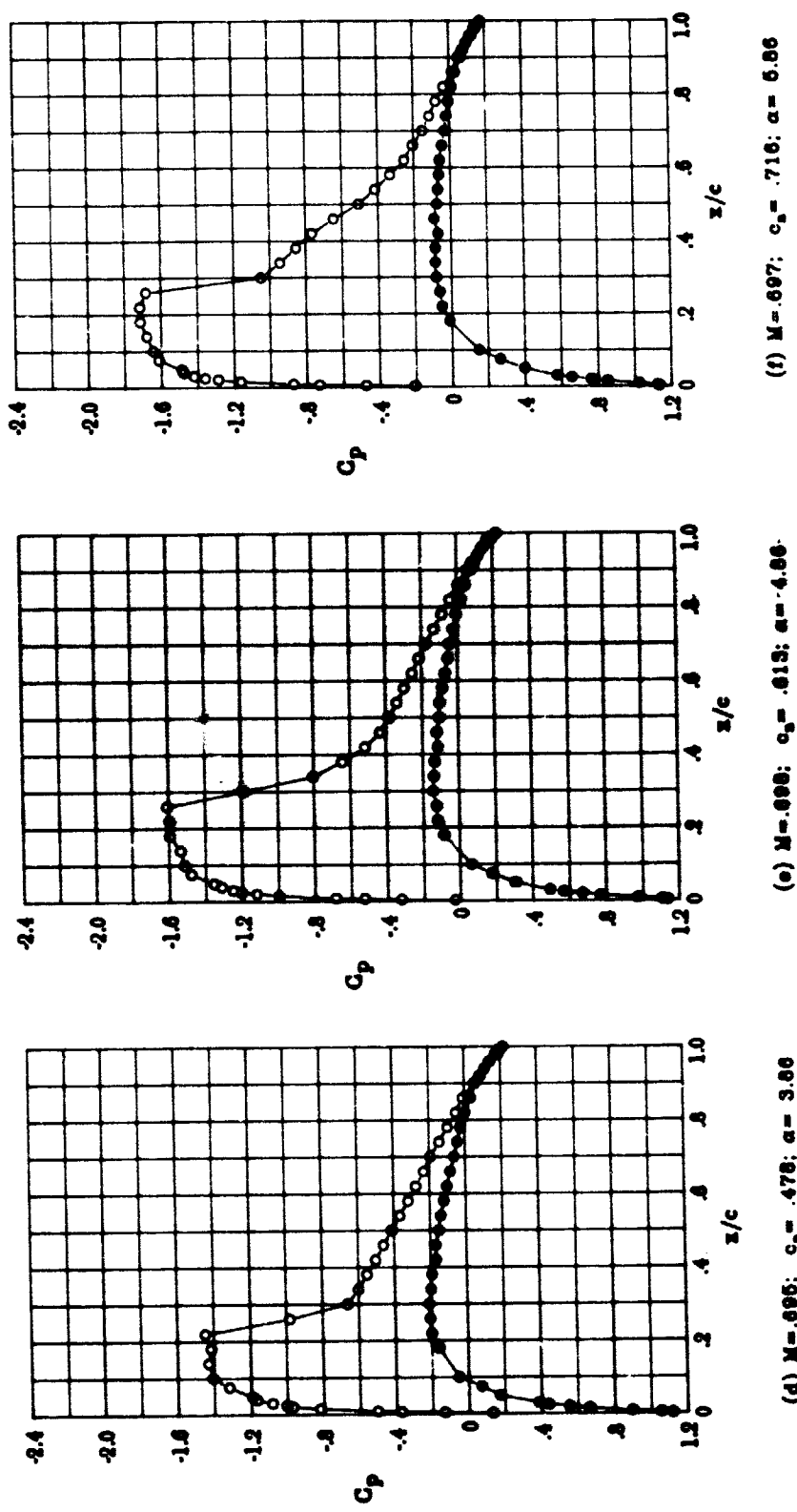
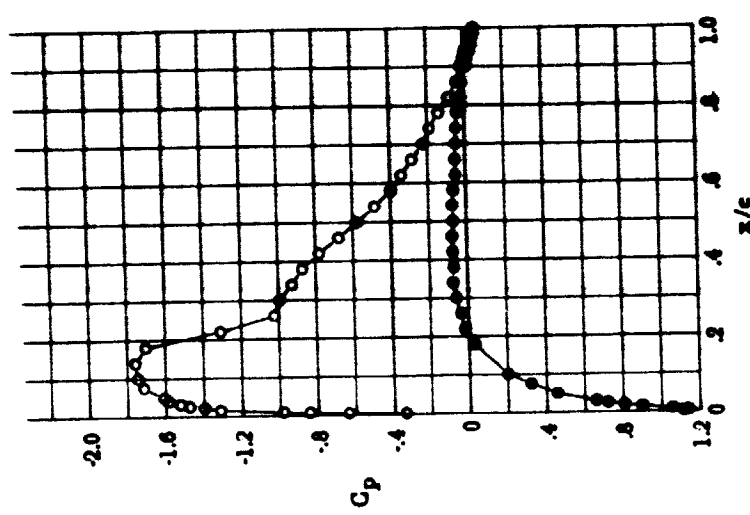


Figure 15.- Continued.



(6) $M = .99$; $c_0 = .726$; $a = 6.00$

Figure 15.- Concluded.

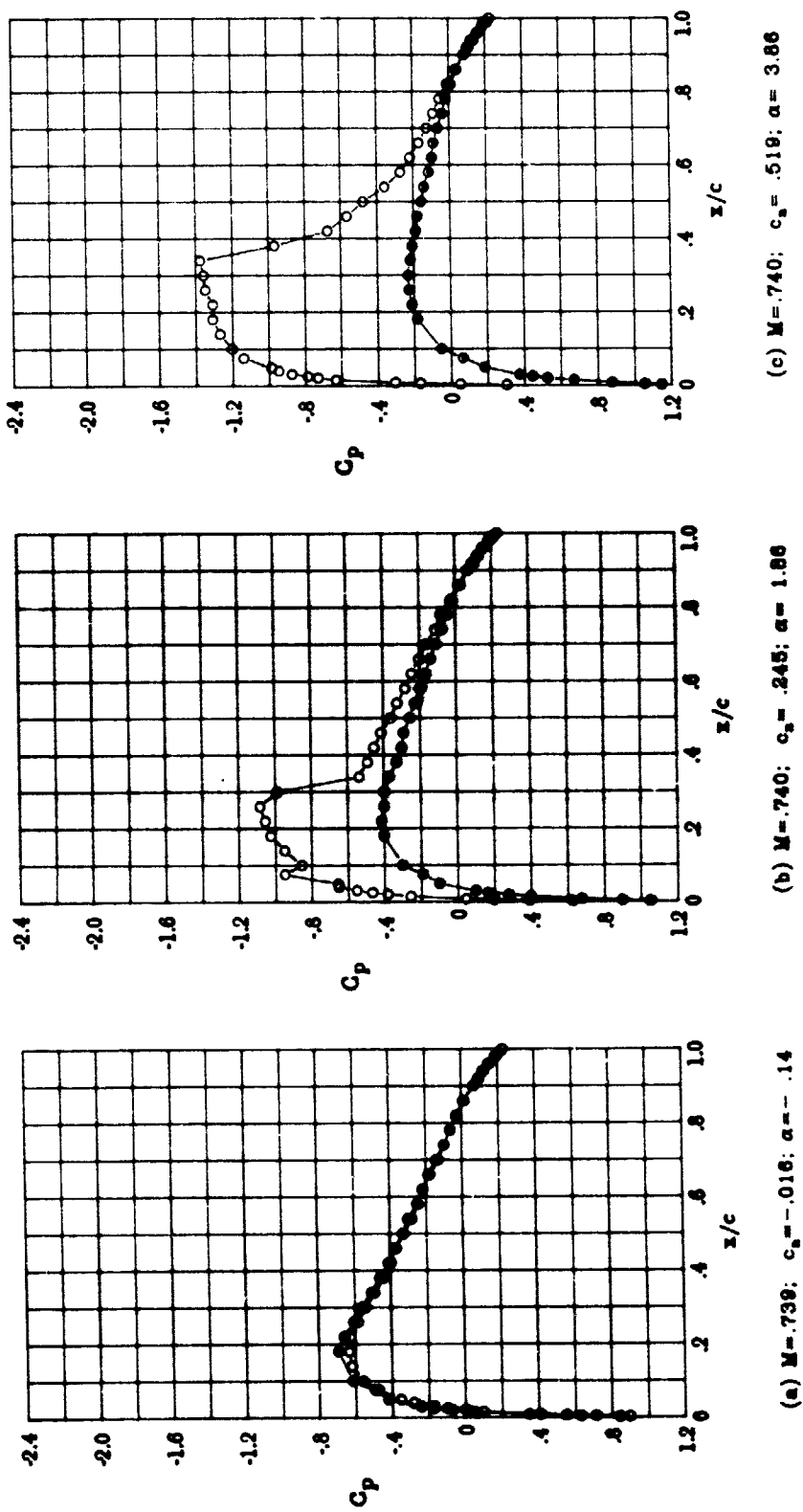
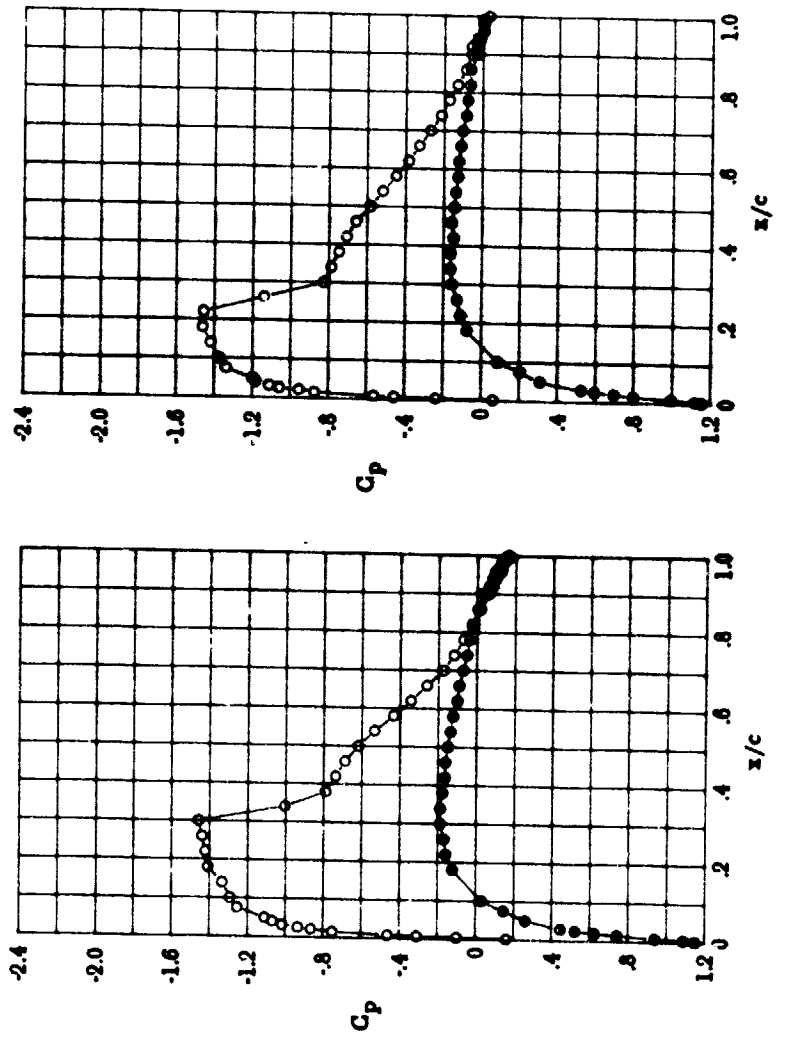
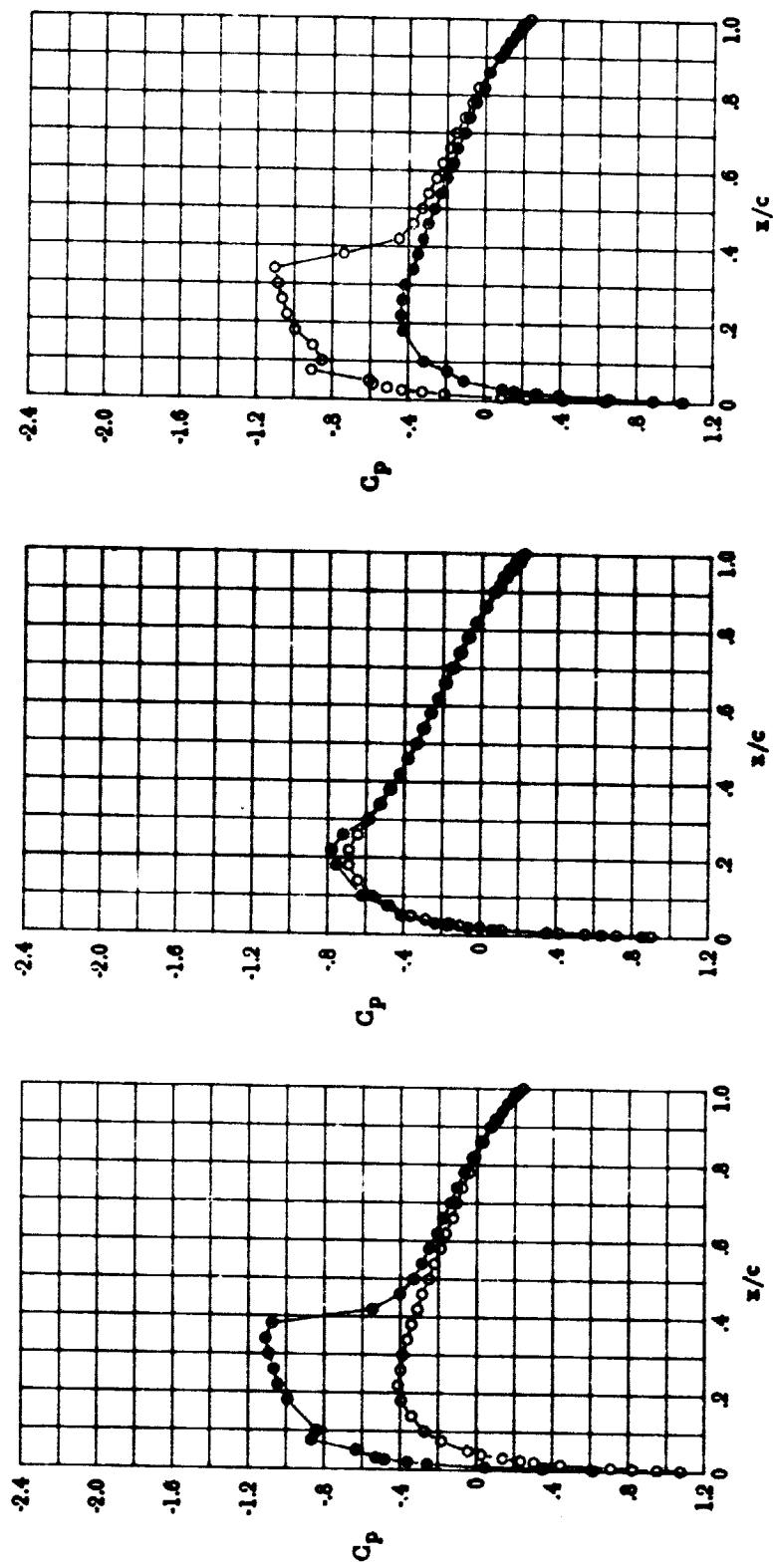


Figure 16.- Chordwise pressure distributions for NACA 0012 airfoil.
 $Rn = 3.0 \times 10^6$; $M = 0.74$; transition fixed.



(e) $M = .741; c_a = .691; \alpha = 5.86$

Figure 16.- Concluded.



(a) $M = .766; \alpha_a = -.292; \alpha = -.214$
 (b) $M = .766; \alpha_a = -.016; \alpha = -.14$
 (c) $M = .766; \alpha_a = .268; \alpha = 1.86$

Figure 17.- Chordwise pressure distributions for NACA 0012 airfoil.
 $Rn = 3.0 \times 10^6$; $M = 0.76$; transition fixed.

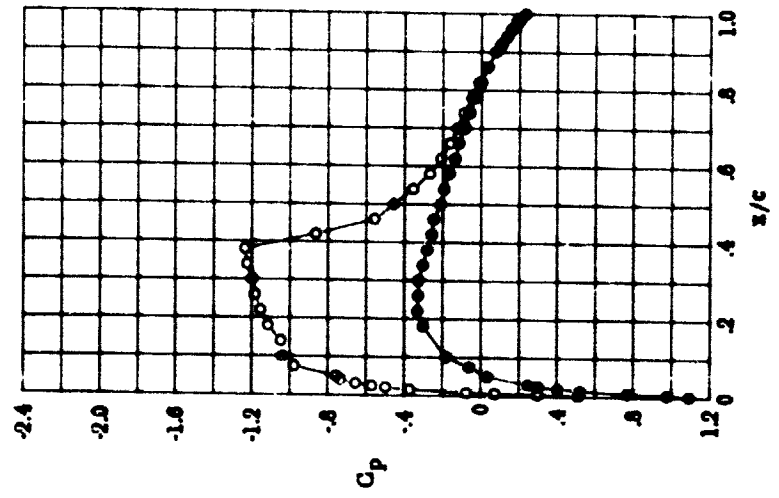
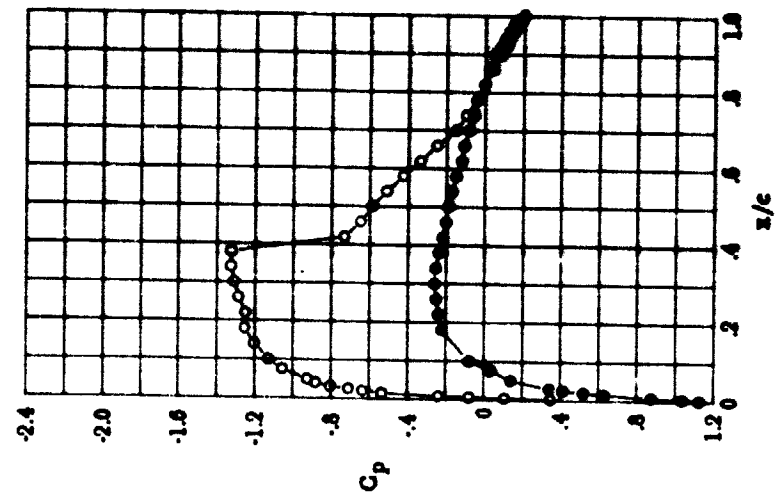
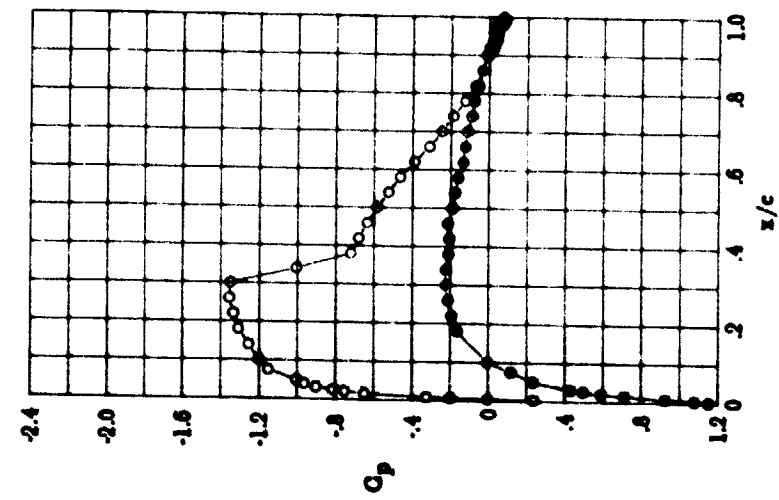
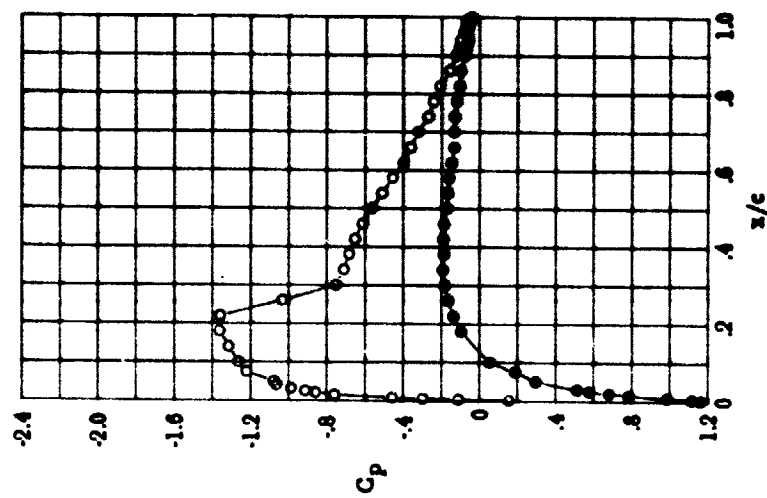


Figure 17.- Continued.



(d) $M = .760; \alpha_0 = .598; \alpha = 6.86$

Figure 17.- Concluded.

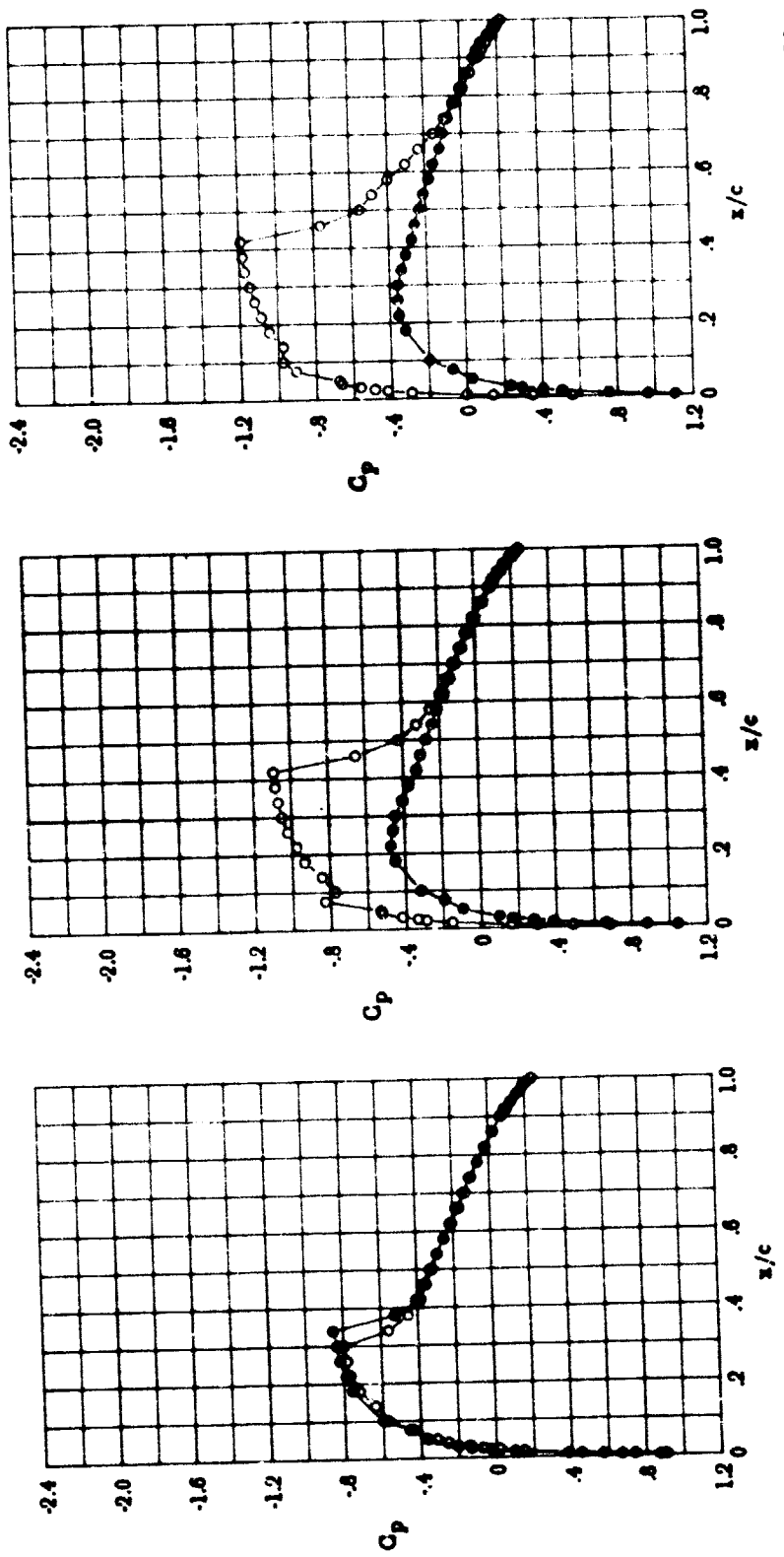
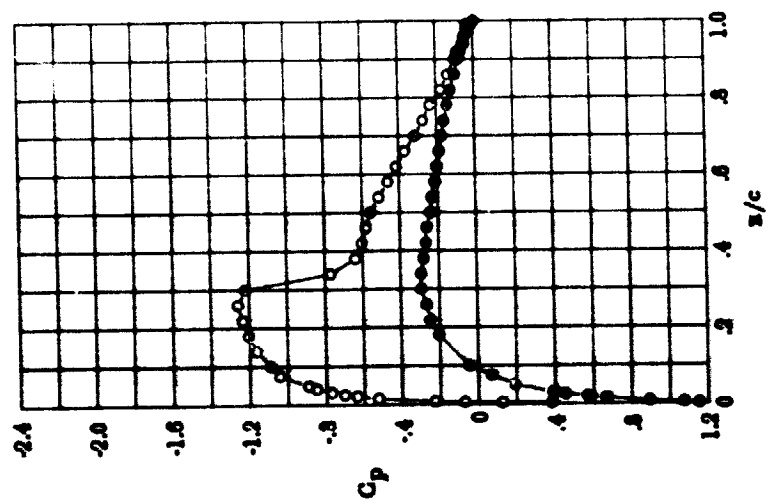


Figure 18.- Chordwise pressure distributions for NACA 0012 airfoil.
 $R_n = 3.0 \times 10^6$; $M = 0.78$; transition fixed.



(d) $M = 0.780$; $c_0 = .447$; $\alpha = 3.86$ (e) $M = 0.782$; $c_0 = .464$; $\alpha = 4.86$

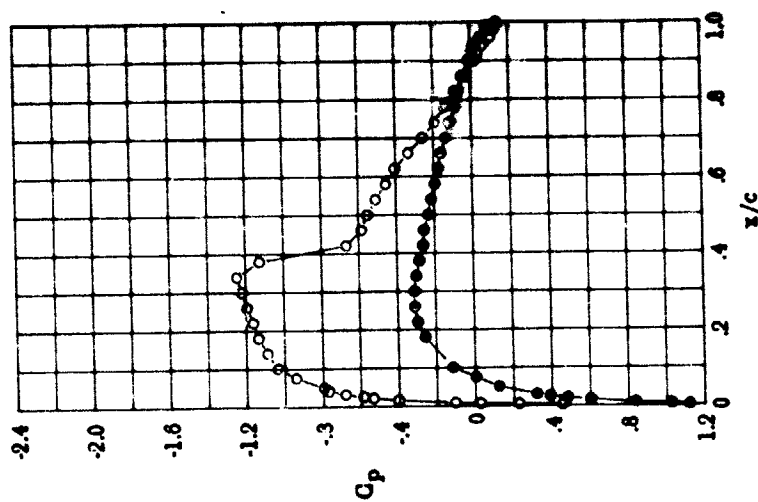


Figure 18. - Concluded.

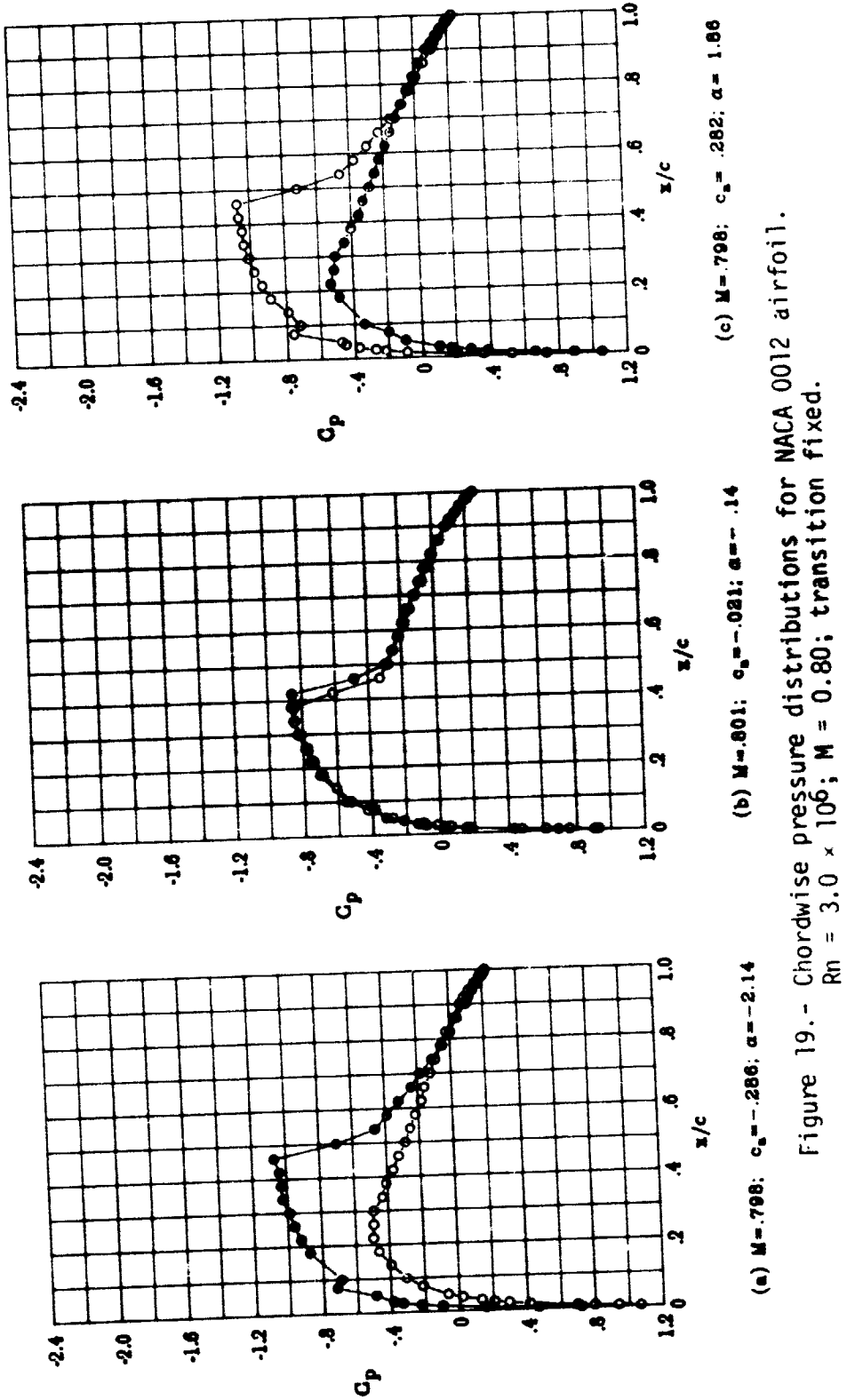
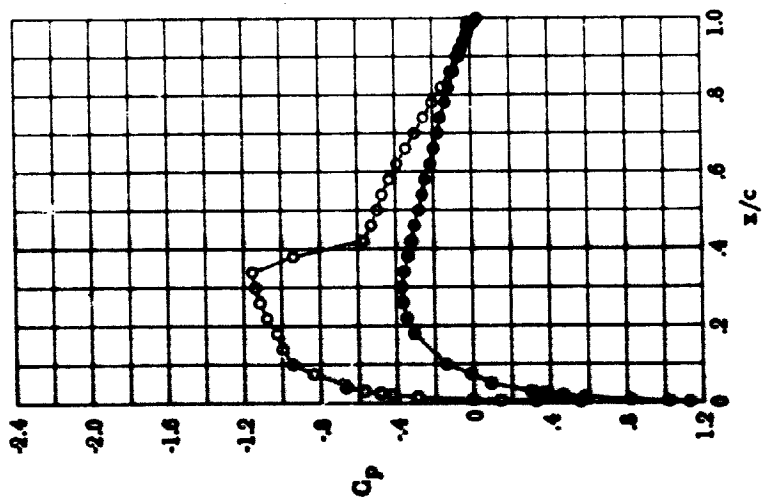
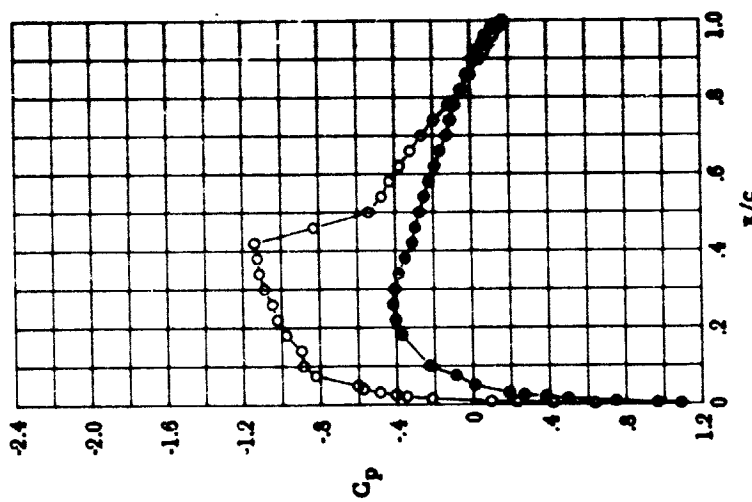


Figure 19. - Chordwise pressure distributions for NACA 0012 airfoil.
 $Rn = 3.0 \times 10^6$; $M = 0.80$; transition fixed.



(e) $M = .802; c_0 = .372; \alpha = 3.86$



(d) $M = .798; c_0 = .367; \alpha = 2.00$

Figure 19.- Concluded.

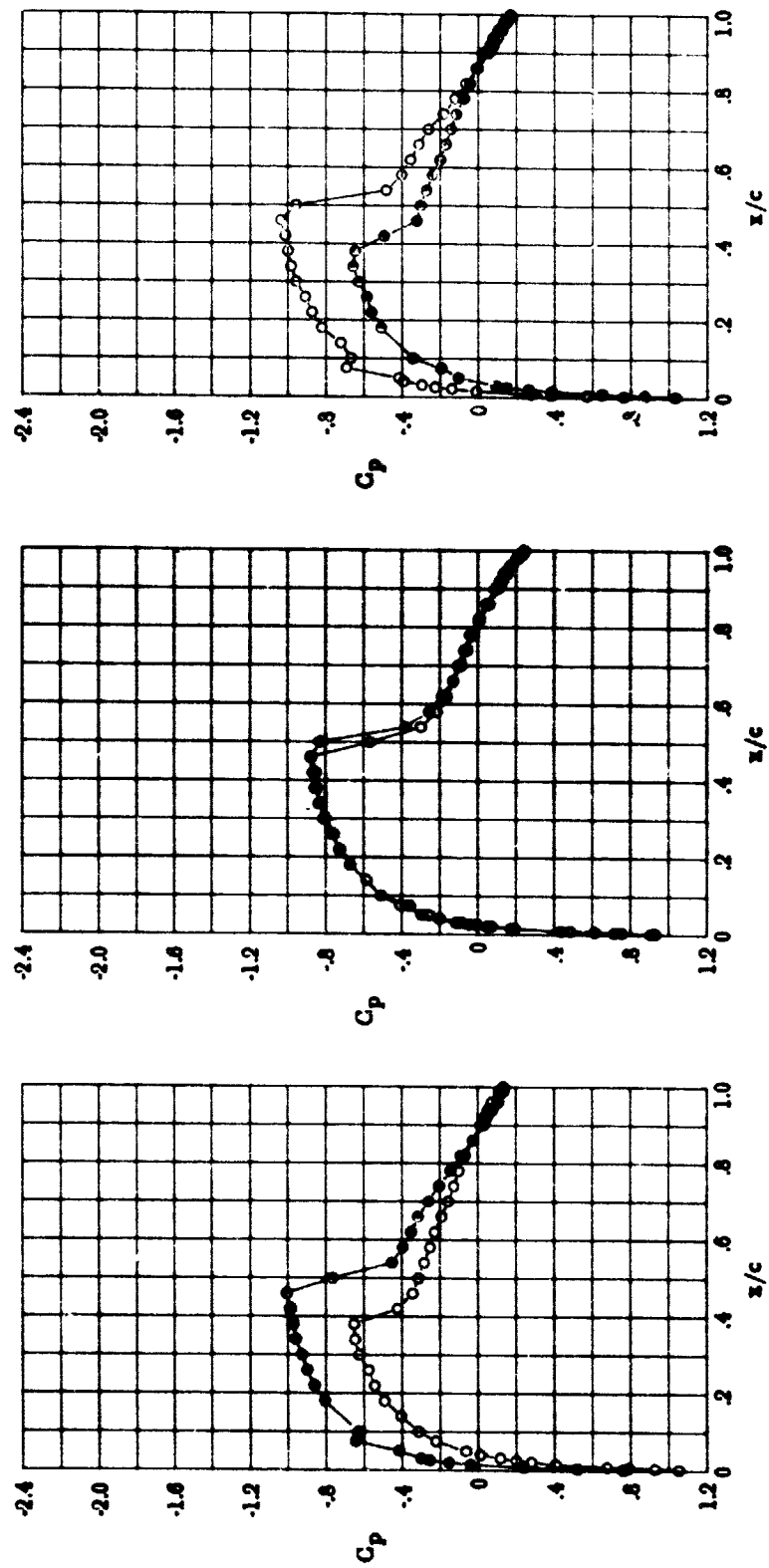


Figure 20.- Chordwise pressure distributions for NACA 0012 airfoil.
 $R_n = 3.0 \times 10^6$; $M = 0.82$; transition fixed.

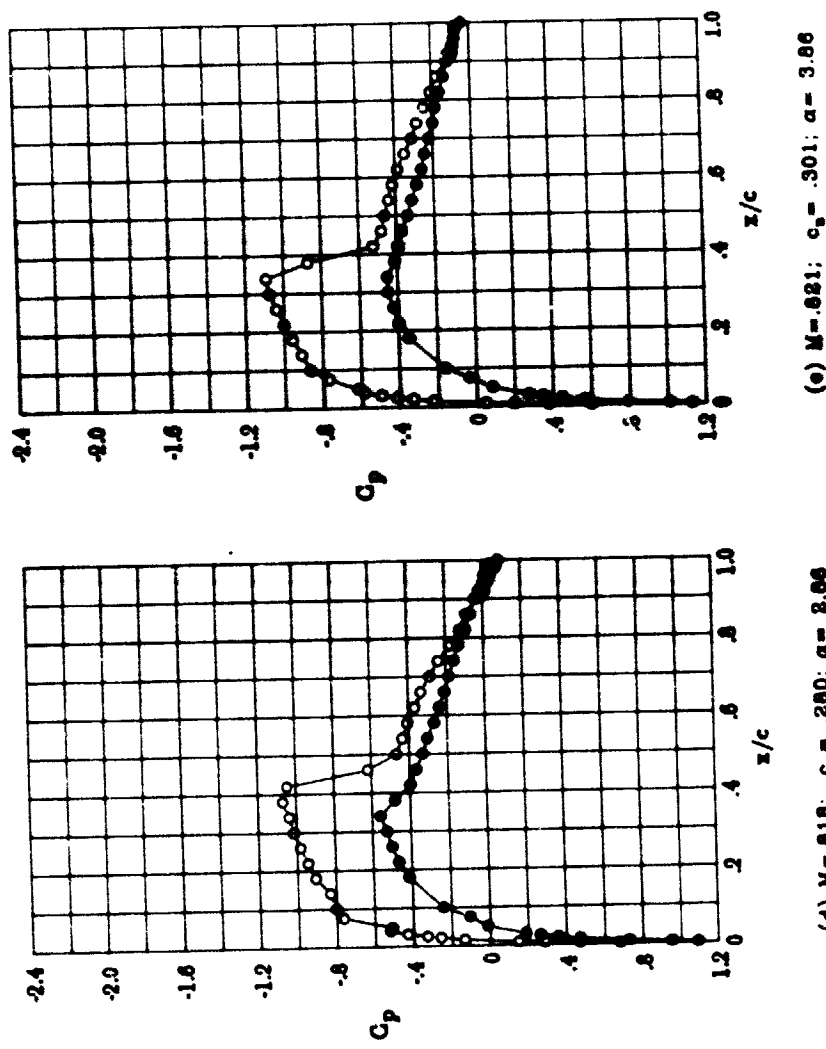


Figure 20.- Concluded.

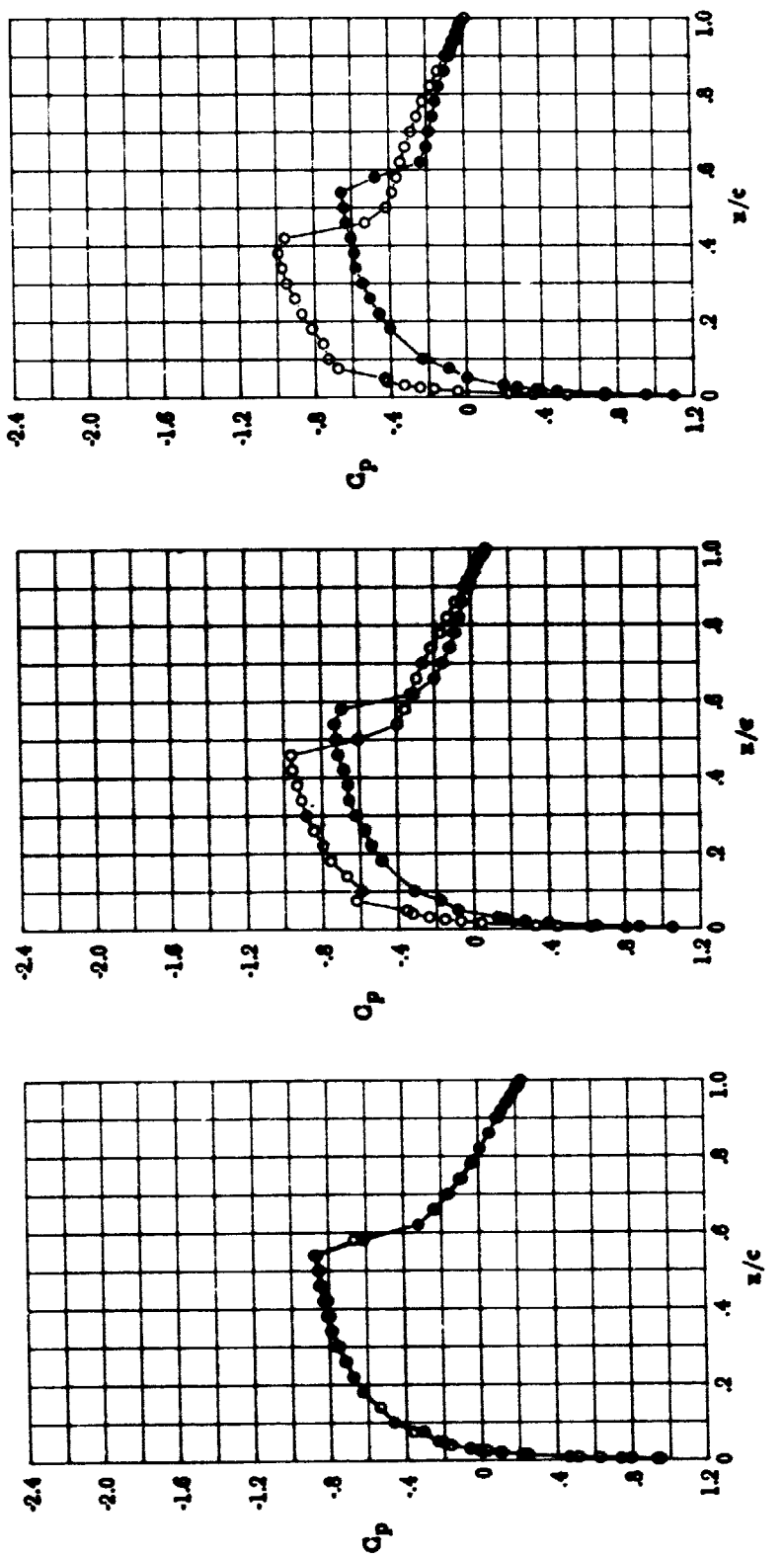
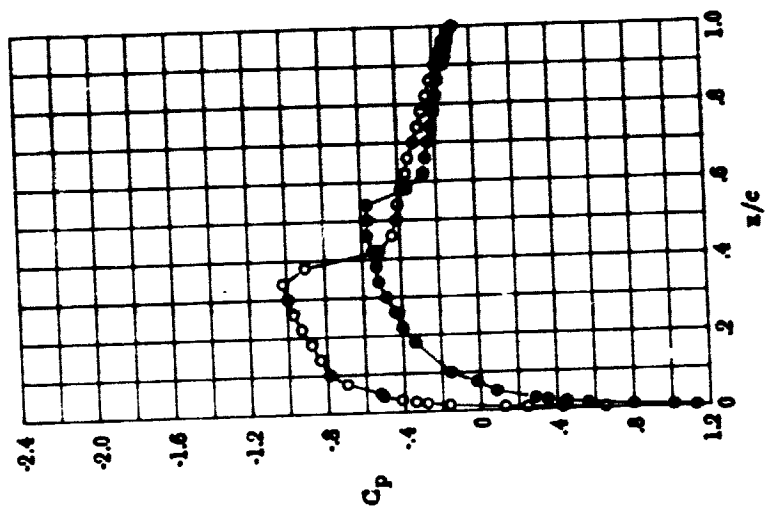


Figure 21.- Chordwise pressure distributions for NACA 0012 airfoil.
 $R_n = 3.0 \times 10^6$; $M = 0.84$; transition fixed.



(d) $M=0.41; c_0= .226; \alpha= 3.00$

Figure 21.- Concluded.

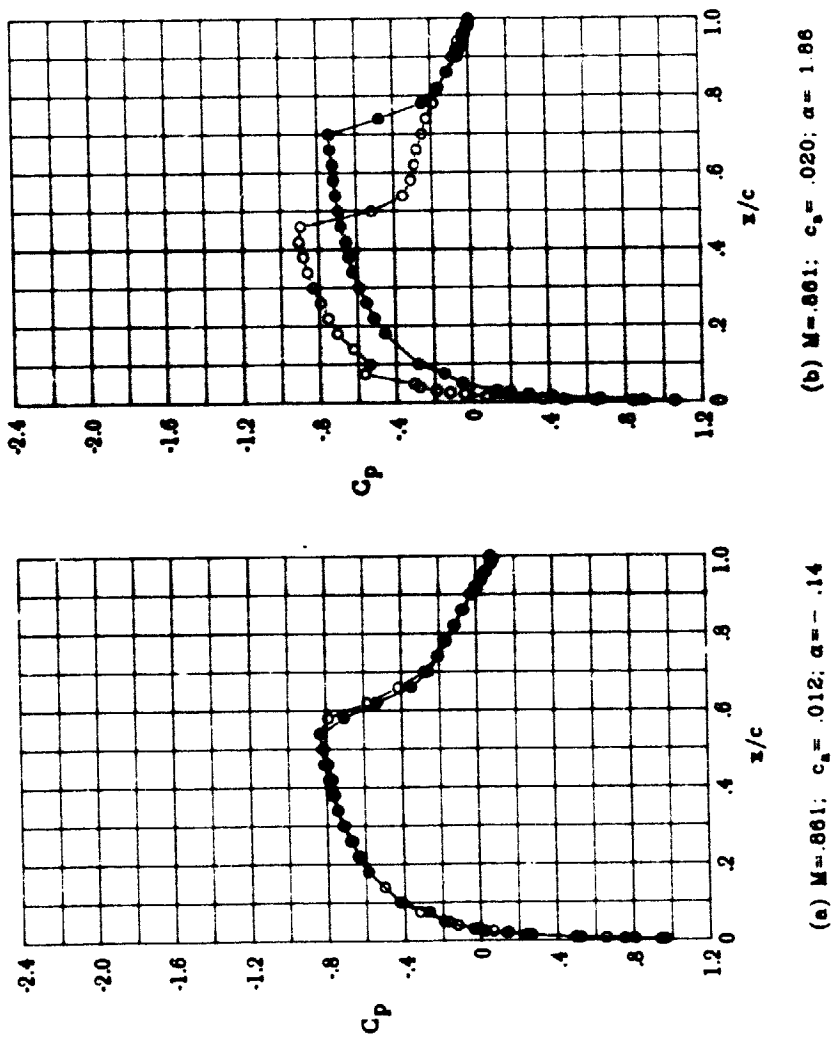
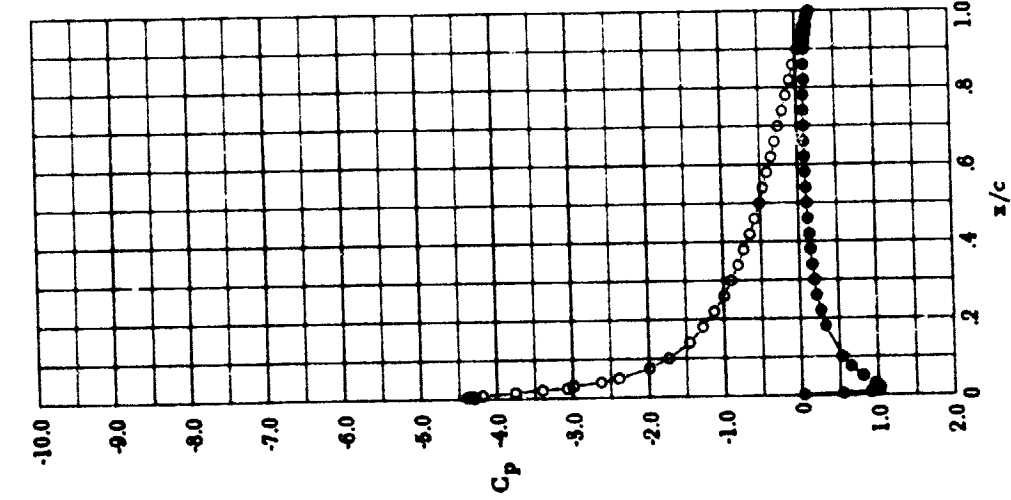
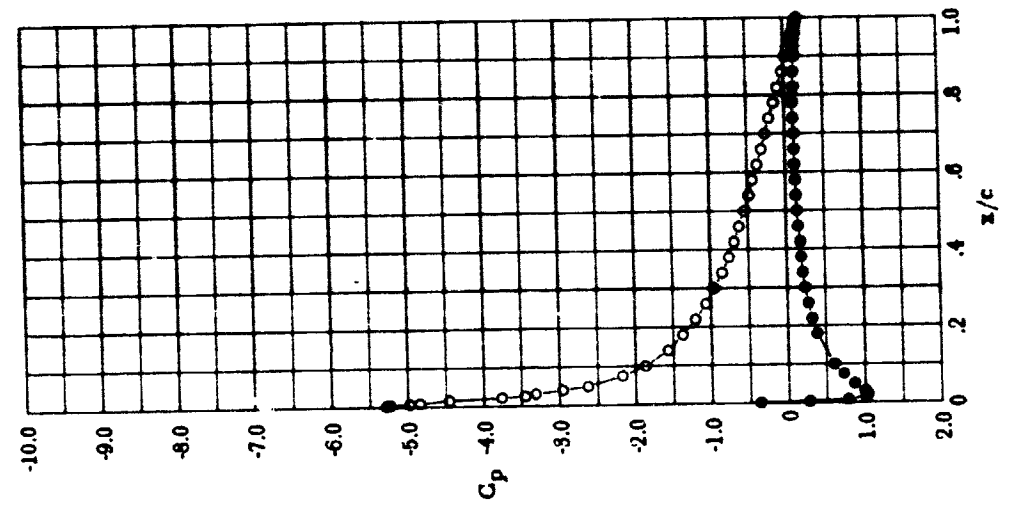


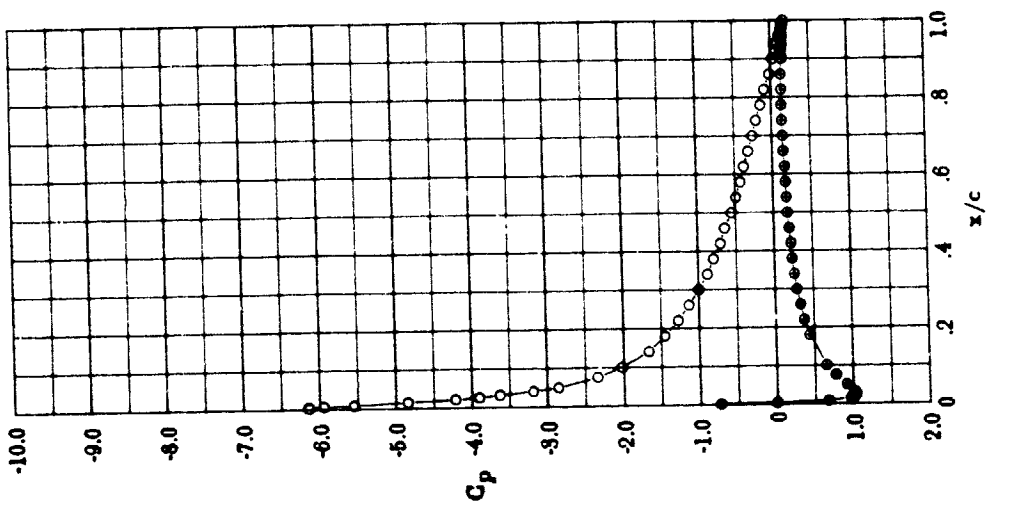
Figure 22. - Chordwise pressure distributions for NACA 0012 airfoil.
 $Rn = 3.0 \times 10^6; M = 0.86$; transition fixed.



(a) $M = .302$; $c_s = .960$; $\alpha = 9.86$



(b) $M = .301$; $c_s = 1.063$; $\alpha = 10.86$



(c) $M = .301$; $c_s = 1.138$; $\alpha = 11.86$

Figure 23. - Chordwise pressure distributions for NACA 0012 airfoil.
 $Rn = 6.0 \times 10^6$; $M = 0.30$; transition fixed.

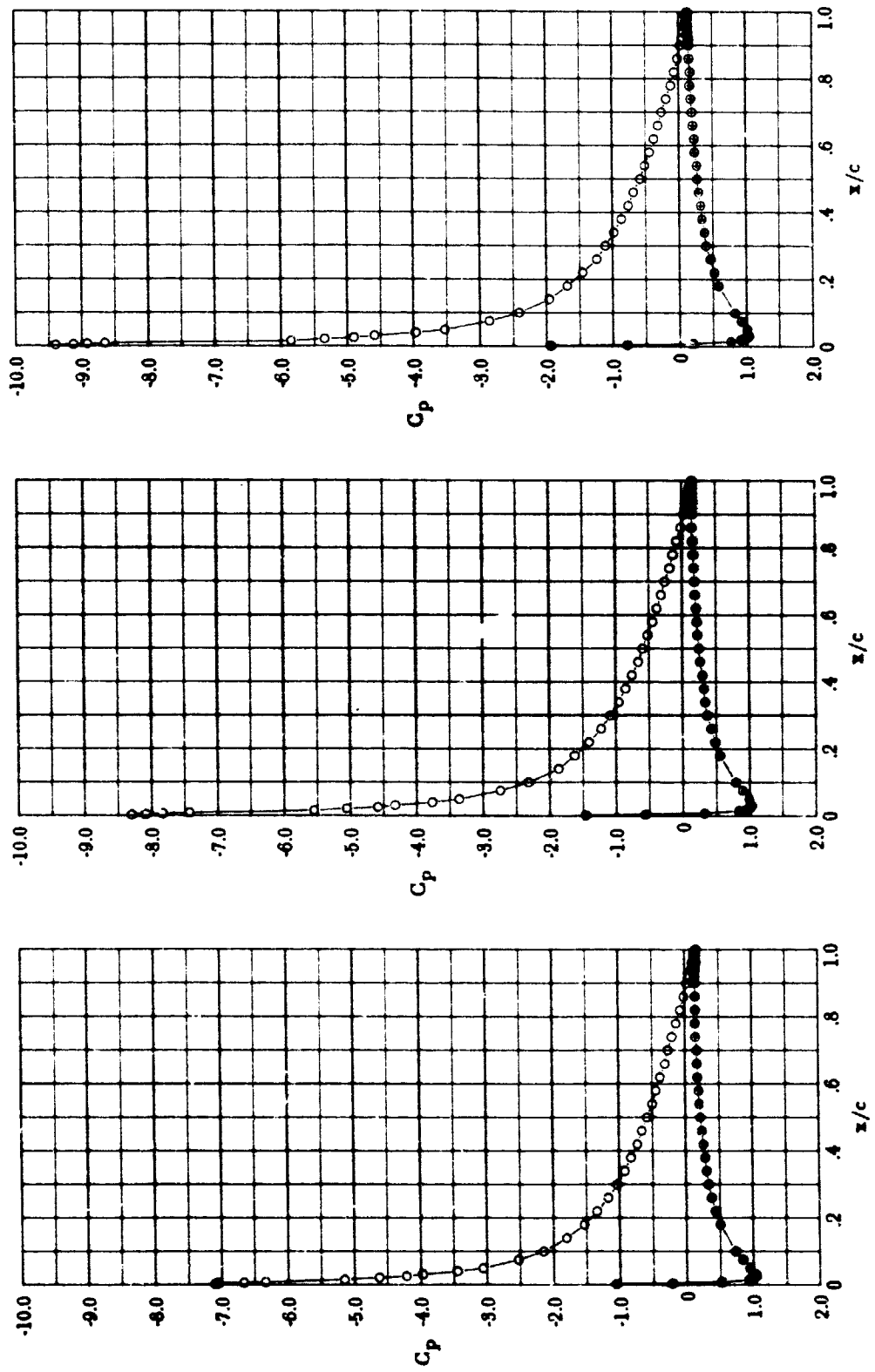
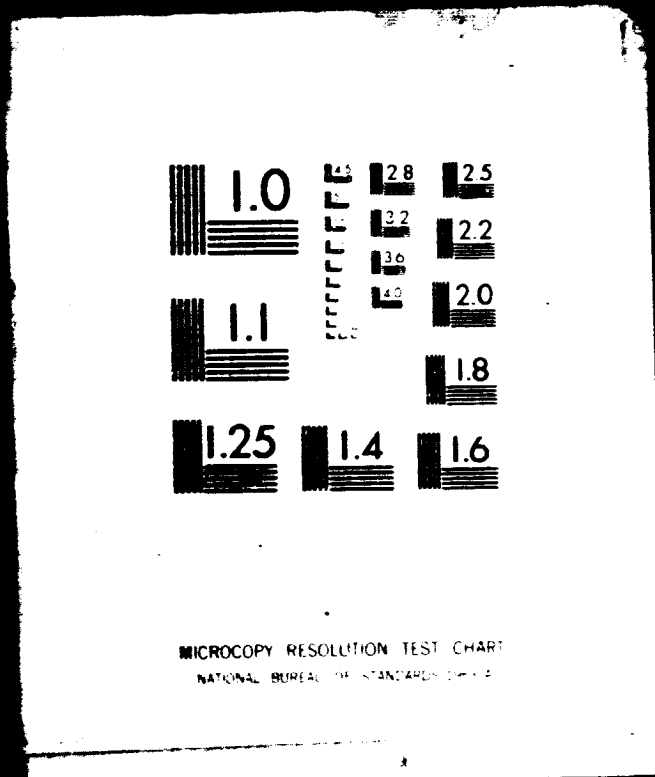


Figure 23.- Concluded.

20F2

N8I-23036

INCLAS



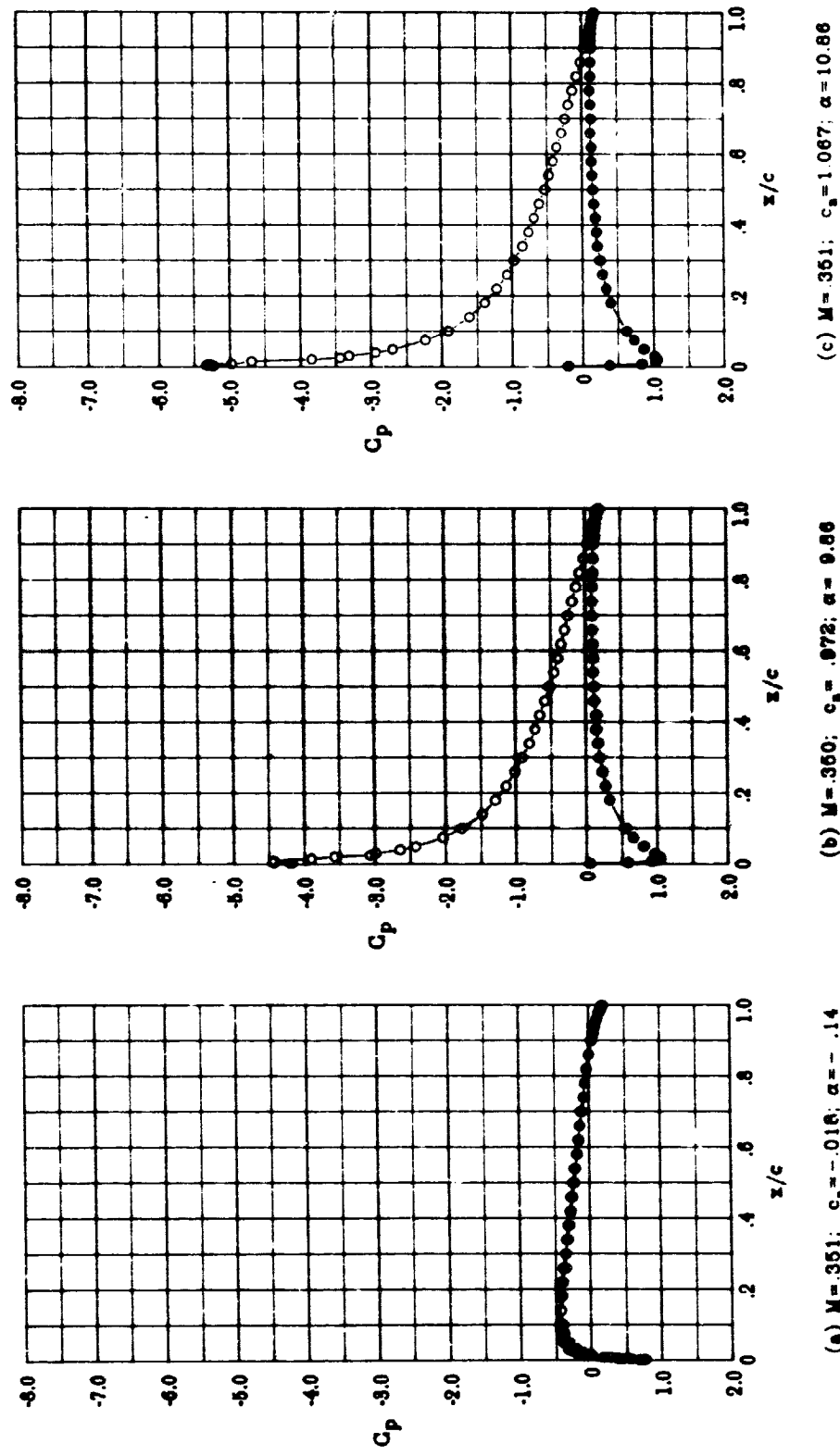


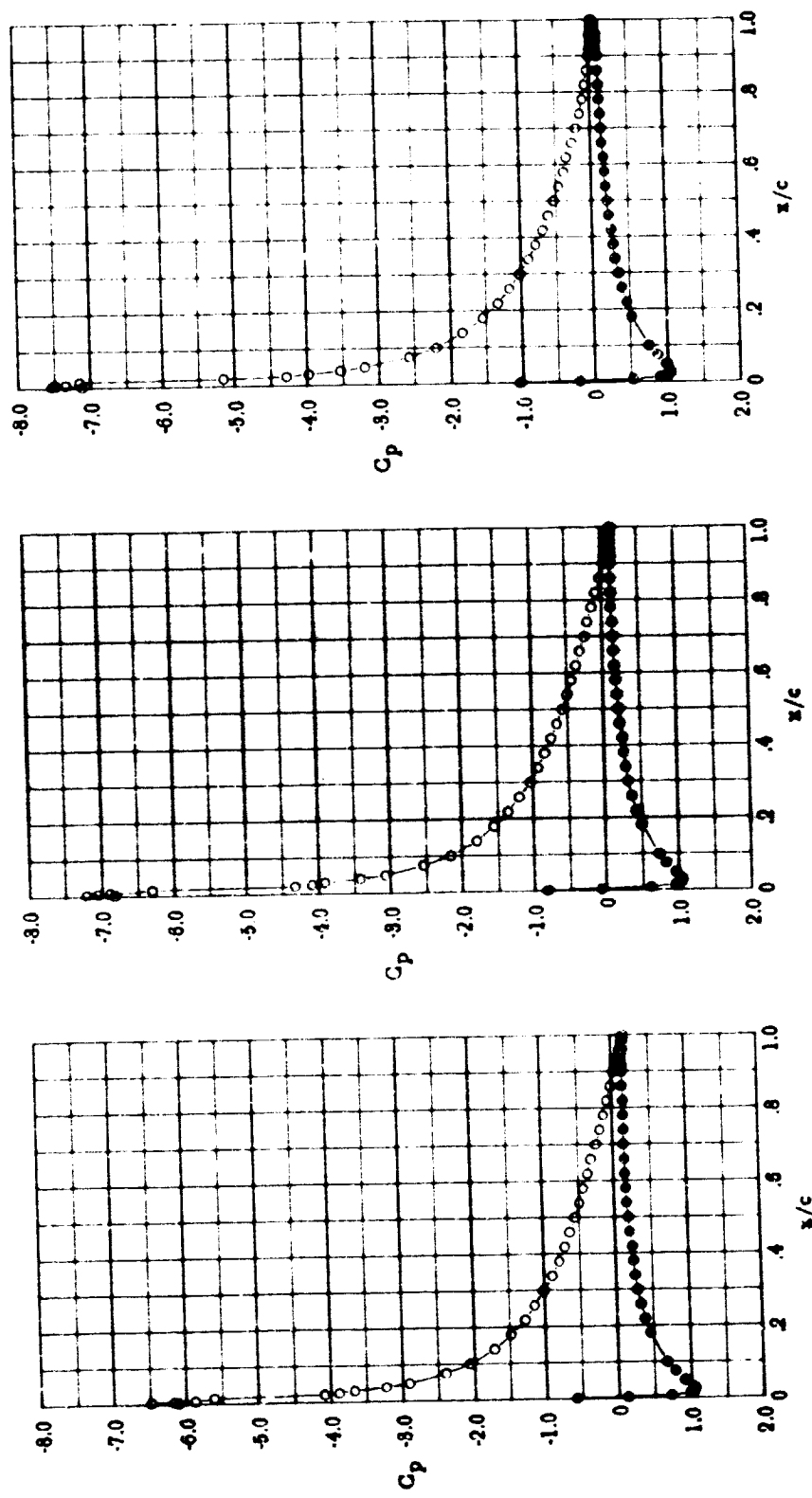
Figure 24.- Chordwise pressure distributions for NACA 0012 airfoil.
 $R_n = 6.0 \times 10^6$; $M = 0.35$; transition fixed.

(f) $M = 3.61; c_a = 1.229; \alpha = 13.86$

(e) $M = .349; c_a = 1.323; \alpha = 12.86$

(d) $M = .351; c_a = 1.156; \alpha = 11.86$

Figure 24.- Concluded.



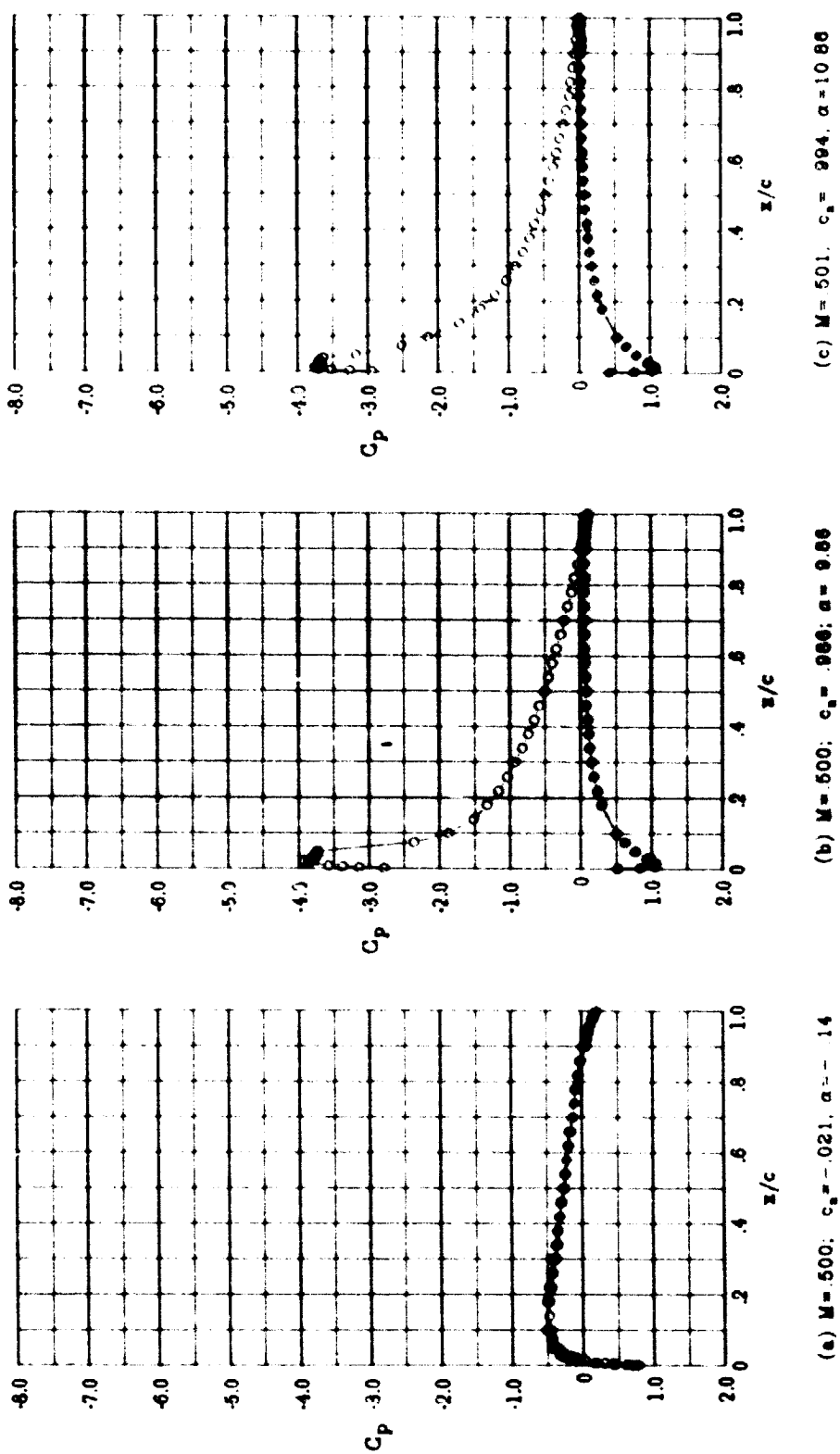


Figure 25.- Chordwise pressure distributions for NACA 0012 airfoil.
 $R_n = 6.0 - 106; M = 0.50$; transition fixed.

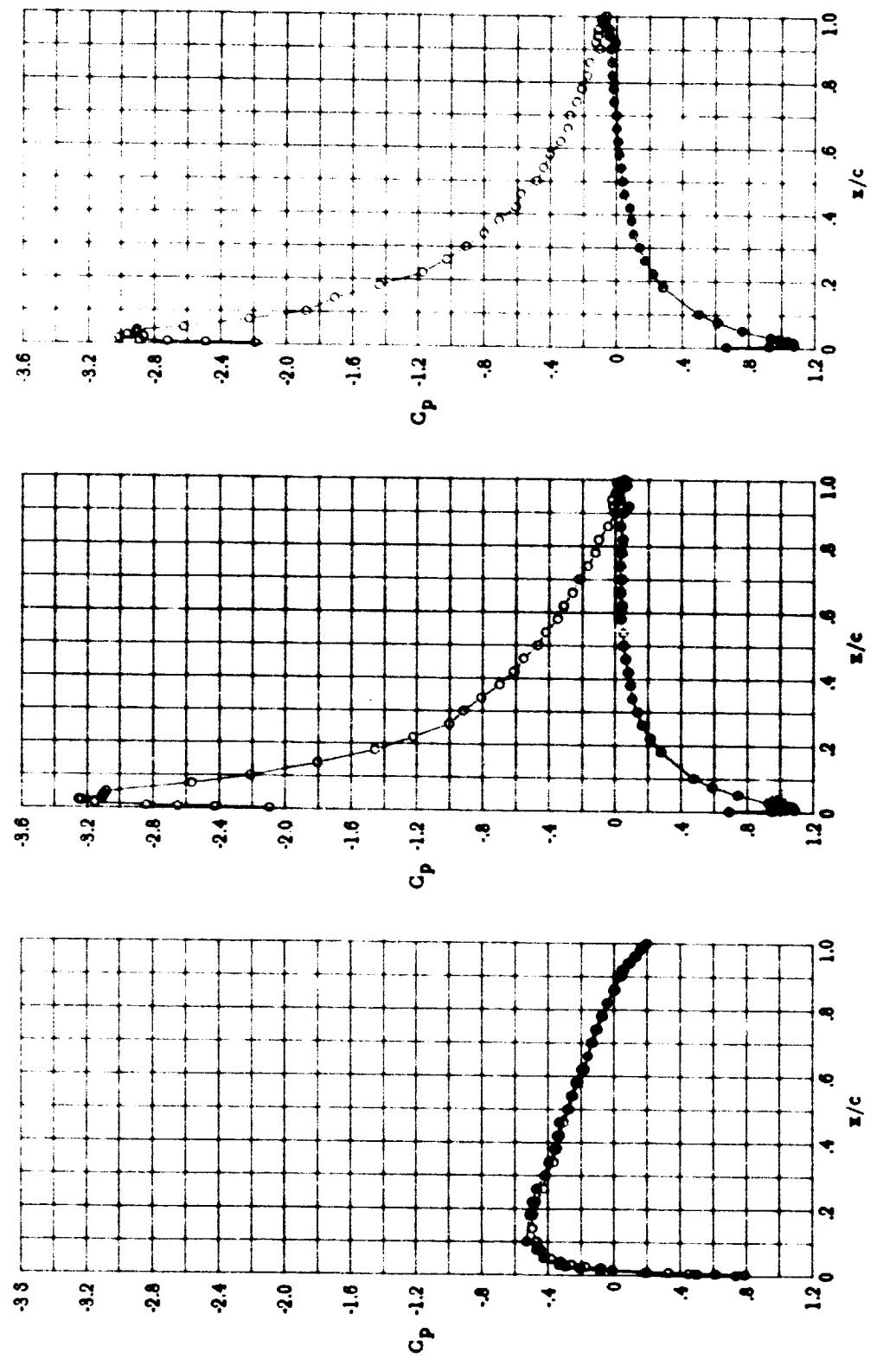


Figure 26.- Chordwise pressure distributions for NACA 0012 airfoil.
 $Rn = 6.0 , 10^6 ; M = 0.55$; transition fixed.

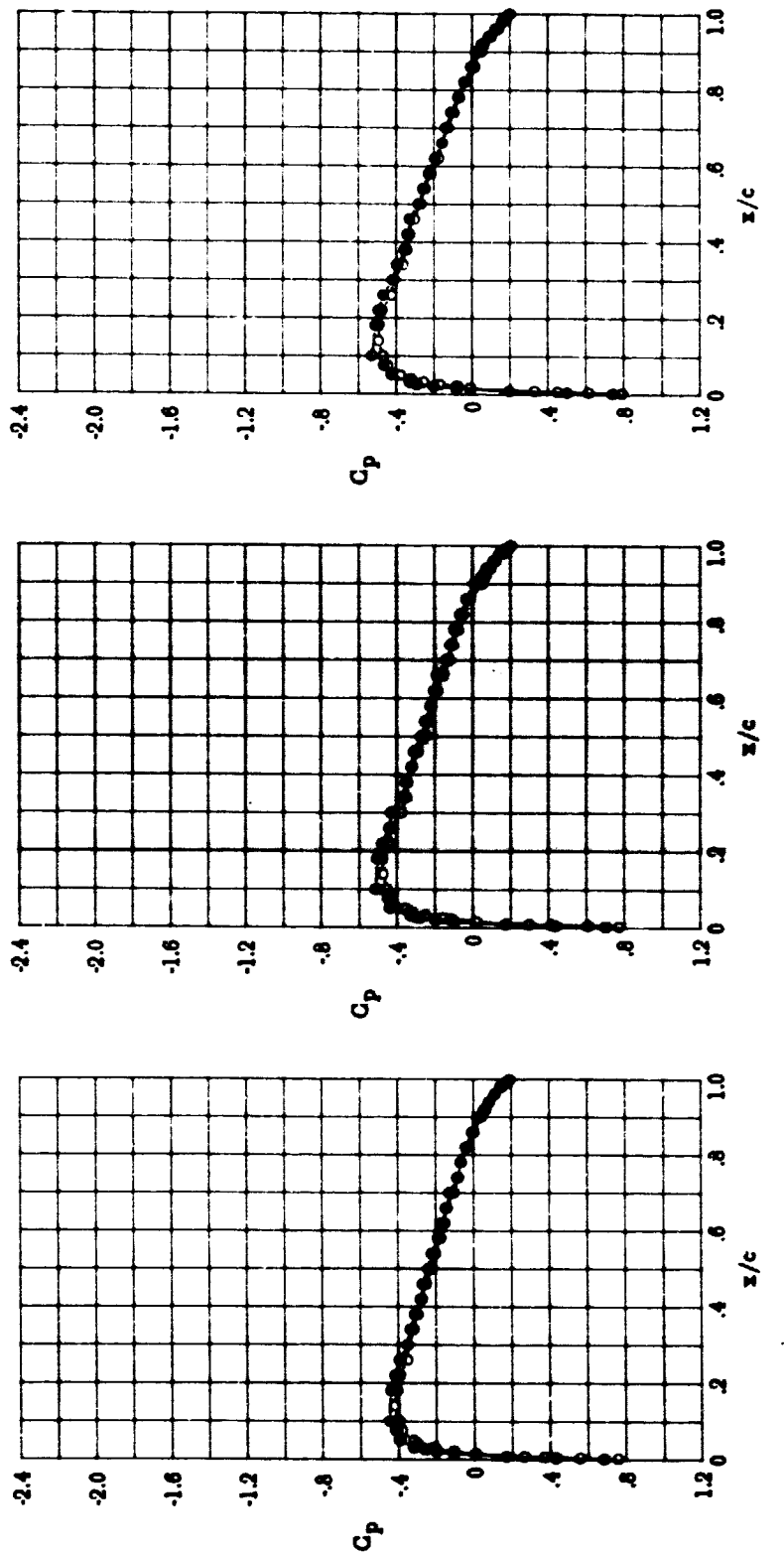
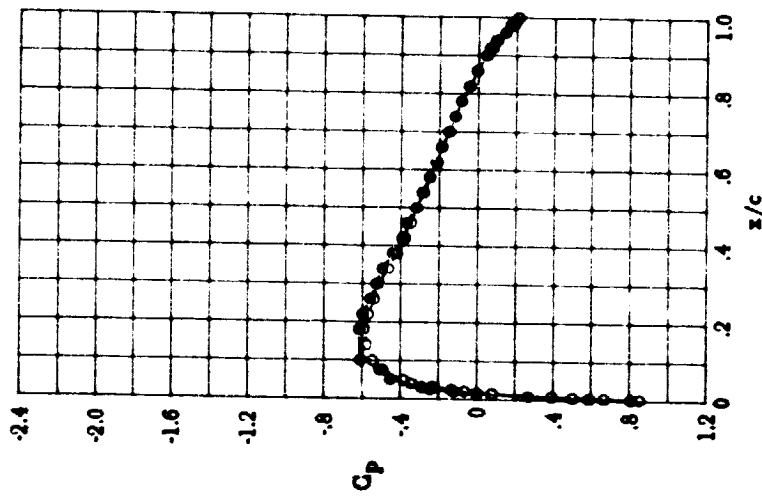
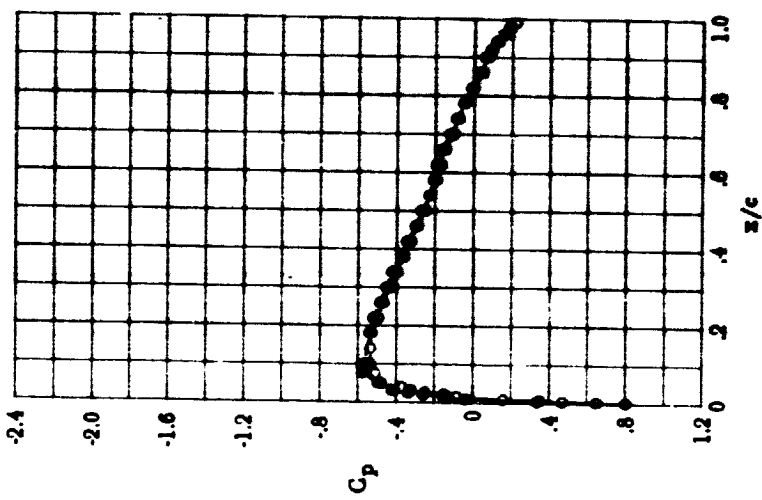


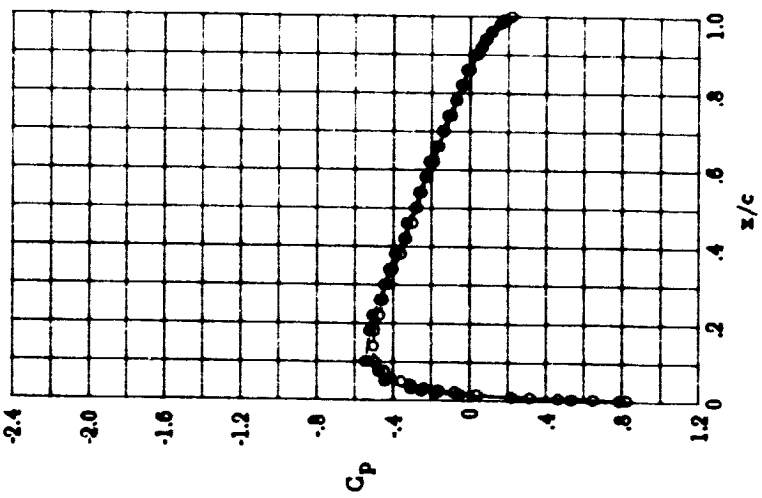
Figure 27. - Chordwise pressure distributions for NACA 0012 airfoil.
 $Rn = 6.0 \times 10^6$; transition fixed; angle of attack near zero.



(f) $M = 7.00$; $c_s = -0.013$; $\alpha = -.14$



(e) $M = .649$; $c_s = -.017$; $\alpha = -.14$



(d) $M = .000$; $c_s = -.017$; $\alpha = -.14$

Figure 27.- Continued.

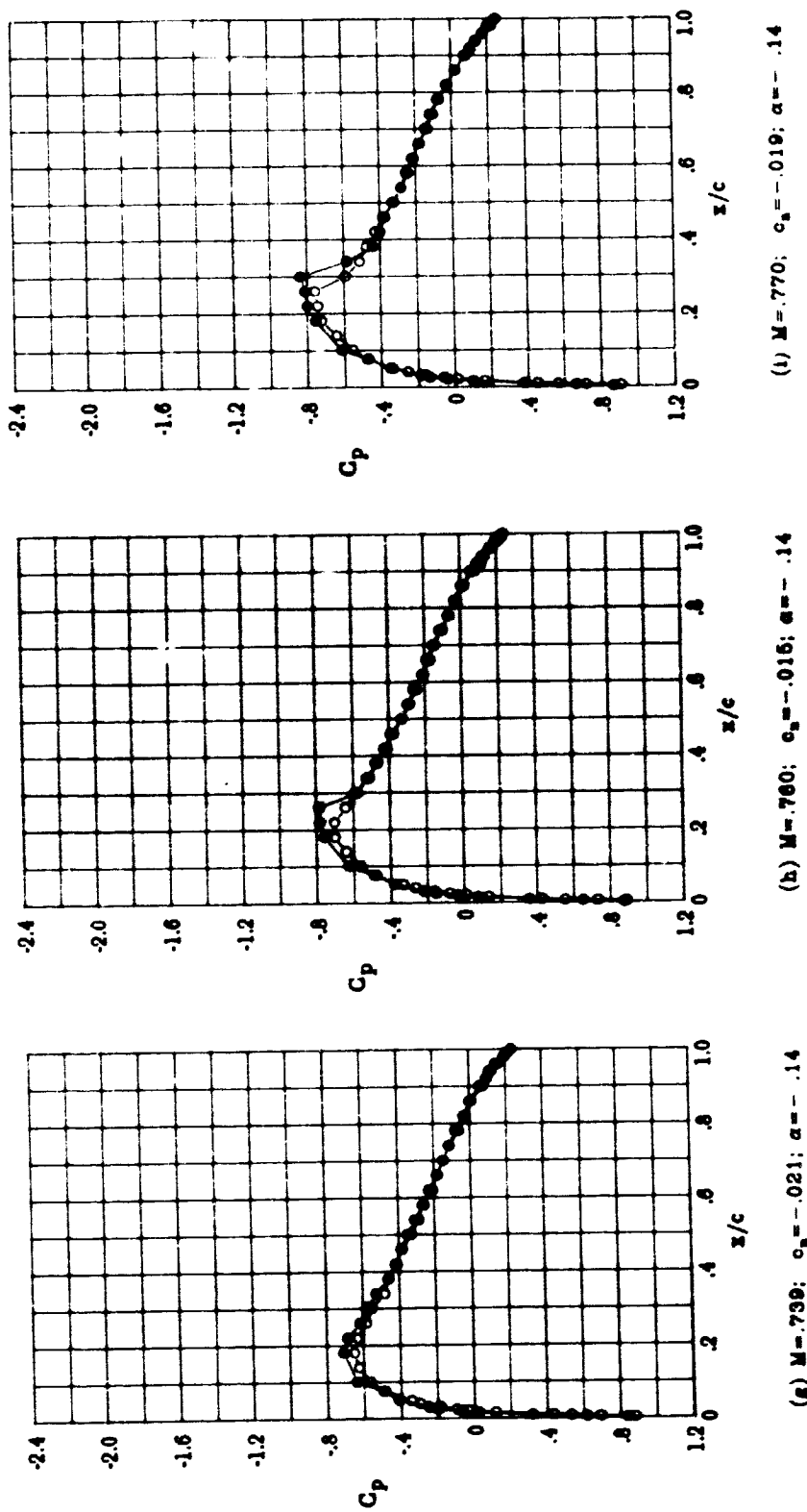


Figure 27.- Continued.

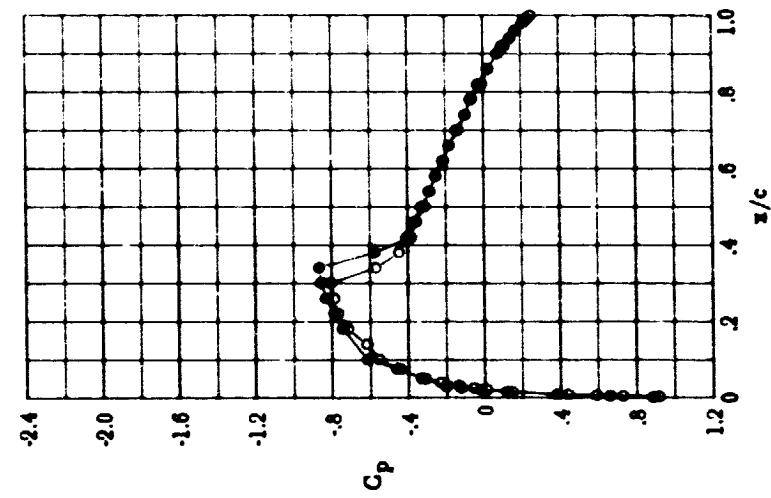
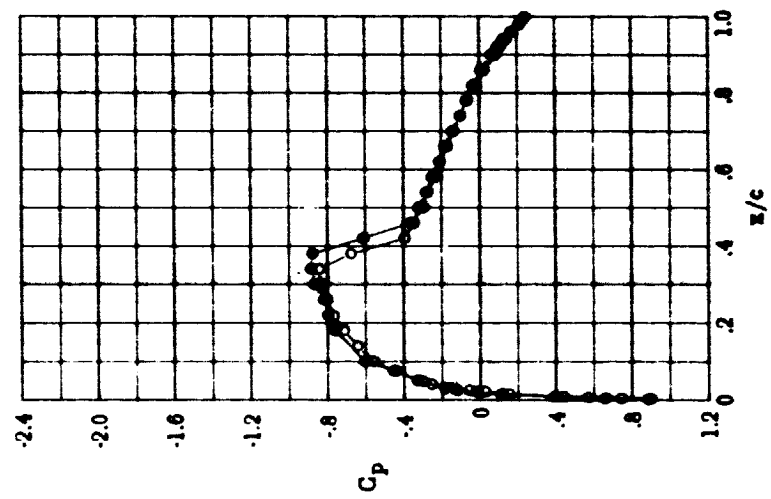
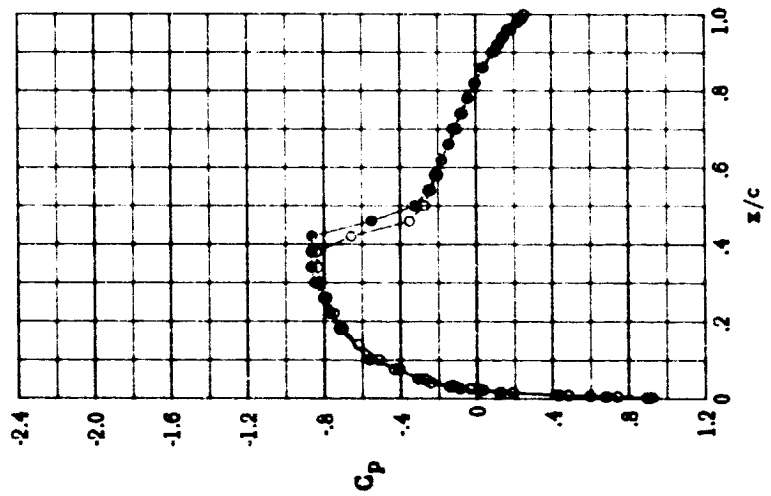


Figure 27.- Continued.

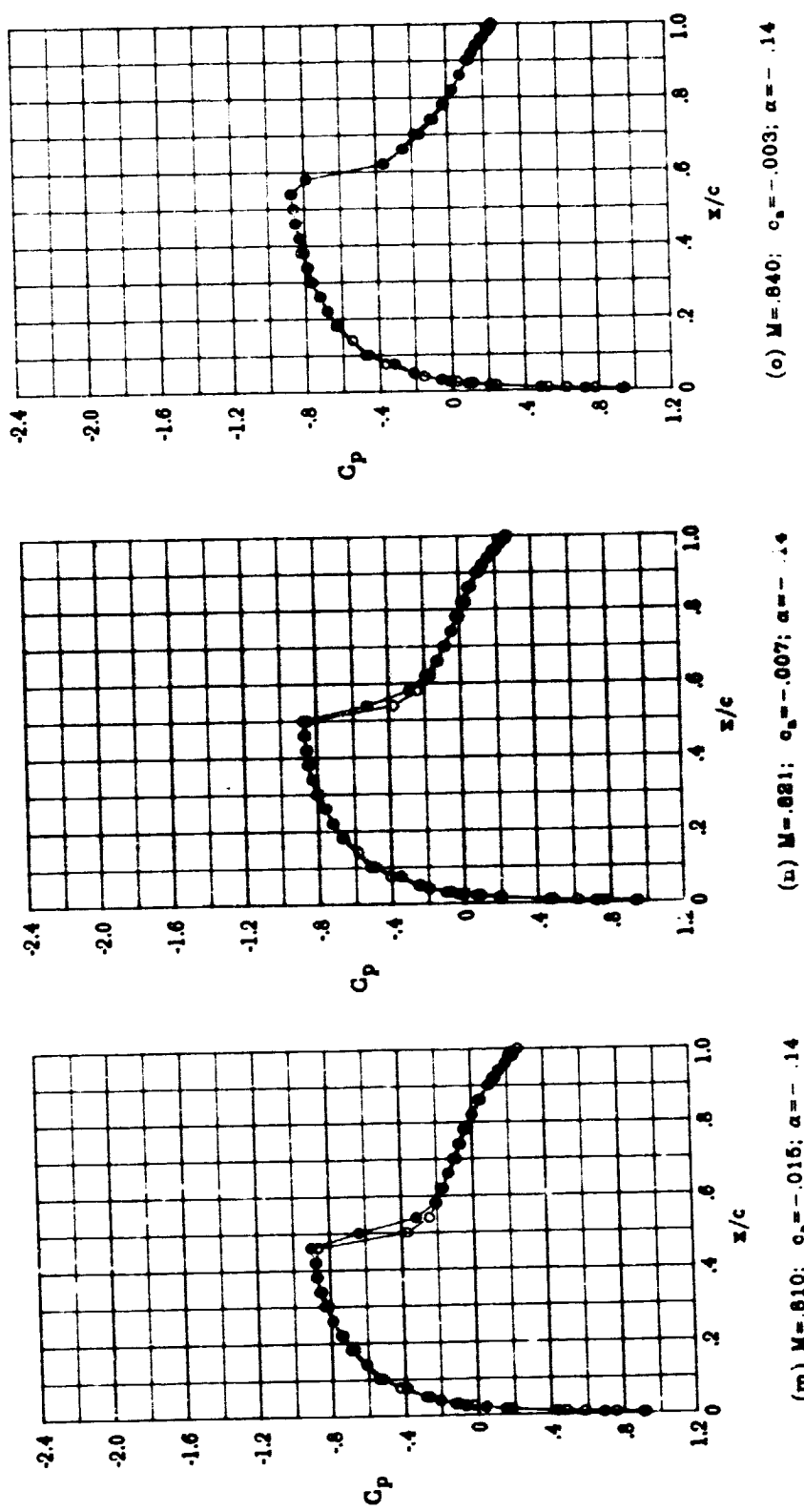


Figure 27.- Concluded.

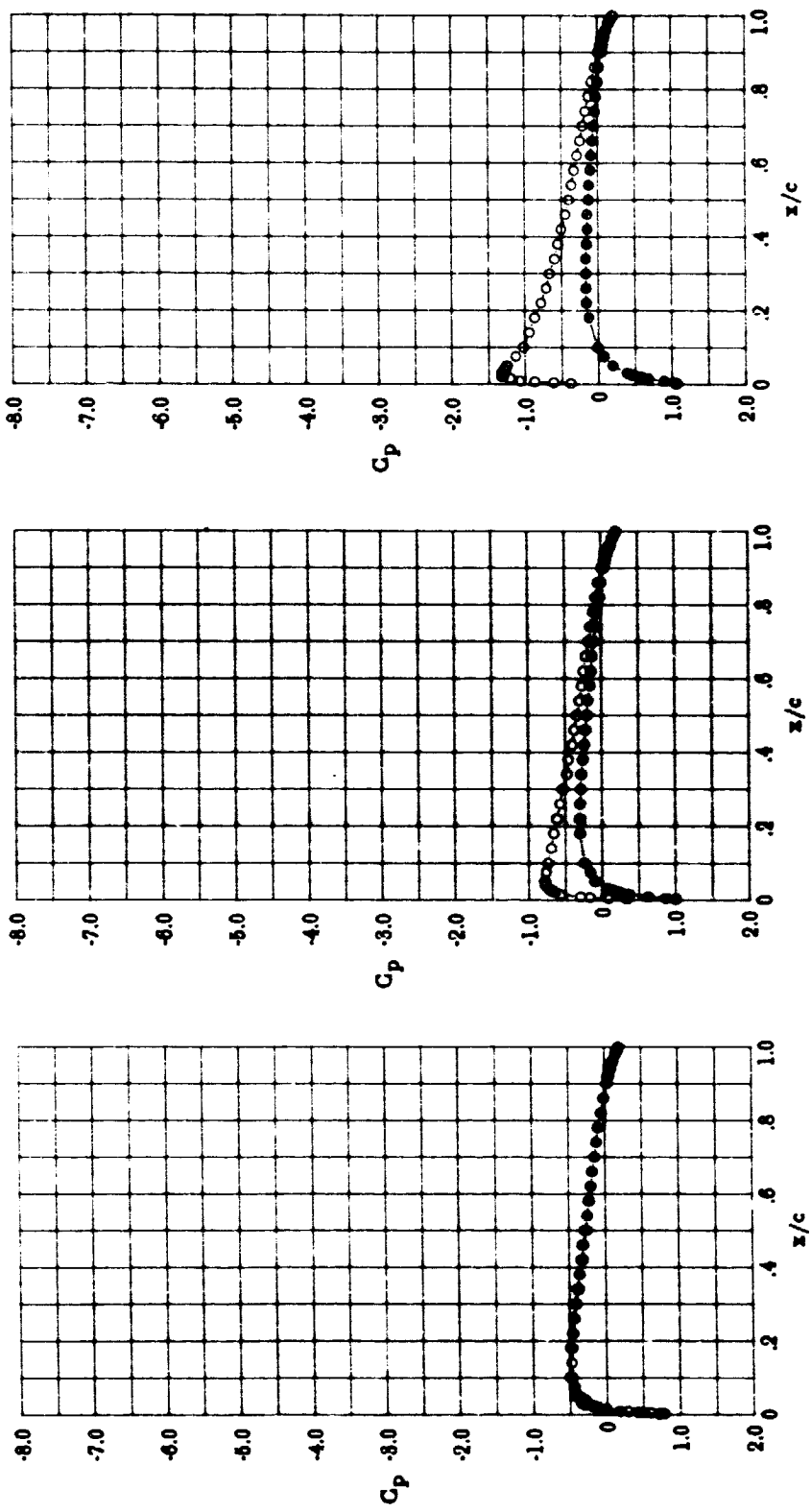


Figure 28. - Chordwise pressure distributions for NACA 0012 airfoil.
 $R_n = 9.0 \times 10^6$; $M = 0.50$; transition fixed.

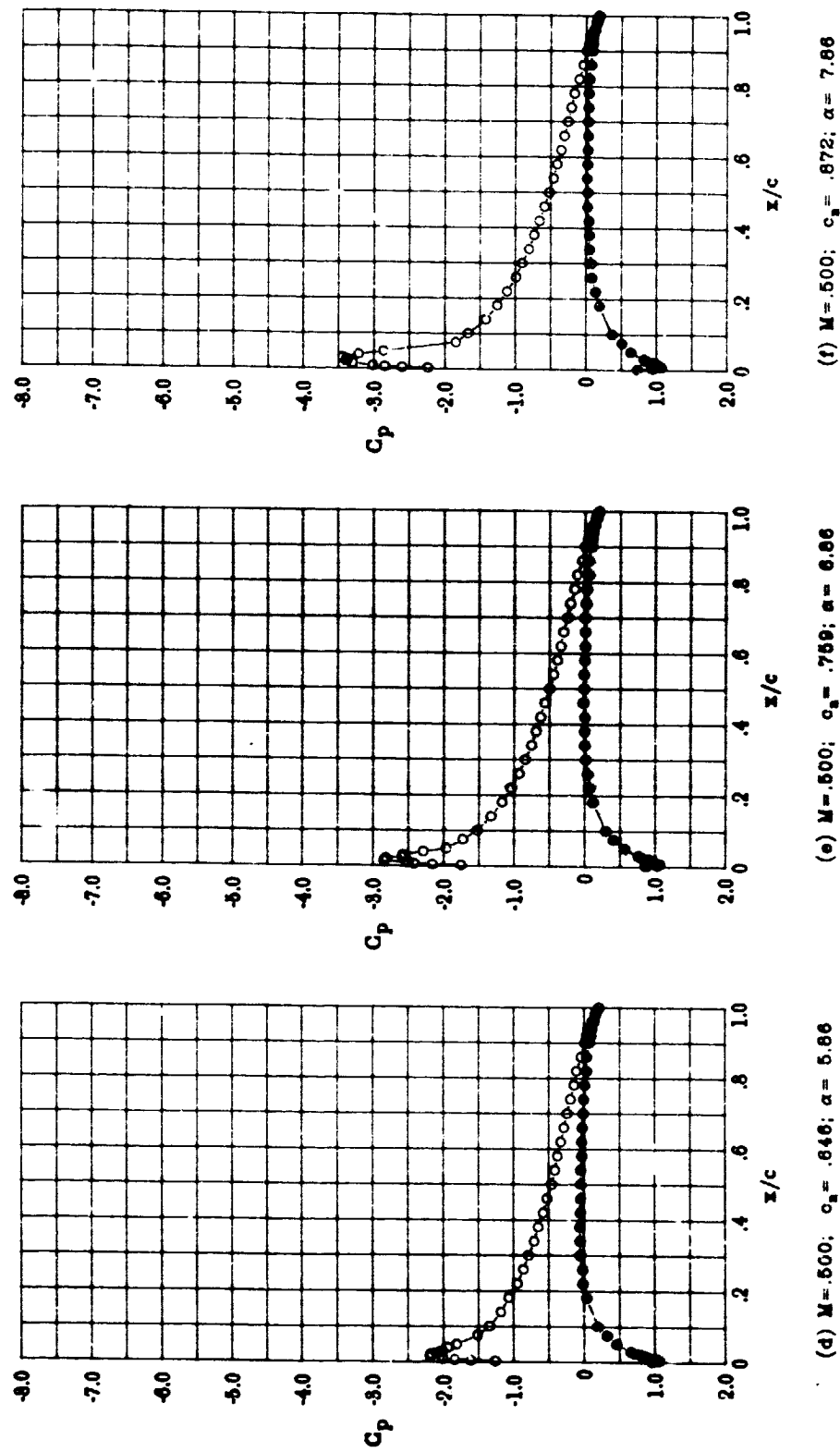
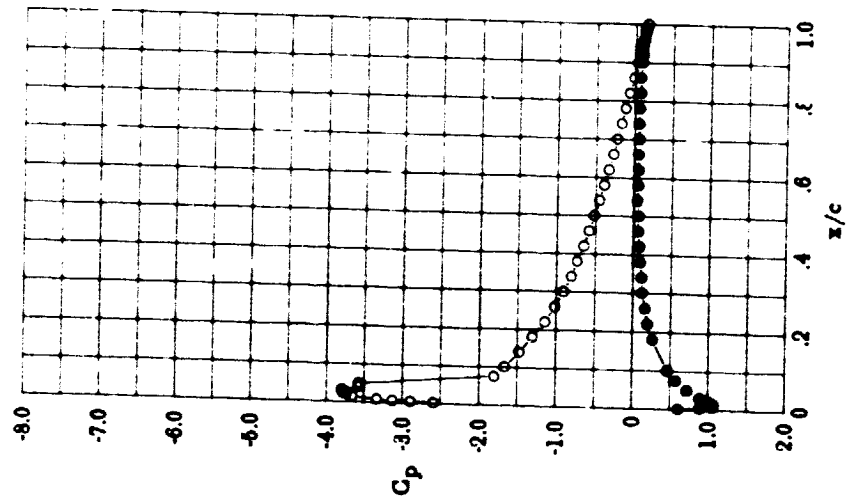
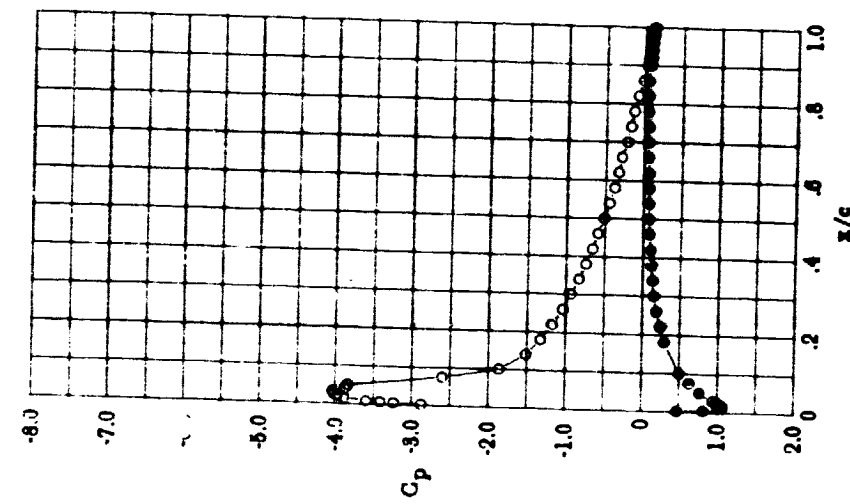


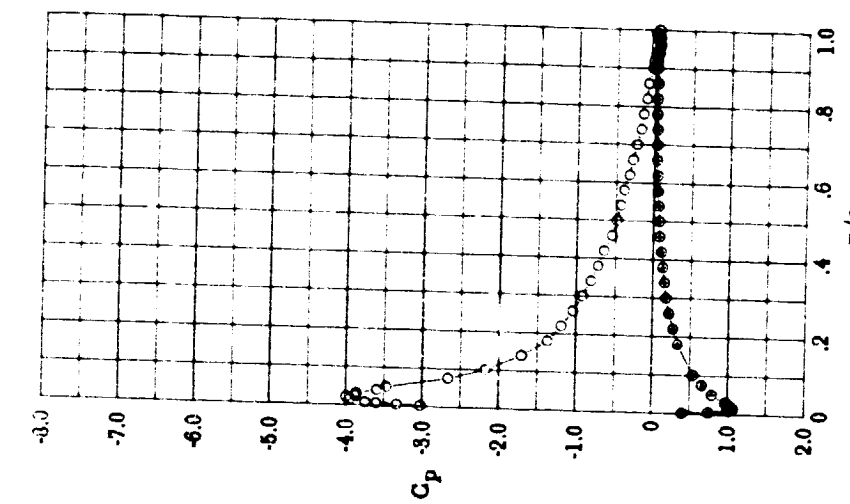
Figure 28.- Continued.



(g) $M = .600; c_a = .934; \alpha = 8.86$



(h) $M = .499; c_a = 1.001; \alpha = 8.86$



(i) $M = .500; c_a = 1.019; \alpha = 10.86$

Figure 28. - Concluded.

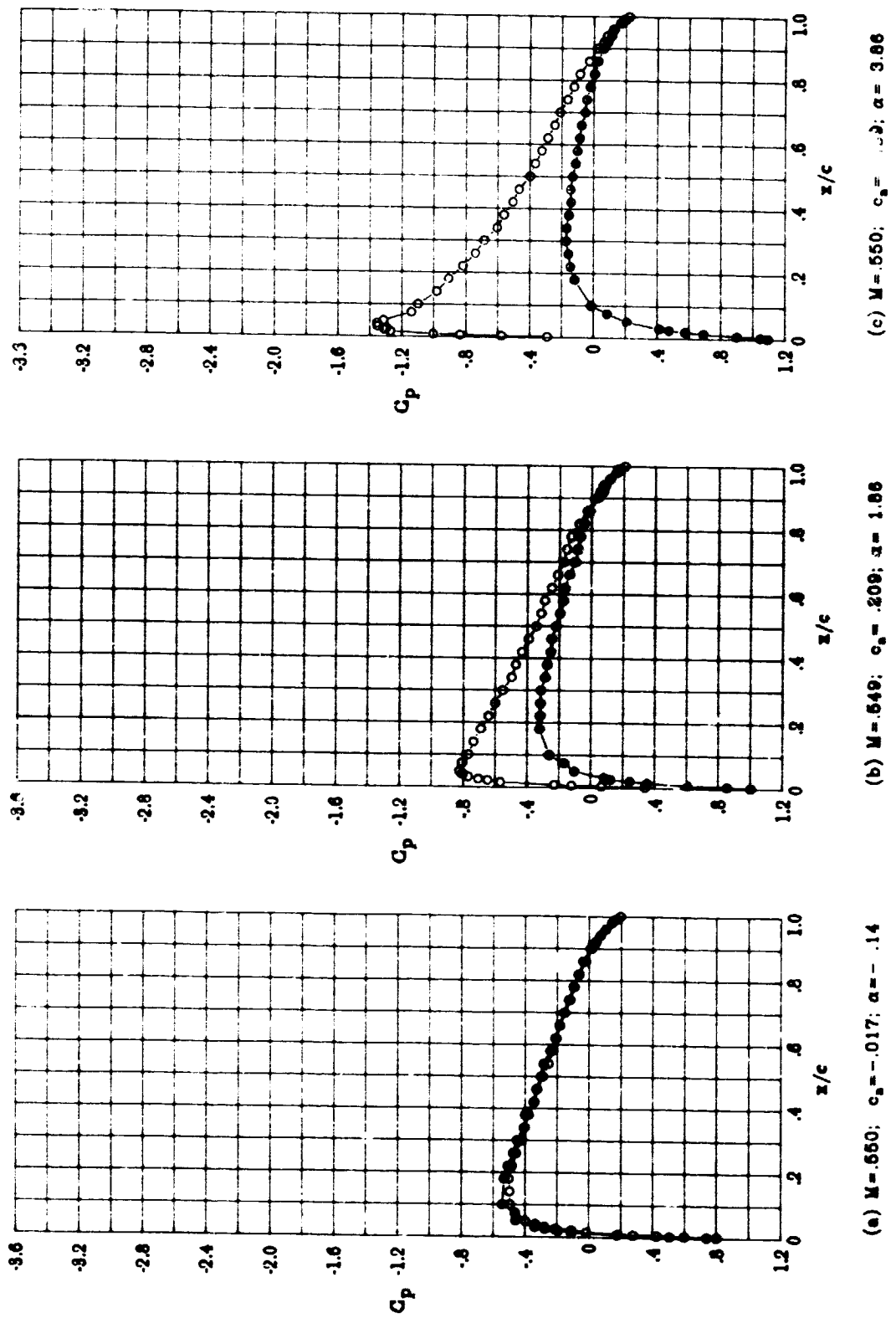


Figure 29. - Chordwise pressure distributions for NACA 0012 airfoil.
 $Rn = 9.0 \cdot 10^6$; $N = 0.55$; transition fixed.

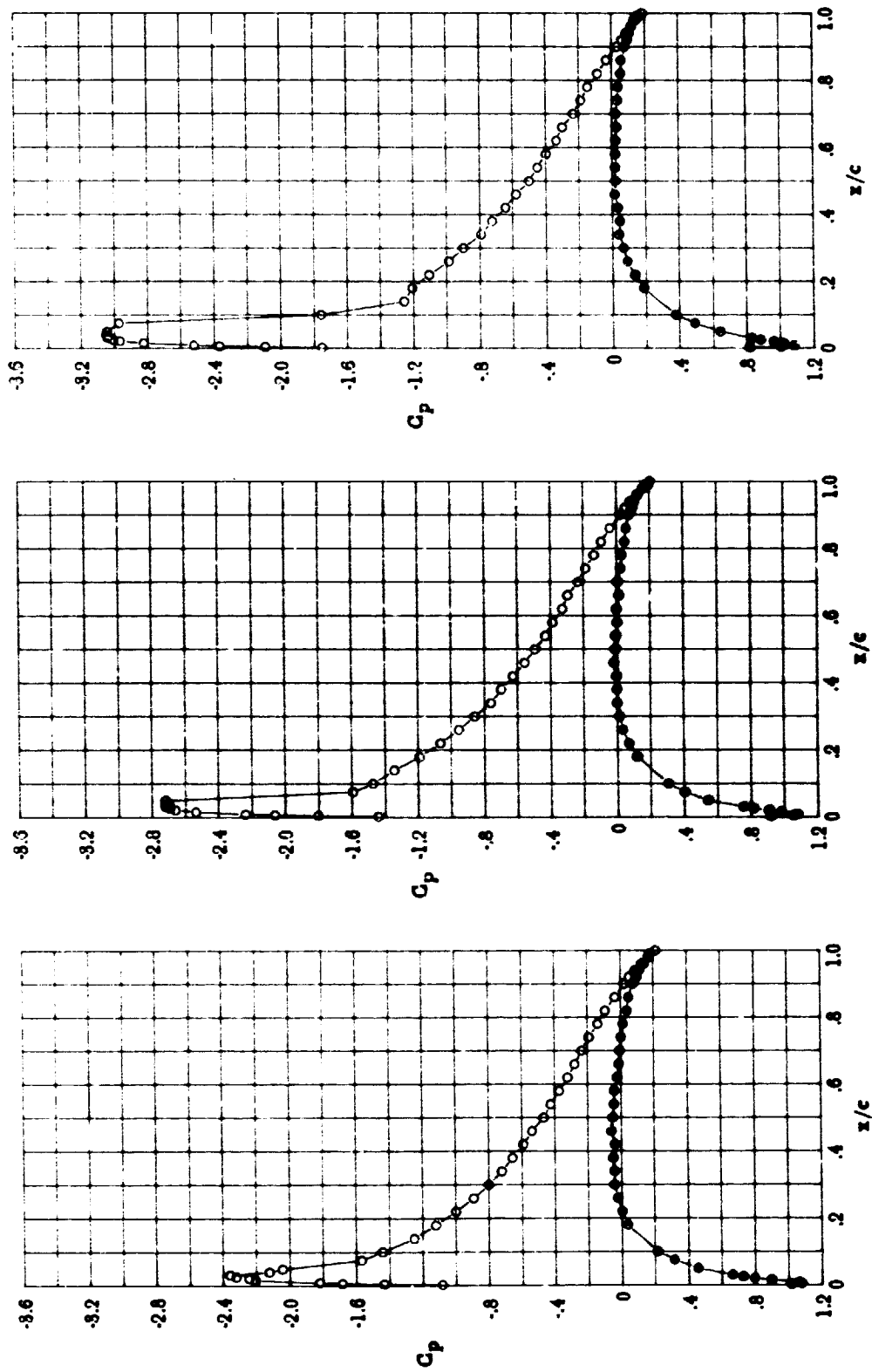
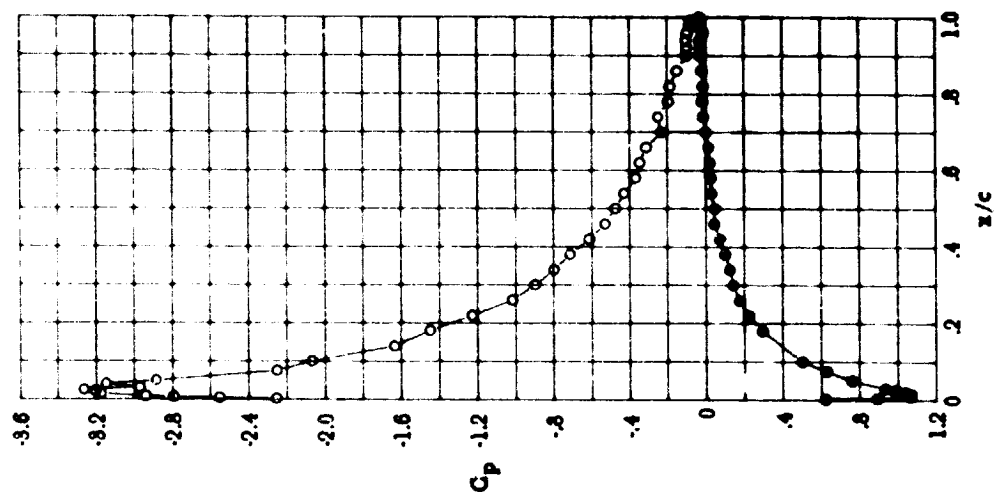
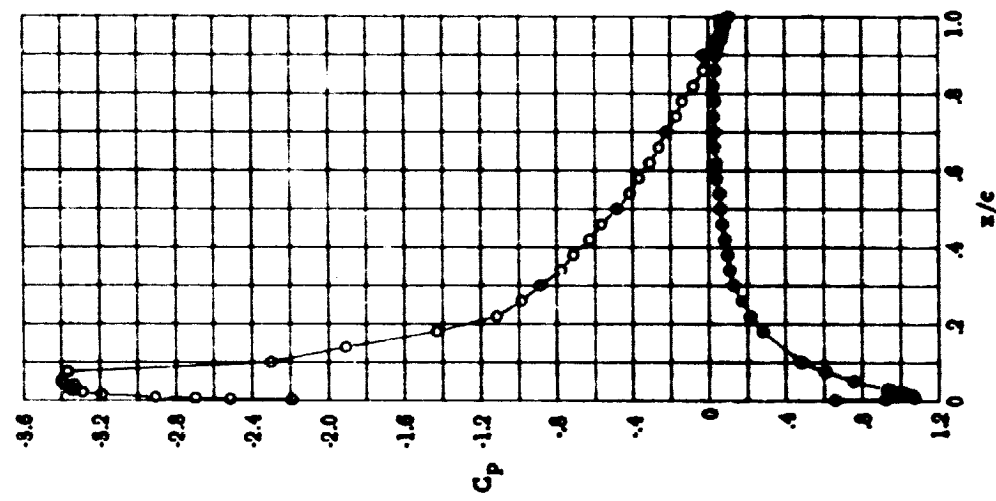


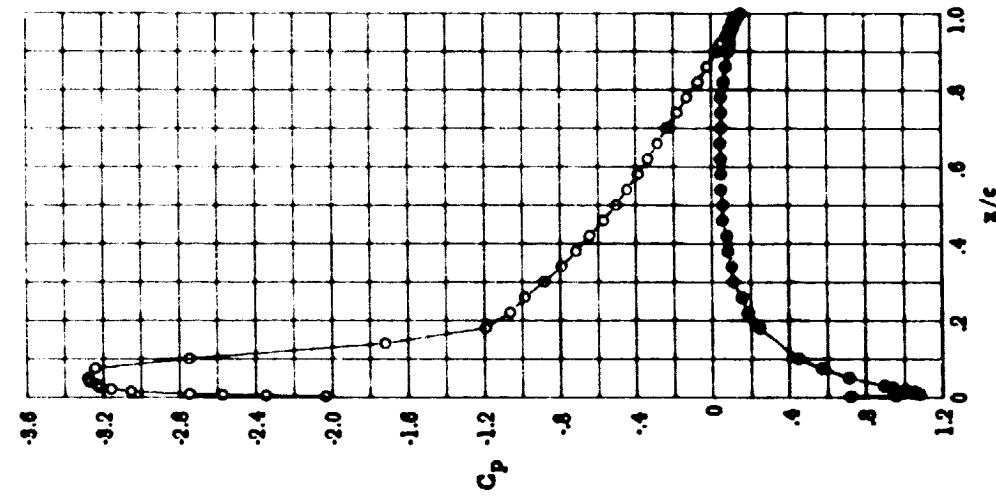
Figure 29.- Continued.



(i) $M = 550$; $c_n = 0.942$; $\alpha = 0.00$



(h) $M = 550$; $c_n = 0.903$; $\alpha = 0.00$



(g) $M = 550$; $c_n = 0.970$; $\alpha = 0.00$

Figure 29. - Concluded.

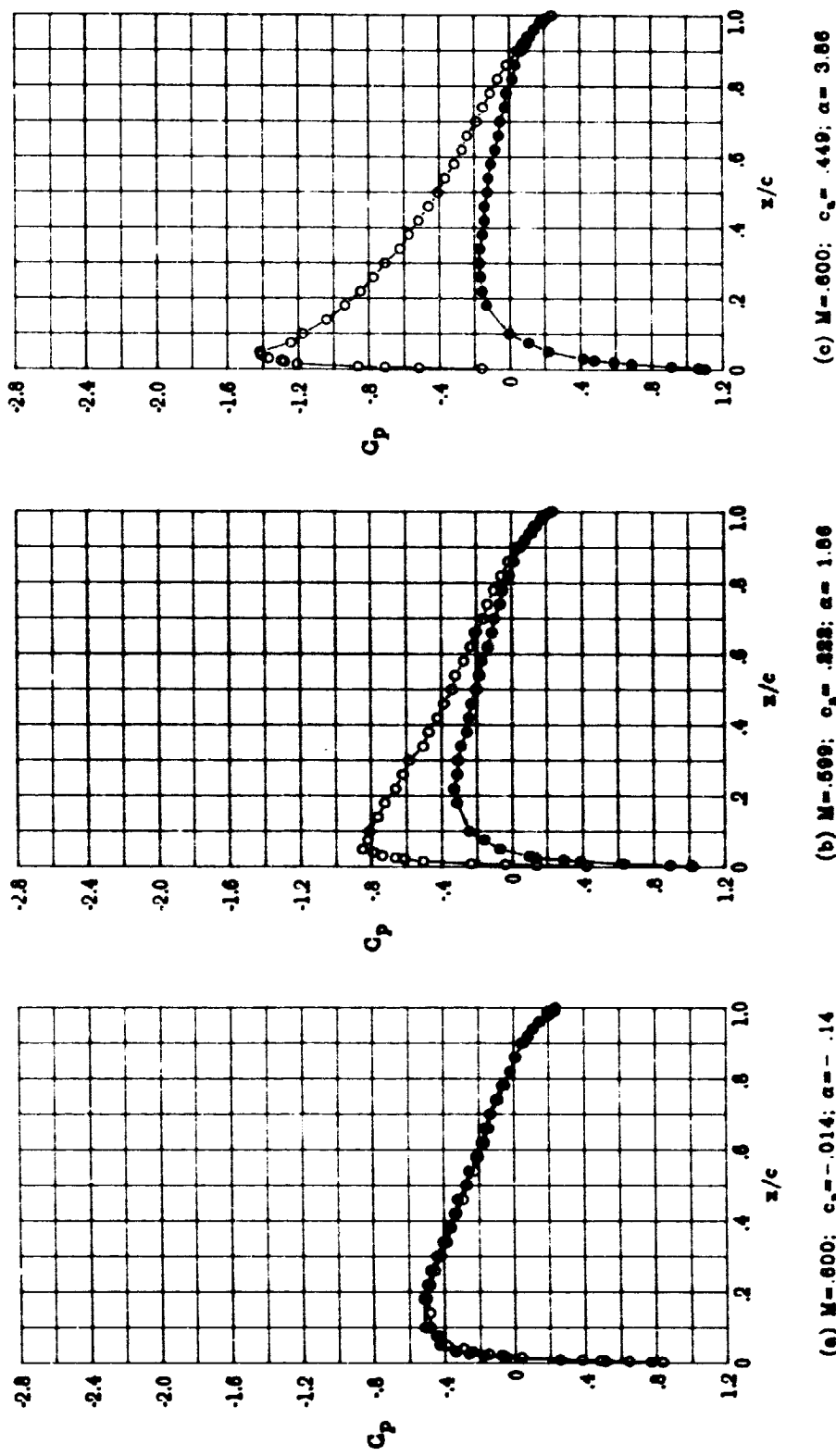
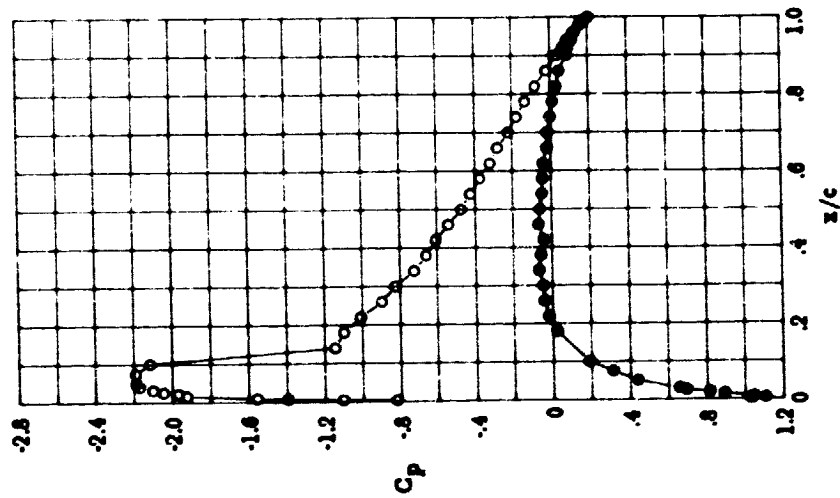
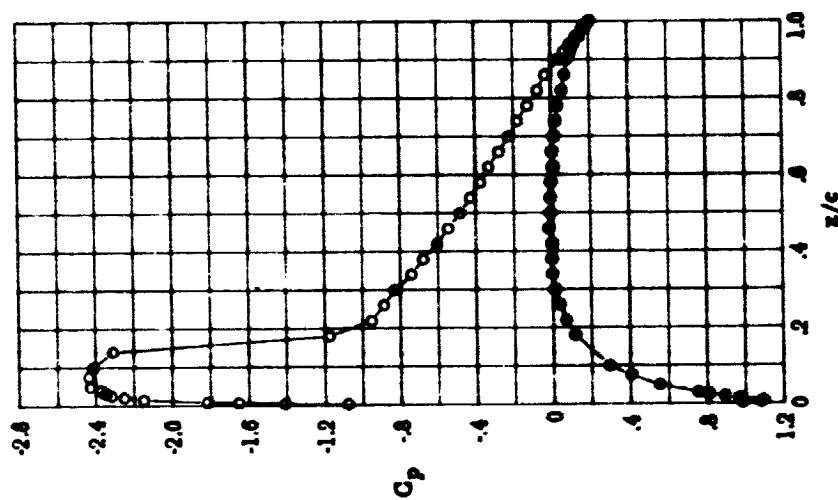
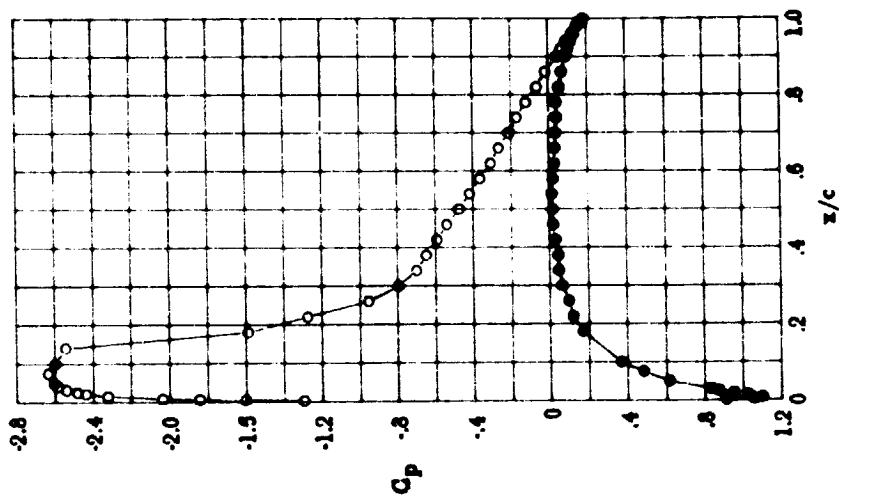


Figure 30.- Chordwise pressure distributions for NACA 0012 airfoil.
 $Rn = 9.0 \times 10^6; M = 0.60$; transition fixed.



(d) $M = 0.800$; $c_0 = .890$; $\alpha = 5.00$
 (e) $M = 0.800$; $c_0 = .815$; $\alpha = 5.00$
 (f) $M = 0.800$; $c_0 = .805$; $\alpha = 7.86$

Figure 30. - Continued.

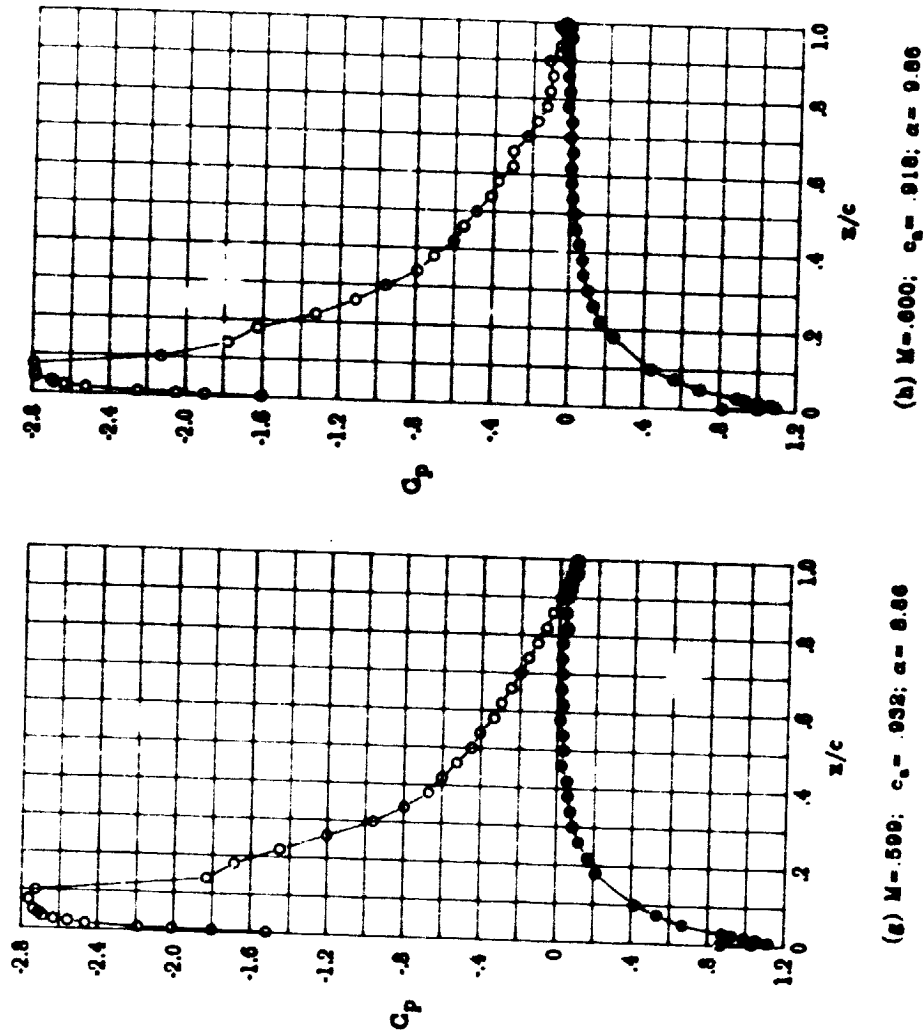


Figure 30.- Concluded.

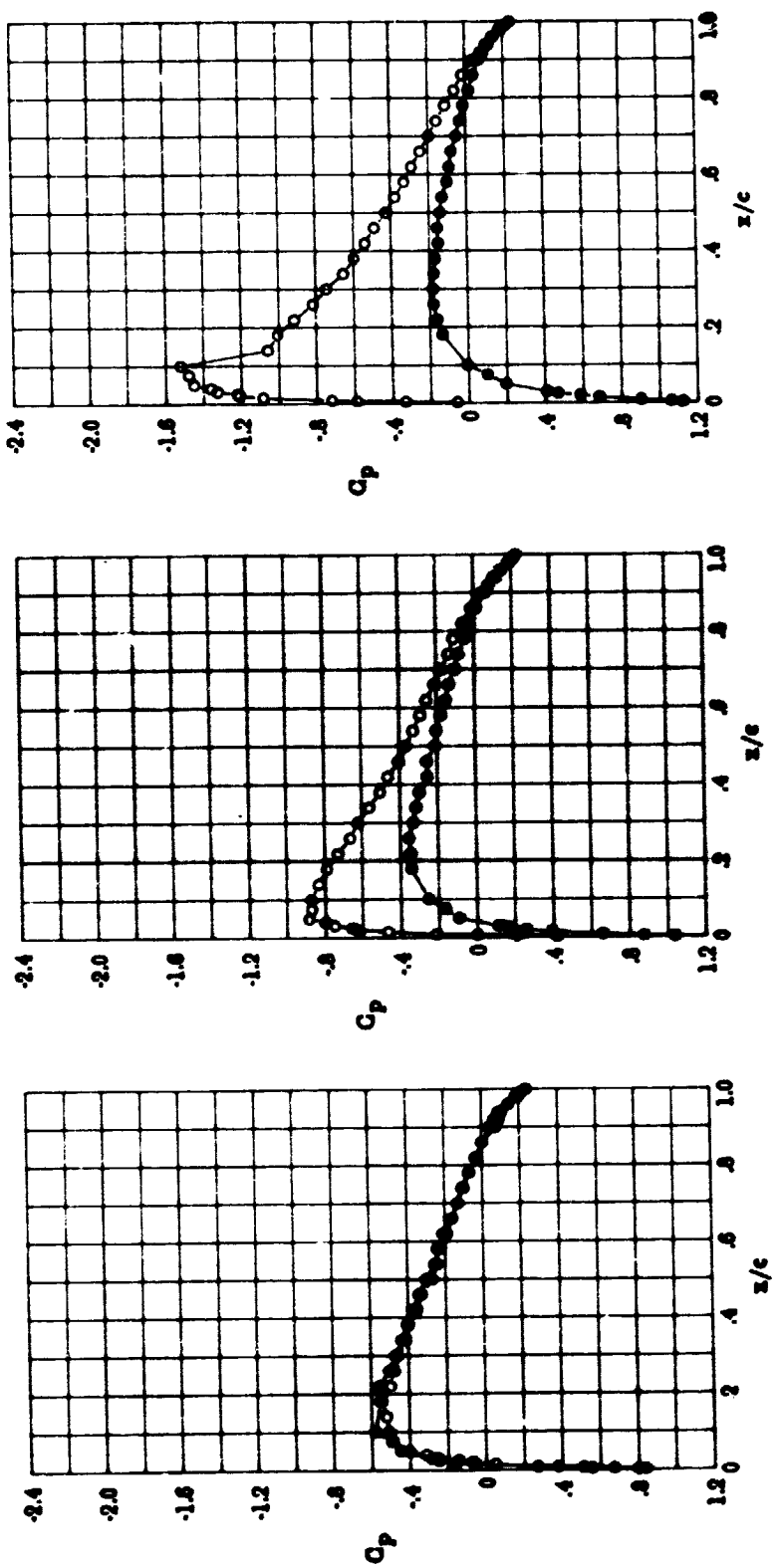


Figure 31. - Chordwise pressure distributions for NACA 0012 airfoil.
 $R_n = 9.0 \times 10^6$; $M = 0.65$; transition fixed.

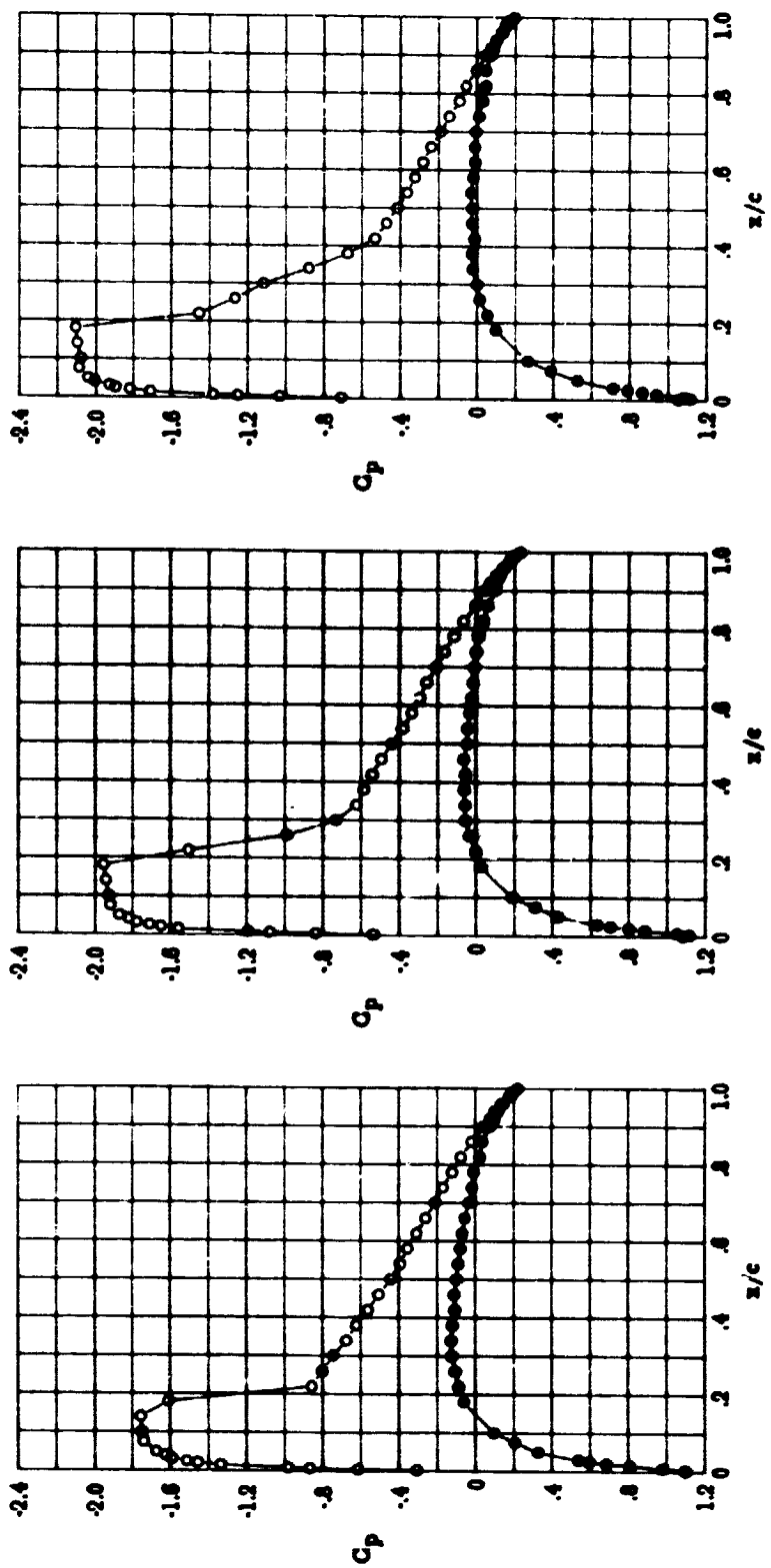


Figure 31. - Continued.

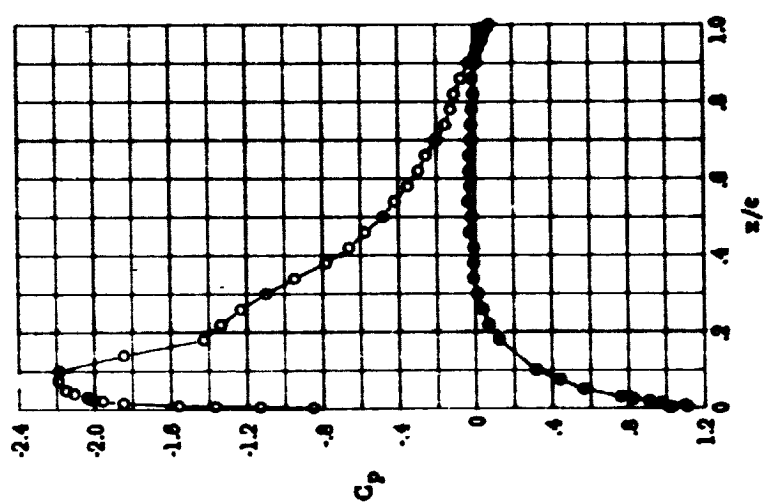


Figure 31.- Concluded.

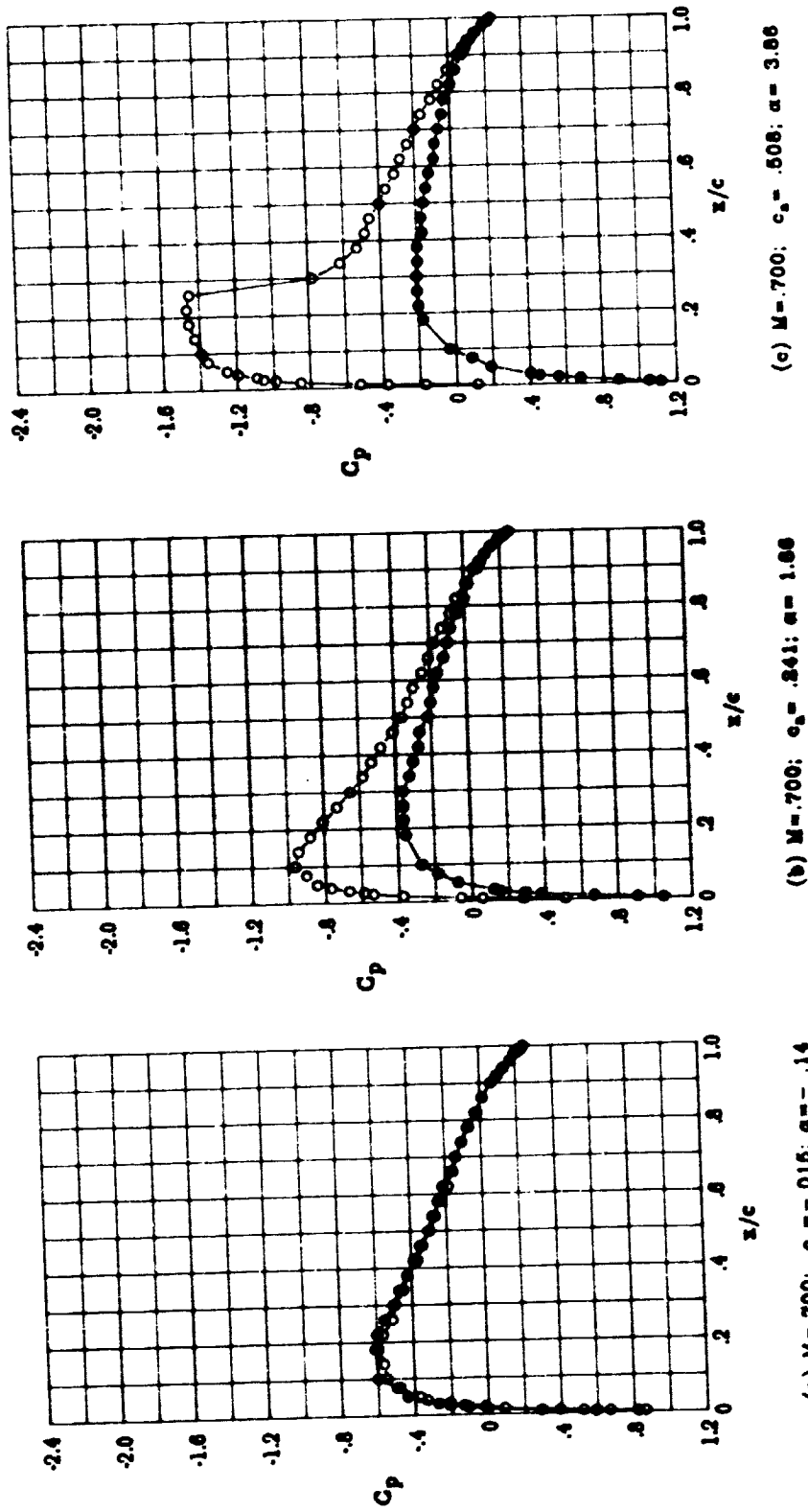
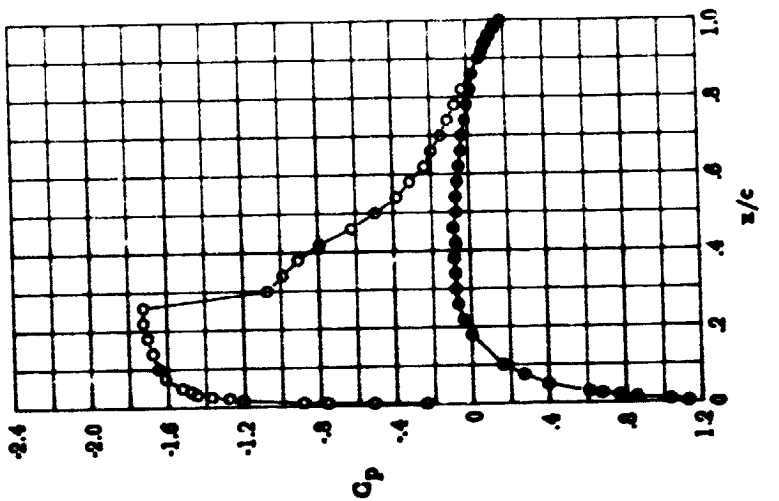
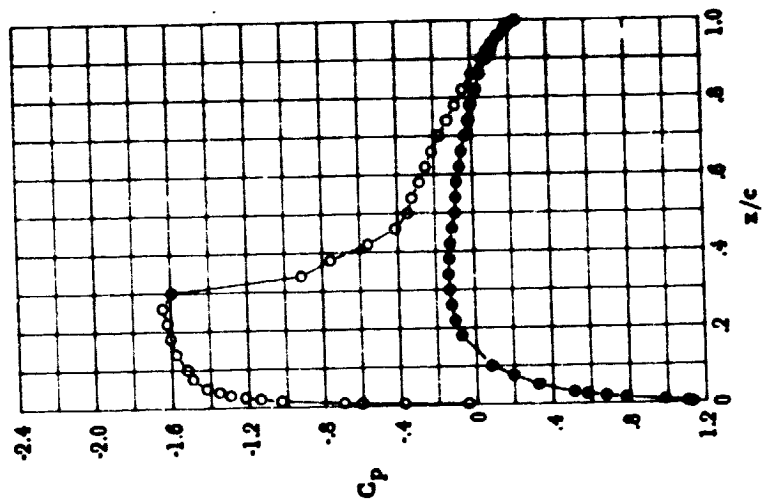


Figure 32. - Chordwise pressure distributions for NACA 0012 airfoil.
 $M = 0.700$; $R_n = 9.0 \times 10^6$; $M = 0.70$; transition fixed.



(d) $M = .600$; $c_a = .650$; $\alpha = 4.86$



(e) $M = .600$; $c_a = .722$; $\alpha = 5.66$

Figure 32.- Concluded.

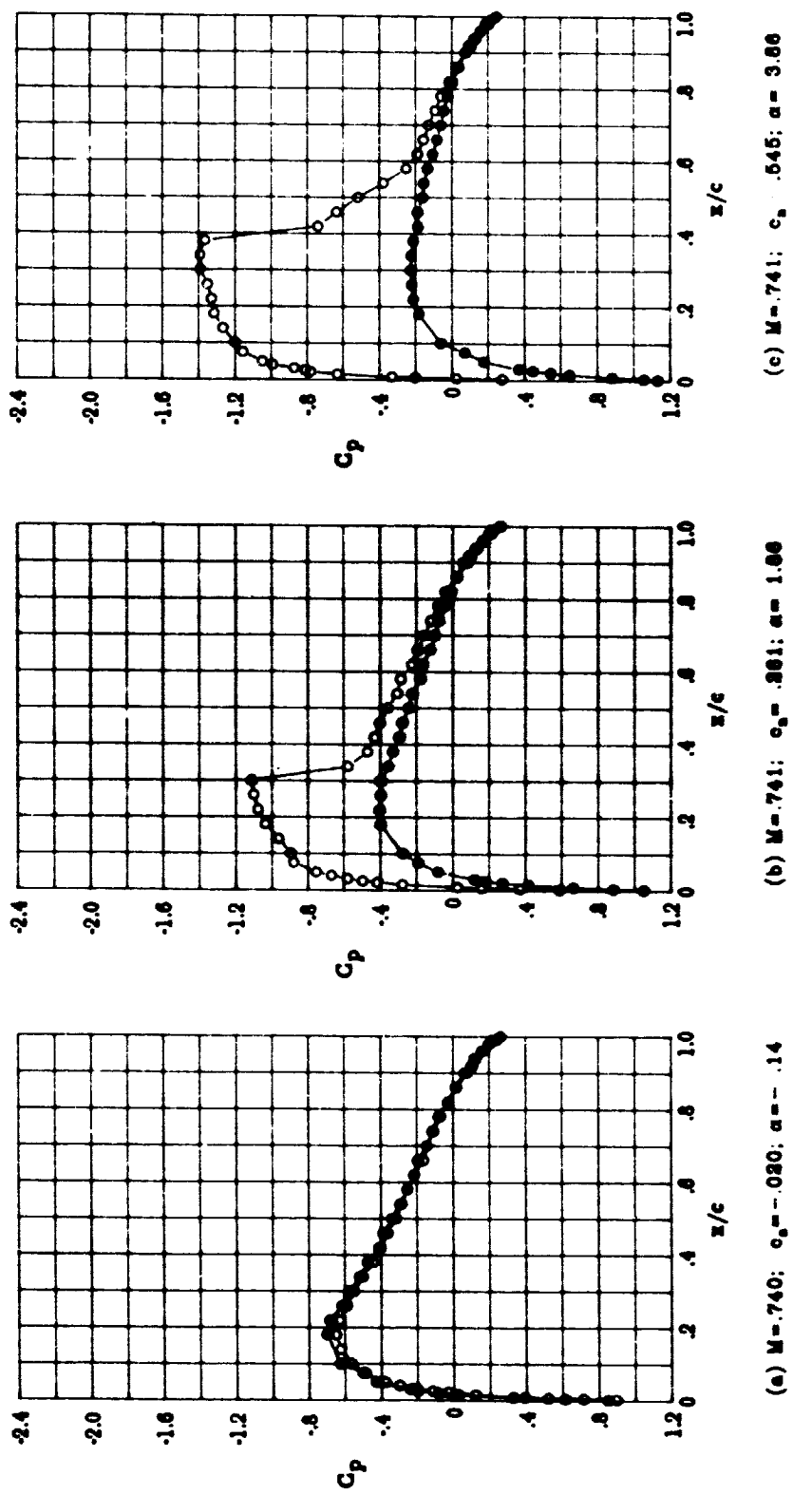
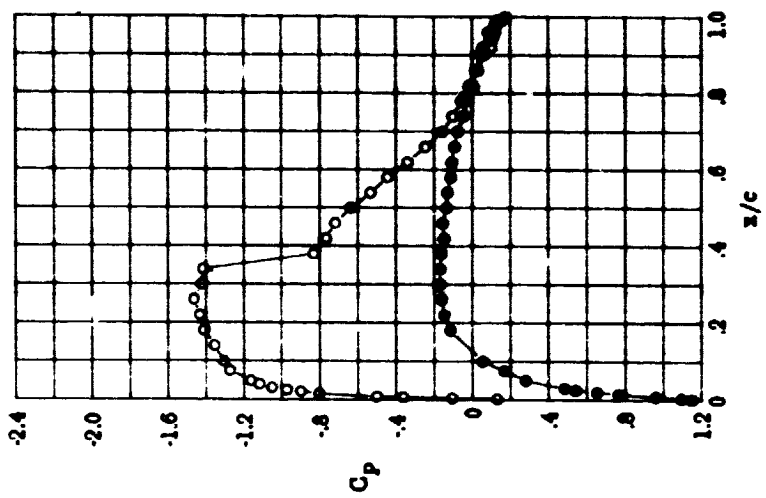


Figure 33.- Chordwise pressure distributions for NACA 0012 airfoil.
 $Rn = 9.0 \times 10^6$; $M = 0.74$; transition fixed.



(d) $M = 0.740; c_a = .922; \alpha = 4.86$

Figure 33. - Concluded.

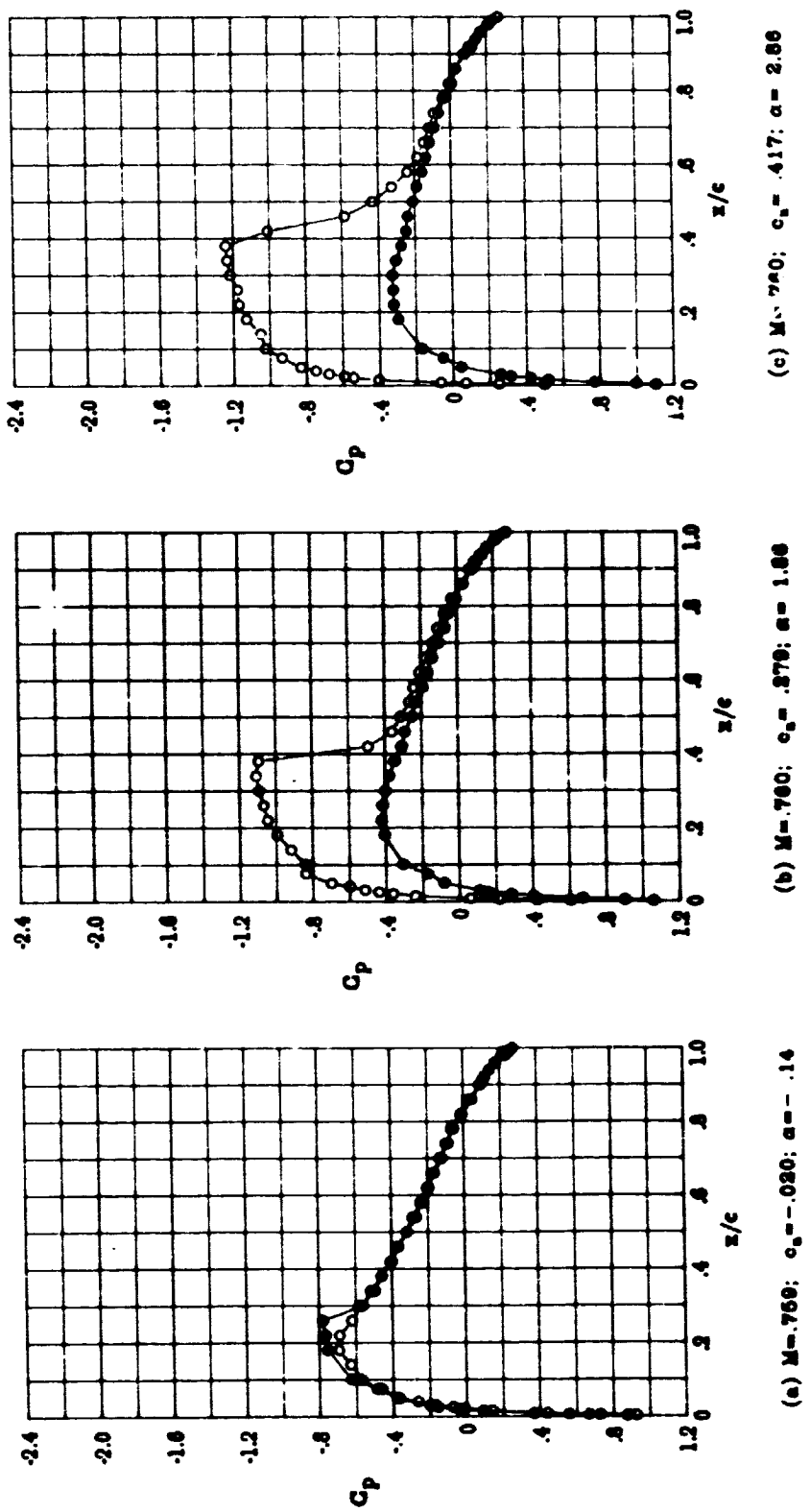


Figure 34.- Chordwise pressure distributions for NACA 0012 airfoil.
 $R_n = 9.0 \times 10^6$; $M = 0.76$; transition fixed.

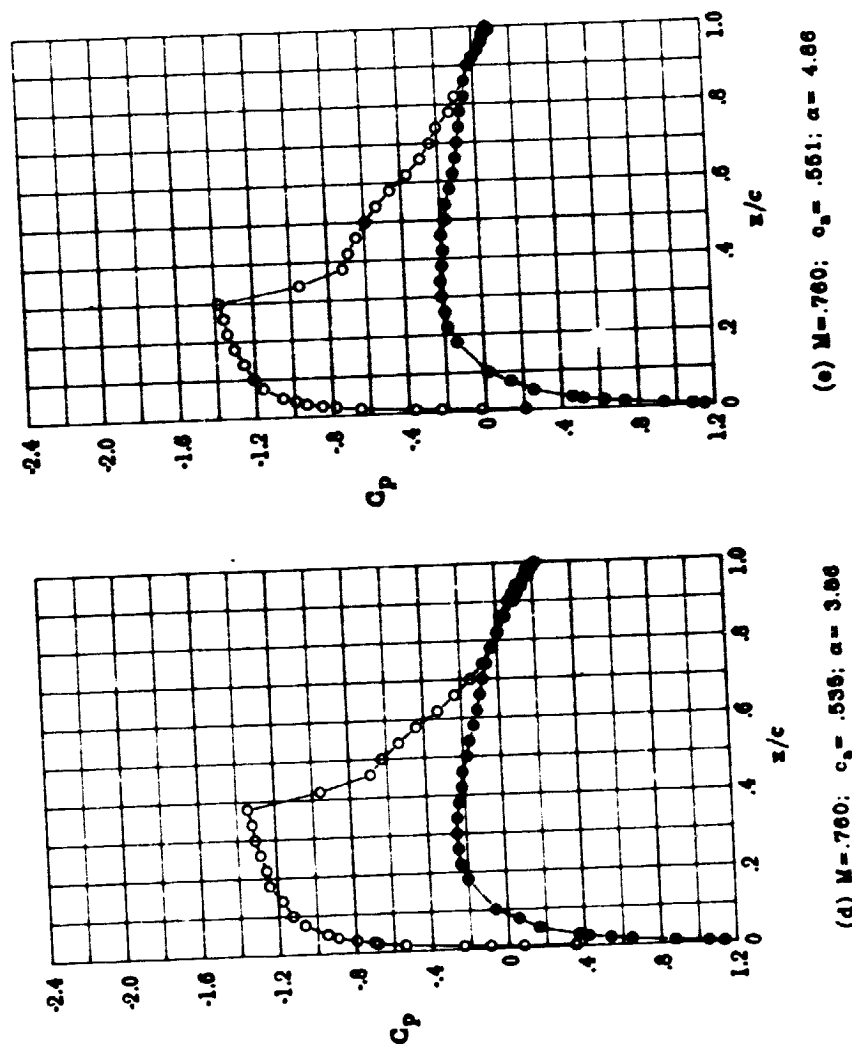


Figure 34. - Concluded.

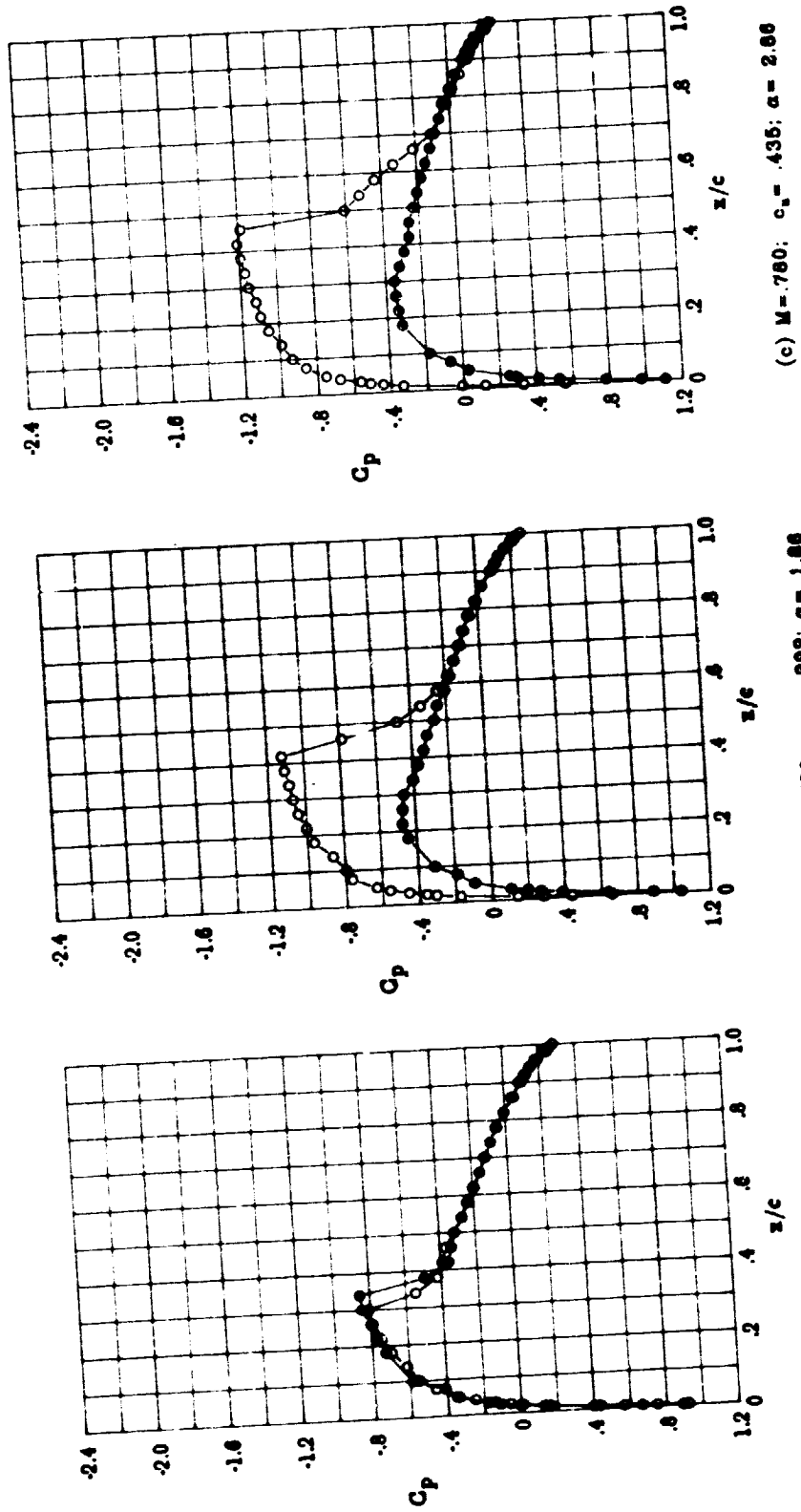
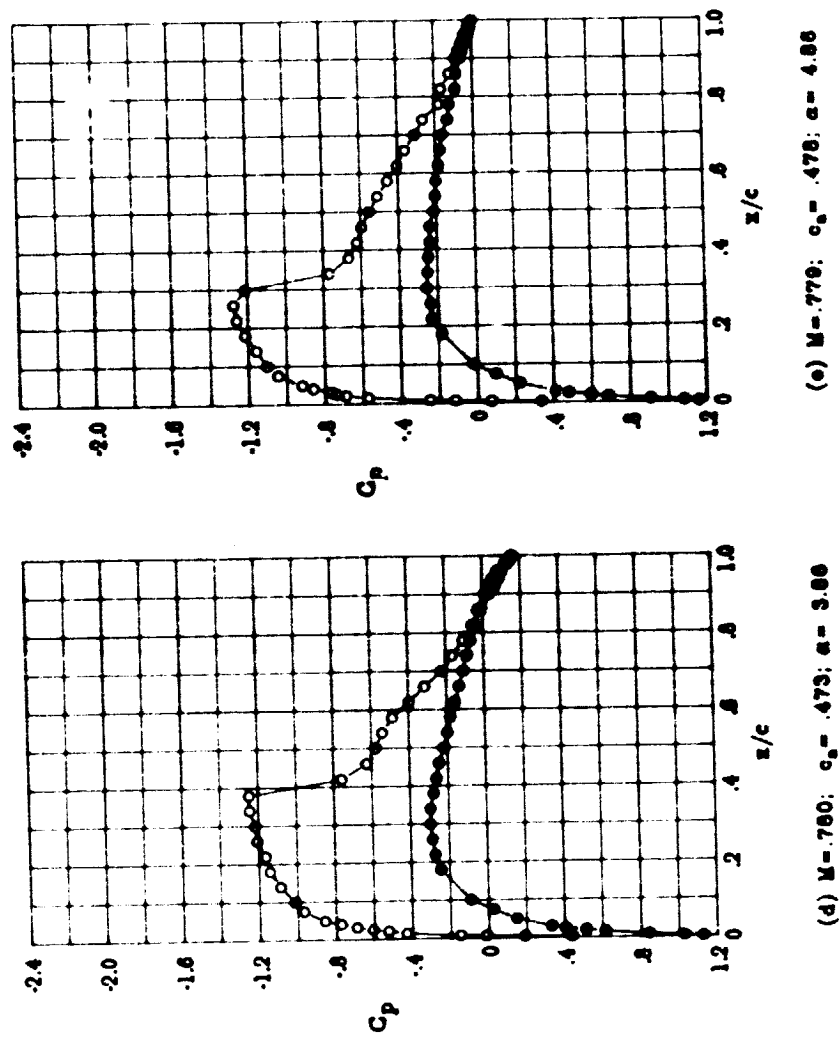
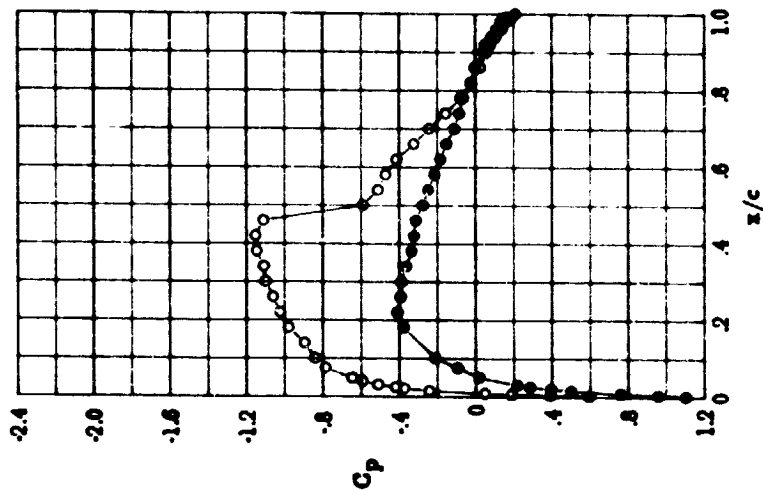


Figure 35.- Chordwise pressure distributions for NACA 0012 airfoil.
 $R_n = 9.0 \times 10^6$; $M = 0.78$; transition fixed.

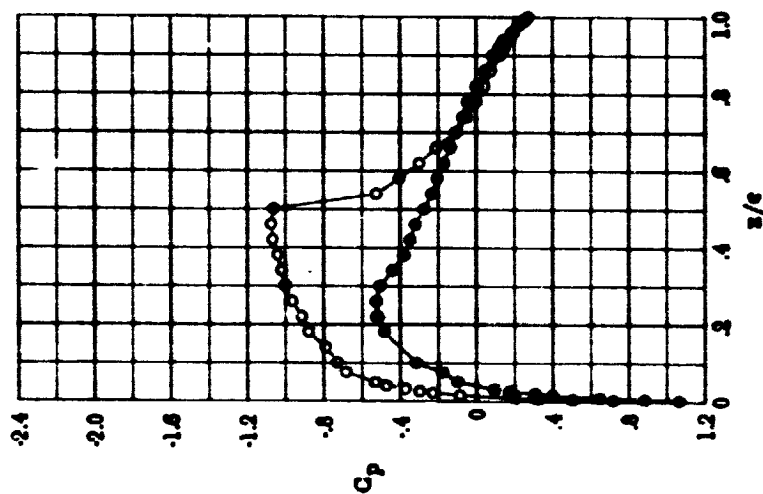


(d) $M = .760$; $c_0 = .473$; $\alpha = 3.06$ (e) $M = .770$; $c_0 = .470$; $\alpha = 4.86$

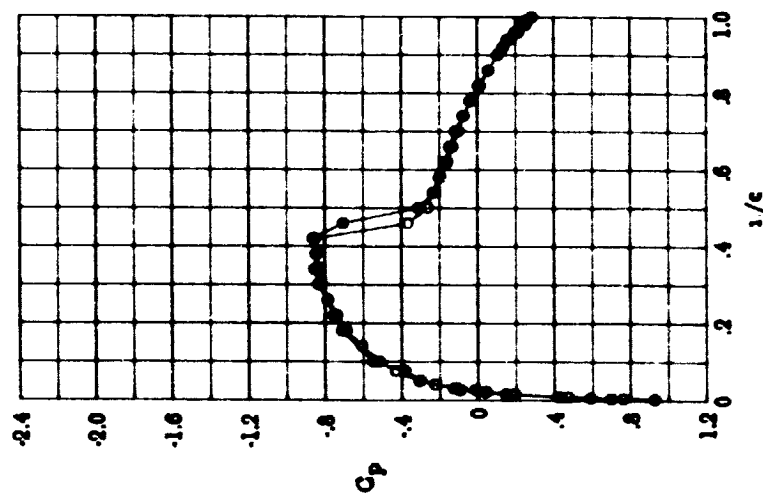
Figure 35.- Concluded.



(c) $M = 700$; $c_a = .390$; $\alpha = 2.66$

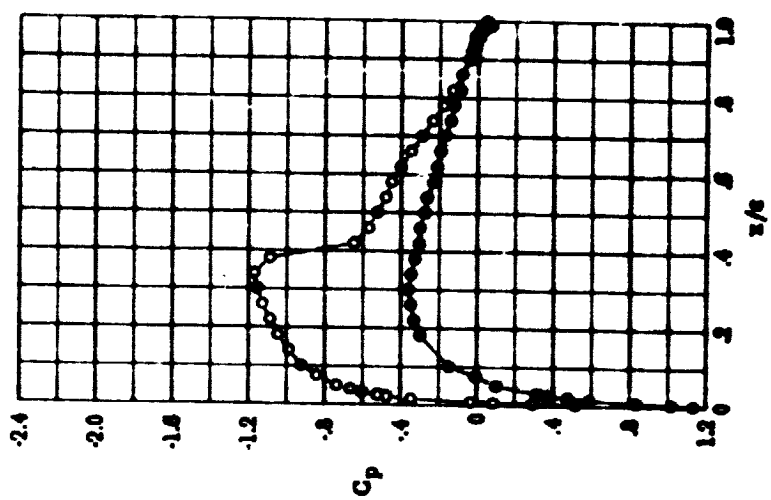


(b) $M = 300$; $c_a = .300$; $\alpha = 1.00$



(a) $M = 100$; $c_a = .016$; $\alpha = 1.14$

Figure 36.- Chordwise pressure distributions for NACA 0012 airfoil.
 $Rn = 9.0 \times 10^6$; $M = 0.80$; transition fixed.



(4) $M_\infty = 0.90$; $c_0 = .305$; $\alpha = 3.03$

Figure 36. - Concluded.

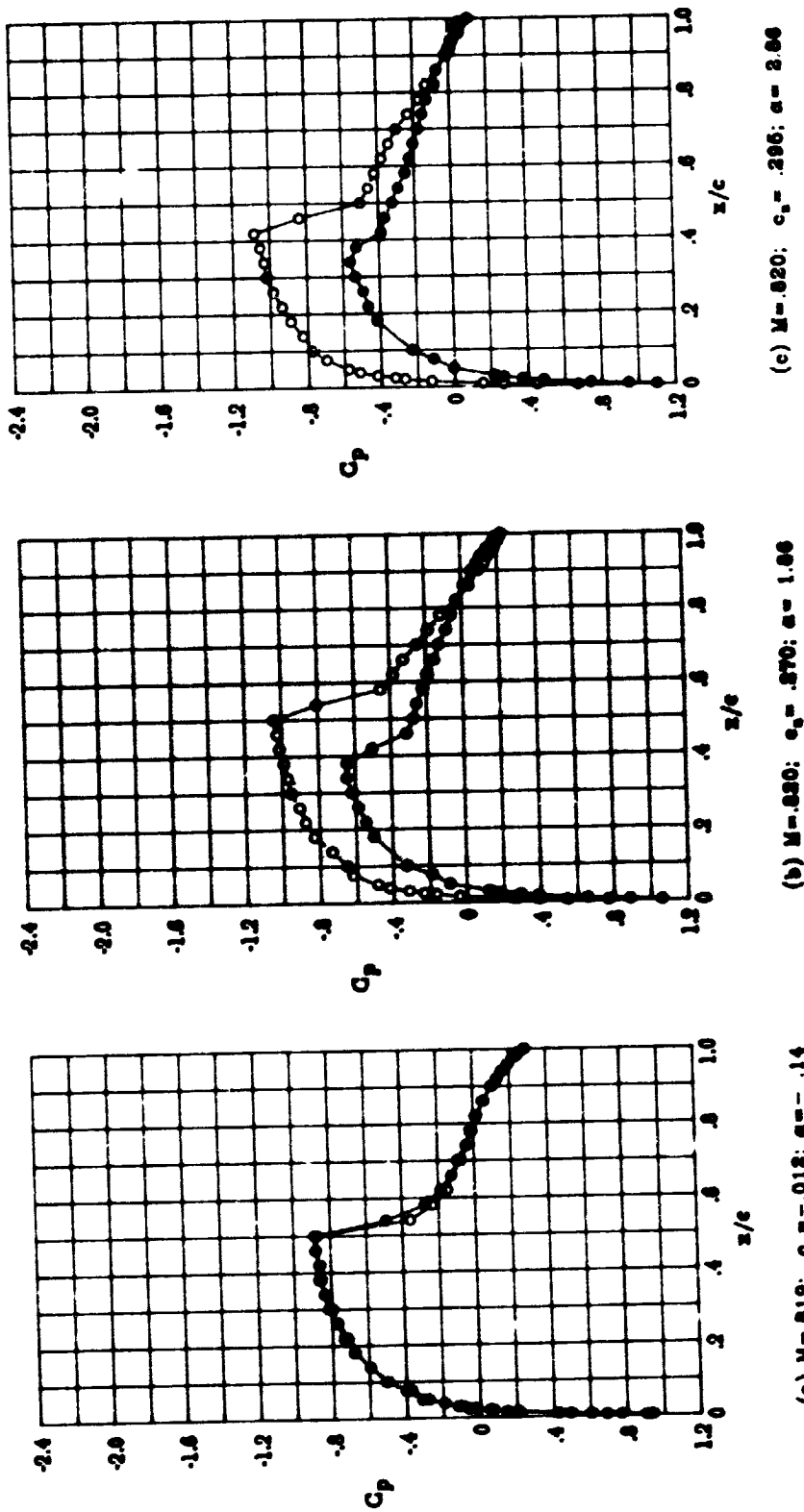
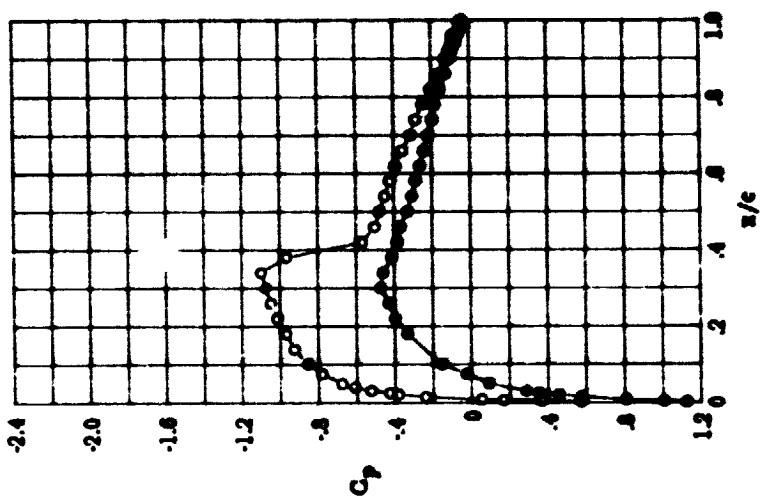


Figure 37.- Chordwise pressure distributions for NACA 0012 airfoil.
 $Rn = 9.0 \times 10^6$; $M = 0.82$; transition fixed.



(d) $M = 0.80$; $c_0 = .318$; $a = 3.66$

Figure 37.- Concluded.

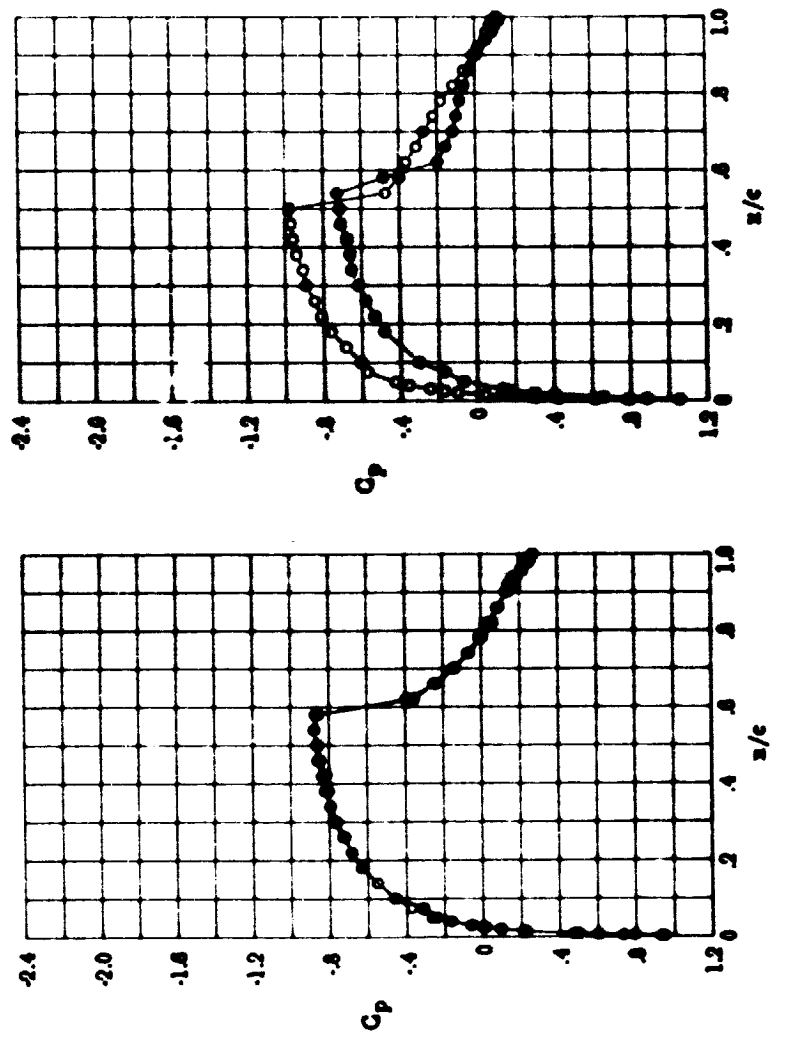


Figure 38. - Chordwise pressure distributions for NACA 0012 airfoil.
 $M = 0.840$; $c_0 = .000$; $\alpha = .14$ (a)
 $M = 0.840$; $c_0 = .170$; $\alpha = 1.00$ (b)
 $Re = 9.0 \times 10^6$; $M = 0.84$; transition fixed.

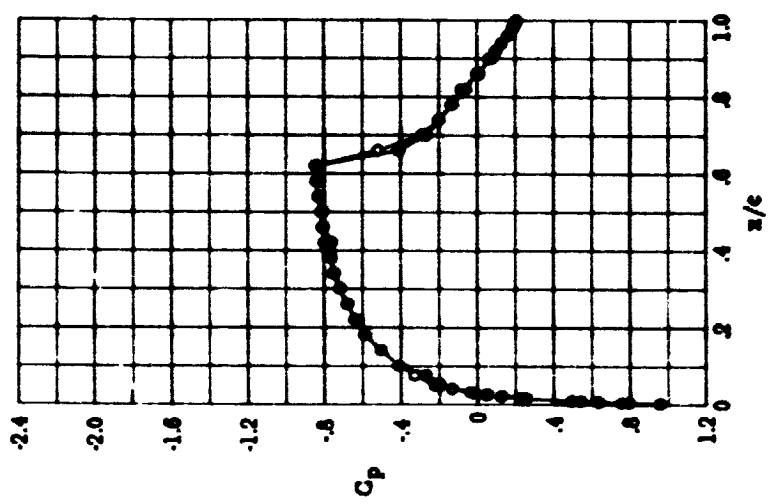


Figure 39.- Chordwise pressure distributions for NACA 0012 airfoil.
 $(\bullet) M = .860; C_L = .011; \alpha = .14$
 $R_n = 9.0 \times 10^6; M = 0.86; \text{transition fixed.}$

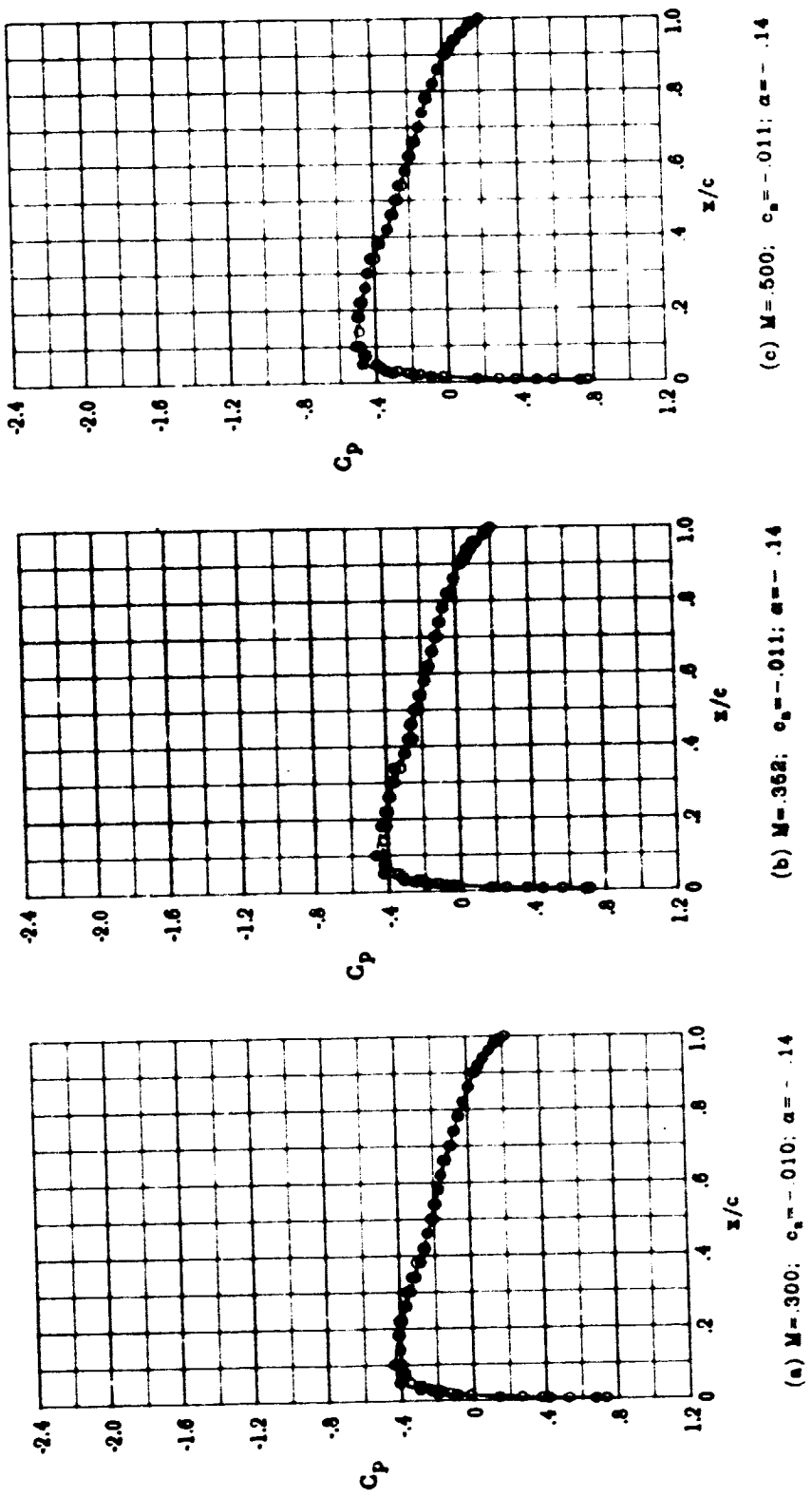
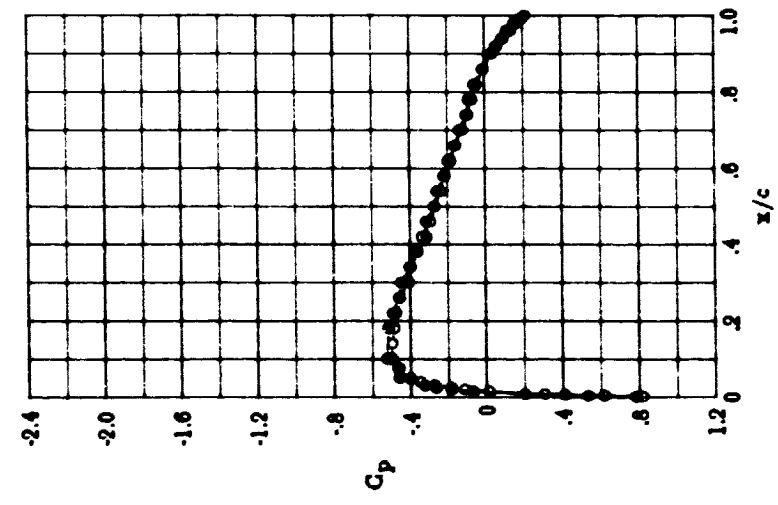
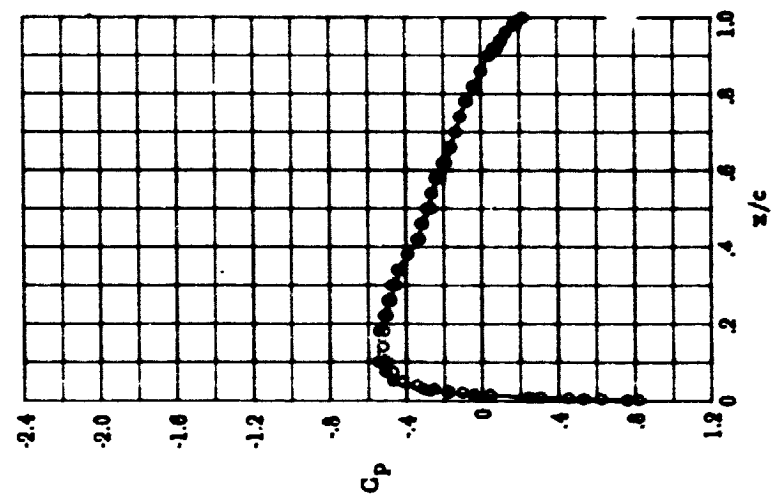


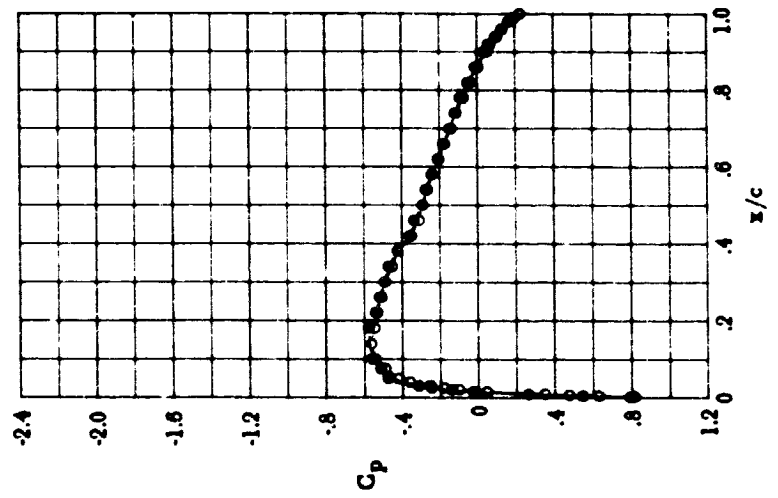
Figure 40.- Chordwise pressure distributions for NACA 0012 airfoil.
 $R_n = 3.0 \times 10^6$; transition free, angle of attack near zero.



(d) $M = .650$; $c_0 = -.011$; $\alpha = -.14$

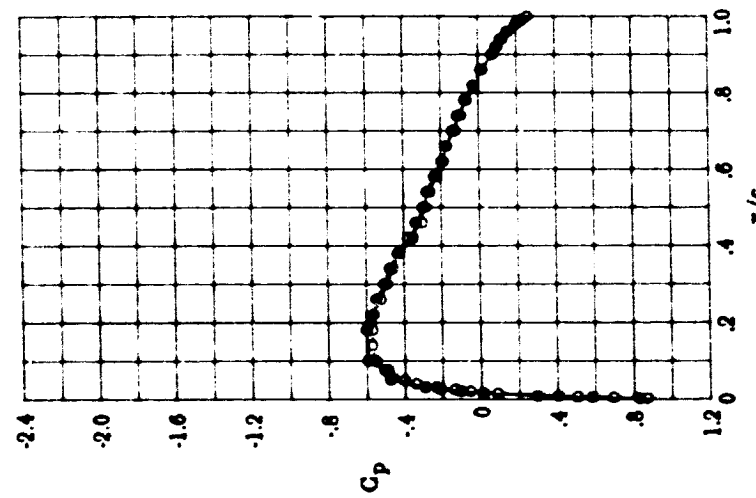
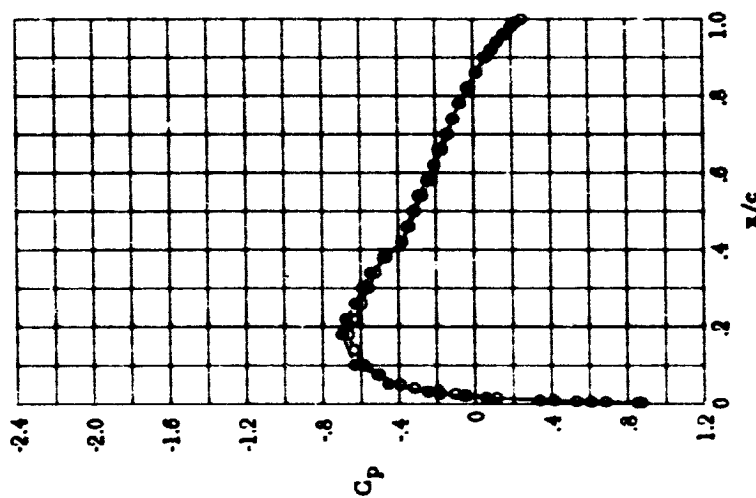
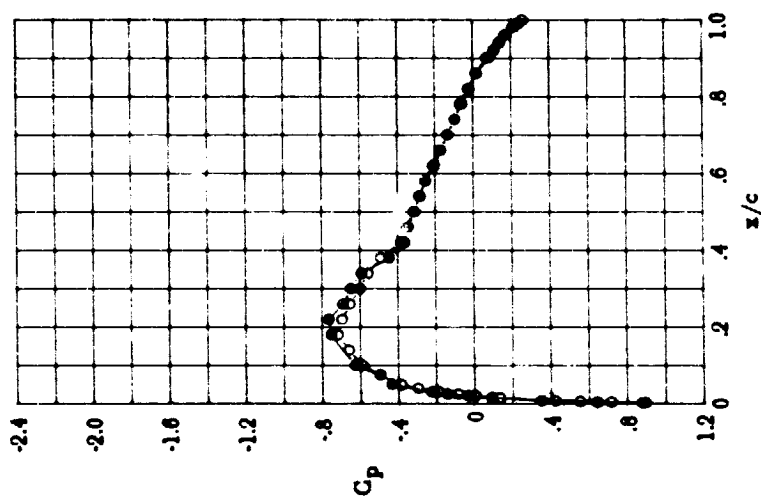


(e) $M = .600$; $c_0 = -.016$; $\alpha = -.14$



(f) $M = .649$; $c_0 = -.010$; $\alpha = -.14$

Figure 40.- Continued.



(1) $M = 0.768$; $c_a = -0.013$; $\alpha = -14$

(b) $M = 0.737$; $c_a = -0.010$; $\alpha = -14$

(c) $M = 0.600$; $c_a = -0.012$; $\alpha = -14$

Figure 40.- Continued.

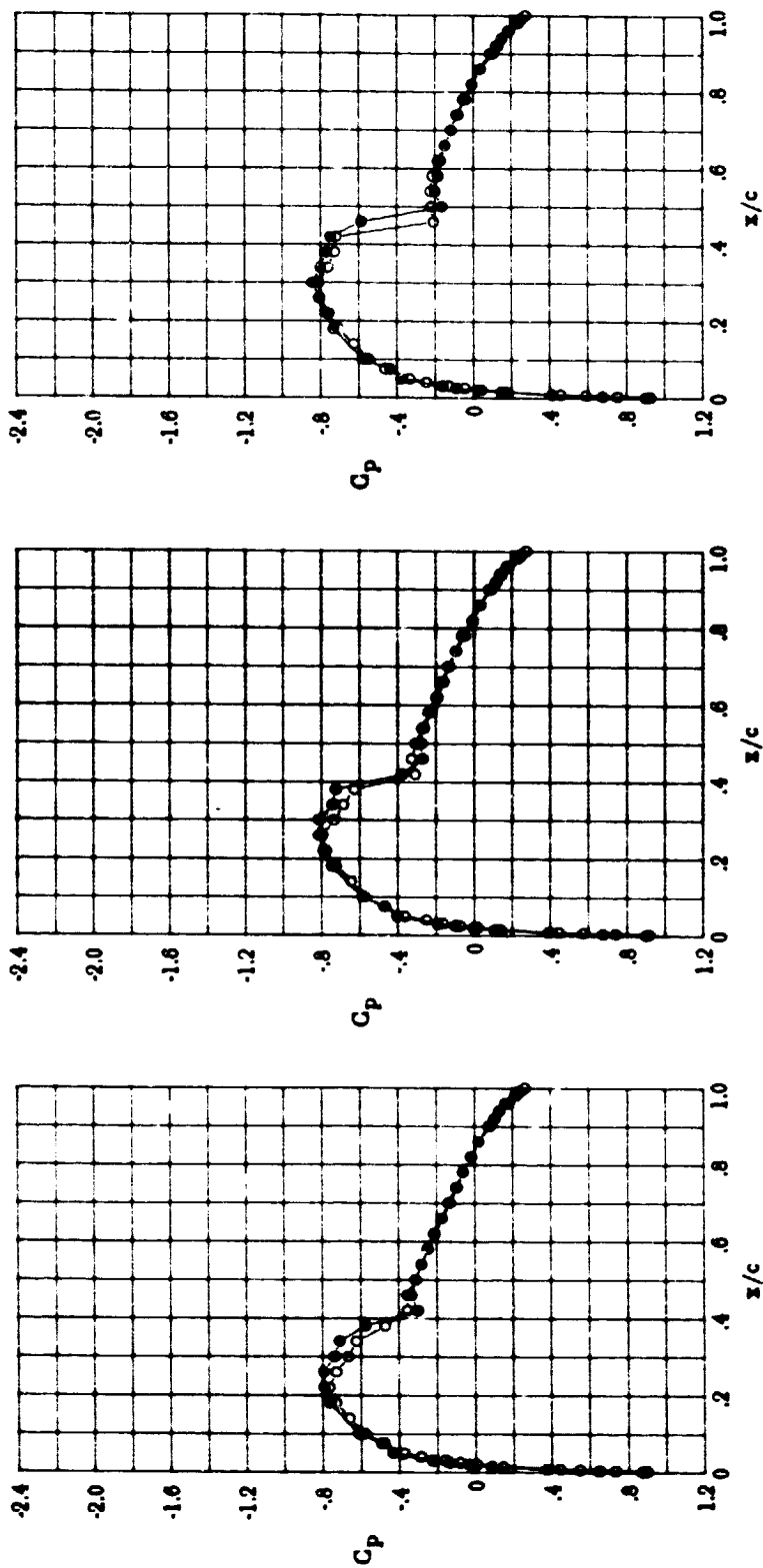
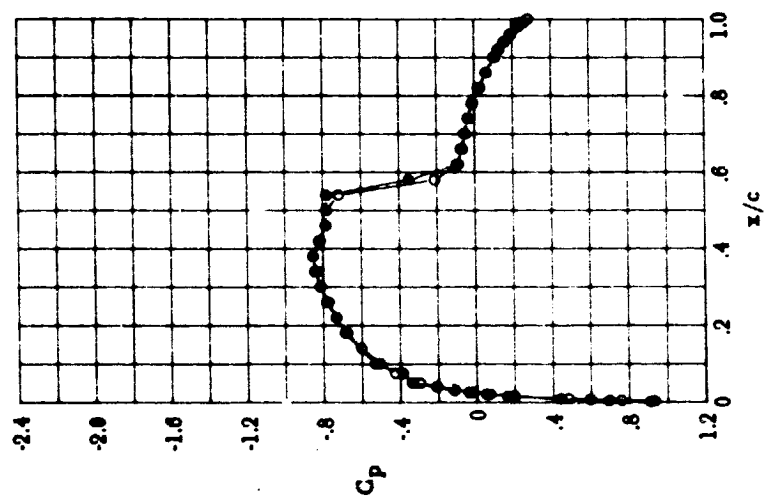
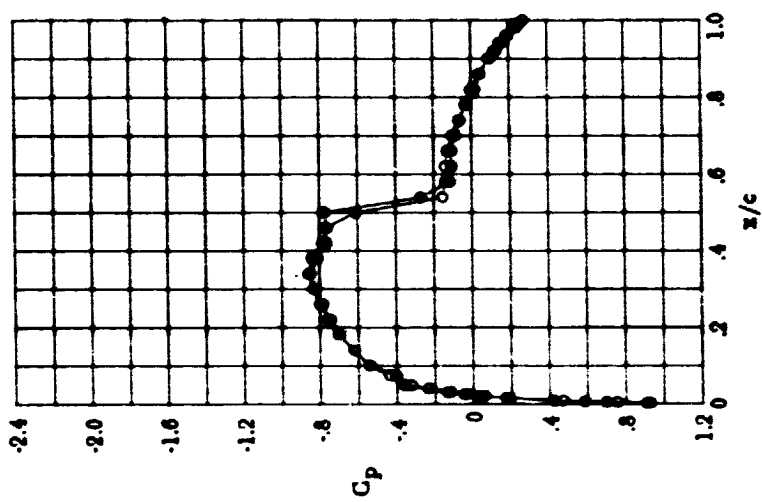


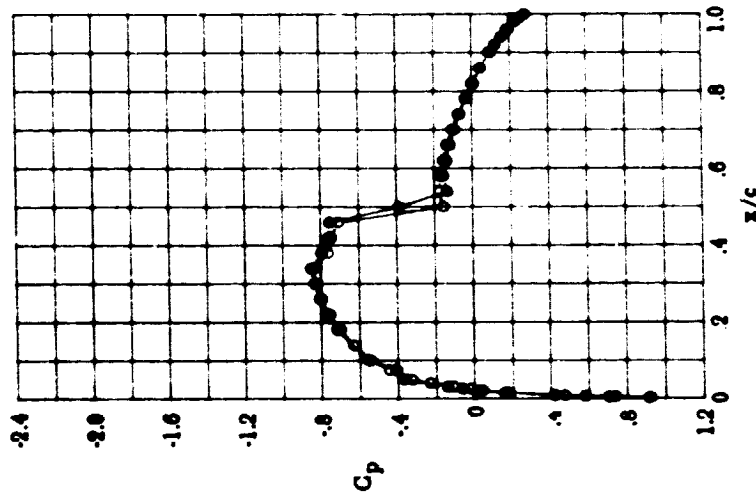
Figure 40.- Continued.



(o) $M = .820; c_0 = -.008; \alpha = -.14$

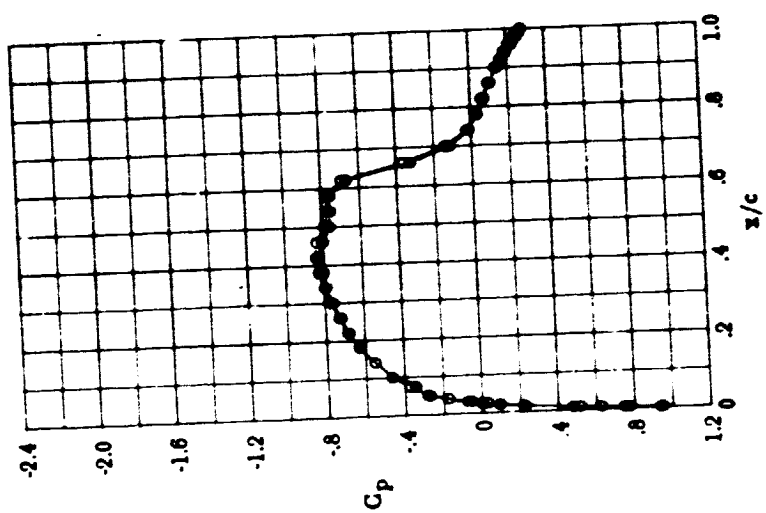


(n) $M = .800; c_0 = -.008; \alpha = -.14$



(m) $M = .800; c_0 = -.011; \alpha = -.14$

Figure 40. - Continued.



(P) $M = 0.41$; $c_a = -0.012$; $\alpha = -1.12$

Figure 40. - Concluded.

END

DATE

FILMED

JUL 8 1981